Universidad de Oviedo

Programa de Doctorado en Biología Molecular y Celular

Departamento de Bioquímica y Biología Molecular

Functional analysis and development of novel marked vaccines against Myxoma virus

Análisis funcional y Desarrollo de nuevas vacunas marcadas contra el virus mixoma

Inés Calonge Sanz

Oviedo 2024

Directores: Dr Francisco Parra, Dr Kevin P. Dalton

Universidad de Oviedo

RESUMEN DEL CONTENIDO DE TESIS DOCTORAL

1.- Título de la Tesis	
Español/Otro Idioma: Análisis funcional y desarrollo de nuevas vacunas marcadas contra el Virus Mixoma	Inglés: *Functional analysis and development of novel marker vaccines against Myxoma virus*

2.- Autor	
Nombre: Inés Calonge Sanz	
Programa de Doctorado: Biología Molecular y Celular	
Órgano responsable: Centro Internacional de Posgrado	

RESUMEN (en español)

La mixomatosis, causada por el virus mixoma (MYXV) de la familia *Poxviridae,* causa una enfermedad severa en el conejo europeo que cursa con inmunodepresión, edema cefálico y anogenital, secreción ocular y nasal, y lesiones nodulares cutáneas llamadas mixomas. No hay un tratamiento específico para esta enfermedad, por ello las medidas profilácticas son cruciales para prevenir y reducir el contagio y transmisión del virus.

Las vacunas actuales utilizan cepas vivas atenuadas o el virus heterólogo del fibroma del conejo, y se administran de forma intradérmica o subcutánea. La respuesta inmune humoral a la vacunación varía considerablemente entre sujetos, e incluso algunos no sufren seroconversión. Además, la presencia de anticuerpos frente al virus mixoma no asegura una protección completa contra un posible contagio. La circulación sostenida del MYXV en la población de conejos silvestres provoca brotes epidémicos en las granjas cunícolas. Las infecciones asintomáticas a menudo pasan desapercibidas debido a que las cepas vacunales y virulentas de MYXV son antigénicamente indistinguibles por los ensayos actuales.

En esta tesis doctoral se propuso desarrollar una herramienta para controlar la enfermedad, basada en una vacuna DIVA, para lo cual se postuló la construcción de un virus mixoma recombinante marcado por deleción de un gen antigénico, además de una prueba serológica diferencial capaz de distinguir animales infectados de los vacunados.

Tras una exhaustiva revisión bibliográfica se seleccionaron 6 proteínas virales candidatas a tener carácter antigénico y a ser delecionadas: M022, M029, M71, M083, M115 y M141. Se procedió al diseño y clonaje de los genes codificantes seleccionadas en vectores de expresión. La producción de cada proteína se optimizó individualmente en los sistemas de expresión heteróloga considerados para ello: procariota y/o basado en la generación de baculovirus recombinantes. Las proteínas M022, M083 y M115 consiguieron purificarse en forma soluble. Mientras M083 no mostró carácter antigénico, las otras dos proteínas mostraron la presencia de epítopos lineales (M115) y conformacionales (M115 y M022).

Ambas proteínas se usaron como antígenos para desarrollar y optimizar protocolos independientes basados en la prueba de ELISA indirecto. Las pruebas iELISA-rM022 y iELISA-rM115 mostraron tener suficiente estabilidad, repetitividad, y un robusto poder discriminatorio en su validación. La potencia diagnóstica se evaluó mediante el análisis ROC, usando 259 sueros de conejo previamente categorizados por una prueba ELISA de referencia. iELISA-

rM022 mostró una sensibilidad diagnóstica del 90.97% y especificidad del 83.65%; mientras que para iELISA-rM15 fueron del 96.77% y 75%, respectivamente. Ambos ensayos mostraron buena sensibilidad en el diagnóstico serológico de muestras de liebre infectadas con ha-MYXV. La reactividad anti-M022 de los sueros mostró predecir perfectamente la supervivencia de conejos vacunados frente un posible contagio.

Los MYXV mutantes se construyeron por recombinación homóloga entre el genoma viral y vectores de transferencia, sustituyendo el gen diana (*m022l, m071 o m115)* por un gen marcador fluorescente. Se consiguió obtener mutantes sobre una cepa vacunal atenuada ΔM022 y ΔM115, pero no ΔM071, así como un mutante ΔM022 en el virus virulento Lu. Su caracterización *in vitro* mostró la viabilidad replicativa de los mutantes, pero una transmisión célula a célula muy limitada y menor producción de viriones extracelulares, mucho más agravada en el virus ΔM115. La falta de M022 supuso una mayor atenuación *in vitro* para Lu que para la cepa vacunal.

En conclusión, a falta de una completa caracterización del sistema DIVA, el mutante ΔM115 es prometedor; su eliminación aumenta la atenuación viral *in vitro* y podría usarse junto a iELISA-rM115, que tiene una elevada especificidad diagnóstica. Además, se propone el potencial uso de iELISA-rM022 para evaluar la protección desarrollada tras la vacunación.

RESUMEN (en Inglés)

Myxomatosis, caused by the myxoma virus (MYXV) from the Poxviridae family, causes a severe disease in the European rabbit, characterized by immunosuppression, facial and anogenital oedema, ocular and nasal discharge, and nodular skin lesions known as myxomas. There is no specific treatment for this disease, therefore prophylactic measures are crucial for preventing and reducing the spread and transmission of the virus.

Current vaccines use live attenuated strains, or the heterologous rabbit fibroma virus, and are administered intradermally or subcutaneously. The humoral immune response to vaccination varies significantly between individuals, with some not achieving seroconversion. Additionally, the presence of antibodies against myxoma virus does not guarantee complete protection against infection. The sustained circulation of MYXV in wild rabbit populations leads to epidemic outbreaks in rabbit farms. Asymptomatic infections often go unnoticed because the vaccine and virulent strains of MYXV are antigenically indistinguishable in current tests.

After an extensive literature review, six viral proteins were selected as candidates for antigenicity and potential deletion: M022, M029, M071, M083, M115, and M141. The genes coding for these proteins cloned into expression vectors. Each protein was individually optimized for production in the considered heterologous expression systems: prokaryotic and/or baculovirus expression vector systems. The M022, M083, and M115 proteins were successfully purified in soluble form. While M083 did not show antigenic properties, the other two proteins exhibited linear (M115) and conformational (M115 and M022) epitopes.

Both proteins were used as antigens to develop and optimize independent protocols based on indirect ELISA tests. The resulting iELISA-rM022 and iELISA-rM115 tests demonstrated good stability, repeatability, and robust discriminatory power during validation. Diagnostic performance was evaluated using ROC analysis on 259 rabbit sera previously categorized by a reference ELISA test. iELISA-rM022 showed a diagnostic sensitivity of 90.97% and specificity of 83.65%, while iELISA-rM115 exhibited a sensitivity of 96.77% and specificity of 75%. Both assays showed good sensitivity in diagnosing serological samples from hares infected with ha-MYXV. Anti-M022 reactivity in sera perfectly predicted the survival of vaccinated rabbits upon

Universidad de Oviedo

exposure to the virus.

MYXV mutants were constructed through homologous recombination between the viral genome and transfer vectors, replacing the target gene (m022l, m071, or m115) with a fluorescent marker gene. Mutants were successfully obtained in an attenuated vaccine strain for ΔM022 and ΔM115, but not ΔM071, as well as a ΔM022 mutant in the virulent Lu strain. In vitro characterization showed the replicative viability of the mutants, but with significantly limited cell-to-cell transmission and reduced extracellular virion production, especially in the ΔM115 virus. The absence of M022 resulted in greater attenuation in vitro for Lu compared to the vaccine strain.

In conclusion, despite not fully characterizing the DIVA system, the ΔM115 mutant appears promising; its deletion increases viral attenuation *in vitro* and could be used alongside iELISA-rM115, which has high diagnostic specificity. Additionally, the potential use of iELISA-rM022 is proposed to evaluate the protective immunity developed after vaccination.

SR. PRESIDENTE DE LA COMISIÓN ACADÉMICA DEL PROGRAMA DE DOCTORADO EN BIOLOGÍA MOLECULAR Y CELULAR

Universidad de Oviedo

Programa de Doctorado en Biología Molecular y Celular

Functional analysis and development of novel marked vaccines against Myxoma virus,

Análisis funcional y Desarrollo de nuevas vacunas marcadas contra el virus mixoma

Memoria presentada por **Inés Calonge Sanz** para optar al grado de Doctora por la Universidad de Oviedo.

Trabajo realizado en el Departamento de Bioquímica y Biología Molecular de la Universidad de Oviedo e Instituto Universitario de Biotecnología de Asturias.

Directores:

Dr. Francisco Parra y **Dr. Kevin P. Dalton**

Oviedo, 2024

Universidad de Oviedo
Universidá d'Uviéu
University of Oviedo

INSTITUTO UNIVERSITARIO DE BIOTECNOLOGÍA DE ASTURIAS

The completion of this research work was possible thanks to the financial support provided by the State Research Agency from the Ministry of Science, Innovation and Universities of the Spanish Government, within the framework of the AGL2017-83395-R research project grant, and the PRE2018-087157 grant for predoctoral contracts for doctoral training.

La realización de este trabajo de investigación ha sido posible gracias a la ayuda económica proporcionada por la ayuda AGL2017-83395-R concedida por la Agencia Estatal de Investigación del Ministerio de Ciencia, Innovación y Universidades del Gobierno de España; así como la ayuda PRE2018-087157 para contratos predoctorales para la formación de doctores.

A mamá, papá,
Óscar y Alba, simplemente
por ser parte de mi vida,

y a Artur, por su apoyo incondicional
y por ayudarme a sacar fuerzas en los
momentos más complicados

RESUMEN

La mixomatosis, causada por el virus mixoma (MYXV) de la familia Poxviridae, produce una enfermedad severa en el conejo europeo que cursa con inmunodepresión, edema cefálico y anogenital, secreción ocular y nasal, y lesiones nodulares cutáneas llamadas mixomas. No hay un tratamiento específico para esta enfermedad, por ello las medidas profilácticas son cruciales para prevenir y reducir el contagio y transmisión del virus.

Las vacunas actuales utilizan cepas vivas atenuadas o el virus heterólogo del fibroma del conejo, y se administran de forma intradérmica o subcutánea. La respuesta inmune humoral a la vacunación varía considerablemente entre sujetos, e incluso algunos no sufren seroconversión. Además, la presencia de anticuerpos frente al virus mixoma no asegura una protección completa contra un posible contagio. La circulación sostenida del MYXV en la población de conejos silvestres provoca brotes epidémicos en las granjas cunícolas. Las infecciones asintomáticas a menudo pasan desapercibidas debido a que las cepas vacunales y virulentas de MYXV son antigénicamente indistinguibles por los ensayos actuales.

En esta tesis doctoral se propuso desarrollar una herramienta para controlar la enfermedad, basada en una vacuna DIVA, para lo cual se postuló la construcción de un virus mixoma recombinante marcado por deleción de un gen antigénico, además de una prueba serológica diferencial capaz de distinguir animales infectados de los vacunados.

Tras una exhaustiva revisión bibliográfica se seleccionaron 6 proteínas virales candidatas a tener carácter antigénico y a ser delecionadas: M022, M029, M71, M083, M115 y M141. Se procedió al diseño y clonaje de los genes codificantes seleccionadas en vectores de expresión. La producción de cada proteína se optimizó individualmente en los sistemas de expresión heteróloga considerados para ello: procariota y/o basado en la generación de baculovirus recombinantes. Las proteínas M022, M083 y M115 consiguieron purificarse en forma soluble. Mientras M083 no mostró carácter antigénico, las otras dos proteínas mostraron la presencia de epítopos lineales (M115) y conformacionales (M115 y M022).

Ambas proteínas se usaron como antígenos para desarrollar y optimizar protocolos independientes basados en la prueba de ELISA indirecto. Las pruebas iELISA-rM022 y iELISA-rM115 mostraron tener suficiente estabilidad, repetitividad, y un robusto poder discriminatorio en su validación. La potencia diagnóstica se evaluó mediante el análisis ROC, usando 259 sueros de conejo previamente categorizados por una prueba ELISA de referencia. iELISA-rM022 mostró una sensibilidad diagnóstica del 90.97% y especificidad del 83.65%; mientras que para iELISA-rM15 fueron del 96.77% y 75%, respectivamente. Ambos ensayos mostraron buena sensibilidad en el diagnóstico serológico de muestras de liebre infectadas con ha-MYXV. La reactividad anti-M022 de los sueros mostró predecir perfectamente la supervivencia de conejos vacunados frente un posible contagio.

Los MYXV mutantes se construyeron por recombinación homóloga entre el genoma viral y vectores de transferencia, sustituyendo el gen diana (m022l, m071 o m115) por un gen marcador fluorescente. Se consiguió obtener mutantes sobre una cepa vacunal atenuada ΔM022 y ΔM115, pero no ΔM071, así como un mutante ΔM022 en el virus virulento Lu. Su

caracterización *in vitro* mostró la viabilidad replicativa de los mutantes, pero una transmisión célula a célula muy limitada y menor producción de viriones extracelulares, mucho más agravada en el virus ΔM115. La falta de M022 supuso una mayor atenuación *in vitro* para Lu que para la cepa vacunal.

En conclusión, a falta de una completa caracterización del sistema DIVA, el mutante ΔM115 es prometedor; su eliminación aumenta la atenuación viral *in vitro* y podría usarse junto a la prueba iELISA-rM115, que tiene una elevada especificidad diagnóstica. Además, se propone el potencial uso de iELISA-rM022 para evaluar la protección desarrollada tras la vacunación.

ABSTRACT

Myxomatosis, caused by the myxoma virus (MYXV) from the Poxviridae family, causes a severe disease in the European rabbit, characterized by immunosuppression, facial and anogenital oedema, ocular and nasal discharge, and nodular skin lesions known as myxomas. There is no specific treatment for this disease, therefore prophylactic measures are crucial for preventing and reducing the spread and transmission of the virus.

Current vaccines use live attenuated strains, or the heterologous rabbit fibroma virus, and are administered intradermally or subcutaneously. The humoral immune response to vaccination varies significantly between individuals, with some not achieving seroconversion. Additionally, the presence of antibodies against myxoma virus does not guarantee complete protection against infection. The sustained circulation of MYXV in wild rabbit populations leads to epidemic outbreaks in rabbit farms. Asymptomatic infections often go unnoticed because the vaccine and virulent strains of MYXV are antigenically indistinguishable in current tests.

After an extensive literature review, six viral proteins were selected as candidates for antigenicity and potential deletion: M022, M029, M071, M083, M115, and M141. The genes coding for these proteins cloned into expression vectors. Each protein was individually optimized for production in the considered heterologous expression systems: prokaryotic and/or baculovirus expression vector systems. The M022, M083, and M115 proteins were successfully purified in soluble form. While M083 did not show antigenic properties, the other two proteins exhibited linear (M115) and conformational (M115 and M022) epitopes.

Both proteins were used as antigens to develop and optimize independent protocols based on indirect ELISA tests. The resulting iELISA-rM022 and iELISA-rM115 tests demonstrated good stability, repeatability, and robust discriminatory power during validation. Diagnostic performance was evaluated using ROC analysis on 259 rabbit sera previously categorized by a reference ELISA test. iELISA-rM022 showed a diagnostic sensitivity of 90.97% and specificity of 83.65%, while iELISA-rM115 exhibited a sensitivity of 96.77% and specificity of 75%. Both assays showed good sensitivity in diagnosing serological samples from hares infected with ha-MYXV. Anti-M022 reactivity in sera perfectly predicted the survival of vaccinated rabbits upon exposure to the virus.

MYXV mutants were constructed through homologous recombination between the viral genome and transfer vectors, replacing the target gene (m022l, m071, or m115) with a fluorescent marker gene. Mutants were successfully obtained in an attenuated vaccine strain for ΔM022 and ΔM115, but not ΔM071, as well as a ΔM022 mutant in the virulent Lu strain. In vitro characterization showed the replicative viability of the mutants, but with significantly limited cell-to-cell transmission and reduced extracellular virion production, especially in the ΔM115 virus. The absence of M022 resulted in greater attenuation in vitro for Lu compared to the vaccine strain.

In conclusion, despite not fully characterizing the DIVA system, the ΔM115 mutant appears promising; its deletion increases viral attenuation in vitro and could be used alongside iELISA-

rM115, which has high diagnostic specificity. Additionally, the potential use of iELISA-rM022 is proposed to evaluate the protective immunity developed after vaccination.

LIST OF FIGURES

LIST OF TABLES

ABBREVIATIONS

Ab- Antibody

BEVS- baculovirus expression vector system

CB- checkerboard/chessboard titration

cELISA- competitive ELISA

CEV- cell-associated enveloped virus

CMV- cytomegalovirus

CV (%)- coefficient of variability

DIVA- Differentiation of infected from vaccinated animals

DMEM- Dulbecco's Modified Eagle Medium

DSe or Se- Sensibility

DSp or Sp- Specificity

EEV- extracellular enveloped virus

EFC- entry-fusion complex

ELISA- Enzyme linked immunosorbent assay

ER- endoplasmic reticulum

FBS- Fetal bovine serum

FFU/ml- Foci forming units/milliliter

FIBV- Hare fibroma virus

FN- False negative

FP- False positive

GSH- gluthation

GST- glutathione S-transferase

GTPV- Goatpox virus

HRP- horseradish peroxidase

ID- intradermal

iELISA- indirect ELISA

IEV- intracellular enveloped virus

IF- immunofluorescence

IM- intramuscular

IMAC- Immobilized metal affinity chromatography

IMV- intracellular mature virus

IPTG- isopropyl β-D-1-thiogalactopyranoside

IUCN- International Union for Conservation of Nature

IV- immature virus

Kb- kilobase

LB-Luria Bertani culture medium

LR (+ or -)- likelihood ratio for a positive (+) or negative (-) result

LSDV- Lumpy skin disease virus

MCS- multiple cloning site

MEM- Eagle's minimum essential medium

MHC-II – Multi histocompatibility complex II

MOI- Multiplicity of infection

MYXV- myxoma virus

NC- negative control

NPV- negative predictive value

NusA- N-utilization substance A

OD- optical density

ORF- Open reading frame

PBST- phosphate buffer

PC- positive control

PF- insoluble fraction, pellet

PPV- positive predictive value

PTM- Post-translational modifications

rBV- recombinant baculovirus

RFLP- Restriction fragment length polymorphism

RFV- Rabbit fibroma virus

RHDV- rabbit hemorrhagic disease virus

ROC- Receiver operating characteristic

SC- subcutaneous

SCT- Scientific-Technical service

SD- standard deviation

SDS-PAGE: sodium dodecyl sulfate–polyacrylamide gel electrophoresis

SEM-standard error of the mean

SF- soluble fraction

SPPV- Sheeppox virus

SQFV- Squirrel fibroma virus

TEM- Transmission electron microscopy

TGN- trans-Golgi network

TIR- Terminal inverted repeats

TK- thymidine kinase

TMB- 3,3’,5,5’-Tetramethylbenzidine

TN- True negative

TP- True positive

VACV- Vaccinia virus

VarV- Variola virus

β-ME- β-mercaptoethanol

CONTENT

CHAPTER 1: INTRODUCTION

THE EUROPEAN RABBIT (*ORYCTOLAGUS CUNICULUS*)

Phylogeny and genetic diversity

The European rabbit (*Oryctolagus cuniculus*) is a Lagomorph classified within the genus *Oryctolagus*. The earliest fossil records of this species, dating back approximately 0.6 million years, were unearthed in southern Spain. These findings, in conjunction with fossil records of other ancestors, suggest that the Iberian Peninsula is likely the region of origin for the European rabbit (Lopez-Martinez, 2008). There are two distinct subspecies that diverged approximately 2 million years ago and have evolved independently: *Oryctolagus cuniculus cuniculus* and *Oryctolagus cuniculus algirus* (Biju-Duval et al., 1991). They show a highly discontinuous geographical distribution, while *O. c. algirus* population is distributed throughout the southwestern region of the Iberian Peninsula, the Canary Islands, the Azores, and Madeira; *O. c. cuniculus* occupies a broader geographical territory, including the remaining portion of the Iberian Peninsula, additional continental European regions, northern Africa, and numerous overseas islands, such as the Balearic Islands and Great Britain (Ferrand & Branco, 2007). They exclusively coexist within a geographic belt spanning the Iberian Peninsula from northwest to southeast, where natural hybridization events between them also take place (Branco et al., 2000)

Habitat, geographic distribution and expansion

The European rabbit is highly adapted to its native ecosystem and the Mediterranean climate, characterized by mild winters and dry summers, and plays a major role in modulating the landscape due to burrowing, foraging and seed dispersal. It relies on a habitat primarily consisting of a combination of scrubland, with sufficient vegetation cover to provide protection against predators, and grasslands that supply it with food. Despite exhibiting some preference for specific forage plants, they can adapt their diet to the plant species available in each habitat and season (Gálvez-Bravo, 2017). Following a diverse and flexible herbivorous diet, allows them to thrive in diverse habitats.

The European rabbit, unlike other leporid species, is prolific and easily manageable in captivity, facilitating its integration into agricultural practices. In fact, rabbits have been significant to human societies for over six millennia, valued for their meat, skin and bones. Historically, humanity introduced rabbits in practically all the lands and newly established settlements (Fox, 1994). Today, the European rabbit is globally distributed in all continents except Antarctica and

is thriving on over 800 islands worldwide (Flux & Fullagar, 1992). The absence of competing species, the scarcity of pathogens, and the lack of natural predators, combined with its prolific reproductive capacity and flexibility in food selection, have all contributed to the expansion and proliferation of rabbit populations in new habitats (reviewed by Naff & Craig, 2012).

The deliberate or accidental introduction of an invasive species into any ecosystem generates a threat to its biodiversity and can severely disrupt the established interactions among native species over time (Zavaleta et al., 2001) In fact, the European rabbit assumes an aggressive role as invasive species, causing significant and destructive role within ecosystems. The exponential surge in the European rabbit population in Australia following its introduction in 1859 sparked a dire situation within native ecosystems. In just 50 years since the release of the initial 13 European rabbit specimens, they managed to completely colonize the continent.

Population dynamics

The population of wild European rabbits in their natural habitat, the Iberian Peninsula, has dramatically declined over the years. It is estimated that the current rabbit population comprises only 5% of what it was 50 years ago. The last assessment of the International Union for Conservation of Nature (IUCN) classified the *O. cuniculus* as a globally threatened species (Lees & Bell, 2008; Villafuerte & Delibes-Mateos, 2019). The emergence of two highly lethal viral diseases, myxomatosis and rabbit hemorrhagic disease (RHD), in the second half of the 20th century (the 1950s and 1980s, respectively) largely contributed to this European rabbit's population loss (Moreno & Villafuerte, 1995; D. Ward, 2005).

The causative agent of myxomatosis which caused devastating losses in the European rabbit population is the subject of this thesis and will be discussed in detail in section 2 of this Introduction. The arrival of Rabbit haemorrhagic disease virus (RHDV) to Europe in the 1980s caused further reductions in the rabbit population density, already affected by several years of myxomatosis outbreaks. This calicivirus was described for the first time in the People's Republic of China, in 1984, and was rapidly dispersed across Asia and Europe (Liu et al., 1984). It is a highly species-specific pathogen with high level of virulence. RHD is characterized by a rapid onset and progression of symptoms such as fever, lethargy, respiratory distress, and bleeding due to internal haemorrhaging (Z. J. Xu & Chen, 1989). It also causes massive hepatic necrosis and alveolar oedema. Mortality rates can be as high as 70-100%, and since there is no treatment, vaccination is the most important prevention measure (F. Fenner, 2010).

The drastic decline of rabbit population from parts of their native Mediterranean ecosystem in the 20th century constituted a major threat for the conservation of Iberian ecosystems and hunting activity (Moreno et al., 2004). In response to that, from the 1980s restocking rabbit populations became a common management practice in Spain, primarily aimed at enhancing game populations within hunting reserves (92%) by translocating wild rabbits form areas with high population densities to regions where populations were sparse or nearly extinct (Calvete et al., 1997). Due to the large number of rabbits involved in each translocation, and the lack of consideration for their origin genetic lineage prior to introduction, the two genetic lineages of *O. cuniculus* (*O. c. algirus* and *O. c. cuniculus*) were often intermixed (Delibes-Mateos et al., 2008).

Rabbit translocations were not successful despite the efforts and the economic investment associated with the process (Cabezas et al., 2007, 2011). The possible transmission of new disease agents into the release area is of high concern, since myxomatosis and RHD diseases have a major impact on native populations.

Ecologic and economic relevance of the European rabbit

O. cuniculus plays a crucial role in the Iberian ecosystem. Over 40 species rely on rabbits, including two endemic and highly endangered apex predators: the Iberian lynx (*Lynx pardinus*) and the Spanish imperial eagle (*Aquila adalberti*) (Delibes-Mateos et al., 2007; Monterroso et al., 2016). Both species rely heavily on this prey, with the rabbit accounting for more than 88% of their diet in both cases (Ferrer & Negro, 2003). A decline in rabbit populations has negatively impacted these apex predators, and consequently, to other trophic interactions of the ecosystem. Regions with higher rabbit densities are positively correlated with greater diversity of raptor species as well as a higher number of individuals (Delibes-Mateos et al., 2007). The recovery of rabbit abundance is also associated with a higher reproductive rate in the Iberian lynx and Spanish imperial eagle populations, and at the same time, the recovery of apex predator populations contributes to the restoration of the relationships that form the structure of the native ecosystem (Monterroso et al., 2016).

The European rabbit is also a major small game species hunted throughout the Iberian Peninsula. Approximately 5.9 million wild rabbits are harvested each year in Spain (FECAZA, 2019). Additionally, the European rabbit is valued for its economic relevance in the meat industry and is a precious hunting game. The consumption of rabbit meat and its trade dates to the Phoenician civilization around 1100 B.C. and remains integral to some Mediterranean countries. The rabbit is the second most-produced species in the EU in terms of numbers.

Currently, in Spain, there are approximately 1439 farms classified as rabbit production, with the majority located in Catalonia, Andalusia, and Castilla-La Manch (*INFORME TRIMESTRAL INDICADORES DEL SECTOR CUNÍCOLA" Subdirección General de Producciones Ganaderas y Cinegéticas, Dirección General de Producciones y Mercados Agrarios).* Rabbit farming offers several advantages compared to other animals: rabbits have a short life cycle and highly prolific reproductive capacity, reaching sexual maturity at an early age (between 9-10 weeks of age), and its gestation period is only 31 days on average. Additionally, rabbit farming can be regarded as a meat production industry that is both economically and ecologically more sustainable than many other livestock sectors as rabbits are highly efficient, capable of converting up to 20% of the protein consumed in their diet into muscle mass (Cesari et al., 2018).

Rabbit meat consumption is experiencing a drastic decline on the European level year after year, even in countries where rabbit meat is a part of their traditional culinary culture, including Spain. In fact, rabbit meat consumption in Spanish households in 2023 during the January-November period dropped by 13.8% compared to the same period the previous year, with a consumption per capita in 2023 of 647 grams (Subdirección General de Producciones Ganaderas y Cinegéticas & Dirección general de producciones y mercados agrarios, 2024) .When it comes to trade in the Spanish rabbit farming sector, exports hold significant economic importance. In the first two months of 2024, Spain exported more than 1200 tons of rabbit meat, resulting in an economic gain exceeding 5.5 million euros.

MYXOMATOSIS

Introduction to the history of myxomatosis

The disease was first described by Professor Giuseppe Sanarelli in domestic European rabbits used for antibody production at the Institute of Hygiene in Montevideo, Uruguay, in 1896 (F. Fenner & Ratcliffe, 1965). The causative agent, called myxoma virus (MYXV) was an endemic virus whose natural host was the South American tapeti *Sylvilagus brasiliensis*, also known as the forest rabbit (Aragão, 1927). In its natural hosts, MYXV infection causes a nonpathogenic condition with benign cutaneous fibromas that persist for several weeks, during which the virus can be mechanically transmitted from one animal to another through the intervention of blood-feeding arthropods. Several species of the genus *Sylvilagus* are susceptible to infection by this virus, developing similar lesions and exhibiting a mild clinical presentation.

In contrast to its natural host, the mortality rate of this disease in European rabbits was initially as high as 99.5%. As early as 1919, well before the identification of the infectious agent

responsible for myxomatosis, Dr. Aragaõ suggested the use of this disease to control the invasive European rabbit population in various territories, including Australia. At that time, the uncontrolled growth of the rabbit population had become a significant ecological, agricultural, and economic issue for the country. Therefore, after numerous unsuccessful attempts to control their population through physical measures such as destroying their burrows and building fences, or the use of poison, the government decided that myxomatosis could be an effective means of population control.

The release of this infectious agent in 1950 in areas near the Murray River in Australia, a humid area with an abundant mosquito population, led to a massive spread of the disease throughout the continent. The implementation of periodic reinoculation programs succeeded in eradicating more than 80% of the rabbit population. (F. Fenner, 2010; F. Fenner & Ratcliffe, 1965).

Shortly after this, myxomatosis (MYXV strain Lausanne, Lu-MYXV) was illicitly introduced into Europe in 1952, rapidly spreading from France to other European countries, ranging from Austria to Spain. Over time, more virulent viral strains gave way to attenuated ones that allowed infected animals to survive for longer durations, thus increasing their opportunities for replication and dispersal. Simultaneously, the selective pressure of the new pathogen led to gradual natural selection in the rabbit population, favoring individuals genetically more resistant to infection (F. Fenner & Ratcliffe, 1965). This coevolution between the pathogen and its host, occurring simultaneously in Australia and Europe, resulted in a reduction in mortality caused by myxomatosis from 99% to 30% just a few years after the infectious agent was introduced into these regions (Spiesschaert et al., 2011). Currently, myxomatosis is an endemic disease in the European rabbit population.

Clinical signs of myxomatosis

Infection by MYXV in its natural host, members of the *Silvilagus* species, only results in a benign infection characterized by the localized formation of a cutaneous lesion restricted to the site of inoculation, although young rabbits are more susceptible to get a generalized disease by MYXV infection, with higher morbidity. The cutaneous fibroma typically emerges around the 4th day post-infection and can persist for up to 40 days. MYXV infection in European rabbits leads to a systemic infection with a high mortality rate (F. Fenner & Ratcliffe, 1965; P. J. Kerr, 2020). However, not all myxoma viruses are lethal to European rabbits. After years of coevolution between the pathogen and the host, owing to their close and continuous interaction both in Europe and Australia, naturally attenuated strains have arisen with lower morbidity and mortality rates (Best & Kerr, 2000; P. J. Kerr et al., 2017; Saint et al., 2001).

The specific clinical signs produced by European rabbit infection with MYXV are variable and depend on the viral strain and the route of inoculation (Best et al., 2000; Chapple & Muirhead-Thomson, 1964). Additionally, the rabbit's individual characteristics, such as its nutritional status, age, immunological state, and potential innate resistance, are variables that can influence the severity of signs following MYXV infection (P. J. Kerr & Best, 1998).

The typical presentation of myxomatosis is known as the nodular form and is a dermatropic form characterized by myxomatous skin lesions. Infected rabbits can have a rapid course of the disease with septicemia and death or manifest a subacute or chronic form of clinical myxomatosis. In this clinical picture, the primary lesion undergoes progressive enlargement, erythema, and thickening over time, and concurrently, edema and inflammation manifest in the eyelids, base of the ears, and the anogenital region. Subsequently, secondary cutaneous macules develop throughout the body, with a predilection for the cranial region and the base of the ears, exhibiting progressive enlargement (F. Fenner & Woodroofe, 1953). Within these epidermal lesions, referred to as myxomas, MYXV concentrates and accumulates, establishing them as the primary infectious loci within the afflicted animal. It is imperative, however, for the virus to attain a density of 10^7 ID_{50}/g to facilitate efficient MYXV transmission via vectors (F. Fenner et al., 1956).

In the context of infections induced by virulent strains, rabbits frequently exhibit edema of the eyelids, mucopurulent blepharoconjunctivitis and nasal secretions approximately one-week post-infection. This, coupled with the associated inflammation, induces severe respiratory distress and results in the inability of the animals to open their eyes. Edema of the perineal region and the external genitalia are also frequently seen in the most virulent strains, together with the presence of lumps and myxomas overall the rabbit’s body, but foremost the head and ears. Virulent infections often lead to the hosts’ death within a span of 10-13 days post-inoculation (F. Fenner & Marshall, 1957). Animals infected with attenuated strains undergo a disease progression analogous to that shown by virulent strains, albeit characterized by a slower and more gradual temporal development. Surviving animals eventually transition from myxomatous lesions to a scab that seals the nodular lesion (Rivers, 1930).

There is a second presentation of the disease characterized by a lower number and smaller size of cutaneous myxomatous lesions but maintaining its immunosuppressive potential. It is also presented with inflammation of the head and base of the ears, perineal edema, blepharoconjunctivitis, serous or purulent rhinitis, and respiratory distress. Even though the amyxomatous form of disease has been detected in wild rabbits, it is typically more frequent to

affect farmed rabbits and cause outbreaks in industrial farms. In this case, the absence of cutaneous lesions reduces the relevance of vectors in the viral transmission process, which predominantly occurs through direct contact between an infected and a healthy rabbit (Joubert et al., 1982; Marlier et al., 1999).

Due to the general depression of the immune system (Jeklova et al., 2008a), rabbits infected with MYXV are susceptible to secondary infections by gram-negative bacteria (e.g., *Pasteurella multocida*, *Bordetella bronchiseptica*), especially in the conjunctiva and the respiratory system, which worsen the animals' health. These opportunistic infections appear to contribute to increased virulence during infections caused by attenuated MYXV strains or amyxomatous strains. Sick rabbits that survive for an extended time often develop bacterial pneumonia (Marlier et al., 1999). In contrast, rabbits infected with virulent MYXV strains that experience more severe disease may die without developing signs of coinfection (F. Fenner & Ratcliffe, 1965).

Pathogenesis

Following intradermal inoculation of MYXV, the virus initially replicates in MHC-II (+) dendritic-like cells at the epidermis-dermis junction. From there, it spreads to epidermal cells and various cell types within the dermis at the inoculation site. The primary lesion forms as a result of the proliferation, hyperplasia, and hypertrophy of epidermal cells, coupled with the disruption of the dermis, leading to fluid accumulation and an edematous appearance. During this initial stage, the virus can also infect endothelial cells of capillaries, which, upon rupture, may cause red blood cells to leak into the surrounding tissues (Best et al., 2000).

Approximately 24 hours post-inoculation, MYXV is detected in the draining lymph node, where it multiplies to high viral titers (> 10^8 pfu/g). Viral replication of virulent strains in lymphoid tissue significantly reduces the number of lymphocytes by inducing widespread apoptosis in lymphocytes adjacent to productively infected cells (bystander apoptosis), even during later stages of infection when MYXV-infected cells are no longer detectable in the node. Additionally, reticular cells proliferate, obliterating the sinuses of the node, and polymorphic cell recruitment occurs. Initially, these pathological events are observed mainly in the T cell zones, but as the infection progresses, they also occur in the paracortical area and the germinal centers of the follicles (Best & Kerr, 2000).

In wild rabbits, which exhibit greater resistance to the virus, infection with virulent MYXV strains presents histopathological characteristics ranging from relatively normal lymphoid tissue to

conditions like those observed in laboratory rabbits susceptible to MYXV. Infections with attenuated strains do not show lymphocyte depletion, as lymphocyte loss due to apoptosis is compensated by lymphocyte influx into the lymph node and cell proliferation associated with the immune response, in both wild and laboratory rabbits. Additionally, there is a lower concentration of polymorphic cells, and the animals are able to eliminate the virus within 2 days (wild rabbits) and 20 days (laboratory/susceptible rabbits) post-infection. (Best et al., 2000).

Subsequently, the virus associates with lymphocytes and other cellular elements in the circulatory system, spreading to additional lymph nodes and distal lymphoid tissues, as well as organs such as the lungs, spleen, and testicles, and mucocutaneous regions like the nasal, anogenital mucosa, conjunctiva, and skin (Fenner & Ratcliffe, 1965). However, viral replication in these tissues does not play a determinative role in the acute death of infected animals (Mims, 1964). MYXV can be detected in MHC-II positive cells in distal regions of the dermis from 4 days post-infection, where polymorphic inflammatory cells also accumulate. Later, the virus infects epidermal cells, causing pathological changes similar to those observed at the primary inoculation site (Best et al., 2000) (Figure 1).

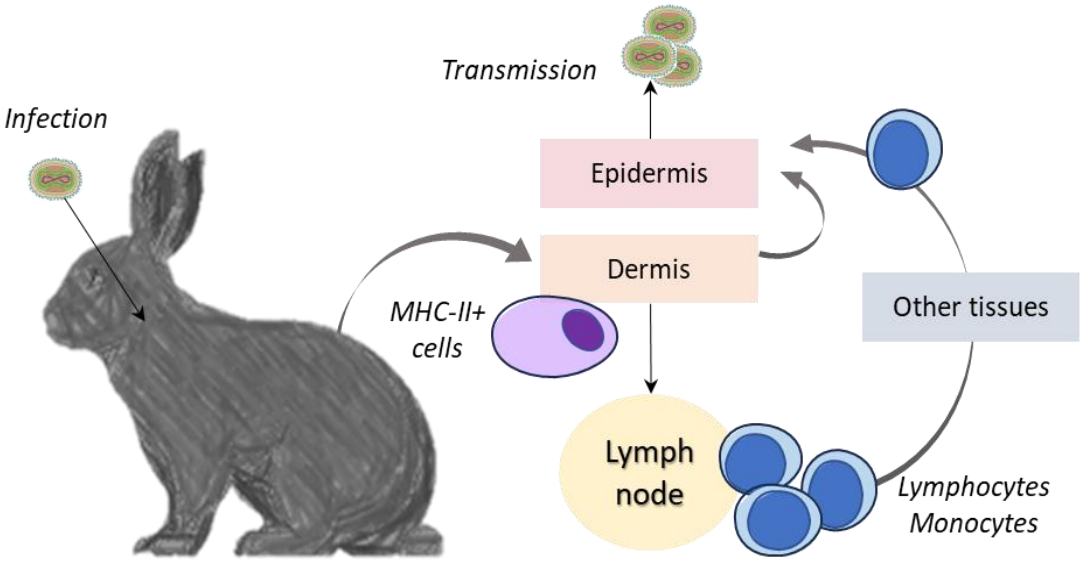

Figure 1. Pathogenesis of MYXV in *O. cuniculus*

The virus is inoculated intradermally by hematophagous arthropods, and MYXV replicates in MHC-II positive dendritic-like cells in the dermis. MYXV replicates within lymphocytes of the paracortex and other cells, in the lymph node draining the inoculation site only within 24 h of inoculation. The virus spreads to other lymphoid tissues, lungs, testes, and skin. After several days, the epithelial lesions and mucocutaneous sites become packed with viruses and become critical sites for transmission by vectors. *Figure based on Kerr and McFadden, 2002.*

Male rabbits exhibit severe pathological effects in their testes following infection even with attenuated strains of MYXV. High viral titers are detected in testes, which can persist for extended periods; even after the virus is cleared, viral DNA is detectable for several months. MYXV infection triggers an influx of inflammatory cells, leading to conditions such as interstitial orchitis and epididymitis, associated with the degeneration of the seminiferous epithelium and disruptions in both steroidogenesis and spermatogenesis. Consequently, the male rabbits experience temporary infertility (Fountain et al., 1997).

Animals that survive the infection with a virulent MYXV strain and have recovered from myxomatosis show high titers of anti-MYXV antibodies higher than those of vaccinated rabbits or, and rabbits infected with more attenuated strains (Fenner et al., 1953). IgMs can be detected at 5-6 days post-infection, often corresponding with the onset of clinical signs, and they persist during the acute phase and recovery phases of the infection. The levels of IgGs peak at around 30 days post-infection and remain at high levels over the next month (P. J. Kerr, 1997). IgG antibodies are passively transferred from does to kittens across the placenta and remain detectable for seven weeks after birth (F. Fenner & Marshall, 1954).

Circulating neutralizing antibodies in their serum are detectable for an extended period and in contrast, the complement-fixing antibody titer falls during the following months and remains steady at moderate titers (P. J. Kerr, 1997). Rabbits that survive the infection have a generalized resistance to subsequent disease; inoculation of such rabbits with a challenge dose of myxoma virus may produce a slight reaction in some cases, and a local lesion at the inoculation site. In this case, the titer of complement-fixing antibody rises. Meanwhile, sera from rabbits vaccinated with fibroma virus (RFV) failed to neutralize myxoma virus before the viral inoculation but reached high titers after the challenge (F. Fenner et al., 1953). Although it may seem that neutralising antibodies might play a relevant role in the acquisition of lifelong immunity to the disease, further investigations have shown that they are not significant, and that resistance would be achieved by the development of an effective cellular immune response (Best & Kerr, 2000).

ETHIOLOGY: MYXOMA VIRUS

Taxonomy

Myxoma virus is the etiologic agent that causes myxomatosis in the European rabbit. It is a member of the family *Poxviridae,* subfamily *Chordopoxvirinae* and genus *Leporipoxvirus.* Members of the *Poxviridae* family are large, enveloped, DNA viruses infecting a wide range of animals, from vertebrate to invertebrate species. Their genome is organized in a linear dsDNA molecule, of 130 to 375 kb long with terminal inverted repeats (TIR) and covalently closed hairpin termini (Geshelin & Berns, 1974). Their large genomes encode hundreds of proteins that include their own RNA and DNA polymerases, transcription factors, etc. in addition to host modulatory factors. Unlike other DNA viruses that must reach the nucleus to replicate, poxviruses are nucleocytoplasmic, and their genome replication occurs in the cytoplasm of the host cell.

The most notorious virus species belonging to the Poxviridae family is Variola virus (VarV), the causative agent of smallpox, a highly contagious and deadly disease, responsible for more deaths throughout history than any other infectious disease. The smallpox vaccine created and popularized in 1796 by Edward Jenner, was the first successful vaccine developed in history, based on using cowpox virus to induce cross-immunity against VarV. Smallpox was the first disease to be officially eradicated, after an intensive global eradication program started in the lates 1960s consisting of strict vaccination campaigns. This historic achievement in global public health was certified by the World Health Assembly in 1980.

The International Committee on Taxonomy of Viruses recognizes four species belonging to the *Leporipoxvirus* genus: Hare fibroma virus (FIBV), Squirrel fibroma virus (SQFV), Rabbit fibroma virus (RFV) also known as Shope fibroma virus, and Myxoma virus (MYXV) (F. Fenner & Ratcliffe, 1965) (Table 1). SQFV and FIBV are the less studied and characterized members of the Leporipoxvirus genus. SQFV was identified in 1936 and is specific to gray squirrels in the U.S. therefore its relevance is reduced to veterinarians and wildlife managers (Kilham et al., 1953; King et al., 1972). FIBV was discovered in the European hare in 1959, becoming the only member naturally occurring outside the Americas. There is evidence suggesting that FIBV may also affect African hares (Karstad et al., 1977).

Table 1. Disease features of leporipoxviruses

AGENT	*DISEASE*	*HOST*	*DESCRIPTION*	*VECTOR*	*LOCALIZATION*
MYXV	Myxomatosis	European rabbit (O. *cuniculus*)	Lethal, multiple skin lesions; systemic affection, collapse of immune system	Mosquito, flea	America, Europe, Oceania
	Fibroma	Tapeti (*S. brasiliensis*), brush rabbit (*S. bachmani*)	Localized cutaneous fibroma, only harmful in very young individuals	Mosquito	America
ha-MYXV	Hare myxomatosis	Iberian hare (*L. granatensis*)	Lethal, multiple skin lesions; systemic affection, collapse of immune system	Mosquito, flea	Europe
RFV/SFV	Rabbit fibroma	Eastern cottontail rabbit (*S. floridanus*)	Cutaneous fibroma, persists for months	Mosquito, flea	North America
SQFV	Squirrel fibroma	Eastern and Californian gray squirrel (*Sciurus* spp.)	Single or multiple cutaneous fibromas	Mosquito, flea	North America
FIBV	Hare fibroma	European hare (*Lepus europaeus*), African hare (*L. capenus*)	Solitary or multiple dermal tumors	Insects	Europe, Africa

[a] Adapted from Mercer et al., 2007.

RFV (also termed SFV in the literature) was identified to be the cause of fibroxanthosarcoma-like tumors in the eastern cottontail rabbit (*Sylvilagus floridanus*) (Shope, 1932b). Although adult rabbits mount a cell-mediated immune response that effectively contributes to tumor regression 10 to 12 days after infection, newborn rabbits and immunocompromised adults can suffer a systemic and lethal disease (Sell & Scott, 1981; Shope, 1932a). RFV is closely related to MYXV, and both induce similar clinical signs in cottontail rabbits. But MYXV leads to a rapidly fatal and widespread infection in European rabbits, contrasting sharply with the benign fibromas induced by RFV that mirrors the signs induced in *S.floridanus* (Shope, 1932a).

Genome organization and gene expression

MYXV has a large and complex genome that is organized in a double-stranded DNA molecule. The complete genomic sequencing of the Lausanne reference strain revealed a 161.8 kb genome, with 11.5 kb in length TIRs and an A/T content of 56.4%. MYXV has an efficiently organized genome with genes aligned one after another, or even slightly overlapping in both directions, with in general, short intergenic regions. The absence of noncoding DNA in the TIRs contrasts to many other poxviruses that show significantly long regions of noncoding DNA within the terminal regions (e.g. 4 kb in Vaccinia virus Copenhagen strain) (Johnson et al., 1993).

The full-length MYXV genome contains a total of 171 open reading frames (ORFs), comprising 159 genes and 12 ORFs duplicated in the TIRs. Every ORF is assigned with a numerical nomenclature in increasing order from the left-end of the genome (from M0.005, M001 to M156), and with the alphabetical character L or R regarding the direction of their transcription, left or right, respectively (C. Cameron et al., 1999).

The central 120 kb of the genome, from M012L to M142R, contains most of the crucial genetic information: genes with putative housekeeping or structural functions highly conserved in all poxviruses. The genes located within this core region have an arrangement that is comparable to the order of genes in the Vaccinia virus (VACV) genome, indicating a degree of genomic structure conservation between poxviruses (Johnson et al., 1993). No myxoma homologs are found to several VACV ORFs (F5L, F6L, F11L, F14L, E11L, O2L, I4L, A25L, A26L, A31R, A36R, A39R–A49R, A53R, and A54L). Amongst them, the lack of MYXV gene homologs to most elements involved in nucleotides biosynthesis could indicate a higher dependency of MYXV to the host cell availability of dNTPs in viral replication. While still encoding a thymidine kinase enzyme (MYXV ORF M061R), MYXV lacks thymidylate kinase (VACV A48R) and a subunit of the ribonucleotide reductase (VV I4L) (Beaud, 1995; Cameron et al., 1999).

Despite their difference in virulence, MYXV and RFV genomes encode a nearly identical set of homologous genes, specifically in the central conserved core. Some ORFs have experienced rearrangements (M156R is duplicated and M009L is partially duplicated in RFV), complete (M000.5L/R) and partial deletions (M008.1L/R, M135R, M136R, M139R, M150R, M152R) in RFV (Cameron et al., 1999; Willer et al., 1999).

Meanwhile, genes presumably involved in immunomodulation or host range, that is, specific to Leporipoxviruses, are mainly located within the 15-25 kb at both terminal regions of the genome (C. Cameron et al., 1999). MYXV, like other poxvirus family members, has developed multiple strategies to disrupt the host antiviral responses. The proteins in these regions are mainly identified as viroreceptors, virokines, anti-apoptotic factors, immune modulators, and host range factors (Nash et al., 1999; Spiesschaert et al., 2011).

Viral genes are transcribed following a cascade mechanism of regulation, in three sequential stages: early, intermediate, and late (Broyles, 2003). Poxvirus promoters are also divided into the early, intermediate, and late temporal categories. These elements are well conserved among the leporipoxviruses, and MYXV consensus promoter sequences are very similar to those in RFV (Willer et al., 1999). The first transcribed and expressed proteins intervene in DNA synthesis (replication and nucleotide metabolism enzymes), whilst those involved in DNA processing and

packaging, and structural proteins are produced in intermediate or late times (Moss & Salzman, 1968).

The transcriptional system of poxviruses is formed by a complex of viral proteins and each stage depends on the activity of the multi-subunit viral RNA polymerase together with class-specific transcription factors (Z. Yang et al., 2011). The beginning and end of each stage is tightly regulated through transcriptional cascades and mRNAs turnovers (Pennington, 1974). In addition, poxviruses encode two conserved mRNA-decapping enzymes that play a crucial role in modulating the shutdown of host protein synthesis during infection, which antagonizes the production of host defenses. These enzymes stimulate the degradation of both cellular and viral transcripts, which influences the gene expression dynamics during infection. Since both enzymes are expressed in different stages during infection, an overlapping manipulation effect of the gene expression is postulated (Parrish & Moss, 2007).

Virion structure

MYXV virions, like the rest of the poxviruses, are large (300×250×200 nm), enveloped, ovoid or brick-shaped, that can exist in two structurally and antigenically different infectious forms: intracellular mature virus (IMV) and extracellular enveloped virus (EEV) (Appleyard et al., 1971) and Figure 2. Based on these differences, each has a distinct role in infection (Smith et al., 2002). IMV particles are surrounded by one double lipidic membrane and are physically robust, resistant to environmental stresses like freezing, thawing, desiccation, which allow them to remain viable outside a host for extended periods. While their stability and resilience facilitate the spread of infection to new hosts, their highly immunogenicity makes IMV poorly suited to virus spread within the host and could explain why these particles are retained within cells, well protected from antibodies and complement (Law & Smith, 2001). The effectiveness of IMV is limited due to its susceptibility to neutralization by antibodies and inactivation by the complement system even in the absence of specific antibodies (Boulter et al., 1971; Vanderplasschen et al., 1997). In fact, strains that produce only IMV are non-virulent and incapable of spreading *in vivo* (Smith et al., 2002). IMV composition notably lacks host proteins, and this is attributed to an exclusion process that is likely taking place during IMV morphogenesis, where non-viral elements from membrane compartments involved in forming the IMV envelope are systematically excluded (Krauss et al., 2002).

EEVs comprise an IMV particle enclosed within an additional lipid envelope that is fragile and easily disrupted. EEV is particularly effective at spreading infection outside the cell due to its resistance to both antibody neutralization and complement systems (Boulter & Appleyard,

1973; Ichihashi, 1996). Whilst several IMV proteins (especially A27 and H3 in VACV) are targets for neutralizing antibodies that prevent infection, the only EEV protein that induces neutralizing antibodies is B5 (Pütz et al., 2006).

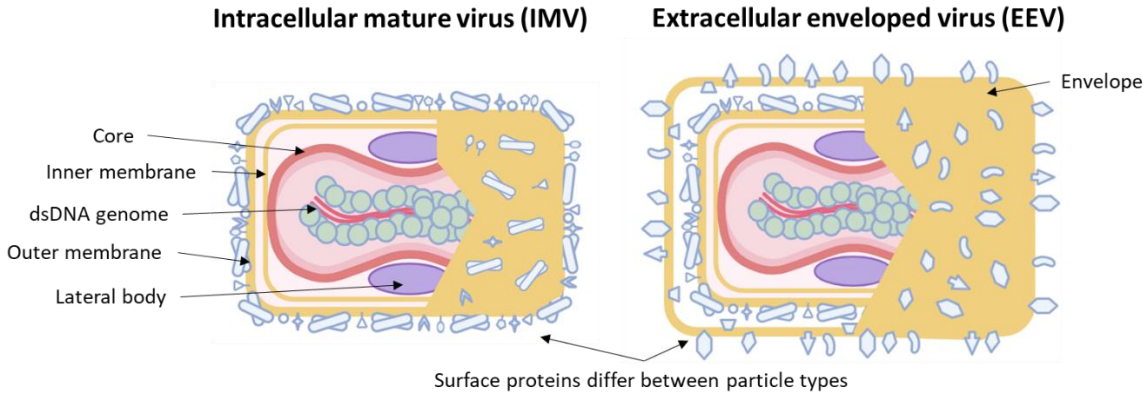

Figure 2. Schematic representation of IMV and EEV poxvirus particles

In cell culture, EEV are responsible for the infection of adjacent cells or spread in a unidirectional manner due to an upward convection current to reach distal cells (Law et al., 2002). This process results in the formation of distinctive comet-shaped plaques with a head generated by the primary plaque and the tail belonging to secondary plaques generated through EEV spread (Appleyard et al., 1971; Payne, 1980).

The outer membranes of EEV (and the cell-associated enveloped form, CEV) contain several virus-encoded and cellular proteins that are absent from IMV (Payne, 1978, 1979). The virus-encoded antigens are A56R, F13L, B5R, A34 and A33R (reviewed in Smith et al., 2002), and their functions have been studied using virus mutants with each individual gene altered, repressed, or deleted. Overall, they contribute to increasing the virulence of the virus and enhancing cell-to-cell transmission through the formation of actin tails beneath CEV attached to the cell surface (in the Vaccinia virus model) (Krauss et al., 2002; Law et al., 2002). These five viral proteins are also present in the intracellular enveloped virus (IEV) together with two additional proteins exclusive to IEV that are involved in the transport of these particles towards the cell surface: A36R and F12L (Hollinshead et al., 2001; Van Eijl et al., 2002).

EEV's resistance to the complement system is attributed to the incorporation of host complement control proteins CD46, CD59, and especially CD55 in its outer envelope (Vanderplasschen et al., 1998). These proteins have been identified in the EEV envelope through immunoblotting and immunoelectron microscopy techniques, confirming their role in protecting the virus from the host's immune response (Krauss et al., 2002).

Life cycle

No specific attachment molecules have been identified for the binding of EEVs to the cell surface (Vanderplasschen & Smith, 1997). However, several IMV membrane proteins mediate initial attachment to the host cell through binding to glycosaminoglycans and extracellular matrix components: D8 binds chondroitin sulfate (Hsiao et al., 1999a), A27 (Hsiao et al., 1998) and H3 (Hsiao et al., 1999; Lin et al., 2000) proteins bind heparan sulfate, and A26 binds laminin (Chiu et al., 2007).

Poxvirus entry depends on the infectious form of the virus. Although IMV and EEV can enter host cells through endocytosis, they differ in their mechanisms of fusion and triggering of macropinocytosis (Schmidt et al., 2012). IMVs can enter cells via low-pH endocytic pathways (Townsley et al., 2006), and neutral pH direct fusion of the viral envelope with the plasma membrane (Carter et al., 2005). The infection pathway chosen by poxviruses is influenced by both the specific viral strain and the type of host cell involved (Whitbeck et al., 2009). Regardless of the route taken, the ultimate goal remains consistent: the entry of the viral core into the cell's cytoplasm.

The additional membrane from EEVs pose an additional barrier to release the naked core into the cytoplasm. Right after binding to the cell surface, the EEV outer membrane is dissolved in a ligand-dependent nonfusogenic process mediated by the EEV proteins B5 and A34, and cellular glycosaminoglycans that is followed by IMV fusion with the plasma membrane (Law et al., 2006).

Surface IMV proteins A16, A21, A28, G3, G9, H2, L1, L5, G3, G9, O3 and J5, form a multiprotein stable structure called entry-fusion complex (EFC) involved in virus core entry and cell-cell fusion processes. All these proteins, apart from O3, are essential genes and thus, are conserved in all poxviruses but do not have homology to any fusion proteins of other non-poxviruses. The EFC has a total mass of 232 kDa that suggests that each of its components are represented once within the complex (Moss, 2012; reviewed in Senkevich et al., 2005). The EFC subcomplex formed by A16-G9 is a target for fusion regulation by A26 protein interaction, an acid-sensitive fusion suppressor protein that prevents premature fusion of IMV membrane with host membranes during virion assembly or exit from the cell (S.-J. Chang et al., 2012). However, MYXV does not encode a VACV A26L homolog, indicating that it exploits different cell entry and exit mechanisms (Villa et al., 2010a). Indeed, MYXV entry into cells is not stimulated by low-pH environments, and it generally forms fewer actin tails than VACV (Irwin & Evans, 2012).

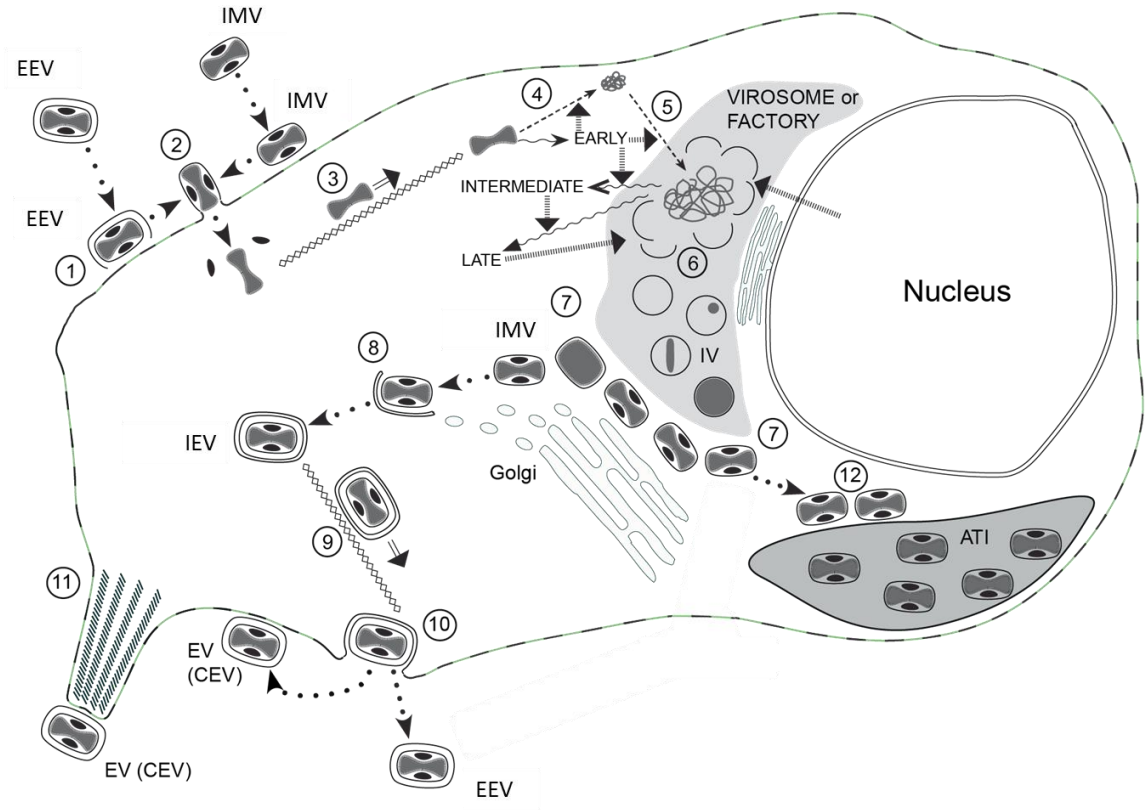

Figure 3. Infectious cycle of poxviruses, based on that of VACV.

(1) Disruption of the outer envelope of EEV particles upon binding to cell surface receptors. (2) IMV fuses directly with the cell membrane to release the lateral bodies and the viral core, (3) which is transported to the perinuclear region. Early genes are transcribed in the core, using the viral gene expression machinery packed into the core, and mRNAs are released to the cytoplasm for the synthesis of viral proteins involved in (4) uncoating the core, (5) viral genome replication and intermediate gene expression, which products lead to late gene expression. New virions are generated from membrane crescents (6) that enclose viral factors and core proteins, and the genomic DNA, and are assembled forming IV. (7) These mature to IMV that are transported to the trans-Golgi for (8) wrapping with a double membrane, producing IEV. (9) These are transported to the periphery of the cell along microtubules. (10) Fusion of the outer IEV's membrane with the plasma membrane leads to the release of enveloped virus (CEV or EEV). The virion can remain attached on the cell surface as CEV, where they would be driven away from the cell surface through actin-driven projections or become free in the medium as EEV. (Adapted from: Family: Poxviridae | ICTV)

Upon entry and fusion, poxviruses transcribe and release a set of early mRNAs into the host cell cytoplasm using the early gene expression machinery that was packed into the virion's core. Although poxviruses encode capping enzymes, viral mRNA translation into protein remains dependent on host ribosomes (Jan et al., 2016). Proteins involved in genome replication and nucleotide metabolism enzymes are produced in this early stage. The synthesis of early proteins is crucial for the following steps of its life cycle: the uncoating of the core and subsequent release of the parental genome into the cell's cytoplasm (Moss, 2013). Viral DNA synthesis is usually

detected in the cell cytoplasm just 2 hours after infection. The newly formed DNA copies serve as templates for the transcription of intermediate and late-stage genes (Yang et al., 2011).

Viral genome replication, intermediate and late transcription, and progeny virion assembly occur in cytoplasmic compartments called viral factories. These discrete sites are specific structures generated by remodeling of endoplasmic reticulum (ER) membranes (Tolonen et al., 2001). A viral factory is formed from every virion that infects the host cell, and even though at first, they are compact structures, their size increases considerably with time (Cairns, 1960). During the uncoating process, the released DNA associates with a subset of early proteins required for genome replication that seem to mediate their association with the cytoplasmic side of the rough ER (Domi & Beaud, 2000; Welsch et al., 2003). Then, as replication progresses, ER cisternae are recruited to the replication sites and fuse together until they completely surround the replication site, while ribosomes are segregated toward the ER membrane facing the cytosol. This wrapping and creation of an independent cytosolic compartment is crucial for efficient viral genome replication (Schramm & Locker, 2005; Tolonen et al., 2001).

Late gene products are mainly structural proteins required for virion assembly, and enzymes destined to be incorporated into the progeny and used for early gene expression during the next round of infection (Broyles, 2003). Virion assembly begins with the formation of rigid crescent-shaped lipidic structures within the viral factories, which expand eventually generating a complete, closed three-dimension sphere configuration known as immature virus (IV). A copy of the dsDNA genome is packaged into this non-infectious structure, which suffers a maturation process involving the proteolytic cleavage of several capsid proteins that results in the IMV particles formation (Moss & Rosenblum, 1973).

Morphogenesis can end at this point with the release of IMVs from the host upon cell lysis. In fact, IMVs represent most of the infectious progeny generated in the infected cell. However, some particles are transported out of the viral factories to the wrapping sites in a microtubule-dependent movement (Sanderson et al., 2000; B. M. Ward, 2005). IMVs acquire two additional membranes derived from endosomes (Van Eijl et al., 2002), or the trans-Golgi network (TGN) (Hiller & Weber, 1985; Schmelz et al., 1994), generating the IEV form (Krauss et al., 2002). Although the mechanism for IEV formation has not been fully unraveled, several viral proteins have been identified as essential for this process: A27/M115, B5/M144 and F13/M022 (Condit et al., 2006). IEVs are transported to the cell periphery in a microtubule-dependent manner, through interactions between the protein A36 from the outer membrane of IEV and kinesin-1, a component of the microtubule transport system (Hollinshead et al., 2001; B. M. Ward & Moss,

2004). The IEV component F12L protein is also involved in the microtubule-dependent egress of IEV to the cell surface (Van Eijl et al., 2002).

Upon reaching the cell surface, the outer membrane of the IEV fuses with the cell membrane, exposing the enveloped virion on the cell surface as a CEV. Some proteins from the IEV outer envelope are deposited on the cell surface during IEV exocytosis, but B5R and F13L in particular, are retrieved from the cell surface through clathrin-mediated endocytosis, eventually reaching the endosomal compartment (Husain & Moss, 2003) (Figure 3).

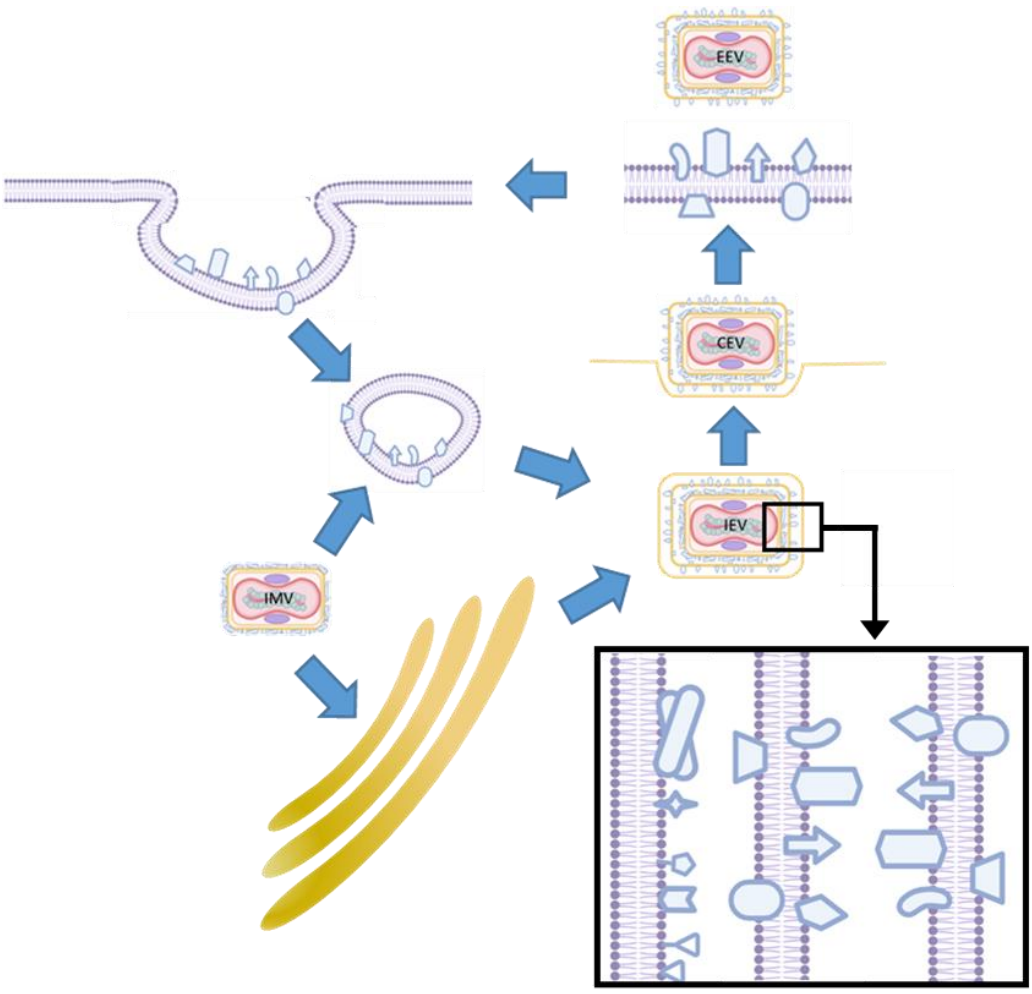

Figure 4. Cycling of proteins in the outer layer of the IEV for re-use during virus wrapping

After fusion with the plasma membrane, the proteins that were attached to the outer membrane in IEV remain in the plasma membrane. They are recycled via clathrin-mediated endocytosis. Adapted from Smith et al. (2002) and Smith and Law (2004).

In VACV, A36 protein that was part of the IEV relocates in the plasma membrane beneath CEV particles, facing the cytosol. There, A36 suffers Src-dependent tyrosine phosphorylation by Src kinases, which in turn are activated by B5R protein exposed on the surface of CEV (Newsome et

al., 2004). This modification regulates the transition between microtubule transport by releasing binding of the virion from kinesin-1 and initiates a signaling cascade that leads to actin polymerization at the plasma membrane beneath the CEV (Frischknecht et al., 1999). Actin tail formation takes place in a polarized manner and drives CEVs away from the cell body and towards neighboring cells for cell-to-cell spread of the virus (Blasco & Moss, 1991; Payne, 1980). A34R and B5R proteins play crucial roles in ensuring that enveloped virions are retained on the cell surface long enough to facilitate actin tail formation and support an efficient cell-to-cell transmission (Blasco et al., 1993). A36 homologs are present in the genome of all orthopoxviruses, but other genera of *Chordopoxviridae* family lack an obvious homolog, leporipoxviruses amongst them (C. Cameron et al., 1999). Nevertheless, MYXV is still able to induce the production of actin tails (Duteyrat et al., 2006) through a functional ortholog, M126, protein with <10% amino acid similarity to VACV A36 that is also recruited to IEVs (Dodding & Way, 2009).

This cell-to-cell spread process is very common for VACV and is characterized by extensive actin tail formation for virion propulsion. However, MYXV less frequently engages in actin tail-mediated cell-to-cell spread, as evidenced by diminished actin tail formation in infected cells (Dodding & Way, 2009). This difference is partly attributed to the absence of a homologous protein to VACV's F11, which is crucial for maintaining the cortical actin layer's integrity (Irwin & Evans, 2012). In fact, MYXV's IEVs migrate to neighbor cells more predominantly through large cytoplasmic corridors, bypassing release into the extracellular space where they could be counteracted by the immune system, which allows the virus to spread while evading immune detection (Duteyrat et al., 2006). This highlights a significant difference in the intracellular mobility and dissemination strategies between the two viruses (Figure 5).

Not all virions are retained on the cell surface, enveloped virions are eventually released by exocytosis as EEV, which are believed to be responsible for viral dissemination within the host (Payne, 1980; Smith et al., 2002). A34R is required for specific infectivity and virulence of the released EEV (Mcintosh & Smith, 1996). Despite being the final stage of the poxvirus morphogenetic pathway, EEV typically constitutes less than 1% of total virion progeny (Payne, 1986). The conserved production of EEV across poxviruses suggests an evolutionary advantage for *in vivo* replication. Although not crucial for infection, the inability to produce EEVs effectively results in significant attenuation of the virus in vivo (Pickup, 2015; Roberts & Smith, 2008). Indeed, it has been suggested that EEVs also mediate immunosuppression by being rapidly and continuously released away from infected cells to neutralize a targeted cell. EEVs would outpace the antiviral and proinflammatory cytokines, as well as Pathogen-Associated Molecular Patterns

(PAMPs) and Damage-Associated Molecular Patterns (DAMPs), released by the infected cells. Otherwise, these molecules could trigger innate immune responses from nearby immune cells. By outrunning these signals, EEVs effectively prevent an immune response from initiating in nearby immune cells, facilitating the spread of the virus without immediate detection or interference from the host's immune defenses (Pickup, 2015).

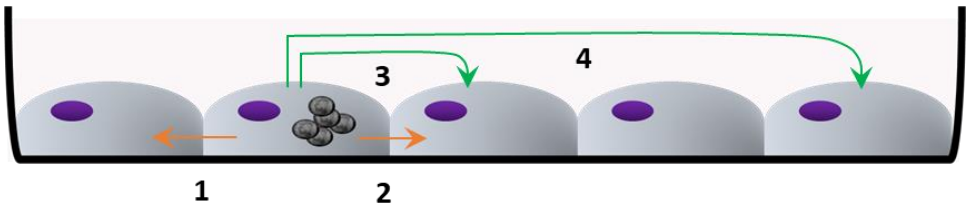

Figure 5. Spread strategies of poxvirus model VACV

Progeny from an infected cell may be spread by (1) releasing IMV to infect adjacent cells by cell lysis, (2) cell-to-cell spread mediated by actin tail formation driven by the CEV particles attached to the cell membrane, EEV released to the environment and (3) infecting adjacent cells or (4) distant cells. Figure adapted from Smith et al. (2002).

Poxviruses can prevent secondary infections through a mechanism called superinfection exclusion that involves the A56-K2 protein complex. This complex is incorporated in the plasma membrane late in infection and can block further viral entry by interacting with the A16-G9 subcomplex of the EFC, stopping additional viruses from entering the cell and ensuring the virus doesn't compete against itself within the host (Wagenaar & Moss, 2007).

Polyclonal anti-VACV antibodies (Ab), targeting both IMV and EEV, can prevent comet plaque formation but only slightly reduce the size of the primary plaque, suggesting a mechanism of virus spread resistant to antibodies which is independent from A56 or A36 proteins, thus also independent of actin tail formation. A33R protein mediates cell-to-cell spread in an antibody resistant manner, possibly through cell junctions (Law & Smith, 2001).

Genetic diversity of MYXV

The evolutionary rate of poxviruses is rapid, they have one of the highest nucleotide substitution rates among other double-stranded DNA viruses (Firth et al., 2010). MYXV specifically, accumulates nucleotide substitutions under a strongly molecular clock-like manner with 9.6×10^{-6} nucleotide substitutions/site/year. This dynamism was likely a consequence of MYXV being subjected to a strong selection process for enhanced transmissibility and better adaptation to its new host (*O. cuniculus*) (P. J. Kerr et al., 2012). The high mutation rate rather provides to the

MYXV genomes a kind of flexibility for several evolutionary routes from which they can attain similar either virulent or more attenuated phenotypes (P. J. Kerr et al., 2015).

There is high variability in the attenuation process, molecular analysis comparing several circulating attenuated MYXV field strains in Australia showed no common changes regarding attenuation events compared to their parental virulent strain following almost 50 years of coevolution with rabbits (Saint et al., 2001). While most of the MYXV genome is highly conserved, the terminal regions (37.2 kb) seem to accumulate most non-conservative nucleotide changes (77.7%), and up to 41% of the total nucleotide changes (Morales et al., 2009). These regions of the genome are the least conserved among poxviruses and correspond with the location of genes encoding host-range and virulence factors. They are rich in repeated elements that can generate heteroduplexes during the replication process, promoting the generation of deletions or insertions, changing the copy number of the repeats that most likely disrupt ORFs affecting the immune modulation and virulence capacities of the viruses (Cameron et al., 1999; Kerr et al., 2010; Kerr et al., 2015). Accumulation of mutations in the TIR regions are presumably involved in the evolution and speciation of leporipoxviruses (P. J. Kerr et al., 2010).

Distribution and host range

MYXV is a natural pathogen of two leporid species that constitute its natural reservoirs in America. The *Sylvilagus brasiliensis* tapeti or tropical forest rabbit is the reservoir practically in all South America, except for Chile and south region of Argentina, where the principal reservoir is *O. cuniculus* (F. Fenner & Ratcliffe, 1965). The brush rabbit, *Sylvilagus bachmani* serves as the source of infection for domestic rabbits in North America, especially the West coast of USA and Mexico (California and Baja California). Due to the low pathogenicity and subclinical manifestations induced in their reservoir hosts, the virus is spread and transmitted without causing clinical infection.

Since its introduction in Australia and Europe in the 1950s as a biological agent to control the *O. cuniculus* population, the virus affects free-living rabbit populations in North America, South America, Europe, and Australia (DiGiacomo & Maré, 1994). Myxomatosis is an endemic disease on the Iberian Peninsula, and amongst the main factors causing the decline of native European wild rabbit population (Calvete et al., 2002).

Besides the *Sylvilagus* and *Oryctolagus* species mentioned above, cottontail rabbits (*S. floridanus, S. nuttalli, S. audubonii*) are also naturally susceptible to develop a larger lesion upon infection. Although other lagomorphs, such as the European and the mountain hares (*Lepus*

europaeus and *Lepus timidus*), that are considered resistant to the infection, sporadic cases of hares suffering systemic myxomatosis were reported in France and Great Britain (Barlow et al., 2014; F. Fenner & Ratcliffe, 1965). However, widespread Iberian hare (*Lepus granatensis*) casualties having the typical myxomatosis clinical signs were reported in Spain and Portugal since 2018, indicating a potential host-species jump of MYXV to a new host (Carvalho et al., 2020; García-Bocanegra et al., 2019).

Genome studies of infected hare showed significant molecular divergence between the Lu MYXV reference genome and the pathogenic agent, which turned out to be a natural recombinant MYXV (ha-MYXV). In addition to the more than 100 identified mutations, the ha-MYXV genome contained a 2.8 kb insertion within the M009 ORF that potentially codes 4 ORFs phylogenetically related to MYXV genes M060, M061, M064 and M065 (Dalton et al., 2019).

The high number of outbreaks reported in recent years over a broad territory indicates an endemic ha-MYXV circulation in the Iberian hare population, with a temporal distribution similar than the one of myxomatosis in wild rabbits: a peak incidence during summer and autumn months, corresponding with the months with higher abundance of vectors (García-Bocanegra et al., 2021). Although at first classical MYXV and the recombinant MYXV were thought to have a specific segregated circulation in rabbits and hares, respectively, ha-MYXV is also pathogenic for the European rabbit and it is even associated with increased mortality in farm rabbits (Abade dos Santos et al., 2020, 2021).

Transmission

The principal mode of indirect transmission is mechanical transport of the virus on mouth parts of arthropod vectors, principally mosquitoes (*Anopheles annulipes, Culex annulirostris*) and fleas (*Spilopsyllus cuniculi*) and subsequent inoculation during biting/feeding. Other Arthropod species such as ticks could also be a competent vector in MYXV transmission (García-Pereira et al., 2021). Mosquitoes, along with other flying vectors such as midges and black flies, play a significant role in transmitting myxomatosis during summer epidemics, due to their seasonal activity which is influenced by changes in weather and environmental conditions. However, when temperatures drop in autumn and winter, their activity decreases since adults die or enter a dormant state. The European rabbit flea (*S. cuniculi)* is less influenced by seasonal changes and flea transmission of myxomatosis occurs throughout the year (Kerr et al., 2015). The occurrence of myxomatosis outbreaks thus depends on the activity and abundance of the arthropod MYXV vectors, which in turn, depend on climatic factors such as temperature and humidity (Camacho-Sillero et al., 2022).

Myxomas have proven to be an important focal point of virus accumulation and hold significant relevance for its dispersal, particularly the facial lesions on the eyelids and at the base of the ears, as they are more accessible to hematophagous vectors (F. Fenner & Woodroofe, 1953). Besides the draining lymph nodes, the highest amount of MYXV is detected in skin from the inoculation site and secondary skin lesions (Jeklova et al., 2008b). When fleas and mosquitoes feed on a diseased rabbit through its cutaneous lesions, they contaminate their mouth parts with a high viral load during the process. However, the infective dose deposited by a mosquito when feeding on a new animal is low. Viral strains with varying degrees of virulence exhibit a similar level of viral concentration in these cutaneous lesions, as well as the same capacity to be transmitted by vectors (Fenner et al., 1956).

Nevertheless, the potential of each strain to persist in circulation is correlated with the efficiency of its transmission. Highly lethal strains, leading to swift mortality in infected rabbits, are typically associated with a lower chance of transmission compared to those strains that allow longer survival of the rabbit. On the other hand, very attenuated strains are also likely to have low transmission rates owing to their insufficient replication in the epidermis, which does not reach the necessary threshold for effective spread (Fenner et al., 1956; Kerr et al., 2003).

In this regard, vectors may play a relevant role in MYXV evolution by favoring the selection of moderately attenuated field strains, since strains that allow for a longer exposure time of myxomatous lesions developed in diseased rabbits to vectors facilitate their natural selection at the population level (Fenner et al., 1956). This phenomenon was observed during an experiment involving the release of the virulent Lausanne strain (Lu-MYXV) in a region of Australia where an attenuated field-derived strain of SLS was endemic in the rabbit population. After an initial increase in infection cases with the virulent Lu-MYXV strain, only attenuated strains were recovered at the end of the outbreak (Fenner et al., 1957).

Epidemiology

Viral infection was the cause of 11.61% lagomorph deaths in northern Spain between 2000-2018, and almost one third of which (29.03%) were due to myxomatosis disease (Espinosa et al., 2020). On the Iberian Peninsula, wild rabbits with symptoms of myxomatosis are observed throughout the year. MYXV circulation can be sustained all year round in particularly abundant populations, if there are enough susceptible rabbits, either recovered adult rabbits or juveniles of the last breeding season. In fact, these populations show high immunity levels against MYXV, demonstrating both IgM and IgG, resulting in a low prevalence of the disease (Marchandeau et al., 2014). Long-term serologic studies of MYXV in wild rabbits in Europe concluded that there is

an association between MYXV seropositivity and rabbit density, population age, sampling season, outbreaks of myxomatosis in the month prior to sampling, mean annual temperature, humidity, and seropositivity to RHDV (Camacho-Sillero et al., 2022; Fouchet et al., 2008; García-Bocanegra et al., 2010; Villafuerte et al., 2017).

The pattern of the spread and severity of the disease observed in rabbit populations is influenced by the transmission rate of MYXV. In populations with a high transmission rate of the virus, many young rabbits have their first contact with the infectious agent while still being protected by maternal antibodies, and while some of them might die, the rest only experiment a mild level of infection (Fouchet et al., 2006). This early exposure results in the effective immunization of the offspring, supporting Zinkernagel's hypothesis, which states that an early-age high level of exposure to the virus is advantageous for the survival of young rabbits (Zinkernagel, 2001).

Female survivors develop maternal antibodies against MYXV that are transmitted to their offspring, providing a temporary passive immunity against the virus during the first 6-9 weeks after birth (Coelho et al., 2023; Fenner & Marshall, 1954; Kerr, 1997). Newborn rabbits' immune system is not fully developed, so they are more susceptible to infections, also to myxomatosis. Maternal antibodies cannot prevent MYXV infection, but they play a key role in reducing the severity of the disease in case of early exposure of juvenile rabbits (< 8 weeks) to the virus, resulting in a mild or attenuated phenotype (Marchandeau et al., 2014).

The study of long-term dynamics of the humoral immunity to myxoma virus revealed a highly dynamic system that demonstrated the seasonality of the disease outbreaks (Coelho et al., 2023). An increase in population reached by the incorporation of newborns and juveniles at the end of the breeding season, decreases the overall antibody level in the population while providing enough susceptible hosts for the virus to circulate (Villafuerte et al., 2017). An abundant and sustained proportion of juveniles resulting from a long reproductive period contributes to a high persistence of the virus (Fouchet et al., 2008). In high abundance populations, a large proportion of juveniles with maternal immunity contribute to increase the contagion of MYXV, which ultimately elevates the overall antibody level of the population and contributes to increase the seroprevalence, thus reducing the impact of myxomatosis (Villafuerte et al., 2017).

Myxomatosis is a seasonal viral disease, and outbreaks often occur following birth pulses as soon as adequate insect vectors are available (Boag et al., 2013; García-Bocanegra et al., 2010). If the breeding season is reduced, and rabbit populations are low, the seasonal peak of myxomatosis

can temporally shift to coincide with the accumulation of enough susceptible rabbits (Mutze et al., 2002). The seroprevalence of MYXV in wild rabbits shows a cyclical pattern on an annual basis, reflecting periodic fluctuations in the immune status of the wild rabbit population within the Mediterranean ecosystem (Camacho‐Sillero et al., 2022; Coelho et al., 2023). Higher seroprevalence levels are found in adult rabbits, followed by juveniles, and least prevalent in young individuals. This pattern suggests an increasing probability of exposure to the virus over a rabbit's lifespan (Villafuerte et al., 2017). Waning of acquired immunity of the survivors over time make them susceptible to re-infections, which reactivate their immune system and contribute to the maintenance of a sustained level of immunity within the population (Fouchet et al., 2006). Most rabbits infected in secondary exposures also develop an IgM response and show mild myxomatosis clinical signs (Marchandeau et al., 2014).

The relative prevalence of clinical myxomatosis in rabbits on farms is also seasonal and has an incidence peak around the end of summer-beginning of autumn (September-October), which happens to coincide with the highest presence of mosquitoes and flies on farms in Spain. Regarding prevalence data of clinical myxomatosis in Spanish farms the 30-year period, from 1988 to 2018, the annual prevalence dropped from 16.5% to 3.2% (Rosell et al., 2019).

DIAGNOSIS

The nodular or classic form of myxomatosis in European rabbits typically presents distinctive clinical signs with characteristic features, such as nodular skin lesions, swelling around the head, ears and genital area, and some respiratory distress and blindness. These clinical manifestations allow for quick presumptive diagnosis and enable a rapid initiation of management and control measures. Clinical signs may vary depending on the strain of the virus, the stage of the disease, and the individual rabbit's immune response. For instance, differential diagnosis of myxomatosis might be more difficult for attenuated strains, since the signs become less obvious, but also for amyxomatous MYXV strains, as they show less ectodermotropism. Laboratory diagnosis is required to confirm the disease, and it usually requires detection of the pathogenic agent (isolation or identification of the MYXV virus, their antigens, or its genome), or the specific immune response (detection of anti-MYXV antibodies in serum).

Direct methods for detection of the causative agent

The biological samples used for detection of MYXV have different origins depending on whether the animal presents the nodular, classic form of the disease, or the amyxomatous form. For the

classic form, samples and biopsies from cutaneous tissue, eyelids, and internal organs, or genital mucosa can be used depending on what suits best in each case. For the amyxomatous or very mild and attenuated cases, samples from the nostrils and conjunctiva can be collected with cotton swabs.

Virus isolation (*in vitro* and *in vivo*)

As previously discussed, poxviruses often have a relatively narrow and defined host range. While MYXV is known to be highly specific to leporids (rabbits and hares) *in vivo* (F. Fenner & Ratcliffe, 1965), many cell lines are permissive to infection. MYXV can be cultured *in vitro* using a variety of established and primary cultures in the laboratory, including various types of mouse and human cancer cells (Sypula et al., 2004). The most common cells used in MYXV studies are the rabbit cell lines RK-13 (rabbit kidney) and SIRC (Statens Serum-Institut rabbit cornea), BHK-21 cells (baby hamster kidney), and the African green monkey kidney cell lines Vero (epithelial), CV-1 (fibroblast), BSC-40 and BGMK cells (Smallwood et al., 2010).

Myxoma virus can be inoculated and cultured within the chorioallantoic membrane of embryonated chicken eggs on the 11th day of incubation. After 3 days at 35°C, viral replication can be detected using a microscope and is characterized by the presence of specific pocks on the chorioallantoic membrane.

Finally, although rabbit inoculation is not used as a diagnostic tool, it is still the only alternative to define the virulence and pathogenicity of specific MYXV strains. In this case, domestic rabbits seronegative for MYXV are used for intradermal inoculation at different doses.

Electron microscopy (EM) Histopathology, and Antigen detection

EM is used to identify the virus by visualization directly from clinical material, without the need for amplification (OIE, 2018). The relatively big size of poxvirus virions allows them to be recognized at levels as low as 10^5 particles/ml of original specimen.

For histopathological analysis tissue samples and biopsies are fixed and pretreated (hematoxylin and eosin staining) to be examined under the microscope, where characteristic tissue structure and cellular changes are assessed to diagnose the disease. Depending on the viral strain and phase of infection, different tissue damage can be detected (Best et al., 2000). Alternatively, immunofluorescence and immunohistochemistry examinations are helpful for pathophysiology studies, to detect specific viral distribution and localization within the affected tissue or sample.

For that, fixed tissues or samples are treated with contrast staining and incubated with anti-MYXV sera or monoclonal antibodies (available from the International Reference Laboratory, in Italy) (OIE, 2018).

The agar gel immunodiffusion (AGID) assay has been routinely used for decades as a qualitative and simple method to detect MYXV in biological samples or anti-MYXV antibodies, although its diagnostic performance (sensitivity and specificity) was assessed only recently (Kwit et al., 2020).

Direct fluorescent antibody test (FAT) provides a quick and direct visualization of the antigen in original fixed cryopreserved tissue, after incubating the samples with fluorescent conjugated anti-MYXV serum. (OIE, 2018).

Molecular detection of the viral genome

PCR has become an increasingly relevant tool for microbial diagnosis due to its affordability, high sensitivity, and high specificity, among other advantages. It is currently the most common direct diagnostic test performed by the WOAH Reference Laboratory on myxomatosis (Lavazza, 2023).

Several conventional PCR protocols for MYXV detection have been developed over the years and are currently available, targeting the M071L gene (Cavadini et al., 2010; Kwit et al., 2019; OIE, 2018) (A PCR strategy targeting the homologous M071L gene in capripoxvirus was previously developed by (Heine et al., 1999), the M022L gene (Farsang et al., (Farsang et al., 2003), and the M135R gene (Belsham et al., 2010).

In addition, conventional multiplex PCR were designed to discriminate between vaccinated (Borghi and SG33 strains) and naturally infected animals, and to detect simultaneous infection of vaccine and wild type strains on a unique clinical sample (Cavadini et al., 2010). The traditional strategy for the analysis and differentiation of MYXV viral strains was based on the comparison of the fragment profile and identification of restriction fragment length polymorphisms (RFLPs), after enzymatic digestion of highly purified whole virus genome (Labudovic et al., 2004). Due to the large MYXV genome size (>160 kb), these restriction analyses are laborious and have a complicated interpretation, thereupon the PCR-RFLP emerged as an alternative method. It is focused on RFLP differentiation from the amplification products of genomic regions, without the need of cultivating the virus *in vitro* (Dalton et al., 2009; Saint et al., 2001).

Quantitative real-time PCR (qPCR) is a molecular technique that offers better sensitivity and the possibility of obtaining quantitative data from the tested samples, such as the determination of viral copy number. A MYXV-specific qPCR was developed targeting the *Serp2* (*M151R*) gene, with

a reliable sensitivity (23 copies) in fresh and paraffin-embedded rabbit tissues (Albini et al., 2012). A MYXV-specific qPCR assay designed for targeting the *M029L* gene showed a wide range of sensitivity, being able to detect 10 MYXV genome copies per sample, and a linear range up to 10^7 copies (Belsham et al., 2010). Furthermore, a broad-range *Leporipoxvirus* specific qPCR was developed and validated, with a sensitivity of 2.5 copies of viral genome. This qPCR assay targets the *m000.5L/R* gene, a gene in the *Leporipoxvirus* genome that has two copies, one in each of the TIRs (Duarte et al., 2013).

m000.5L/R is highly conserved amongst myxoma viruses and has also been used for the development of a validated and robust quadruplex qPCR for the differential diagnosis between MYXV and recombinant ha-MYXV strains in leporid samples. In this strategy, amplification of the *m000.5L/R* gene is combined with the specific *m009L* amplification in MYXV strains, and amplification of a specific region within the *m060L* gene, only present in ha-MYXV genomes. These reactions are validated and normalized by the amplification of a fourth gene, the eukaryotic housekeeping gene 18S rRNA (Dos Santos et al., 2021).

Serologic assays- detection of a specific immune response against MYXV

Serological assays are useful for monitoring the dispersion and field circulation of the virus, allowing an approximation of the extent of the rabbit population affected, for those that cannot be clinically recognized. The classical assays used for detection of specific antibodies to MYXV are neutralization, complement fixation, immunofluorescence, and agar gel double-immunodiffusion, the latter being the only one implemented during epidemiological studies in Australia (F. Fenner et al., 1953; Gilbert et al., 1989; Sobey et al., 1966). Subsequently, indirect enzyme linked immunosorbent assays (ELISAs) were shown to have significantly higher diagnostic sensitivity and specificity over the tests mentioned above, as well as additional advantages, such as time required, less volume of sample needed, the possibility of using hemolyzed sera, constituting a more reliable alternative for myxomatosis survey studies (Gelfi et al., 1999; Kerr, 1997).

ELISA

The first ELISA developed for epidemiological studies used the Lu-MYXV whole virion as antigen for an indirect ELISA (iELISA). Positive-control serum from a rabbit immunized with RFV and hyperimmunised with the Lu strain, previously titered in neutralisation assay (Kerr, 1997). A second iELISA protocol is available, this time the antigen is the Lu strain French derivative, the

Toulouse 1 (T1) strain. Immune sera are obtained from intradermally vaccinated rabbits, using the SG33 French attenuated strain. This ELISA had 100% specificity and sensitivity and could also detect anti-RFV antibodies in serum samples from animals vaccinated with the heterologous vaccine, unlike IFT or CF tests, that give a negative result even when these vaccinated animals are protected from myxomatosis (Gelfi et al., 1999). Therefore, this assay is appropriate in kinetic studies of the immune response stimulation after vaccination either with homologous or heterologous vaccines (Marlier et al., 2000). No cross-reaction with other Poxviruses was observed in either of the two different iELISAs.

The WOAH Reference Laboratory for Myxomatosis (Italy) developed and optimized an in-house competitive ELISA (cELISA) that they currently use as the serologic routine test used in their facilities. It uses the 1E5 monoclonal antibody (MAb) which recognizes the immunodominant IMV envelope M071L viral protein. The cELISA allows the detection of all anti-MYXV Ig types, thus having a higher specificity than iELISA (OIE, 2018). All reagents and the protocol can be obtained by demand to the WOAH Reference Laboratory.

The iELISA protocols described by Kerr (1997) and Gelfi et al. (1999) were used to assess the prevalence of myxomatosis on different occasions: in wild rabbit populations on two Indian Ocean islands (Gelfi et al., 1999), in wild rabbit populations across the Iberian Peninsula (Villafuerte et al., 2017), in rabbit farms in Belgium 2001(Marlier et al., 2001), ; and in wild rabbits in south-eastern Australia (Kerr et al., 2010), respectively. cELISA has also been used in sero-surveillance of myxomatosis in Romania (Baraitareanu et al., 2014) and in monitoring the dynamics of the humoral response upon homologous vaccine application through different inoculation routes (Manev et al., 2018).

Two Spanish commercial kits based on indirect ELISA were developed during recent years. “CIVTEST Cuni Mixomatosis” (HIPRA S.A., Girona, Spain), with 100% sensitivity and 95% specificity, and INgezim Mixomatosis R.17.MIX.K1t (Ingenasa, Madrid, Spain), with a reported sensitivity and specificity rates of 98% and 99%, respectively. Their optimized protocols allow for easier seroprevalence studies and assessment of success of vaccination campaigns on farms. E.g. serological analysis of wild rabbits sampled across the Iberian Peninsula (Villafuerte et al., 2017).

Anti-MYXV -seropositive rabbits have higher survival rates than seronegatives, but they can also have higher susceptibility to suffer other infections due to the immunosuppressive effects that may cause in rabbits with a poor physiological status (Santoro et al., 2014). Regarding the relevant role of immunoglobulins in resolving poxvirus infection, serological evaluation of the

antibodies against MYXV are used as biomarkers for successful vaccination (Dalton et al., 2015; Manev et al., 2018). However, seroconversion may not always be indicative of protection.

PREVENTION STRATEGIES

There is no treatment for myxomatosis therefore preventative measures are essential to mitigate the spread and the impact of the disease. In accordance with the Terrestrial Animal Health Code (WOAH), there are specific guidelines established to regulate the trade of rabbits and their products whose follow-up is crucial for preventing the spread of diseases among rabbit populations. Significant focus is placed on managing the interaction between domesticated and wild rabbit populations, as the latter are often primary reservoirs of various viruses. One of the key strategies outlined is the implementation of effective measures to isolate rabbit farms from external threats. This involves the construction of fences or walls designed to restrict the access of unauthorized individuals and wild fauna, potential carriers of diseases.

Another critical aspect of disease prevention is the strict enforcement of quarantine protocols for newly introduced animals. Quarantine periods should exceed the incubation period of prevalent viruses, which typically ranges from 15 to 20 days, ensuring that any incoming animals are free from infection and do not pose a risk to the existing farm population.

Maintaining high standards of hygiene is paramount. This involves the regular cleaning and disinfection of facilities and work equipment, which helps in creating a sanitary environment conducive to rabbit health and farms are also encouraged to implement strategies to guard against vector transmission, a common method of disease spread (Rosell et al., 2019; Salaün et al., 2015). These comprehensive measures form the basis of a robust approach to preventing the spread of rabbit diseases and ensuring the overall health and safety of both domestic and wild rabbit populations.

PROPHYLAXIS: VACCINATION

Types of vaccines: (heterologous vs homologous)

The host immune response to MYXV, like to other poxvirus, is a complex mechanism that involves both cellular and humoral arms of the immune system. The large genome of MYXV contains numerous genes that encode for immunomodulatory proteins that ensure host immune system evasion. Since cell death pathways are innate mechanisms used by the host cell in response to

viral infections, many of these viral proteins are involved in antagonizing cellular apoptotic induction, allowing the completion of their life cycle and progeny production (Smith et al., 2013).

A robust cellular immune system stimulation is needed to control the spread and clear a MYXV infection, as well as providing long-term protection (Kerr & Mcfadden, 2002). On this basis, inactivated vaccines are mostly ineffective for poxviruses and only live vaccines have succeeded on inducing a protective immune response (McKercher, 1952).

Non-live vaccines were developed as an alternative strategy due to potential benefits over live vaccines: their non-transmissibility and safer profile, amongst others. DNA vaccines encoding pathogen-specific antigens are thought to be good T-cell inductors and therefore, one would think that they could be a suitable option (McConkey et al., 2003). However, the plasmid-derived vaccination with MYXV genes, whose homologous genes in Vaccinia virus are protective antigens, resulted in non-protective responses even with co-expression of cytokine genes (Adams et al., 2004).

In accordance with this data the only commercially available vaccines against MYXV are live virus vaccines, either heterologous based on the leporipoxvirus RFV, or homologous vaccines based on live attenuated MYXV strains.

Heterologous vaccines use the live RFV as antigen, also belonging to the Leporipoxvirus genus. This poxvirus is endemic in the eastern United States and its natural host is the Eastern cottontail (*Sylvilagus floridanus*). In this host, RFV infection causes large, flat, wart-like subcutaneous fibromas on the face, feet, legs, and perineum (Shope, 1932b). Although these are usually localized lesions that regress after several days or weeks, newborn or immunocompromised individuals can suffer a more severe generalized fibromatosis. RFV is nonpathogenic in the European rabbit, and it only causes a benign fibroma (Kerr et al., 2015). The attenuated nature of RFV might be attributed to the partial or complete absence of 7 ORFs in its genome, which are known to encode virulence factors in MYXV, such as Serp-1 and M135R (Willer et al., 1999). Shope (1932a) demonstrated that RFV is immunologically related to MYXV and that convalescent rabbits from RFV acquired resistance to fatal myxomatosis.

Commercial heterologous vaccines against MYXV are based on the original Shope OA strain, the Boerlage strain, or closely related strains. They have been used since 1955 on rabbits older than 3 weeks of age, since they are safe for young rabbits. Despite inducing early immunity against MYXV, their effectivity is limited over time (P. Fenner & Woodroofe, 1954; Jerabek, 1980). The variability on the level of protection induced upon vaccination might depend on different elements such as differences in the adjuvant used, the vaccine dosage or the vaccination

strategy itself (differences in administration route, the number of dosages, etc.) (Alfonso & Pagés-Mantè, 2003; Cabezas et al., 2006; Marlier et al., 2000).

Homologous vaccines consist of attenuated live MYXV strains. The first attempts to generate vaccines involved the attenuation of several field MYXV strains that were extensively serial passaged in cell culture (McKercher & Saito, 1964). The resulting attenuated strains showed a safe profile in rabbits since they were incapable of spreading to unvaccinated rabbits under field conditions. Although they caused a very mild systemic reaction, they stimulated immunity to challenge with virulent virus up to 7-9 months after vaccination (Saito et al., 1964a). The homologous MYXV-based vaccines induce a stronger protective immune response than the heterologous vaccines. Due to the immunosuppressive effect of MYXV in rabbits, homologous vaccines frequently induce more side effects (primary and secondary skin lesions, edema, and rash at the injection point) than heterologous vaccination. This immune depression is especially harmful to young and immunocompromised rabbits, exacerbating their vulnerability to adverse reactions and underlying subclinical infections (Jeklova et al., 2008b; Manev et al., 2018).

Attenuation of virulent virus strains through serial passage in cell culture relies on the virus gradually adapting to that specific and restrictive environment. During this process, the virus often undergoes genetic mutations that restrain its ability to replicate effectively in its natural host. Although several homologous vaccine strains are currently available (SG33, MAV, Borghi, Leon162, etc.), and used in the formulation of commercial vaccines available in Europe.

There is no clear consensus on the specific mutations that are responsible for the attenuated phenotype. SG33 strain lost some relevant immunomodulatory genes like Serp-2, *M148R*, *M149R*, *M150R*, *M152R*, *M153R*, *M154R* and M-T1; Borghi strain suffered mutations in Serp-2, M-T4 and *M131* genes (Braun et al., 2017; Cavadini et al., 2010). The MAV strain experienced 14.2 kb deletion. Besides other mutations, it included the loss of the *M006L* to *M009L* region in the left TIR, and the *M148R* to *M008.1R* region in the right TIR. Two immunomodulatory proteins (*M007L* encodes M-T7 and *M008.1L* encodes SERP1) were amongst the genes lost in the first deletion, whilst the second deletion implied the truncation of *M148R* and loss of *M149R*, *M150R*, *M151R*, *M152R*, *M153R*, *M154L*, *M156R*, and *M008.1R*, all encoded proteins with immunomodulation roles (Barrett et al., 2001; Braun et al., 2017).

Based on the current knowledge on MYXV virulence genes and genomic analysis, directed attenuation of the virus has been used to overcome the immunosuppressive effect produced by homologous vaccines. Simultaneous deletion of M007L, M010L, M011L genes in the naturally attenuated MYXV Ur strain led to a well-tolerated vaccine by adult and juvenile rabbits but had

a limited protection against MYXV challenges (Adams, van Leeuwen, & Kerr, 2008). Insertional inactivation of the M065R ORF of the Ur strain resulted in a replication-defective vaccine that produces an abortive infection after the expression of early viral genes (Barrett et al., 2007). Besides being a safe vaccine candidate as it cannot replicate within the host, it stimulates B cell and T cell responses. Immunization with the M065 defective virus only protected rabbits from lethal viral challenge on boosted individuals, as neutralizing antibodies that are barely detectable in prime-vaccination, rise after the boost or/and a challenge infection. However, this vaccine strain only shows a good degree of protection in short-term trials, comparable with the duration of protection by heterologous RHDV vaccines (Adams, Leeuwen, McFadden, et al., 2008)

RHD together with myxomatosis are two major viral threats to rabbits, therefore combined vaccines have been designed to deal with both diseases simultaneously. One of the first combined vaccines available since 1999 was known as Dercunimix® (Merial Laboratoire) and was designed as the combination of two already commercial vaccines: the live attenuated SG33 MYXV strain and an inactivated preparation of RHDV field strain AG88 in aluminium hydroxide adjuvant. Although vaccination with Dercunimix® does not affect the safety or the efficacy compared to the SG33 vaccine alone, the author recommends the performance of a primary vaccination with the SG33 vaccine at 4 weeks of age, followed by this combined vaccine at 10 weeks of age and successive booster administrations of SG33 and Dercunimix® vaccines every 4 and 12 months, respectively (Lemiere S, 2000). Castomix (Pharmagal-Bio Ltd.) is also a vaccine designed for active immunization against both diseases, of rabbits from 10 weeks of age onwards, that combines a dose of the attenuated MYXV strain MAV with the inactivated RHDV strain PHB. Its protective effect lasts at least 9 months; thus, revaccination is required after that period.

Additionally, bivalent vaccines were developed for the prevention of both myxomatosis and RHD using a laboratory attenuated MYXV strain with a good safety profile as a vaccine vector. Recombinant viruses were constructed by inserting the RHDV GI.1 capsid gene (VP60) into different locus of the MYXV genome (Bertagnoli et al., 1996; Spibey et al., 2012). VP60 directed insertion could improve the safety of the resulting vaccine virus, by targeting the thymidin-kinase (TK) gene (Jackson & Bults, 1992a; Jackson & Bults, 1992b), or the MGF/M11L locus, which would affect both ORFs coding for the two virulence factors MGF (myxoma growth factor) and M11L (Graham et al., 1992; Opgenorth et al., 1992). This confers the strain a good safety profile, as the vaccine virus is unable to disseminate beyond the area around the injection site, or to spread from the vaccinated animal. Although this highly attenuated vaccine strain is safe for use in young rabbits, according to the manufacturer's instructions it must be administrated to rabbits

from 5 weeks onwards. The onset of immunity against MYXV and RHDV is 3 weeks after vaccination, and the protection lasts for one year (Spibey et al., 2012).

Following the emergence of the novel RHDV in 2010, RHDV GI.2, which proved highly virulent in younger rabbits and vaccinated adults, the EU licensed a novel trivalent vaccine offering protection against MYXV and the two current RHDV circulating strains (Reemers et al., 2020).

Vaccination either with monovalent Mixohipra-H or multivalent Nobivac Myxo-RHD PLUS vaccines, induce a humoral response that protect rabbits from ha-MYXV infection. Despite this, concerns have arisen about this situation, since this finding still points out that wild rabbits may contribute to the spread of ha-MYXV in hares. Neither homologous (Mixohipra-H) nor heterologous (Mixohipra-FSA) commercial vaccines against the classic MYXV virus effectively protect hares from a deadly recombinant MYXV (ha-MYXV) infection, at least at the recommended doses. Seroconversion and survival were only observed in 66% of hares vaccinated with 10 times the recommended doses for the heterologous Mixohipra-FSA vaccine (Abade dos Santos et al., 2022).

Immune response to vaccination

While antibody titers are not the only parameter correlated with protection against myxomatosis (Manev et al., 2018), they are the only immune response factor that can be readily measured in a standardized way. It seems clear that, as with other poxvirus infections, a robust cellular response is required for control and clearance of an MYXV infection, and that both are also necessary for providing long-term protection (Kerr, 2012).

The overall health condition of the rabbit is of vital importance for an effective immune response following vaccination. Immune-depressing factors in field circumstances, such as stress and other diseases, may negatively affect the rabbit's serological response to vaccination on an individual level (Alfonso & Pagés-Mantè, 2003).

The route of administration of the vaccine is also critical. Studies have shown greater effectiveness of the intradermal (ID) route in inducing a robust immune response against MYXV compared with the subcutaneous (SC) or intramuscular (IM) routes (Dalton et al., 2015; Manev et al., 2018). ID administration allows a longer contact between the antigen and the antigen-presenting cells with a high number of dendritic cells in the derma compared with the subcutaneous tissue (Levin et al., 2015). Successful ID administration of the RFV antigen (heterologous vaccine) induces the development of nodules at the inoculation site, whose

presence and size correlate to a positive humoral response to vaccination (Alfonso & Pagés-Mantè, 2003).

Intradermic vaccine application using a Dermojet device proved 100% efficient (Dalton et al., 2015). However, it is important to consider the technical challenges involved in handling and using vaccination devices like Dermojet for intradermal vaccination on a farm setting. Although this tool was designed to facilitate ID inoculation, it requires proper handling, including regular cleaning and maintenance, to ensure proper usage. Otherwise, it leads to unsuccessful vaccinations and variability in the induced humoral responses amongst rabbits (Alfonso & Pagés-Mantè, 2003).

Vaccination with monovalent vaccine against myxomatosis induced higher antibody titer in comparison to bivalent vaccine (Manev et al., 2018).

Myxoma virus causes immunosuppression in rabbits (Jeklova et al., 2008a). Homologous vaccines offer longer protection, but they are also more immunosuppressive and can be detrimental for the general health status of the rabbit, and even exacerbate underlying subclinical infections or increasing their susceptibility to the virus and other infections. Since homologous myxomatosis vaccines contain a live, attenuated virus that still retains part of its immunosuppressive effect. Vaccinating infected animals or those not in optimal health can compound the immunosuppressive effect of the vaccine with that of the disease. Additionally, if there is active virus circulation on a farm, vaccinating can facilitate the spread of the disease.

An important aspect to consider in this context is maternal immunity interference. Serological studies have revealed that kits retain the immunity passed on from their mothers until about 28-30 days of age and consequently, vaccinating animals younger than 30 days does not ensure effective immunization. The safety and efficacy of vaccines have been established in animals as young as 30 days old. Therefore, vaccinating weaned kits at this age is a viable option, especially in cases where these animals are earmarked as future breeders. However, considering that the ideal time for the first vaccination (primovaccination) is typically recommended at around two months of age, there is a vulnerability gap between the loss of maternal immunity and primovaccination, in which the kits remain unprotected.

Vaccination protocols and schedules

Regulations

Vaccines produced against myxoma virus must comply to the veterinary vaccine guidelines. The viruses employed for as vaccines against myxomatosis are RFV or MYXV attenuated strains. For

both, a validation test must be carried out for each route of administration indicated, in which candidate strains are administered to specific pathogen-free rabbits with the minimum age at which they can be vaccinated, at a dosage of no less than 10 times the working concentration. Body temperature needs to be monitored, and rabbits are checked for abnormal local or systemic reactions for 28 days.

The efficacy of the vaccine is tested by experimentation in which rabbits are vaccinated with the corresponding dose of the vaccine strain, and after 21 days or more, are challenged using a virulent strain (usually Lu strain) and the infection progress is assessed for a further 21 days. If at least 80% of vaccinated rabbits do not show signs of myxomatosis, the test is valid, and the vaccine's protective efficacy is confirmed. If positive, the duration of immunity needs to be tested.

Vaccine strains also need to pass several tests to check their safety in different situations. For instance, an overdose safety test (RFV vaccines are tested subcutaneously whilst MYXV attenuated strains are tested using intradermal administration), a safety test in pregnant rabbits and sucking rabbits, and a stability test (that studies if reversion to virulence is possible).

Strategies for domestic/farmed rabbit populations

Developing an ideal vaccination program against myxomatosis in rabbits is a complex task due to the complex nature of the disease. Several vaccination plans have been established to simplify the issue, but they may be specifically modified and supervised by a veterinarian familiar with the specific situations and peculiarities of each farm. Implementation of a successful vaccination program ensures a robust population immunity which involves immunizing enough animals to create a communal barrier against infection, thereby impeding the transmission and spread of the virus.

The common protocol involves a mixed vaccination plan that begins with administering a heterologous vaccine for the initial vaccination and is followed by a revaccination with a homologous vaccine after at least a couple of months, and from then with boosting doses every six months to provide a stronger protection (Marlier et al., 2000).

The type of vaccine administered may depend on the infection pressure and risk situations intrinsic to the farm (management conditions, recurrent cases of myxomatosis, etc.), or extrinsic (level of disease incidence in the geographical area, farm density, etc.). Vaccination plans using the heterologous vaccine exclusively are optative in situations of low infection pressure, although in these cases revaccination must be performed every 4 months. In situations with

medium to high-risk, it is advisable to initiate vaccination using the homologous vaccine and to continue administering it every 6 months.

In many vaccination strategies, the systematic immunization of fattening rabbits is not a standard practice, primarily due to the intensive labor required compared to the relatively short raising period (they are often culled around 12 weeks of age). Instead, the focus is generally placed on the vaccination of breeding rabbits, who are considered valuable assets for the farm. By consistently and properly vaccinating these breeders, high levels of immunity are maintained, which in turn contributes to a strong level of immunity across the farm's population. This strategy is effective in reducing the likelihood of disease contagion and spread.

Control and prevention programs: vaccination of wild rabbits

The eradication of myxomatosis in rabbit populations presents a complex challenge. Despite the availability of vaccines against MYXV, certain peculiarities of the disease prevent its complete eradication. The existence of multiple strains of the virus, each with a different degree of virulence, complicates the management of the disease. The subtle nature of some attenuated and amyxomatous strains hinder the identification of infected rabbits, thus challenging the control of the disease. Asymptomatic carriers are crucial in the transmission of the virus and often go unnoticed, acting as reservoirs for MYXV, perpetuating its presence and spread.

Vaccination campaigns of wild rabbits against myxoma virus are not only expensive but also logistically complex, encompassing everything from the capture and handling of animals to the technical aspects of preparing the vaccine and correctly administering it. Furthermore, these campaigns are typically conducted in a “blind” and non-systematic manner, meaning that vaccines are administrated to animals without consideration of factors such as their sex, age or serological status. The highly variable spatial-temporal pattern shown by the virus, highly influenced by the circulating strains and population density, compromises the success of these campaigns (Ferreira et al., 2009).

Several elements are critical for the success of a vaccination campaign, such as the time of vaccination, the body/health status of the animal prior to vaccination, the type of vaccine, the proportion of vaccinated animals, etc. Firstly, vaccination might be more effective if performed after the breeding season but before the annual myxomatosis outbreak (Guitton et al., 2008), but since the emergence of outbreaks can vary across different regions and over time, this can be tricky to assess (Calvete et al., 2002; P. J. Kerr & Best, 1998). The intensity of the immune response after vaccination of free-living adult rabbits is determined by the body condition of individual rabbits at the time of vaccination (Cabezas et al., 2006, 2007).

Although systematic vaccination of juvenile rabbits with the homologous vaccine before the disease outbreak has short-term negative effects on their survival, it could also improve their overall survival rates in high-density systems (Calvete et al., 2004; Guitton et al., 2008)).

Attempts to vaccinate adult rabbits from densely populated areas, with a high prevalence of natural antibodies against MYXV, are likely to yield unsatisfactory results attributed to the interfering effect of the naturally acquired antibodies against MYXV with the immunisation process (Cabezas et al., 2006). In fact, blind vaccination against myxomatosis with live RFV during translocation program does not affect to the average survival of individuals, when compared to non-vaccinated animals (Rouco et al., 2016). Conversely, in populations where the virus's transmission rates are low and do not support sustained immunity, myxomatosis shows an epidemic pattern, thus juveniles born in the subsequent breeding season are most at risk due to their lower seroprevalence rates prior to the outbreak (Ferreira et al., 2009).

Alternative vaccination strategies

Transmissible vaccines

The restricted host range of MYXV reduces the risk of affecting non-target species in nature, making it a good candidate as a vaccine vector in terms of safety. Strain 6918, an attenuated MYXV field isolate, was selected from a field survey of strains circulating in Spain, since it showed a good ability to disseminate within the rabbit population (horizontal transmission). Although 6918 infection was non-lethal, it maintained high immunogenicity and protected against lethal challenges in direct inoculations (Bárcena, Pagès-Manté, et al., 2000). The 6918-strain genome closely resembles those of highly pathogenic wild-type virus strains, differing in the disruption of 4 genes (*M009L, M036L, M135R, M148R*), two of which are known to be virulence factors of MYXV (*M135R, M148R*) (Morales et al., 2009). Under laboratory conditions, it showed over 50% transmission in co-housed rabbits, with the immunity conferred by transmission being protective. However, onward transmission efficiency dropped significantly.

In addition, MYXV 6918 strain was genetically engineered to create a bivalent and transmissible vaccine against both diseases, RHD and myxomatosis. The horizontal transmission in laboratory trials gave over 50% of both RHDV and MYXV seroconversion rates in non-vaccinated rabbits just one month after initial contact with immunized rabbits. Although the vaccine transmission efficiently induced a protective immune response in all seropositive rabbits, the proportion of seropositive rabbits in a second passage was reduced to less than 10% (Bárcena, Morales, et al., 2000). Given that this involves the environmental release of the vaccine virus, safety considerations are just as crucial as its potential effectiveness. The recombinant virus

demonstrated lack of adverse effects, regardless of dosage, administration route, rabbits' age, or health status. The minimal effect on immunosuppressed rabbits was particularly relevant due to the prevalence of immunocompromised individuals in the wild (Torres, Ramírez, et al., 2001). This recombinant virus showed similar efficacy in a limited field trial where as well as inducing a high antibody response against both viruses in vaccinated rabbits, the recombinant vaccine disseminated among the population and seroconverted around 50% of the un-inoculated rabbits (Angulo & Bárcena, 2007; Torres, Sánchez, et al., 2001). The use of transmissible vaccines is not widely supported due to the added risk of reversion to high virulent phenotypes, but according to mathematical models, the limited capacity of spreading associated with the recombinant 6918VP60-T2 virus would reduce the chance of reversion and provide a safer approach to this issue, whilst still enhance the infectious disease control (Nuismer et al., 2016; Nuismer & Bull, 2020).

Marked vaccines

It is clear that this issue is not satisfactorily resolved, we envisage the use of mark vaccines would greatly help in the control of this disease, as happened with Aujeszky's disease (AD), a herpesvirus infection of pigs caused by the Pseudorabies virus (PrV). AD was the first animal disease in which the idea of developing a genetically engineered live DIVA vaccine successfully implemented (Van Oirschot et al., 1986). The target-deletion of virulence PrV genes that were non-essential for the viral viability resulted in attenuated marker vaccines that since then, have constituted the main strategy for AD eradication programs worldwide (Freuling et al., 2017; Van Oirschot, 1999).

The design and implementation of differential serologic diagnostics to distinguish between vaccinated and naturally infected animals are crucial for the success of veterinary eradication programs, as exemplified by the Aujeszki's disease eradication. The presence of a natural reservoir of MYXV poses significant challenges to the hypothetical eradication of this infectious disease in rabbit farms. Indeed, a complete eradication of myxomatosis would require simultaneous efforts in enhanced DIVA vaccination strategies and coordinated actions involving wildlife management and rabbit population control. However, implementing the DIVA approach would enable accurate identification of naturally infected animals, thereby improving the ability to track the disease prevalence among vaccinated individuals.

A more recent example of the usefulness of this disease control strategies, was the design of a differential serological DIVA assay for capripoxvirus. In their work, Berguido et al., (2023) illustrate the development of an iELISA based on the truncation of a conserved protein that is

consistently found among many attenuated poxviruses of the genus *Capripoxvirus*, including sheeppox virus (SPPV), goatpox virus (GTPV) and lumpy skin disease virus (LSDV) strains. The assay was designed to detect antibodies that recognize a specific protein fragment of the non-structural B22R protein that is only present in the full-length wild-type conformation. This approach was based on genetic differences between virulent capripoxvirus field strains and most of the commercially available attenuated vaccines.

Current live MYXV vaccines do not feature common deletions. To overcome this limitation, the present thesis focuses on the identification of candidates within the MYXV genome that encoded non-essential antigenic proteins that could be deleted in an attenuated MYXV strain in order to develop an effective DIVA vaccine.

CHAPTER 2: JUSTIFICATION

The ongoing coevolution of MYXV and its host towards equilibrium in morbidity and mortality rates within wild rabbit populations does not mitigate the high concerns associated with potential MYXV outbreaks in Europe, where myxomatosis is an endemic disease. The ecological and economic impacts underline the need of proactive monitoring and management strategies in order to mitigate the spread of MYXV.

There is no effective treatment for the disease, therefore, prophylactic measures are highly relevant for preventing and reducing viral transmission. Live vaccines are the only proven method to be efficient in protecting rabbits from MYXV challenge. Despite the wide use of homologous MYXV vaccines, myxomatosis is prevalent throughout the territory, with certain farms showing an endemic disease pattern (Rosell et al., 2019). The use of vaccines in rabbit farms only provides partial protection and is not sufficient to prevent the disease and spread of the virus (Kritas et al., 2008; López‐Lorenzo et al., 2021). Shedding of infectious MYXV in conjunctivae and nasal secretions was observed in vaccinated animals exposed to virulent challenge virulent field strains, regardless of the clinical form (nodular or amyxomatous) of the disease (Marlier et al., 2000).

The specific environment on rabbit farms, where high densities of animals are kept in close contact, creates an ideal environment for the transmission of bacterial and viral pathogens. Immune suppression caused by bacterial coinfections that cause respiratory diseases, can promote the transmission of attenuated MYXV strains. In fact, bacterial coinfections increase the virulence of amyxomatous MYXV strains (Marlier et al., 1999). These factors could be contributing to the persistence of myxomatosis in rabbit farms, since unrecognized cases of myxomatosis in asymptomatic vaccinated rabbits might contribute to an ongoing transmission of MYXV in commercial rabbitries (Marlier et al., 2001).

Managing and preventing myxomatosis outbreaks in rabbit farms involve a combination of strategies that when combined with a correct vaccination schedule, are aimed at reducing transmission, and enhance immunity of the population. Adopting adequate biosecurity measures within the farm, such as maintaining regular cleaning and disinfection of the installations, preventing rabbit exposure to vectors for MYXV through physical barriers and chemical control of vector populations, are essential preventive measures that farms should implement to prevent myxomatosis outbreaks. Conducting serosurveillance of the incoming animals prior to their integration with the rest of the population could prevent the introduction and spread of the virus. Moreover, evaluation of the individual immune status of vaccinated

rabbit populations over time provide the effectiveness and vaccine coverage on the population level.

Ultimately, early detection of myxomatosis within the farm is a crucial, cost-effective measure that can minimize the financial burden associated with the culling of rabbits during widespread outbreaks. Myxomatosis disease surveillance is not a straightforward process. While passive diagnosis of the classic or nodular myxomatosis typically relies on the detection of the characteristic skin lesions, the amyxomatous form mainly displays non-pathognomonic respiratory signs and overall immunosuppression that can often lead to its misdiagnosis (Joubert et al., 1982; Marlier et al., 2001).

Serologic surveillance is currently not effective for detecting active infections in vaccinated rabbits due to the complexity immunogenicity of the MYXV virion. Since all commercially available vaccines against myxomatosis are live attenuated, the antigenic profiles of virulent and vaccinal strains are virtually identical, making it impossible to distinguish between the two specific situations. Under these conditions, the generation of a DIVA vaccine would be strategically relevant in the control of the disease (Van Oirschot, 1999). Besides the DIVA vaccine itself, this management strategy involves the design and generation of a differential serologic test that could correctly identify the humoral response induced in an infected rabbit, from the one induced upon vaccination (Bertolotti et al., 2015). The implementation of both elements would offer a robust solution for the control of myxomatosis in a rabbit farms' scenario, and hopefully guarantee the maintenance of long-term disease-free conditions.

CHAPTER 3: OBJECTIVES

On this basis, the main purpose of the present Doctoral Thesis is to engineer a DIVA vaccine for MYXV. This vaccine will consist of two essential elements: a recombinant attenuated MYXV strain marked by the deletion of an antigenic gene to generate a differential serologic profile, and an antigenic-specific diagnostic test to selectively identify naturally infected animals from vaccinated ones.

This principal objective can be broken down into several specific sub-objectives that give a deeper detail into the different relevant research areas. The sub-objectives described below outline the necessary steps that need to be addressed, providing a clearer roadmap, for the research to ultimately achieve the principal objective:

1. Identification and validation of antigenic MYXV proteins
    a. Selection of the MYXV protein candidates
    b. Production of soluble candidate proteins in different heterologous expression systems
    c. Examination of the antigenic properties of the candidates

2. Development of an antigen-specific test for serological diagnosis
    a. Design and optimization of the protocol specific for the assay
    b. Validation of the specificity and sensibility of the serological test under laboratory conditions
    c. Evaluation of the test ability to be used as a diagnostic tool

3. Generation of an attenuated MYXV virus marked by gene deletion
    a. Site directed deletion of the gene candidates
    b. *In vitro* characterization of the mutant MYXV DIVA candidates
    c. *In vivo* characterization of the mutant MYXV DIVA candidates

Given that the main objective involves designing and generating of two independent elements that will eventually complement each other, some of the tasks described above can be approached in a non-sequential manner.

CHAPTER 4: MATERIALS & METHODS

MATERIALS

Expression vectors

pTriEx-™-1.1

The pTriEX™-1.1 vector is a high copy plasmid designed to allow the expression of heterologous proteins in multiple expression systems: bacteria, insect, and vertebrate cells. The vector contains a β-lactamase (*bla*) gene that confers resistance to ampicillin, and the genes of interest are cloned between the *NcoI* and *XhoI* sites in the multiple cloning site (MCS). The target ORF expression in *E. coli* is under the control of the T7 promoter which is regulated by the *lac* operon. Target genes can be translated in hosts that constitutively express the T7 RNA polymerase and induced in those containing also the *lacI* gene (lac repressor). The pTriEX-1.1 also contains the very late p10 promoter, and two flanking baculovirus sequences (upstream lef-2, 603 flanking region and downstream ORF1629 flanking region) surrounding the gene of interest, for the expression of the transgene in insect cells. Finally, the introduction of pTriEx1.1 in vertebrate cell lines through transfection protocols can also result in transient or stable expression of the transgene, which is mediated by the hybrid promoter composed of the constitutive cytomegalovirus (CMV) immediate early enhancer fused to the chicken β-actin promoter.

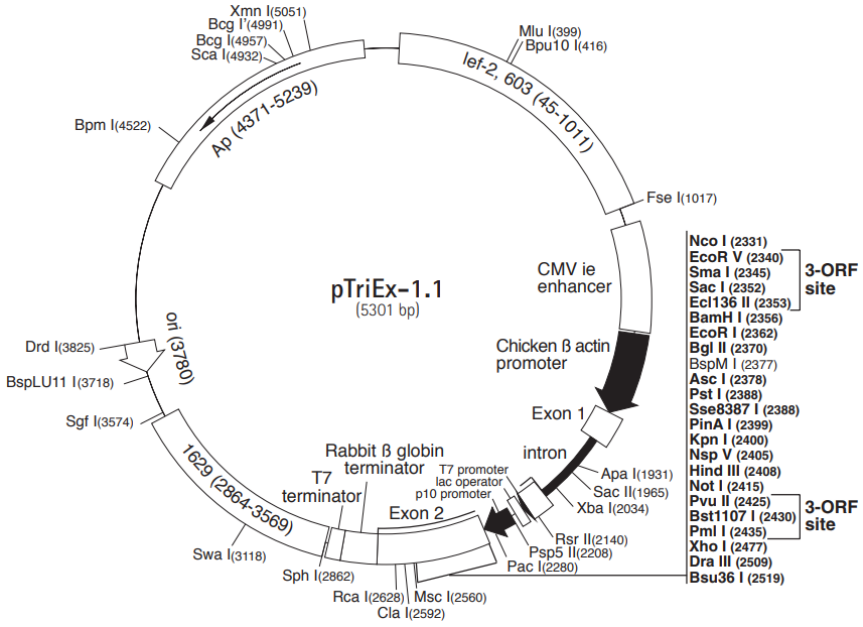

Figure 6. Vector map of the pTriEX-1.1 plasmid

Key features of the construct are illustrated, including the promoter elements for all the expression systems: T7 promoter for bacteria, p10 promoter for insect cells, and the hybrid CMV+ β-actin promoter for mammal cells. Restriction enzyme sites of the MCS are indicated along with their position. The map was obtained from the Novagen User's manual.

The gene of interest can be strategically cloned in the vector without a stop codon to allow the addition of polyhistidine tag (8xHis) at its C-terminal region, therefore producing a histidine-tagged recombinant protein.

pET-28a(+)

The pET-28a(+) high-copy number plasmid is a vector designed for bacterial expression. It contains the aminoglycoside phosphotransferase gene that confers resistance to kanamycin. Heterologous genes can be cloned fused to N-terminal and C-terminal histidine tags (6xHis), and their expression is under the control of the T7 promotor, regulated by the operon *lac.* The vector also contains the regulator element *lacI* that represses the transcription by binding the *lac* operator in the presence of glucose. Protein expression is induced after the addition of either lactose, or the analogous to the metabolite allolactose, isopropyl β-D-1-thiogalactopyranoside (IPTG), to the culture media.

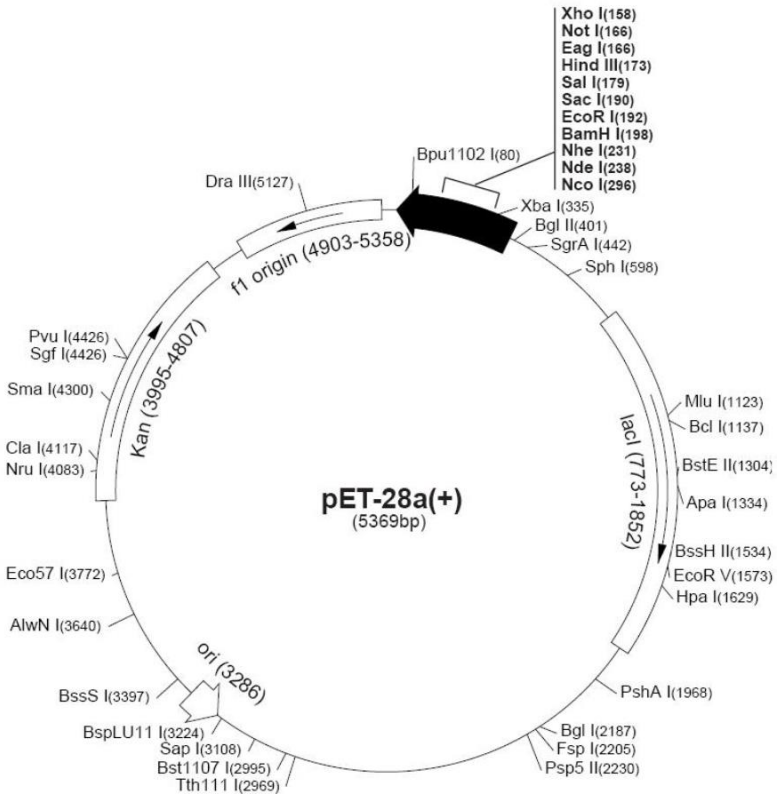

Figure 7. Vector map of the pET-28a(+) plasmid

Key features and restriction sites are illustrated. The map was obtained from the Novagen user's manual

pEt44a(+)

The expression vector pEt44a+ codes for the 54.9 kDa N-utilization substance A (NusA) protein, a highly soluble and functional protein that can be expressed as a N-terminal tag fused to the gene of interest when it is cloned in the same reading frame as the tag, playing a passive role in enhancing the solubility on the fusion protein (Nallamsetty & Waugh, 2006). Like the pEt-28a(+) vector, the fusion construct is also expressed under the control of the T7 promoter, that is regulated by the *lac* operator. The transcription inhibitor LacI is also included in the vector.

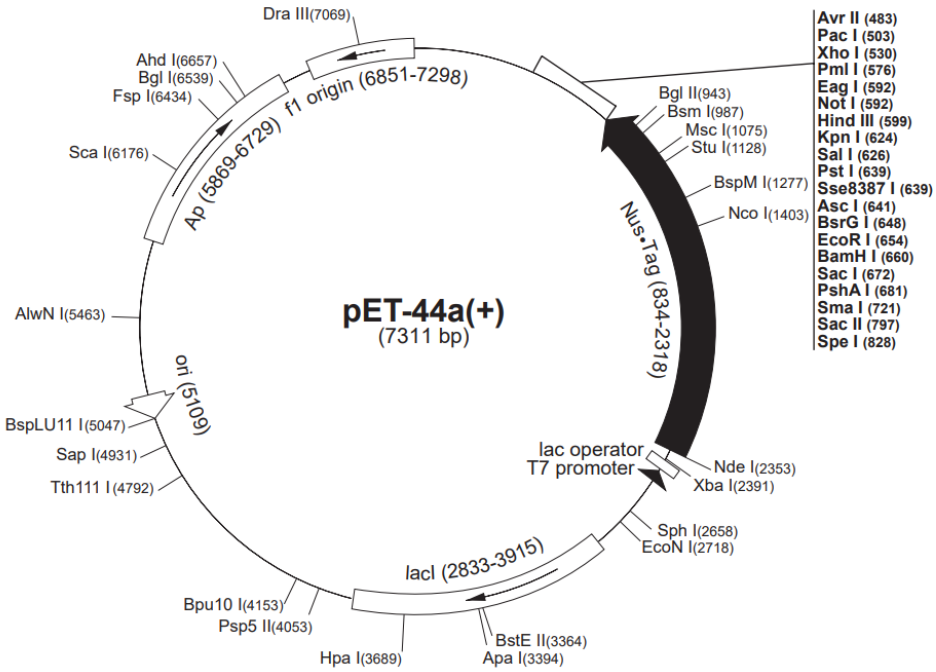

Figure 8. Vector map of the pET-44a(+) plasmid

Schematic map illustrating its key features, including the Nus fusion protein tag, and the T7 promoter. The map was obtained from Novagen user's manual

.

pGEX-2T

The pGEX-2T plasmid is a bacterial expression vector under the prokaryotic synthetic promoter *tac*¸ regulated by the *lac* operon. This expression vector also contains the *lacI* repressor that blocks the transcription at the *lac* operon level, the β-lactamase gene that confers ampicillin resistance, and the glutathion S-transferase (GST) gene as a solubility tag. GST is a highly stable and soluble 26 kDa enzyme that folds into its native tridimensional structure rapidly after being translated in a prokaryotic system. pGEX-2T vector includes this tag at the 5'-end from the transgene cloned in the vector, therefore producing a recombinant fusion polyprotein with GST

in its N-terminal region, separated with a thrombin site. Besides increasing its solubility, the recombinant GST-tagged proteins can be purified easily by affinity chromatography.

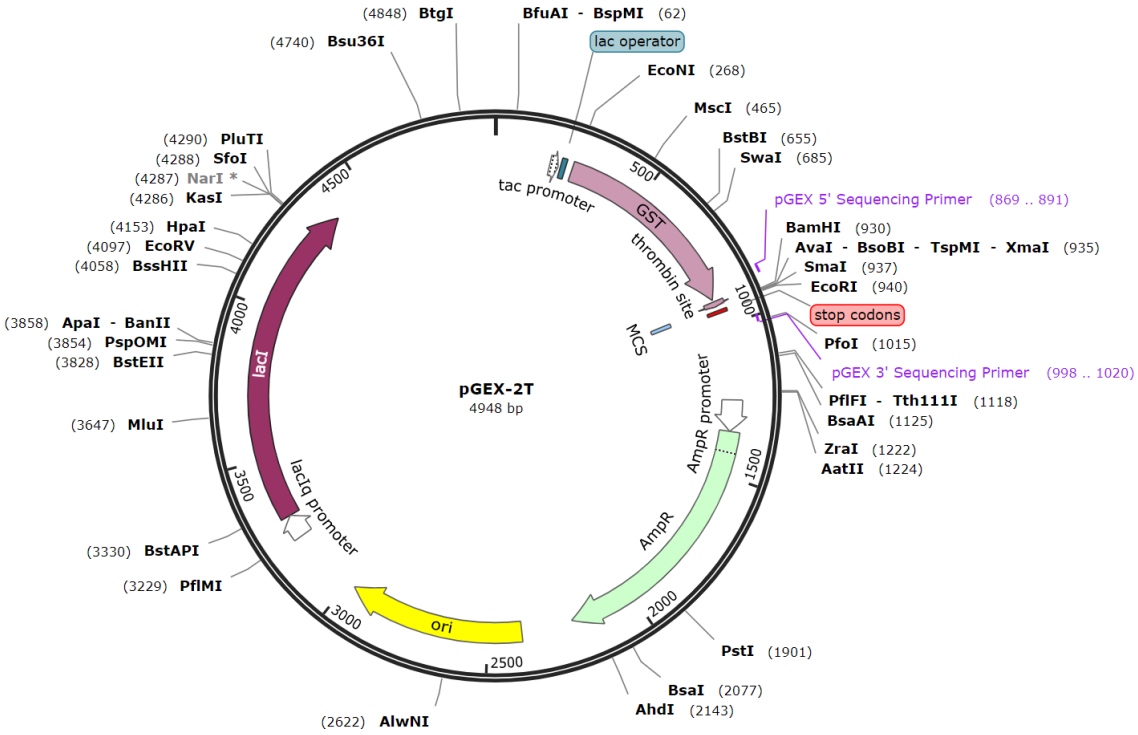

Figure 9. Vector map of the pGEX-2T plasmid

Schematic map illustrating its key features, including the GST-fusion tag and the inducible hybrid *tac* promoter, for bacteria expression. The map was generated in SnapGene Viewer.

Transfer vectors

pΔM071tdTmt and pΔM115gfp

These plasmids were designed *in silico* in the lab and ordered to be synthetized by IDT. pΔM071tdTmt or pΔM115gfp plasmids contained a reporter gene flanked by approximately 500 bp downstream (left flank, LF) and upstream (right flank, RF) homologous sequences of either *m071l* or *m115l* MYXV ORFs.

Reporter genes were cloned to maintain the same orientation as the genes being replaced, mimicking the conditions from the original viral genome, and both GFP and tdTomato genes, were cloned under the control of a synthetic early/late poxvirus promoter.

pHiFi

pHiFi plasmid was constructed and provided by Dr. K. Dalton. Briefly, the pHiFi contains genes encoding the selectable marker proteins, guanosine phosphoribosyl transferase (gpt), eGFP and β-glucuronidase (β–gus). These marker genes were cloned between the restriction enzyme sites

*EcoR*I and *Hind*III of pUC19 (Thermo Fisher Scientific). Selectable marker genes were under the control of p7.5 (*gpt*) or pE/L (*eGFP* and β–*gus*) and separated by multiple cloning sites OV2 and OV3 (Figure 10). Restriction sites within OV2 and OV3 can be used to clone homologous regions to the MYXV genome immediately surrounding the target gene, to direct homologous recombination for recombinant virus construction.

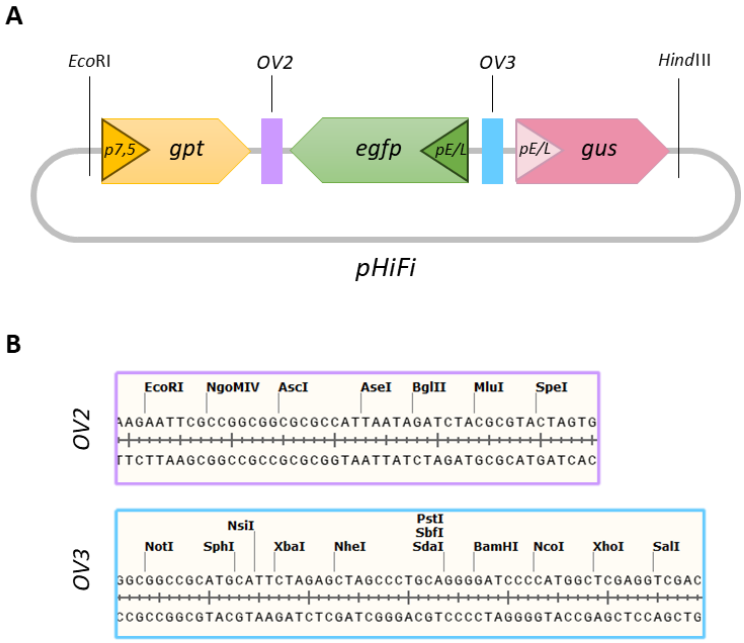

Figure 10. Feature map of the transfer vector pHiFi, illustrating the key elements.

A) pHiFi includes the marker gene eGFP for fluorescence-based identification, and two resistance genes: *gpt,* driven by the p7.5 poxvirus promoter, and *gus* driven by the pE/L promoter. B) The regions OV2 and OV3 have single restriction sites, allowing for the cloning of desired flanking regions essential for homologous recombination.

Commercial antibodies

Table 2. Antibodies and their working dilution regarding their technical use

Antibody	Manufacturer	Working dilution
Mouse Anti-6X HisTag monoclonal antibody	Sigma-Aldrich, Taiwan	1:3000-1:4000 in WB 1:125 in IF
Mouse Anti-GST monoclonal antibody	Sigma-Aldrich, Israel	1:4000 in WB
Rabbit Anti-GFP (N-terminal) antibody	Sigma-Aldrich, Israel	1:5000 in WB
IRDye® 800CW conjugated Goat (polyclonal) anti-Mouse IgG (H+L), Highly Cross adsorbed	LI-COR Biotech,	1:20000 in WB

Goat anti-rabbit IgG (H+L) Highly Cross-adsorbed secondary antibody, conjugated with Alexa Fluor Plus 800	Invitrogen, USA	1:20000 in WB
Goat HRP-conjugated anti-rabbit IgG (whole molecule)	Sigma-Aldrich, USA	1:6000; 1:12000 in ELISA
Goat anti-rabbit IgG (H+L) Cross-Adsorbed Secondary Antibody, conjugated with Alexa Fluor™ 350	Life Technologies, Eugene, USA	1:1000 IF
Goat anti-rabbit IgG (H+L) Secondary Antibody, conjugated with Alexa Fluor ™ 488	Life Technologies, Eugene, USA	1:1000 IF
Goat anti-rabbit IgG (whole molecule) Secondary Antibody conjugated with FITC	Sigma-Aldrich, USA	1:250 IFAT
Goat anti-mouse IgG (H+L) Secondary Antibody, conjugated with Alexa Fluor ™ 633	Life Technologies, USA	1:1000 IF

Note: Immunofluorescence staining (IF), Indirect immunofluorescence antibody technique (IFAT), Western blot (WB)

Sera

The rabbit sera samples used in this Thesis were derived from three distinct sources, and for this reason were separated in 3 different panels. PANEL 1 and PANEL 2 were obtained from experimental vaccination/challenge experiments performed before the commencement of this Thesis, in which New Zealand White rabbits were vaccinated and subsequently challenged with Lu-MYXV. PANEL 3 comprised samples from naïve young rabbits that had not been exposed to MYXV vaccination or challenge.

Anti-MYXV rabbit immune sera from experimental vaccination/ challenge experiments

Anti-MYXV immune sera had been previously obtained from animal experimentation using New Zealand White rabbits that were vaccinated and subsequently challenged with Lu-MYXV. Two experiments were performed before the commencement of this thesis.

PANEL 1: Procedures for this experiment were approved by the Animal Ethics Committee of the University of Oviedo and authorized by the Consejería de Agroganadería y Recursos Autóctonos of the Principlaity of Asturias, Spain. The authorization code PROAE 22/2017 was assigned to the authorization. All the procedures were carried out in accordance with Directive 2012/63/EU of the European Parliament and the Spanish RD53/2013. A total of 161 rabbit sera samples were obtained from this experiment.

PANEL 2: This experiment was carried out at the University of Leon in the Animalario facility. The experiment was approved by the ethical committee board of the University of Leon. A total of 18 rabbits were used. Six were infected experimental, while 12 were vaccinated and one month later used in challenge experiments. Blood samples were obtained at 4 different time points, obtaining a total of 64 sera samples.

To obtain sera; peripheral blood was collected from the marginal ear of vaccinated/challenged rabbits at different time post vaccination/challenge to allow for a study of kinetics of anti-MYXV Ab production following vaccination/challenge. Blood was allowed to clot, and the sera separated using standard protocols and stored at -20°C until used. The presence of anti-MXYV Abs in all sera were confirmed using commercially available ELISAs.

Sera from naïve young rabbits

A total of 12 non-vaccinated 2-month old wild rabbits (*O. Cuniculus*) were kept in individual cages and were subjected to weekly blood sampling, obtaining a total of 34 samples. In general, whole blood (0.5-1ml) was collected into sterile tubes from jugular veins and sent to the laboratory, where sera were separated as described above.

Viral strains

MYXV Lausanne

Lausanne myxoma virus strain (Lu-MYXV) is considered the international reference MYXV strain (ATCC VR-115). This viral strain, also called Brazil Campinas/1949, as it was isolated in Brazil in 1949, and kept in the *Laboratoire de Bacteriologie in Lausanne* (Switzerland). It experienced less than five rabbit passages; maintained a very virulent profile, with almost 100% mortality rate in laboratory rabbits. In June 1952, Lu-MYXV was used in the epizootics in Europe, through the inoculation and later liberation of two wild rabbits in a region close to Paris (F. Fenner & Marshall, 1957). The virus has since been endemic in Europe.

MYXV Lausanne-GFP

Lausanne-GFP myxoma virus strain (Lu-GFP-MYXV) was produced in the laboratory as part of the Master´s final research project entitled “Diseño de un virus recombinante de Mixoma Virus (Lausanne) con expresión de GFP” by Sandra Presa Muñiz (Máster en Biotecnología del medio ambiente y la salud, course 2015-2017, University of Oviedo).

MYXV vaccine Léon162

The León162 (L162) MYXV strain (denominated Vac-MYXV in this thesis) is an attenuated strain was isolated in 1976 by Laboratorios Ovejero S.A., León, Spain, commercial name Pox-Lap, although this vaccine is not currently commercially available in Spain. The original isolate was passed 40 times in embryonated hens' eggs and 120 passes in cell culture (Arguello Villares 1986). The vaccine was used for many years on the Iberian Peninsula as a homologous live-attenuated strain. Our laboratory isolated the vaccine strain in cell culture (RK-13 cells) from a vaccine vial (Z008A) and was passaged a maximum of 3 times to amplify a working stock.

Prokaryotic cells

One-Shot™ TOP10 chemically competent E. coli.

The One-Shot ™ TOP10 chemically competent cells have a high transformation efficiency (ThermoFisher Scientific). Their genotype is F- mcrA Δ(mrr-hsdRMS-mcrBC) Φ80lacZΔM15 Δ lacX74 recA1 araD139 Δ(araleu)7697 galU galK rpsL (StrR) endA1 nupG. This strain is suitable for cloning and stable production of high amounts of plasmid copies. The *rec*A1 genotype helps reducing the non-specific DNA recombination, and the mutation in endonuclease I (*end*A1) gets rid of the non-specific digestions.

DH5α chemically competent E. coli.

DH5α chemically competent cells (genotype F- Φ80lacZΔM15 Δ(lacZYA-argF) U169 recA1 endA1 hsdR17(rk-, mk+) phoA supE44 thi-1 gyrA96 relA1 λ-) also have high transformation efficiencies, are suitable for rutinary subcloning events. This strain contains the *recA1* and *endA1* mutations that improve the stability of the plasmid insertion, besides increasing the yield and quality of the DNA produced. The lacZΔM15 mutation produces a dysfunctional β-galactosidase enzyme and facilitates the blue/white screening of the transformed bacteria in the presence of X-gal when the plasmid used carries the lacZα gene. Therefore, only the cells that incorporate the plasmid DNA have the functional enzyme that can metabolise the substrate X-gal into a blue product easily distinguishable by the naked eye.

BL21 (DE3) chemically competent E. coli.

The BL21 (DE3) strain's (Invitrogen) genotype is F^{-}*ompT* *hsd*S_B ($r_b^{-}m_b^{-}$) *gal dcm* (DE3). This strain is deficient in the cytoplasmic Lon protease and the outer membrane protease VII (OmpT), in its DNA restriction/methylation system, and its methyltransferase activity. It contains a lambda DE3 prophage carrying the T7 RNA polymerase gene under the control of the mutated *lac* operon

promoter, lacUV5. BL21(DE3) cells are suitable for the inducible high-level expression of heterologous genes.

Eukaryotic cell culture

Spodoptera frugiperda 9 (Sf9)

The insect cell line Sf9 (ATCC® CRL-1711™) (ThermoFisher Scientific) was bought and used according to the manufacturer's instructions. This is a clonal isolate derived from the *Spodoptera frugiperda* cell line IPLB-Sf-21-AE (Vaughn et al., 1977).

High-Five™

The High-Five™ (HF) or BTI-Tn-5B1-4 (ATCC®CRL-10859™) is a *Trichoplusia ni* (cabbage looper) cell line (Granados et al., 1994) that was bought from ThermoFisher Scientific and used according to the manufacturer's instructions.

RK13 cells

RK13 (ATCC® CCL-37™) cell line was isolated from the kidney of a rabbit (*O. cuniculus*). They show epithelial morphology and were obtained from Ovejero Laboratories in 2007. The cell line is the same ATCC CCL-37 but it has been cleared for any potential contamination with bovine viral diarrhoea virus (BVDV).

METHODS

Molecular biology techniques

Nucleic acid manipulation

DNA extraction. Plasmid DNA was produced and extracted from bacteria cultures of different volumes, depending on the purpose for each extraction. Precultures of 2 to 4 ml of individual colonies grown at 37°C with agitation overnight, in LB supplemented with the corresponding antibiotic were used for screening and selection the vector-transformed bacteria clones. The GenElute™ HP Plasmid Miniprep kit (Sigma, USA) was used as described in the manufacturer's guidelines to extract the plasmids produced by the cultured cells. Larger bacteria cultures (100-200 ml) were used for isolating higher amounts of the corresponding plasmid DNA, using the

PureLink™ HiPure Plasmid Filter Maxiprep kit (Invitrogen, Lithuania) in accordance with the manufacturer's instructions.

The QIAmp® DNA mini kit (QIAGEN, Hilden) was used for genomic and viral DNA extraction, following manufacturer's guidelines. Parental MYXV and mutant virus were amplified on RK13 monolayers cultured in 6-well plates until a broad cytopathic effect was noted. MYXV-infected cell cultures were harvested by scrapping the bottom of the well, lysed by freeze-thaw cycles and sonication, and used as starting material for DNA extraction using this kit.

DNA restriction enzyme digestion. Restriction enzymes were used to perform restriction analysis of the cloned plasmids to check the success of the ligation event. All the restriction enzymes mentioned in this Doctoral Thesis were purchased from Thermo Fisher Scientific and belong to their FastDigest product line. They exhibit a high performance and fast digestion activity (10-15 minutes in optimized conditions), and all of them are compatible since they are active in the same digestion buffer.

DNA fragment purification. The Wizard® SV Gel and PCR Clean-up System (Promega, USA) was used to extract and purify diverse DNA molecules, from DNA bands extracted from low-melting agarose gels to PCR products in the amplification reaction mix, and DNA fragments after enzyme digestion. The protocol provided by the manufacturer was followed, and the samples were eluted in 20-50 µl, depending on the starting sample.

DNA quantification. Concentration of the double-stranded DNA samples (plasmids, vectors, extracted DNA, etc.) was measured by fluorometry quantification, using the broad range Qubit dsDNA BR Assay kit (Invitrogen, Eugene, Oregon, US) and the Qubit 2.0 or 4.0 Fluorometers (Invitrogen). Alternatively, some samples were analysed in the NanoDrop Spectrophotometer (ThermoFisher Scientific).

DNA sequencing. The sequence of the DNA fragments and amplicons was obtained by the Sanger sequencing method in the Scientific-Technical Service (SCT) of the Universidad de Oviedo. DNA samples (0.5-1 µg) were sent with the corresponding primer at concentration 5 µM and analysed by the ABI PRISM® 3130xl Genetic Analyzer (Applied Biosystems).

DNA amplification by polymerase chain reaction (PCR)

The polymerase enzyme used throughout this Doctoral Thesis for cloning purposes was the *LA Taq* DNA Polymerase (TaKaRa, China), together with the provided buffer, a proof-reading polymerase with 3'- 5' exonuclease activity that can amplify long and accurate fragments from

their templates. The PCR mix was constituted of the reagents from the *LA Taq* kit (2.5 U/µl TaKaRa LA *Taq*, LA PCR Buffer II 1X, 2.5 mM $MgCl_2$, dNTP mixture of 0.4 mM each) with the addition of the DNA template, and the specific upstream and downstream primer pair at 0.2 µM each.

The GoTaq® Green Master Mix PCR, 2X (Promega,) was used for screening of the viral recombinants, since this mix can be directly loaded onto agarose gels after the amplification reaction. This product is a ready-to-use solution containing optimal concentration of *Taq*DNA polymerase, dNTPs, $MgCl_2$ and the corresponding buffer. The PCR mix was constituted of GoTaq® Green Master mix, 1X, 0.4 µM of the specific upstream and downstream primer pair, and < 250 ng of DNA template, completing with nuclease-free water to 25 µl.

All reactions were carried out in the Mastercycler Personal thermocycler (Eppendorf, Hamburg, Germany).

Agarose gel electrophoresis

For agarose gel electrophoresis of DNA samples, a gel matrix of 1% agarose in TAE buffer (40mM Tris-acetate, 2 mM EDTA, pH 8) acted as support for the DNA movement. The fluorescent Safe View™ Classic Nucleic Acid stain (Applied Biological Materials Inc.) was added to the agarose to visualize the nucleic acids through UV exposure. The samples to be analysed were mixed with 6X Orange DNA Loading Dye (Thermo Scientific, Vilnius) before being loaded into the wells, and the Gene Ruler 1 kb Plus DNA ladder (Thermo Scientific, Vilnius) was added as marker. Samples were run at 90 mV for 30-40 minutes, and the gel was visualized using a transilluminator.

Generation of prokaryotic expression vectors for the characterization of antigenic MYXV protein candidates

pTriEX-*m022l,* pGEX-*gst-m022l* containing the full-length MYXV ORF*m022l* were generated in the laboratory. pET-28a(+) containing the full-length ORF*m029l* and ORF*m115l,* and partial ORF*m071l*, ORF*m083l* and ORF*m141r,* were designed and were synthesized commercially (Genscript).

Generation of multivalent expression vectors for the characterization of MYXV M022, M071 and M115 proteins

The GST-m022l expression cassette in pGEX-*gst-m022l* was cloned in the pTriEX-1.1 expression vector (Figure 11). Additionally, the full-length ORF*m071l* and ORF*m115l* genes were also cloned into pTriEX-1.1 using amplicons generated from Lu-MYXV viral gDNA extracted from a RK13

infected culture as template. For each cloning reaction, a pair of primers were designed with the appropriate restriction sites (*Bsa*I and *Xho*I for GST-*m022l* amplification; *Nco*I and *Xho*I for *m071l* and *m115l*) and were synthetised and purchased from SIGMA (Table 3). The cycling conditions for PCR amplification of the *m022l* candidate gene involved a gradient of annealing temperatures for the first 5 cycles of amplification of (45, 46.4, 48.4, 50.9, 54.4, 57.1, 58.9 and 60ºC) to identify the condition giving the highest specificity and efficiency of primer binding. The protocol followed was initial denaturation at 95ºC for 5 minutes, 5 cycles of 95ºC for 30 seconds, 30 seconds at one of gradient temperatures mentioned, and 2 minutes at 72ºC, and then 40 cycles of 95ºC for 30 seconds, 57ºC for 30 seconds, and 72ºC for 2 minutes, with a final 5-minute extension at 72ºC. The cycling conditions for PCR amplification of the ORFm071l and ORFm115l from gDNA were 3-minute denaturation at 94 ºC, 30 cycles of 94ºC for 30 seconds, 55ºC for 30 seconds, and 68ºC for 45 seconds, followed by a final 5-minute final extension at 68ºC.

Table 3. Sequences of primers used in the cloning PCR for the generation of GST-m022l and full-length ORFm071l and ORFm115l amplicons

PCR AMPLICON	***AMPLICON SIZE***	***PRIMER ID***	***NUCLEOTIDE SEQUENCE (5'-3')***
GST-m022l	1835 kb	Fw_m022l_BsaI	GTCATACTGCACGGTCTCAC**ATGTCCCCTATACTAG**
		Rv_m022l_XhoI	CATTGCACTAGTCTCGAG**GTTTTTTACCACCG**
m071l	1003 pb	Fw_m071l_NcoI	CAGTCAGTCACC**ATGGCGTCTCCTAGCAAAAC**
		Rv_m071l_XhoI	TGACTGACTGCTCGAG**CACGATGTACGTGATTAACG**
m115l	595 pb	Fw_m115l_NcoI	CAGTCAGTCACC**ATGGATAGAGTGTTGTCG**
		Rv_m115l_XhoI	TGACTGACTGCTCGAG**TAGAGCGCCCGTTTGAGC**

Note: Bold bases indicate the region that hybridizes with the target sequence on the template DNA. Underlined bases represent the restriction sites of BsaI, NcoI or XhoI enzymes, as appropriate.

PCR amplicons were analysed by agarose gel electrophoresis and purified using the Wizard PCR Clean-up system (Promega). GST-m022l amplicon was digested at 37ºC for 20 minutes with the BsaI-FD and XhoI-FD (Thermo Scientific, Vilnius) restriction enzymes in FastDigest 10X buffer, while the m071l and m115l amplicons were digested with NcoI-FD and XhoI-FD (Thermo Scientific, Vilnius). Then, digested DNA products were column purified and cloned in a 3:1 molar ratio (insert to vector) into the pTriEX-1.1 vector at the NcoI and XhoI sites. Ligation reactions were catalyzed by the T4 DNA ligase enzyme overnight at 16ºC.

The resulting recombinant plasmids, designated as pTriEX-gst-m022l, pTriEX-m071l and pTriEX-m115l were introduced into chemically competent *E.coli* DH5α cells via heat shock transformation, followed by selection in presence of ampicillin. Multiple colonies were screened

for the presence of the recombinant vectors and correct target gene insertion by restriction enzyme analysis and confirmed by colony PCR and Sanger sequencing.

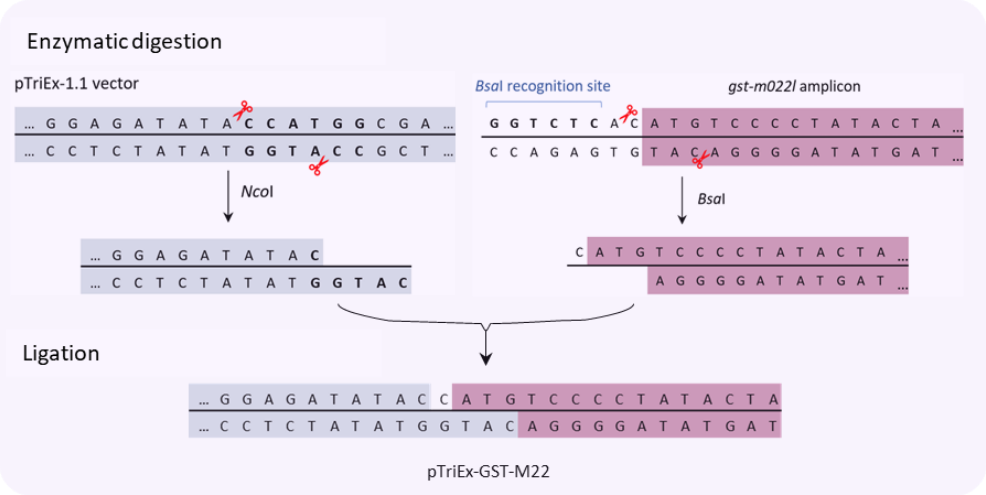

Figure 11. Schematic presentation of the pTriEX-GST-m022l construction.

5'-end ligation of the 1,8 kb fragment GST-m022l amplified from pGEX-GST-M022L double-digested with BsaI and XhoI. The resulting construct loses the restriction site at this end.

Generation of pHiFiΔm022lgfp, pHiFiΔm071ldTmt, and pHiFiΔm115gfp transfer vectors

Δm071l*tdTmt* and Δm115*gfp* expression cassettes were amplified using a PCR cloning process from the pΔM71*tdTmt* and pΔM115*gfp* plasmids, respectively. A *Bgl*II restriction site was incorporated at the 5' end of the amplicon, and a *Xho*I restriction site was incorporated at the 3' end of each amplified cassette. And the Δm022l*gfp* cassette was amplified from the *F1F2* ΔM022*gf* vector (Figure 12).

PCR amplifications were performed *using* the TaKaRa LA Taq® kit reagents in a 50 µl reaction volume containing PCR buffer II (with $MgCl_2$) 1X, 0,4 mM of each dNTP, 0.2 µM of each primer (Table 4), 2.5 U of Taq polymerase, and 30 ng of template DNA (pΔM71*tdTmt,* pΔM115*gfp and F1F2* ΔM022*gfp*). Initial denaturation was conducted at 95°C for 5 minutes, followed by 35 cycles of 95°C for 30 seconds (denaturation), 56°C for 30 seconds (annealing), and 72°C for 2 minutes (extension), with a final extension at 72°C for 5 minutes. Amplification products were purified and quantified using the BR dsDNA kit (Qubit 2.0).

pHiFi was digested with *Bgl*II, *Xho*I and *Not*I, to release a 750 pb fragment corresponding to the eGFP gene, plus a small 40 pb fragment generated from the *Xho*I and *Not*I combination in the

OV3 MCS. The 3 amplicons (Δm022*gfp-BX*, Δm071*tdTmt-BX* and Δm115*gfp-BX)* were digested with *Bgl*II and *Xho*I, pHiFi was digested with *Not*I too. Digestion products were purified, quantified, and the amplicons were mixed with the linearized pHiFi vector at a molar ratio 3:1 (insert to vector) using 2.5 Weiss Units of T4 DNA ligase (Thermo Fisher Scientific) and incubating 30 minutes at 22°C.

Table 4. Primers used in PCR cloning for the generation of ΔM022gfp-BX, ΔM071tdTmt-BX and ΔM115gfp-BX amplicons.

PCR AMPLICON	***PRIMER ID***	***NUCLEOTIDE SEQUENCE (5'-3')***
Δm115gfp-BX	Fw_LF_m115l_*Bgl*II	GTCAATCAAGAGATCT**GCTAAGGTGTTTATGGGCCCCATC**
	Rv_RF_m115l_*Xho*I	CATAGGATCGCTCGAG**TTAAAGTAAATGAACCCCGTTAC**
Δm071tdTmt-BX	Fw_LF_m071l_*Bgl*II	GTTAAGTATTAGATCTG**TGTCCACGGTCTGTTTCTTCGTG**
	Rv_RF_m071l_*Xho*I	CATAGACCTACTCGAG**CCTAAGGAATTGGCCGCAGATAC**
Δm022gfp-BX	Fw_LF_m022l_*Bgl*II	GTTAACCATAAGATCT**TTCACGAACCTATACGCCTC**
	Rv_RF_m022l_*Xho*I	CTAAGTAGACCCTCGAG**TTACGTTATCAGAACTGTTG**

Note: Bold bases indicate the region that hybridizes with the target sequence of the template DNA. Underlined bases represent restriction sites of BglII and XhoI enzymes.

Competent cells (One Shot TOP10 Chemically Competent *E.coli*) were transformed with 5 µl of the ligation mixture and incubated overnight on LB-ampicillin-agar plates at 37°C. Multiple colonies were piked and screened for the presence of the recombinant vectors and correct target gene insertion by restriction enzyme analysis with *Bgl*II and *Not*I. confirmed by colony PCR and Sanger sequencing. The plasmids from clones giving the expected restriction pattern were sequenced by Sanger sequencing and used for further experiments.

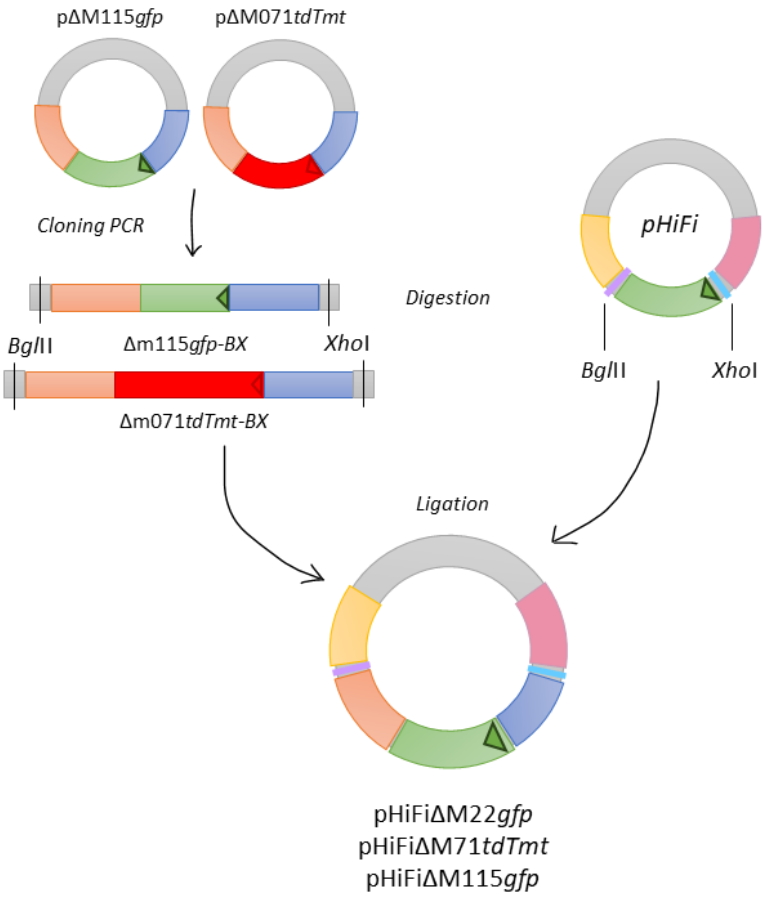

Figure 12. Construction of the pHiFiΔM022gfp, pHiFiΔM071tdTmt, and pHiFiΔM115gfp transfer vectors.

A cloning PCR added a *Bgl*II restriction site at 5'end and *Xho*I site at the 3'end of the generated amplicons (ΔM022gfp-BX, ΔM071tdTmt-BX and ΔM115gfp-BX) that contained the reporter fluorescent gene (eGFP or tdTomato) and flanking regions (LF, RF) from the corresponding target genes (*m022l, m071l, m115l*). Inserts and pHiFi3 vector digested with *Bgl*II and *Xho*I were ligated leading to the generation of the transfer vectors; pHiFiΔM022*gfp*, pHiFiΔM071*tdTmt*, and pHiFiΔM115*gfp*.

PCR validation of recombinant Vac-MYXV mutant isolates

The purity of recombinant viruses following selection and 3 rounds of plaque purification was verified by PCR analysis and subsequently confirmed by DNA sequencing (Broder & Earl, 1999). Each plaque isolate was amplified using 300 µl of each sonicated foci isolate, on 70% confluent RK13 cultures in 6-well tissue culture plates (seeded at 5×10^5 cells/well seeded 18 h prior to infection). Following 7 days of incubation, cultures were harvested by scrapping the surface of each well, and cells were homogenized, lysed by three freeze-thaw cycles, and sonicated in an ice water bath for three consecutive 30-second intervals. 200 µl of each infected cell lysate was used for DNA extraction using the QIAamp® DNA mini kit (QIAGEN, Hilden).

Two PCR reactions were designed for this validation (Table 5). The first one involved using a forward primer that hybridized to the 5' region upstream of the target gene, and the reverse primer that hybridized within the fluorescent marker sequence (gfp). The second reaction involved two primers that hybridize in the genes flanking the target locus; therefore, amplification would occur independently of the viral genome template. PCR reactions were performed with the GoTaq® Green Master Mix PCR, at the conditions described previously (*DNA amplification section*). Initial denaturation was conducted at 95°C for 5 minutes, followed by 35 cycles of 95°C for 30 seconds, 56°C for 30 seconds, and 72°C for 1 minute, with a final extension at 72°C for 5 minutes. Amplification products were directly analyzed in a 1% agarose gel. The amplicons of foci clone isolates with the correct band pattern were purified and quantified using the BR dsDNA kit (Qubit 2.0) and sequenced by Sanger (Table 6).

Table 5. Primers used in the PCR validation reactions for the mutant MYXVs

ID PRIMER	*5'-3' NUCLEOTIDE SEQUENCE*
Δm022 Fw in	GGACACGGATACCATCGATTTTAC
Δm022 Rv in	GTGGAGTGAGACGATGGATG
TransVect gfp Rv1	CCACAAGTTCAGCGTGTCC
Δm115 Fw in	GGAGACATTACAGCGAACATCC
Δm115 Rv in	CTACATCCACTCATTCCAG

Table 6. Primers used for sequencing and characterization of mutant MYXV

ID SEQUENCING PRIMERS	*5'-3' NUCLEOTIDE SEQUENCE*
Δm022 Fw out	GACGGAGAGGAAAGACGTTC
Δm022 Fw in	GGACACGGATACCATCGATTTTAC
Δm022 Rv out	GAATCCGTTCAAGCACATGAATCG
Δm022 Rv in	GTGGAGTGAGACGATGGATG
Δm115 Fw out	GACGAGGTCATTAACGACAAG
Δm115 Fw in	GGAGACATTACAGCGAACATCC
Δm115 Rv out	GGATGCAACGCACGACTC
Δm115 Rv in	CTACATCCACTCATTCCAG
F- GFP in	CTTGAAGTTCACCTTGATGCC
TransVect gfp Rv1	CCACAAGTTCAGCGTGTCC
TransVect gfp Fw2	GCTTCATGTGGTCGGGGTAG
TransVect gfp Rv2	GTACAACTACAACAGCCAC

Protein manipulation techniques

Protein quantification. Protein quantification was performed using the Qubit® 2.0. Fluorometer (Thermo Fisher Scientific) with the Qubit Protein Assay kit (Invitrogen). Samples were measured at least in duplicate.

Polyacrylamide gel electrophoresis

Protein extracts obtained from cell lysates, and the purified recombinant protein samples were analysed by a discontinuous electrophoretic system based on a method developed by Ulrich K. Laemmli, the sodium-dodecyl sulphate-polyacrylamide gel electrophoresis (SDS-PAGE). Stacking gel at pH 6.8 and 3.5 % of acrylamide (in 0.5 M Tris-HCl pH 6.8, 0.4% SDS), and a resolving gel at pH 8.8 and 10-12 % acrylamide (in 1.5 M Tris-HCl pH 8.8, 0.4% SDS). The samples were mixed with Laemmli loading buffer, giving a final concentration of 0.125 M Tris-HCl, 2% SDS, 0.62% 2-mercaptoethanol, 8.75 % Glycerol and bromophenol blue colorant; and heated at 90°C for 10 minutes.

The monomeric acrylamide and N,N'-metilenbisacrylamide in their corresponding buffers, were mixed with the compounds TEMED and ammonium persulphate (APS), which are the source of the free radicals needed to initiate the polymerization reaction. The mixture was then poured between two glass plates, where the polymer matrix settled. The molecular mass marker, PageRuler™ Prestained NIR Protein Ladder (Thermo Fisher Scientific), was added to every gel to determine de approximate mass of the proteins of interest. After loading the protein samples, a voltage gradient (150 mV) was applied to the tank containing Tris-Glycine buffer.

At the end of the run, the proteins in the gel were visualized through a non-specific stain with Coomassie Brilliant Blue solution (45% methanol, 10% acetic acid, 0.25% Brilliant blue), to confirm their presence and abundance. Afterwards, the gel was destained with a solution composed of 7.5% acetic acid and 10% methanol until the protein bands could be seen individually. The molecular marker LMW (Thermo Scientific™) was used to do a semiquantitative determination of the amount of the purified recombinant protein stocks.

Western blot

The recognition and identification of specific proteins in a complex mixture was conducted by the Western blot immunoassay. After the initial protein separation according to their size by SDS-PAGE, samples were transferred to a 0.2 µm nitrocellulose membrane (Bio-Rad) through a semi-dry electro transfer system (Semi-Phor TE70, Hoefer Scientific Instruments, California, USA). In this system, a sandwich set up was prepared in which the polyacrylamide gel was in

contact with the nitrocellulose membrane, and with two pieces of blotting filter paper soaked in transfer buffer (25 mM Tris, 192 mM glycine, 20% methanol, pH 8.8). Three more transfer buffer-soaked filter papers must be underneath the nitrocellulose membrane. The filter papers are in direct contact with the plate electrodes, so that after applying a constant voltage the proteins migrate from the gel to the membrane.

Subsequently the membrane was blocked with a 5% skimmed milk solution in PBS for one hour at room temperature, or overnight at 4°C. Then, it was washed with PBST (PBS with 0.5% Tween-20) twice for 5 minutes each time, membranes were incubated with primary antibodies diluted in PBST with 0.5% skimmed milk at their working dilutions (*see Materials*). After one hour of incubation on a shaker at room temperature, the membrane was washed again with PBST, and the corresponding conjugated secondary antibody diluted 1:20000 in PBST with 0.5% skimmed milk was added. Since the secondary antibodies are conjugated with fluorescent dyes, this last incubation was done in the dark to avoid dampening their performance by photobleaching. One hour later, the membrane was thoroughly washed with PBST, and it was visualized using the Odyssey Infrared Imaging system (LI-COR Biosciences).

Dot-blot

This immunodetection technique was used to determine the antigenicity of the "native" conformation of the purified recombinant viral protein stocks. In brief, a small volume of the purified proteins was directly added (placed in dots) to a nitrocellulose membrane and left to air dry. In the next step, the free sites of the membrane were blocked with the 5% skimmed milk in PBS solution, to prevent the non-specific binding of the antibodies. After one hour of incubation, the membrane was washed twice with PBST, and a 1:300 dilution of the MYXV-positive control and MYXV-negative control rabbit sera in PBST containing 0.5% skimmed milk were added. Following two consecutive washes with PBST, the secondary anti-rabbit IgG antibody, conjugated to a fluorophore, was added to the membrane, and incubated for 45 minutes at room temperature. After that, the membrane was washed with PBST, and the result of the assay was visualized in the Odyssey system.

Cellular biology techniques

Culture of prokaryotic cells

Cells in suspension were cultivated at 37°C with agitation in Luria-Bertani (LB) broth (SIGMA, USA). For the preparation of solid medium, 15 g/l of agar was added to the LB media. These commercial competent *E.coli* strains were either used for the plasmid DNA propagation, or the

expression of heterologous gene. When needed, the addition of ampicillin (final concentration of 100 µg/ml) or kanamycin (final concentration of 50 µg/ml) were added to the liquid or solid media culture. LB was supplemented with glycine betain and sorbitol (LB-B/S) in a few expression screening conditions of the recombinant proteins.

Screening of recombinant protein expression in E.coli

Each recombinant plasmid construct (pTriEX-m022l, pGEX-2T-m022l, TriEX-gst-m022l, pTriEX-m071l and pTriEX-m115l) or purchased expression vector (pET28-m029l, pET28-m071l, pET28-m083l, pET28-m115l, pET28-m141r) was transformed into BL21(DE3) E. coli cells following the protocol provided by the manufacturer. Individual colonies grown from a single positively transformed bacteria were isolated and selected in LB-agar plates containing the corresponding selection antibiotic after an overnight incubation at 37°C.

Small-scale BL21(DE3) cultures from these colonies were grown in 2-3 ml of LB/selection antibiotic media to confirm correct expression of the intended construct. Expression was induced with 1 mM IPTG for 1 hour in a shaker at 37°C. Non-induced aliquots from the same colonies were used as negative controls for each colony. Then, bacteria cultures were centrifuged at 2600 g for 10 minutes, and the resulting pellets were resuspended in Laemmli 1X dissociation buffer for further analysis by SDS-PAGE and Western blot.

Scale-up of recombinant protein expression in prokaryotic system

A single colony of bacteria transformed to express each recombinant viral protein was selected and was used to inoculate larger culture volumes (usually 50 ml LB + selection antibiotic). The initial solubility screening protocol included the bacteria culture incubation at 37°C until reaching the mid-log growth phase (OD600 ≈ 0.5), and protein expression induction by addition of 1 mM IPTG for 1.5 hours. Then, cells were harvested by centrifugation at 4°C for 10 minutes at 2600 g, and pellets were stored at -20°C.

Expression of recombinant proteins in native conditions

Bacteria pellets of transformed BL21(DE3) thawed on ice and resuspended in lysis buffer, PBS containing 1 mM DTT, 1% Triton X-100, DNaseI (2.5 µg/ml) and Lysozyme (0.2 mg/ml). Samples were incubated on ice for 30 minutes and were sonicated on ice avoiding foam formation in a probe sonicator (Digital Sonifier ® from Branson, Connecticut, US). Bacteria were lysed using a setting of 20% amplitude, applied in 3 cycles of 2 minutes of active sonication each, delivered in 20-second pulses (On) interspersed with 30-second rest (Off) intervals. Cell debris was removed by centrifugation at 41400*g* at 4°C for 25 minutes, and supernatants (soluble fraction, SF) were

collected to further purification of the corresponding recombinant proteins. The pellet, containing the insoluble components, was resuspended in the same buffer and the same volume previously used for the lysis (insoluble fraction, PF).

In this study, induction and incubation conditions were optimized to improve the yield of native recombinant proteins in the soluble fraction. This involved varying some parameters for each construct, such as the incubation temperature (18°C, 30°C, 37°C), inducer concentrations (0.2 mM, 1 mM IPTG), incubation time (1 h, 1.5 h, 3 h, overnight), and media composition (LB alone or LB-B/S).

Solubilization screening of recombinant proteins

Pellet from induced bacteria cultures were thawed on ice and resuspended in 20 mM Tris-Cl pH 7.4 lysis buffer containing 10 mM imidazole, DNaseI (2.5 µg/ml) and Lysozyme (0.2 mg/ml) and protease inhibitors. After 30 minute-incubation, cells were sonicated (20% during 2 working minutes, 20 seconds on and 30 seconds off) and clarified at 900g for 30 minutes at 4°C. The pellet (P1) was discarded, and the supernatant (S1) was divided in 4 Eppendorf tubes and were centrifuged at 20000g for 1 hour at 4°C. The resulting pellets (P2) were resuspended in Tris-Cl buffer pH 7.5 non-supplemented, or supplemented with 1% of either Tween-20 (A), IGEPAL/NP-40 (B) or Triton X-100 (C) non-ionic detergents, followed by one hour of incubation in rotation at 4°C. The samples were centrifuged at 20000g during 1 hour at 4°C, supernatants (S3, S3-A, S3-B, S3-C) were stored at -20°C and the process was repeated with the corresponding pellets (P3, P3-A, P3-B, P3-C), which were resuspended in Tris-HCl buffer pH 7.5 without detergents or containing 2% of the same non-ionic detergents. Then samples were centrifuged at 20000g during 1 hour at 4°C, supernatants (S4, S4-A, S4-B, S4-C) were collected, and the pellets were resuspended in buffer R. All samples were stored at -20°C and they were analysed by SDS-PAGE and Western blot (targeting the marker tag) to evaluate the efficacy of recombinant proteins solubilization mediated through consecutive incubations with each detergent.

Isolation and solubilization of bacterial inclusion body recombinant proteins

The protocol followed for the isolation and solubilization of inclusion bodies was developed by integrating several steps and guidelines established in other reference protocols, to ensure more reliable outcomes (A. Kumar et al., 2012; Qiagen, 2003).

Bacteria pellets of induced BL21(DE3) were frozen at -20°C, thawed on ice and resuspended in resuspension buffer (buffer R): 100 mM NaH_2PO_4, 10 mM Tris, 10 mM imidazole, pH 8.0. Following sonication and incubation with DNase I (10 µg/ml), bacteria lysates were cleared by

centrifugation at 21130 g, 20 minutes at 4°C. The supernatant (S1) was discarded, and the pellet (P1) containing the insoluble components, including inclusion bodies, was washed once with a buffer containing Triton X-100, pH 8 (buffer W). Upon resuspension, the samples were incubated for 1 hour at 4°C on a rocking platform, clarified at 21130 g, 20 minutes at 4°C. After each washing cycle, supernatants (S2, S3) were removed, and the final pellet (P3), enriched with inclusion bodies, was resuspended in freshly prepared solubilization buffer (buffer S), consisting of buffer R supplemented with 8M urea. Modifications of this buffer were also explored, such as the addition of 10 mM β-mercaptoethanol (β-ME) alone, or in combination with 1% Triton X-100, to improve the yield of soluble purified protein. Samples resuspended in buffer S (and derivates) overnight incubation on a rocking platform at 4°C was followed by a final centrifugation at 21100 g for 20 minutes. Finally, supernatants containing denatured proteins (S4) were collected and stored at -20°C.

Culture of eukaryotic cells

Insect cell clines Sf9 and HF can grow either as an adherent monolayer or in suspension, at 28°C in a non-humidified, ambient air-regulated incubator. They were maintained in Sf-900™ II SFM (1X) media (Gibco, UK) supplemented by 1X of the antibiotic and antimycotic product Anti-Anti (Gibco, USA) and although serum addition is not required, in some situations, Foetal Bovine Sera (FBS) (Gibco, Brazil) was added to a final concentration of 2-5%.

Mammalian cell lines RK13 were grown in Dulbecco's Modified Eagle Medium (DMEM) (Gibco/Thermo Fisher Scientific, UK) containing glucose and L-glutamine, and supplemented by anti-anti 1X and FBS to a final concentration of 5-10% (DMEM-5 or DMEM-10, respectively). Mammalian cell lines were cultured in a humidified incubator at 37°C and 5% CO_2 concentration.

Baculovirus Expression Vector System (BEVS)

To generate the recombinant baculovirus (rBV), Sf9 cells at around 85% confluence in 35 mm culture dish were co-transfected using the transfection reactive Cellfectin™ II Reagent (Gibco, Carlsbad, Canada), with a mixture of 500 ng of linearized AcMNPV and 500 ng of the transfer vector pTriEx-1.1 containing the selected viral transgene: r*m022*-pTriEx-1.1, r*m071*-pTriEx-1.1 and r*m115*-pTriEx-1.1 (see section … for vector construction) (Figure 13). The strategy was based on (Zhao et al., 2003).

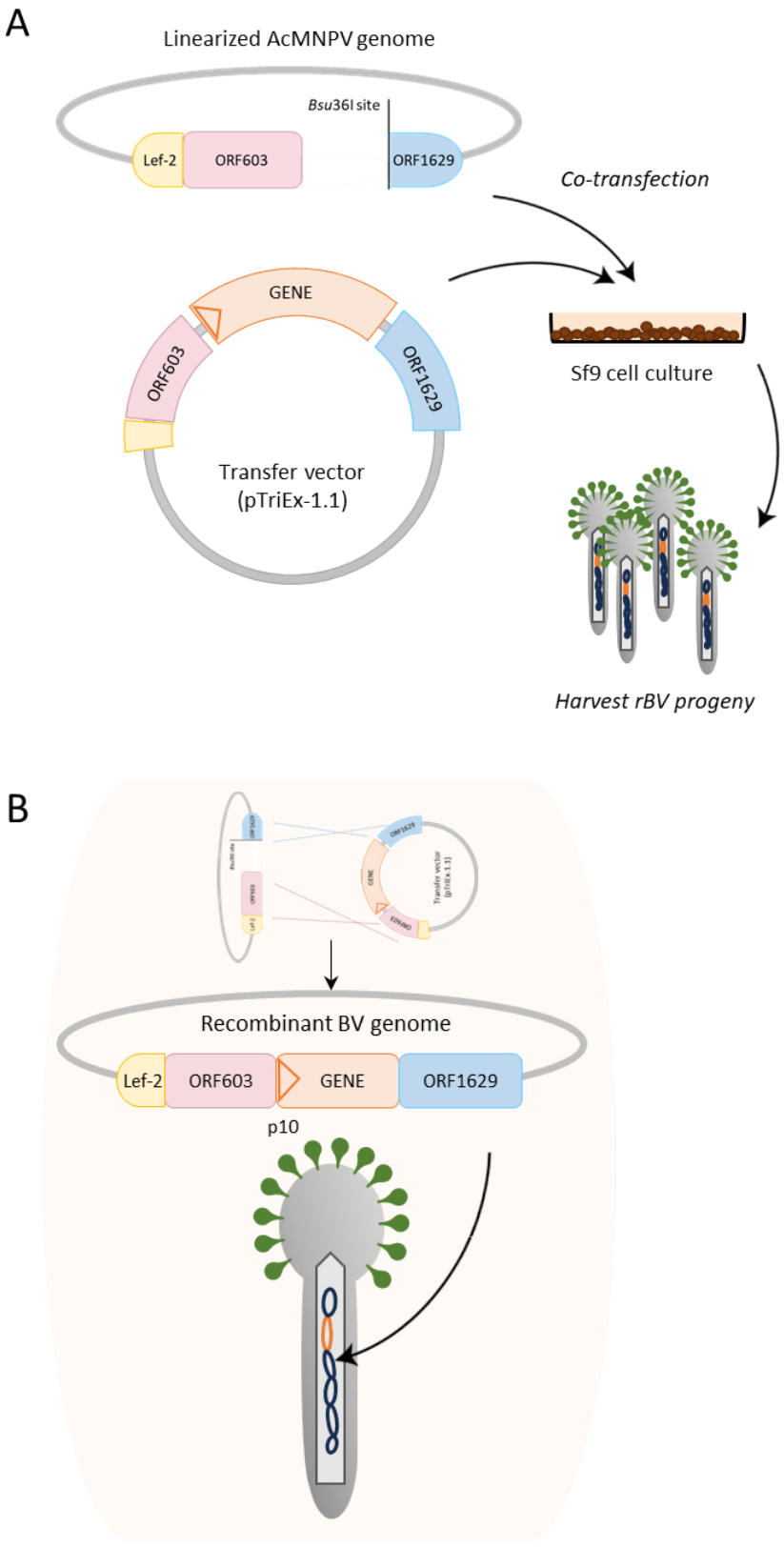

Figure 13. Construction of rBVs using a knockout viral AcMNPV genome lacking a functional ORF1629.

A) Schematic design of the elements involved in the generation of the rBVs: a donor plasmid containing the gene of interest, the viral genome, and a culture of insect cells. B) Recombination events occurring inside a cell that has been cotransfected with both elements, and the resulting rBVs.

Supernatants (P0) containing the recombinant baculovirus were collected 72 h after transfection and centrifuged for 10 minutes at 15900 g to get rid of cellular debris. P0 samples were used to infect at 1:20 (v/v) dilution a fresh Sf9 culture in Insect-XPRESS™ Protein-free Insect Cell Medium (Lonza) supplemented with 5% FBS in a T75 culture flask. Cells were incubated 96h in a humified incubator at 28°C, and baculovirus were harvested from the cultures by collecting the supernatant. They were centrifuged at 300 ×g for 10 minutes to remove any cellular debris and were stored at 4°C until further use, as virions are stable and can maintain their integrity up to years stored in serum-supplemented growth media in this condition. Further viral amplification and serial passaging might result in accumulation of mutations and defective particles (Kool et al., 1991).

Recombinant baculovirus (rBV) titration

The virus titer of each recombinant baculovirus stock (rBV-M022, rBV-M71, rBV-M115) was determined by plaque assay. Sf9 cells were seeded in a 6-well plate and incubated at 28°C to a 60-70% confluence (1×10^6 Sf9/well and incubated at 28°C overnight). Then, cells were washed and incubated with serum-free Insect-XPRESS media whilst serial dilutions of the baculovirus stock were made also in serum-free media. Supernatant from each well was discarded and replaced with 0.5 ml of each virus dilution, from 10^{-3} to 10^{-7}. The plates were incubated for 1 hour at 28°C and the inoculum was then removed from each well and replaced with 2 ml of 1.5% agarose in Insect-XPRESS overlay. After this, another 2 ml of media supplemented with 10% FBS are added on each well.

Plates are incubated >5 days and cell monolayers are stained with 0.1% neutral red solution and incubated >1 hour. Neutral red is a dye that can only be uptaken by living cells and accumulated inside their lysosomes. The viral plaques can easily be detected as white spots within the monolayer, and the number of plaques formed in the wells incubated with the highest dilutions are used to calculate the stock titer:

$$PFU/ml\,of original\ stock = \frac{dilution\ factor\ \times\ number\ of\ plaques\ per\ well}{volume\ of\ inoculum\ per\ well\ (in\ ml)}$$

Protein production in BEVS

Viral titer determination is crucial for setting the optimal infection conditions to obtain maximum yields of every recombinant protein, regardless of the viral lot used for the infection.

Besides the cell types (Sf9 or HF) and harvest time, the multiplicity of infection (MOI) given by the number of infectious particle per cell (PFU or FFU/cell) was optimized for each production.

50 ml of Sf9 suspension cell culture was set up at 1×10^6 cells/ml in serum-free Sf-900™ II SFM medium and infected at a MOI of 5, to synchronise the infection. The culture was incubated at 28°C and 100 rpm shaking conditions for 48 hours, and subsequently harvested at 300 ×g for 10 minutes (Allegra X-22R Centrifuge, Beckman Coulter), and the cell pellet was frozen at -20°C until the recombinant proteins' purification process.

Transient protein expression in mammalian cells

RK13 cells were seeded in 6-well plate at a density of 5×10^5 cell/well and after overnight incubation at 37°C (and 5% CO_2). At 80-90% of cell confluency, wells were washed with PBS and incubated with Opti-MEM™ (1X) Reduced Serum medium (Gibco, UK) for > 30 minutes. The Lipofectamine 2000 reagent (Invitrogen, Carlsbad, Canada) was used for the transfection reaction of the viral proteins cloned into the pTriEX.1.1 expression vectors: r*m022*-pTriEx-1.1, r*m071*-pTriEx-1.1 and r*m115*-pTriEx-1.1, into the RK13 cells. For each construct, transfection mixes A and B were prepared in 150 µl of Opti-MEM, following the recommended guidelines. 2-5 µg of DNA: pcDNA3.1- eGFP, as a transfection control, r*m022*-pTriEx-1.1, r*m071*-pTriEx-1.1 and r*m115*-pTriEx-1.1, was diluted in mix A; and 8 µl of Lipofectamine 2000 was diluted in mix B. All the volume of mix A was transferred to the mix B and mixed thoroughly and incubated at room temperature for 20 minutes. Afterwards, each transfection mix was added onto one of the wells in the 6-well plate, and incubated until next day at 37°C.

Then, media was changed to DMEM-10 and incubated for another 24 hours. To check the recombinant protein expression of each transgene, and regarding that none of them are secreted proteins, cells were harvested as follows: media was removed from the wells, cells were washed with sterile PBS and 300 µl of 3X Tripsin/EDTA was added to detach cells from the bottom. Trypsin was neutralised by addition of 600 µl of DMEM-10 and cells were resuspended and collected into a 1.5 ml tube, pelleted at 2000 rpm for 10 minutes in Biofuge pico (Heraeus Instruments) and stored at -20°C.

Indirect immunofluorescence (IF) staining for recombinant proteins detection

RK13 cells were cultured in complete DMEM, in 35 mm FluoroDish cell culture dish (Thermo Fisher) until they reached 60-70% confluence. Cells were fixed with 4% PFA in PBS (Thermo Fisher, Kandel, Germany) at room temperature for 20 minutes, washed twice with PBS prior to permeabilization with PBS-0.1% Triton X-100 for 20 minutes. Cell monolayers were washed

three times with PBS and blocked with PBS-0.1% Triton X-100-1% BSA solution at room temperature for 1 hour. Then, the primary anti-HisTag antibodies (1:125) or anti-MYXV positive rabbit serum (1:100) diluted in PBS-0.1% Triton X-100- 0.1% BSA were added at the working dilutions, and samples were incubated 1 hour at room temperature, or overnight at 4°C. Monolayers were washed thoroughly with PBS-0.1% Triton X-100 and then the conjugated secondary antibodies diluted in PBS-0.1% Triton X-100- 0.1% BSA were added at the corresponding working dilutions described in the Materials section. One hour later, samples were washed again with PBS-0.1% Triton X-100 and were kept at 4°C until visualization of fluorescence in the ECLIPSE Ts2 microscope (Nikon).

Affinity chromatography protein purification

Glutathione S-transferase (GST) affinity chromatography

GST-fused proteins were purified with Glutathione Sepharose 4B matrix, comprising agarose-based Sepharose beads covalently bonded to glutathione, a GST enzyme substrate. The matrix, prepared in a propylene column, was equilibrated with phosphate buffer before addition of clarified supernatants from exogenous expression systems. Following 1 hour incubation in a rotator at 4°C, the stopper at the bottom of the column was removed and samples were allowed to pass through the column by gravity. GST-fused proteins were selectively captured and retained in the glutathione-Sepharose matrix, and the rest of protein and components on the solution were discarded in the flowthrough. Then, to eliminate any possible contaminants with light affinity for the matrix, it was washed three times with 10 matrix volumes of cold binding buffer, which was let to pass the column by gravity. The target recombinant protein was released from the matrix by adding five matrix volumes of the elution solution (20 mM GSH-TrisCl pH 8), each volume collected in an independent 1 ml tube. Two further rounds were performed using a 40 mM GST pH 8 buffer.

Metal ion affinity chromatography (IMAC) under native conditions

Viral proteins marked with polyhistidine tag (HisTag) were isolated by Immobilized Metal Affinity Chromatography (IMAC) purification. This technique is based on the high affinity of histidine residues for transition metal ions that are attached to the stationary phase of the column. In this specific protocol, Chelating Sepharose Fast Flow resin from GE Healthcare was utilized as the medium for immobilizing nickel ions. These ions were introduced into the resin using a 0.3 M nickel solution, preparing the matrix for effective binding with histidine-tagged recombinant proteins. The matrix was first equilibrated with five volumes of cold buffer containing 10 mM imidazole. The sample was then applied and incubated at 4°C for one hour with rotation,

allowing viral proteins with polyhistidine tags to bind to the resin. Non-target proteins were washed away in the flowthrough. Subsequently, the column was washed with ten matrix volumes of the same buffer, now containing 50 mM imidazole, to remove weakly bound proteins. This strategy uses a low imidazole concentration initially to minimize non-specific binding, followed by a higher concentration for washing off loosely attached proteins. Finally, the target proteins were eluted six times in one matrix volume of buffer with 250 mM and 500 mM imidazole.

Metal ion affinity chromatography (IMAC) under denaturing conditions

IMAC column was charged with nickel ions using the same protocol as in the previous section and then the matrix was equilibrated with ten column volumes of buffer S (100 mM NaH_2PO_4, 10 mM Tris, 10 mM imidazole, 8M urea, pH 8.0). The sample containing the recombinant proteins solubilized from the inclusion bodies in buffer S, was applied to the column, homogenized with the matrix, and incubated at 4°C for two hours in a tube rotator. The sample was passed through the column, and the matrix was washed with ten column volumes of wash buffer (100 mM NaH_2PO_4, 10 mM Tris, 10 mM imidazole, 10% glycerol, 1% Triton X-100, 8 M urea, pH 6.3). Finally, the recombinant protein bound to the nickel ions chelated in the matrix, was eluted several times applying one column volume of elution buffer (100 mM NaH_2PO_4, 10 mM Tris, 10% glycerol, 8 M urea, pH 4.5) each time.

Post-purification dialysis

Eluates containing sufficient protein concentration were combined for each protein construct and loaded into a prepared dialysis cellulose membrane (Sigma Aldrich, Germany) with a 14 kDa exclusion size. The loaded dialysis membrane was immersed in the dialysis buffer (PBS) and was incubated overnight at 4°C. For an efficient exchange, a magnetic stir bar was placed in the beaker and a magnetic stirrer was used to ensure gently and constant movement of the dialysis solution around the membrane. The protein sample was collected and mixed with glycerol to a final concentration of 20%, for cryopreservation. Subsequently, the concentration of recombinant protein in solution was determined, and was aliquoted for long-term storage at -20°C.

ELISA

Commercial indirect ELISA test

The INgezim Mixomatosis R.17.MIX.K1t (Ingenasa, Madrid, Spain) is an iELISA kit with a reported sensitivity and specificity rates of 98% and 99%, respectively. As it was the only commercially

available kit developed for the diagnosis of myxomatosis in rabbits in the moment of this study, it was selected as the gold standard serologic test against which the iELISA tests developed in this Doctoral Thesis were compared.

The analysis of rabbit sera by the commercial iELISA targeting MYXV-specific IgG antibodies was performed following the manufacturer's instructions. Briefly, 100 µl of a 1:200 rabbit sera dilution in 1X sample solvent was added to the plate and incubated 1 hour at 37°C. After washing the plate 3 times with 300 µl of Wash solution, 100 µl of conjugate solution were added to each well and the plate was incubated 1 hour at room temperature (25°C). Wells were washed five times with 300 µl wash solution, and 100 µl of substrate solution 3,3',5,5'-Tetramethylbenzidine (TMB) was added to each well. The plate was incubated this time for 10 minutes at room temperature, but in the darkness, while the enzymatic reaction took place. 100 µl of a 0,5M sulfuric acid solution (stop solution) was added to stop the reaction, and then the absorbance at 450 nm (Optical Density at 450 nm, OD_{450}) was measured in the Varioskan® Flash plate reader (Thermo Scientific).

To validate the test, two replicates of the positive and negative controls were added in every run. A valid assay would give a (OD_{450}) Positive mean/(OD_{450}) Negative mean ratio > 5.

The immune status of each animal was determined after calculating the positive and negative cut off values for each run. The positive cut off value was calculated as the mean OD_{450} of the negative control + 0.2, samples with higher OD_{450} were considered seropositive. The negative cut off value for each run was calculated as the mean OD_{450} + 0.15 and samples with lower OD_{450} were considered seronegatives. Samples with OD_{450} between both cut off values were considered doubtful.

A total of 259 rabbit serum samples, of which 161 sera samples were obtained from panel 1, 64 from panel 2, and 34 from panel 3, were tested by the commercial iELISA test (INgezim Mixomatosis, Ingenasa S.A). The outcomes derived from this analysis determined the serological status of each sample and categorized them into either positive or negative serology based on the presence or absence of antibodies against MYXV, respectively.

Indirect ELISA using the whole MYXV as antigen

This indirect ELISA was developed as a *in house* assay, trying to simulate the gold standard (commercial iELISA) test for the detection conditions of antibodies against MYXV. For that, a Lu-GFP-MYXV stock purified by ultracentrifugation was used as antigen, after total protein quantification. The amount of antigen, sera dilution and secondary antibody dilution, were

optimized following the checkerboard (CB) titration method (Walker, 2009) that consists of a systematic experimentation in which two different reagents are tested in a matrix against each other at different concentrations, in a checkerboard-like pattern, to determine the combination that produces the best results (Crowther, 2009). The selection criteria in this Doctoral Thesis for this purpose was choosing the combination giving the highest P/N ratio without compromising the signal strength and analytical performance.

In brief, 1 µg/ml solution of Laus-GFP-MYXV in 0.05M C-B pH 9.5 buffer was used to coat the bottom of the wells from a Costar® Assay 96-well plate (Corning Incorporated, Kennebunk, USA), and the plate was incubated overnight at 4°C. After washing the plate two times with PBS and the non-ionic detergent Tween 0.05% (PBST), the wells were blocked with 3% BSA in PBST during 2 hours at room temperature; washed 3 times with PBST and incubated for 1 hour at room temperature with 1:200 dilutions of rabbit sera in blocking buffer. The plate was washed again with PBST and then the goat anti-IgG rabbit conjugated with HRP was added at a 1:6000 dilution in blocking buffer. The plate was incubated 1 hour at room temperature and after washing again the wells with PBST, the substrate TMB was added to the wells, the plate was incubated in the dark for 10 minutes, and the stop solution (sulfuric acid 3N) was added to each well. The absorbance at OD_{450} was measured in a plate reader.

Indirect ELISA for antibody detection against antigenic proteins of MYXV

The indirect enzyme-linked immunosorbent assay (iELISA) was the technique chosen to detect the presence of antibodies raised against these two viral proteins (rM022 and rM115) in rabbits' sera. Since ELISA protocols were first developed, they showed better performance in MYXV serodiagnosis than other serologic methods (OIE, 2018). The assay conditions in the CB titration that resulted in the highest OD_{450} positive/OD_{450} negative (P/N) ratio, as well as raw OD_{450} within the acceptable range for the positive control (of around 1.5) were considered to set up the final iELISA protocol.

As a result of the optimization process, two independent protocols for each of the proteins rM022 and rM115 were obtained. Briefly, each well of a Costar® Assay 96-well plate coated with 100 ng of purified rM022 in PBS for the iELISA-rM022 test or with 25 ng of purified rM115 in PBS for the iELISA-rM115 test, and incubated overnight at 4°C. After washing the wells two times with PBST, they were blocked with the blocking buffer composed of 3% BSA in PBST, during 1 hour at 37°C. Next, the plate was incubated for an hour at 37°C with 100 µl of sera diluted in blocking buffer 1:400 for the rM022-iELISA, or 1:100 for the rM115-iELISA. Then, the wells were washed five times with PBST, and 100 µl of the secondary antibody, diluted 1:12000 or 1:6000

for rM022-iELISA or rM115-iELISA, respectively, in blocking buffer was added to the wells. After further incubation of 1 hour at 37°C, unbound conjugate antibody was removed after five washes with PBST. 100 µl of TMB (SIGMA-Aldrich, China), a substrate for the enzyme HRP, was added to each well and the plate was incubated at room temperature (RT) in the dark. TMB's oxidation results in a blue colour product with a maximum absorbance at 605 nm. After 10 minutes of incubation, the enzymatic reactions were stopped by adding 100 µl of 3N sulfuric acid (H_2SO_4), that turned the colour of the solution into yellow, with an absorbance peak at 450 nm. Finally, the OD of each well was measured at 450 nm by the Varioskan® Flash plate reader (Thermo Scientific), driven by the SkanIt Software (Thermo Scientific).

Validation

To ensure that the data obtained after performing these diagnostic assays is reliable, each one was validated individually. To this end, stability, precision, sensitivity, and specificity were determined for both recombinant iELISAs.

For the assessment of antigen stability, the 96-well plates were coated with the corresponding amount of each antigen (rM022 or rM115) and blocked, following the optimized protocol. Afterwards, the blocking buffer was removed, and the plates were oven dried at 37°C. Then, the plates were sealed and stored at 4ºC and tested for stability with several replicas of the positive and negative control samples after a day (day 1), and a week (day 7) and a month (day 30) (B. Kumar et al., 2021).

To evaluate the overall reliability and applicability, the precision/repeatability and reproducibility of each assay were assessed by analysing their intra-assay (within-run) and inter-assay (between-runs) variability, respectively. Whilst intra-assay variability assesses consistency within a single experiment, inter-assay variability assesses consistency across different experimental runs.

The intra-assay variability refers to the inherent variation observed when the same assay is run multiple times under the same conditions, which can be due to small differences in sample handling, volume of added reagent, equipment performance, etc. This variability was evaluated for every serological assay (iELISA-MYXV, iELISA-rM022 and iELISA-rM115) by calculating the coefficient of variability (CV) of eight replicates of the control samples (PC and NC), tested at the corresponding working dilutions for each serological assay. The CVs were obtained as the ratio between the SD and the arithmetic mean of the eight replicates within the same test run:

$$\text{CV}\ (\%) = \frac{Standard\ deviation\ (SD)}{Mean\ (\bar{x})} \times 100$$

The inter-assay variability states the reproducibility between the same assays done across different experimental setups, therefore it can be influenced by differences in reagent lots, environmental conditions, equipment calibrations, different operator manipulation, etc. The CV of PC and NC replicates analysed in three different plates were calculated for every serological assay (iELISA-MYXV, iELISA-rM022 and iELISA-rM115) to assess the between-run variability.

Additional accuracy descriptives of a diagnostic test are the Positive Predictive Value (PPV) and the Negative Predictive Value (NPV) of the test. PPV is referred to as the probability that individuals with a positive test result does reflect the true positive disease status, whilst the NPV is a measure that indicates the reliability of a negative test result. PPV and NPV were calculated as follows:

$$\text{PPV}\ (\%) = \frac{TP}{TP + FP} \times 100 \quad ; \quad \text{NPV}\ (\%) = \frac{TN}{TN + FN} \times 100$$

Where true positives (TP) are individuals who tested positive and had the disease, false positives (FP) are those who tested positive but did not have the disease, true negatives (TN) are those who tested negative without having the disease, and finally, false negatives (FN) are individuals who tested negative but did have the disease.

The Likelihood Ratio for a positive result (LR+) is referred to as the ratio of the probability of a positive test result in the analysis of truly positive samples (Se) to the probability of a positive test result in a true negative sample (1-Sp): LR+ = (Se)/(1-Sp). The Likelihood Ratio for a negative result (LR-) is referred to as the ratio of the probability of a negative test result in truly positive samples (1- Se) to the probability of a negative result in truly negative samples (Sp): LR- = (1-Se)/(Sp).

Data processing and standardization

Raw OD_{450} measurements and relevant information about the sera samples were compiled in Microsoft Excel. For each run, the mean blank OD_{450} value was subtracted to the control and samples raw OD_{450}. The resultant background-subtracted values were expressed as a relative OD percentage (ROD, %) using the formula:

$$\text{ROD}\ \% = \frac{OD.S - \bar{x}OD.NC}{\bar{x}OD.PC - \bar{x}OD.NC} \times 100$$

where OD.S is the OD of any sera sample; $\bar{x}$OD.NC is the mean OD_{450} of the negative control replicates; $\bar{x}$OD.PC is the mean OD of the positive control replicates.

Statistical analysis

The receiver operating characteristic (ROC) method was used to evaluate the diagnostic ability of the three iELISA tests (iELISA-Lu, iELISA-rM022 and iELISA-rM115). A ROC curve was generated for each test, representing the true positive rate (Se) in the Y axis, and the false positivity rate (1-Sp) values across all possible thresholds. The optimal threshold or cut-off value for each iELISA test, defined to as the point that classified most of the individuals correctly, was estimated maximizing the Youden's Index (J) statistic value in a function such that:

$$J\ (x) = Se(x) + Sp(x) - 1 = Se(x) - (1 - Sp(x))$$

Area under the curve (AUC), diagnostic sensitivity (DSe), specificity (DSp), PPV, NPV and LRs were calculated with 95% confidence interval, for the threshold value established to each iELISA test. Cohen's Kappa (κ) test was used to evaluate the test agreement (Landis & Koch, 1977).

Descriptive analyses were carried out, providing distributions of relative and absolute frequencies for the qualitative variables, and measurements of position and dispersion for the quantitative variable qualitative variables. The Shapiro Walk test or Kolmogorov-Smirnov test, and F test were performed for studying the distribution of datasets, in the assessment of normality and equal variances, respectively. Differences in quantitative variables between two groups were studied with the Student's t test, with Welch's correction in case of different variances; or with the Wilcoxon signed-rank test. Differences among more than two groups were studied with the Kruskal-Wallis test, with post hoc pairwise Dunn's test analyses.

The statistical analysis was carried out using the GraphPad Prism software (version 8.0.2) with a significance level of 0.05.

Indirect immunofluorescence antibody technique (IFAT)

Rabbit kidney RK13 cell line (CCL-37) was seeded in 96-well flat-bottom cell culture plates (Sarsted, Nümbrecht) at a density of 7×10^5 cells/ml, in Eagle's minimum essential medium (MEM) supplemented with 10% FBS. Once adherent to the plate at 70% confluence, they were infected at a MOI of 0.001 with the ha-MYXV strain diluted in MEM without serum. One column of each plate was left uninfected to observe the background signal produced by each serum at its lowest dilution in the absence of the virus. Cells were incubated at 37°C with 5% CO_2 for 72 hours, until cytopathic effects were evident. Subsequently, the cells were fixed with a mixture of 70% methanol-30% acetone (v/v) cold (stored in the freezer) for up to 30 minutes at room temperature. After removing the fixative, the cell monolayer was washed twice with PBS-Tween 0.05%, incubating for 5 minutes with the buffer in each wash.

Blocking was carried out by incubating the cells with 5% skim milk in PBS-Tween 0.05% for more than 30 minutes at room temperature (it could have been incubated with agitation and at 37°C to enhance blocking). Afterward, the monolayer was washed twice with PBS-Tween 0.05%, and 50 µl of rabbit serum dilutions in PBS, starting from 1:8 and going up to 1:4096, were added. They were incubated for one hour with agitation at 100 rpm at 37°C, and the cells were washed twice with PBS-Tween 0.05%. A secondary anti-rabbit IgG antibody labeled with FITC at a dilution of 1:250 in PBS was added, and it was incubated for one hour with agitation at 100 rpm at 37°C. Finally, the monolayer was washed twice with PBST the liquid was removed, and the cells were observed under an inverted fluorescence microscope (Nikon Eclipse Ti-S, TI-F). The titer of each serum was estimated as the reciprocal of the last dilution with specific and positive fluorescence in both replicates.

Cellular virology methods

MYXV propagation and purification

MYXV stocks were generated by virus amplification on RK13 cultures using 150 cm^2 flask. Cells were seeded the day before and were let grow to a semiconfluent monolayer. Growth media was removed, and cells were infected at a MOI of 0.02-0.05 with the corresponding virus inoculum diluted in 5 ml of serum-free DMEM media, per flask. Cultures were incubated at 37°C for 1 hour and afterwards, 25 ml of complete DMEM media was added to each flask.

Infected RK13 cultures were incubated for 72-96 hours, depending on the progression of the infection, until the cytopathic effect generated by the MYXV infection was evident throughout the monolayer. Then, cells were scraped from the bottom of the flasks and harvested into the growth medium itself. Following harvest, cell suspensions were transferred into 50 ml conical tubes and span down at 1930 g at 4°C in a refrigerated centrifuge, for 15 minutes. Supernatants were discarded and cells were resuspended in swelling buffer and incubated on ice for 20 minutes prior to storage at -80°C.

A protocol adapted from the methodology described by Smallwood et al. (2010) was used for viral purification. The suspension was thawed and sonicated in an ultrasonic bath sonicator for two rounds of 1-minute with 1-minute rest in between. Then, it was transferred into an autoclaved Dounce homogenizer prechilled on ice and homogenized applying 20 strokes with a loose pestle. The homogenate solution was transferred to a centrifuge tube and spun 1040 g for 15 minutes at 4°C in a refrigerated centrifuge. Supernatant was saved and the pellet was resuspended in 10 mM Tris-HCl, pH 8 buffer, and centrifuged at 1930 g for 15 minutes at 4°C.

Supernatant was saved again and this step was repeated once more, to remove cell debris from the lysate solution.

A sucrose cushion was prepared into a 10 ml ultracentrifuge tube, pouring 4 ml of a cold 36% sucrose solution in 10 mM Tris-HCl, pH 8. The supernatant obtained in the previous steps containing the viral particles amplified in the infected cell culture, was gently poured on top of the sucrose layer without disturbing the interphase or mixing both solutions. The centrifuge tubes were filled to within 0.5 cm from the top and were balanced in pairs. Then, the tubes were loaded into buckets and centrifuged for 80 minutes at 18000 rpm in SW28 rotor (Beckman Coulter) at 4°C.

The supernatant was discarded carefully and the pellet, containing the virus particles, was resuspended in 200 µl of cold 10 mM Tris-HCl pH 8 and stored at - 80°C until further need.

MYXV titration

The concentration of infective MYXV particles in all stock generated by viral amplification, or after purification by ultracentrifugation, was determined by foci assay titration. This method is based on the ability of MYXV in forming clumps of cells called viral foci, in infected cell cultures. Since each focus results from a single infectious virus particle, by counting the number of foci generated at a certain dilution, the number of infectious particles in solution can be determined. The titer is expressed in foci forming units/ml of culture (FFU/ml).

Virus stocks at –80°C were thawed at room temperature, homogenized and sonicated for 15-15 seconds in a bath sonicator. Serial tenfold dilutions of the corresponding MYXV stocks were prepared in serum-free DMEM, adding 1 part of virus stock (or previous dilution) to 9 parts of diluent. The process was repeated until the desired range of dilutions (usually between dilutions 10^{-7} to 10^{-9}) was reached. RK13 cells seeded in a 6-well tissue culture plate and around 80% confluent were infected with 300 µl of the dilutions to each well of the plate. Following an incubation of 1.5 hours at 37°C in a humidified CO_2 for virus adsorption, the inoculum was removed and 2 ml of warm 1.5%-agarose in MEM was added to each well. Once solidified, 1 ml of complete DMEM was added on top of the agarose gel matrix formed in each well. Cells were incubated at 37°C for a period of 72 hours (or 6 days in case of recombinant MYXVs).

After the incubation period, foci were identified by different strategies. For wild type and non-tagged MYXV (e.g. Lu-MYXV, Vac-MYXV), cells were fixed with a 35% formaldehyde by overnight incubation at 4°C, and then stained with crystal violet solution at room temperature for 30 minutes. The crystal violet solution was removed, and wells were rinsed with water to eliminate

any excess stain, before inverting the plate to air-dry the wells. Foci were counted under an inverted microscope or with a magnifying lens.

$$FFU/ml\ of original\ stock = \frac{dilution\ factor\ \times\ number\ of\ foci\ per\ well}{volume\ of\ inoculum\ per\ well\ (in\ ml)}$$

For the recombinant MYXV strains, Lu-ΔM022gfp, Vac-ΔM022gfp, Vac-ΔM71tdTmt and Vac-ΔM115gfp, staining is not needed since stock titration is readily performed by counting green or red fluorescent foci under a fluorescent microscope.

Generation of Vac-MYXV by homologous recombination using the transfer vectors pΔM071tdTmt or pΔM115gfp

For the generation of a marked vaccine against myxomatosis, specific ORFs encoding candidate antigenic proteins were deleted from the MYXV genome by insertional inactivation using homologous recombination. LF and RF segments surrounding the target gene direct the insertion of the reporter gene into the MYXV genome.

A culture of subconfluent RK13 cells were infected with the parental Vac-MYXV strain at a MOI of 0.005 and following 1.5 hours of incubation in DMEM without serum, cells were transfected with 0.5 µg of the corresponding transfer vector, or the transfection control vector pcDNA-eGFP using Lipofectamine 2000 (Invitrogen) according to manufacturer's instructions (Figure 14). Following overnight incubation, culture media was changed to DMEM-5 and 48h later, cells were harvested, lysed by three freeze-thaw cycles, and supernatants were stored at -20°C (P0). The progeny was amplified in a fresh culture of RK13 cells, and recombinant viruses were isolated by focus purification and further amplified to increase their population in the total pool. The selection process of recombinant Vac-MYXV involved isolating cells associated with green or red fluorescent foci 48 hours post-infection.

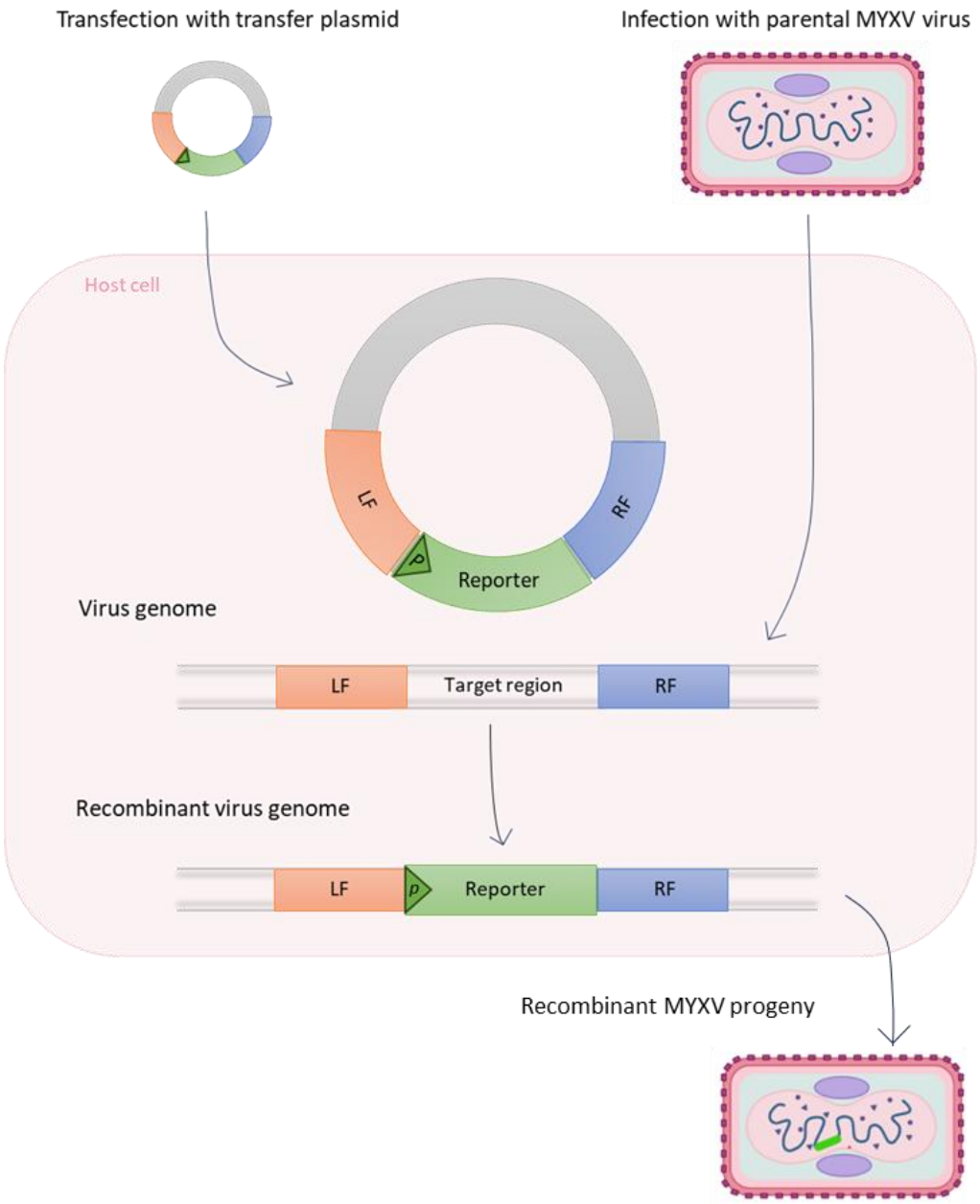

Figure 14. Generation of recombinant MYXV viruses by homologous recombination.

Cells are both infected with the parental MYXV and transfected with a plasmid transfer vector. This vector contains either a foreign gene or a reporter gene, under the control of a poxviral promoter (*p)* in either way and left (LF) and right (RF) flanking viral DNA sequences that direct the homologous recombination event during the replication cycle of the virus, to a specific genomic location within the parental MYXV genome (target region). The resulting modified DNA genome is packaged to form progeny recombinant myxoma viruses that are released to infect new host cells.

Transmission electron microscopy

Virions for electron microscopy were purified by ultracentrifugation following the protocol described above. For uranyl acetate negative staining, Formvar/carbon supported copper grids (Merk) were placed on 10 µl sample drop facedown on parafilm sheet and incubated for 10 minutes at room temperature. Following this sample absorption step grids were placed (again facedown) onto a drop of uranyl acetate (supplied by the technical staff at the Servicios Cientificos Tecnicos, of the University of Oviedo) for 30 seconds. Excess stain was removed by gently touching the edge of the grid on to 3M blotting paper. The grid was then washed twice with drops of sterile water and dried before analysis.

Samples were visualized at 100000x and an accelerating voltage of 100kW in the JEM 1011 (JEOL) compact high-performance TEM of the SCTs facilities of the University of Oviedo.

Data analysis

Microsoft Windows Excel was used for data processing and handling, while GraphPad Prism software (version 8.0.2) was used to perform all statistical analyses and graphical presentations.

DNA sequences were analysed and aligned in the GeneiousPrime software (version 2023.2.1), while the design of transfer vectors and oligonucleotides were performed in Geneious Prime or the VectorNTI softwares.

ImageJ analysis software (1.54g) was used in the measurement of MYXV virion dimensions using TEM images.

CHAPTER 5: IDENTIFICATION AND VALIDATION OF ANTIGENIC MYXV PROTEINS

SELECTION OF CANDIDATE ANTIGENIC MYXV PROTEINS

The main goal of this chapter was to describe the steps taken for the identification of antigenic MYXV proteins for use in diagnostic ELISAs from a selection of candidate targets. The fundamental criteria of this selection laid in the protein's ability to be recognized by the immune system of the host in a detectable manner. The protein should also be non-essential as it will potentially be used to construct a knockout DIVA MYXV vaccine.

The antigenicity of the MYXV protein candidates was specifically evaluated based on their ability to be recognized by rabbit antibodies from a MYXV-seropositive serum sample. The MYXV proteins that were initially designated as suitable candidates and their predicted functions are summarized in Table 7. Amongst these six candidates, there were proteins located within or associated to the membrane of IMVs and EEVs particles. The preselection also included immunomodulatory proteins, given their significant role in virulence and host-pathogen interactions, or MYXV targets with predicted homologies to proteins that have been successfully used in the development of immunological based assays for other poxviruses.

Table 7. MYXV proteins selected for expression trials and their predicted localization and putative functions.

CANDIDATE MYXV PROTEINS	**Predicted MW** (kDa)	**POXVIRUS HOMOLOGS**	**Localization in the virion**	**Putative function**
M022	41.51	F13L / ORFV-B2L	EEV	IMV wrapping
M29	12.81	E3L / SPPV34 / SPV032L	Cytoplasmic	PKR inhibition *
M71	36.85	H3L / (P32) GPTV-074	IMV	IMV-morphogenesis protein
M83	32.23	D8L	IMV$^{\Delta}$	Cell adhesion
M115	21.58	A27L / GTPV-117 / SPPV-117	IMV	Fusion protein and EEV formation
M141	23.7	A56L	EEV-Membrane associated	OX-2 homologue *

* Predicted immunomodulatory, host range, or antiapoptotic functions

BIOINFORMATIC ANALYSES OF THE MYXV PROTEIN CANDIDATES AND THEIR (PUTATIVE) FUNCTIONAL ROLES

M022

M022 is homologous to the VACV protein F13L (also termed p37) protein, which has been extensively characterized biochemically and functionally. In Uniprot, F13 (OPG057) is defined as an envelope phospholipase with hydrolase activity which consists of 372 amino acids. It is a multifunctional protein. Some of the putative roles attributed to F13L are related to membrane biogenesis of IEV and/or membrane fusion, and in cell-to-cell transmission since deletion of the F13L gene failed to produce mature EEV (Blasco & Moss, 1991) (Bryk, Brewer and Ward 2018) and host-cell interactions. Some of these roles are related to the presence of certain domains within the F13L protein. M022 of MYXV has not been specifically studied, but the presence of such domains in M022 can be predicted based on the amino acid sequence (prosite.expasy.org) and comparisons with F13L.

F13L (P37) contains 3 regions of functional or structural interest. Firstly, it has a phospholipase D (PLD)-like domain (amino-acid position 312-319), but despite the sequence homology to the PLD conserved HxKxxxxD (HKD) motif, no phospholipase D activity was detected in cells expressing the viral protein (Sung et al., 1997). Yet, the F13L protein does exhibit broad specificity phospholipid-metabolizing activities, such as phospholipase C, phospholipase A and triacylglycerol lipase activities (Baek et al., 1997). The (H)DK motif in the PLD of F13L is needed for B5R colocalization in endosome-like vesicles, indicating that B5R recruitment is induced by a putative catalytic activity of F13L (Hiller & Weber, 1985; Husain & Moss, 2001). EEV proteins F13L and B5R are required for the wrapping process of IMV in the *trans*-Golgi, and production of the IEV. Single mutations in the conserved active site of the PLD also showed a reduction on the EEV formation and loss of efficient cell-to-cell spreading (Roper & Moss, 1999; Sung et al., 1997).

F13L suffers post-translation modifications (PTMs) *in vivo* on two highly conserved cysteine residues at positions 185 and 186 (C185, C186), consisting of the addition of palmitate, a 16-carbon saturated fatty acyl moiety via thioester or ester linkage to cysteine (Grosenbach & Hruby, 1998; Hirt et al., 1986).

Finally, F13L has also been implicated in the budding process. The tetrapeptide sequence of tyrosine-X-X-leucine (YxxL) is a viral late assembly domain (L domain), a motif that putatively mediates assembly and egress of viral particles, first identified in the *Lentiviridae* viral family. The YxxL motif is required for efficient EEV release and regular plaque formation and is well conserved in the F13L homologs within the *Orthopoxvirus* genus.

M029

The MYXV *m029l* ORF is well conserved and encodes a 12.81 kDa protein orthologous to the VACV E3L protein known for its role in counteracting the host's interferon response by disrupting the interferon-inducible cellular protein kinase (PKR) activity (Romano et al., 1998).

M029 interacts with PKR indirectly via dsRNA bridging viral enzyme targets dsRNA, preventing the overall shutdown of global protein synthesis by the mentioned pathways that is essential for the host's antiviral response. dsRNA is a common byproduct of viral infection that targets the activation of PKA and 2'−5' oligoadenylate synthetase pathway, resulting in inhibition of translation initiation by eIF2α phosphorylation, and RNA degradation through ribonuclease L activation, respectively. This interaction appears to be crucial for M029 host range functions.

Moreover, M029 has a direct protein-protein interaction with RHA/DHSX9, a cellular RNA helicase with several regulatory roles in cellular transcription and translation processes. RHA/DHX9 upregulates MYXV replication in a cell-specific fashion, showing pro-viral regulatory effects (Rahman et al., 2013).

M071

The *m071l* ORF encodes a MYXV protein predicted to be homologous to the VACV H3L protein, which is the major IMV envelope protein (Zinovieva et al., 1994). H3L protein is expressed late in infection, accumulated in the cytoplasmic viral factories, and post-translationally incorporated into IMV membranes via a hydrophobic C-terminal anchor tail (da Fonseca et al., 2000a).

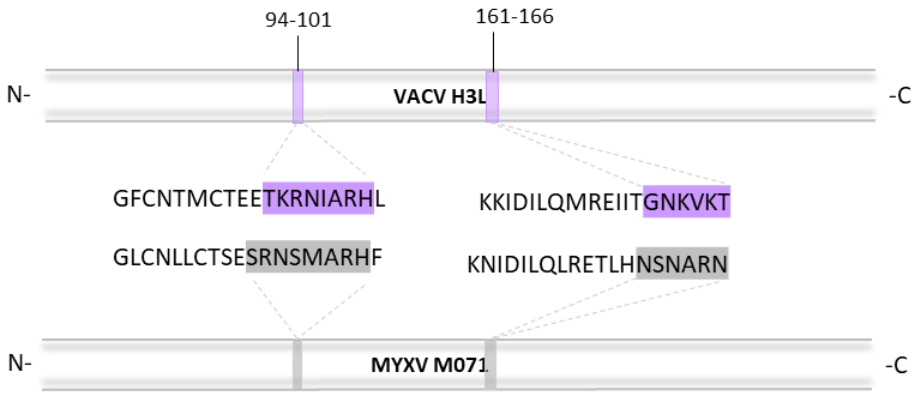

Figure 15. Schematic representation and conservation of the putative GAG-binding sites in M071.

Nucleotide sequence in purple indicate GAG-binding sites in VACV H3L protein (SOU90113.1) and the sequence highlighted in grey indicate the homologous region in MYXV M071 protein (NP_051785.1).

During virus entry H3L binds to cell surface heparan sulphate (HS) through two putative GAG-binding sites constituted by hexapeptide sequences rich in basic amino acids (Lin et al., 42000). Although both proteins show a 35.8% sequence identity, M071 seems to lack these conserved binding sites (Figure 15).

VACV H3L also is involved in the IV to IMV maturation process, absence of the protein results in great reduction of IMV and consequently, of IEV and EEV particles production (da Fonseca et al., 2000b; Lin et al., 2000). It is also an immunodominant viral antigen that induces both T-cell and B-cell immune reactions and is a target for neutralizing antibodies (Davies et al., 2007; Khlusevich et al., 2022).

M083

The *m083l* ORF encodes a putative chondroitin sulfate binding protein, homologous to the VACV IMV membrane D8L protein. D8L is a type I transmembrane protein that facilitates the attachment of the virus to the cell surface by interacting preferably with chondroitin sulfate molecules (Hsiao et al., 1999b; Matho et al., 2014; Niles & Seto, 1988). However, recent studies have indicated that M083 does not play a significant role in the attachment of virions to the cell surface. Instead, it is suggested that the M083 protein locates in the outer membrane of CEV particles (Wolfe et al., 2018). While not definitive, the proteomic analysis of MYXV IMV composition failed to detect the M083 protein (Zachertowska et al., 2006).

M115

The M115 ortholog is the VACV A27 protein (12.57 kDa) with 23% sequence identity. It is a conserved protein in poxviruses with relevant roles in multiple stages in the virus life cycle, such as binding, entry, intracellular trafficking, and egress.

Despite lacking a transmembrane domain, A27 is exposed on the IMV membrane surface by interacting with the A17 integral membrane protein (D. Rodriguez et al., 1993a; Wang et al., 2014). The A26 protein is indispensable for endocytosis of VACV and is incorporated into the mature virion through the formation of a disulfide bond with A27 (S.-J. Chang et al., 2012; Howard et al., 2008). Although A26 has a relevant role in VACV membrane fusion suppression, MYXV does not encode an A26 homologous suggesting an alternative entry and exit strategy (Villa et al., 2010a). Additionally, A27 intervenes in transporting immature IMV progeny generated in the cytoplasmic viral factories to the trans Golgi network, in a microtubule-dependent manner. Hence, it is indirectly involved in IMV wrapping process and generation of IEV particles (Sanderson et al., 2000).

A27 features an N-terminal region abundant in basic residues that exhibit GAG-binding activity, which is essential for the protein attaching to cell surface heparan sulfate molecules during viral attachment. This interaction initiates membrane fusion mediated by A27L, facilitating the entry of the virus (Hsiao et al., 1998). Besides this heparin binding domain (HBD), VACV A27 protein has two other motifs: a coiled coil domain (CCD) and leucine zipper domain (LZD) (Vázquez et al., 1998) (Figure 16).

Figure 16. Schematic representation of the domain structure of VACV A27 (110 aa)

The heparin binding domain (HBD) for binding to the cell surface glycosaminoglycans (HS), coiled-coil domain (CCD) for oligomeric assembly and interaction with A26, and leucine zipper domain (LZD) for IMV membrane association through binding with A17.

A27 forms trimeric structures through oligomerization mediated by the α-helices corresponding to the CCDs. The N-terminal region of CCD is involved in the assembly of two parallel α-helix and one antiparallel α-helix. In addition, two of these trimers then are stacked upon one another involving residues at the C-terminal regions of the CCD, resulting in the formation of a hexameric assembly. Despite displaying some differences, hydrophobic CCD residues involved in the coiled-coil structure formation are relatively conserved in ortholog proteins (Chang et al., 2013).

M141

The *m141r* ORF encodes a cell surface protein with putative homology to the VV A56R protein of the EEV envelope particle, also known as hemagglutinin (Jackson et al., 1999). M141R belongs to the immunoglobulin (Ig) family and since it has significant amino acid similarity (23%) to the rabbit CD200 (OX-2) cellular protein, it is also known as vOX-2 (Cameron et al., 1999). CD200 is a membrane glycoprotein within the immunoglobulin superfamily, found on diverse cell types including endothelial cells, B and T cells, and neurons. It features two immunoglobulin (Ig) domains: a variable-like Ig domain at its N terminus and a constant-like Ig domain near its C terminus. CD200 engages its specific receptor, CD200R, specifically through the N-terminal V-like Ig domain (Hatherley & Barclay, 2004). Although M141R shows the highest amino acid conservation and similarity to cellular CD200 in its only Ig domain, to the V-like Ig CD200 domain, it does not bind to the rabbit CD200R.

M141R has the ability to modulate the immune response limiting the activation of myeloid-lineage cells, which in turn reduces the release of stimulatory signals for CD8+ T lymphocytes activation. M141R expression also decreases IFN-γ production by CTL cells in response to nonspecific T-cell activators (Cameron et al., 2005; Zhang et al., 2009).

PREDICTED BIOCHEMICAL CHARACTERISTICS OF THE MYXV CANDIDATES

M022

The ORF *m022l* of MYXV encodes a protein expressed during the late phase of the viral infection. The full-length M022 protein is a polypeptide of 371 aa with a theoretical molecular weight (MW) of 41.5 kDa and pI of 8.39 (Q77PA6). The protein has not been fully characterized so far and its structure and function has only been predicted due to homology with VACV F13L (Figure 17).

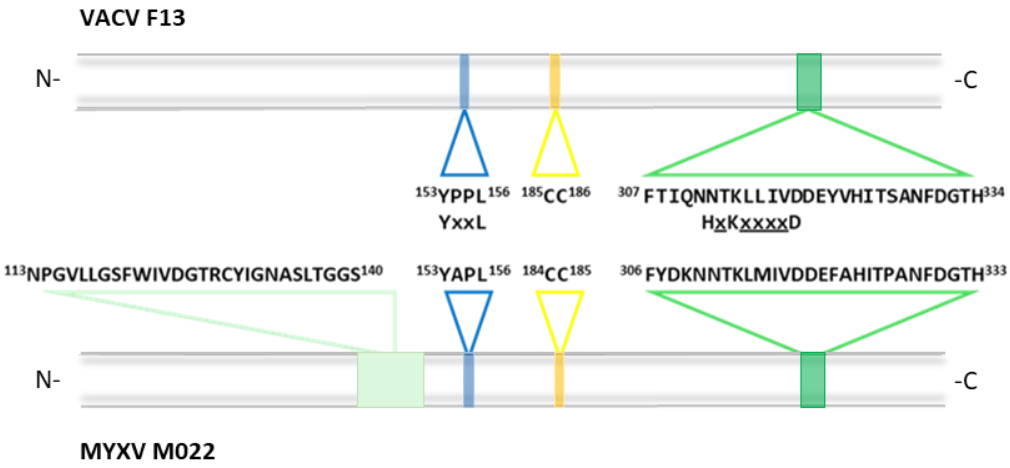

Figure 17. Schematic representation of the 371 amino acid sequence of M022 and comparison of its putative motifs with VACV F13L protein

Predicted YxxL-motif is displayed in blue, S-palmitoylation sites are displayed in yellow (residues C188-C189), the PDL active site (aa 306-333) is displayed in green, specifically identifying the conserved "(H)KD motif" -N, K and D- within this domain.

The hydropathicity analysis using the Kyte and Doolittle amino acid scale (ProtScale, Expasy) reveals no evidence of a signal peptide in M022 and indicates the presence of two hydrophobic regions of 27 amino acids near the center of the protein (Figure…). Although the Grand average of hydropathicity (GRAVY) score of -0.074 calculated regarding its amino acid composition indicated that the protein is slightly hydrophilic, the fatty acid modifications acquired during the palmitoylation process are expected to be responsible for its hydrophobic behavior (Hirt et al., 1986). The TMHMM-v.2.0 (DTU Health Tech) tool analysis of the protein sequence did not predict any transmembrane regions in M022, in agreement with the literature.

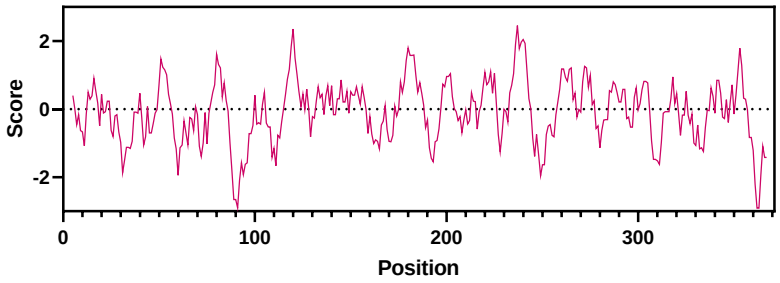

Figure 18. Kyte-Doolittle hydrophilicity plot of the MYXV M022 protein

The plot represents the hydrophilicity profile (Y-axis), with positive values indicating hydrophobic regions and negative values indicating hydrophilic regions, along the 371 amino acid sequence of M022 (X-axis) (ProtScale, Expasy).

Regarding its functional domains, similar to F13L, M022L features a putative HKD catalytic motif characteristic of the PLD-like domain (306-333). However, it displayed a substitution at the

histidine (H) position within the conserved HxKxxxxD motif, which was replaced by an asparagine (N) (Koonin, 1996; Sung et al., 1997) (Figure…). The analysis performed by the SMART (Simple Modular Architecture Research Tool) and InterPro (ELIXIR Core Data Resource) bioinformatic tools identified a second PDL domain between positions 113 to 140. It was predicted as catalytically inactive since it lacked two of the residues from the catalytic site (Table…). Regarding the results of domain prediction analyses, M022L was described as a member of the phospholipase D family, like VACV F13L and K4 proteins. Due to the absence of functional H and K residues in the first PLDc domain (113-140 aa) and the partially conserved HKD motif in the second PLDc domain (306-333 aa), the protein is expected to lack PLD enzymatic activity. These two motifs have been already described and identified in several poxvirus proteins (Koonin, 1996).

M029L

MYXV M029 is 115 aa in length and shares 24% identity with VACV E3L, mainly in the C-terminal two-thirds of the sequence, including the predicted dsRNA binding domain found in E3L. Despite being approximately 13 kDa smaller than E3L, and missing much of the N-terminal region, M029 retains a critical tryptophan residue (W8) that aligns with the W66 residue in E3L protein, which is vital for its immunomodulatory activity (Barrett et al., 2001). The hydropathic Kyte and Doolittle analysis predicted an overall predominantly hydrophilic character for M029, corroborated with by a GRAVY index of -0,291 (ProtScale, Expasy). The TMHMM-v.2.0 (DTU Health Tech) analysis tool did not predict any transmembrane regions, despite the presence of a pronounced hydrophobic peak around position 80.

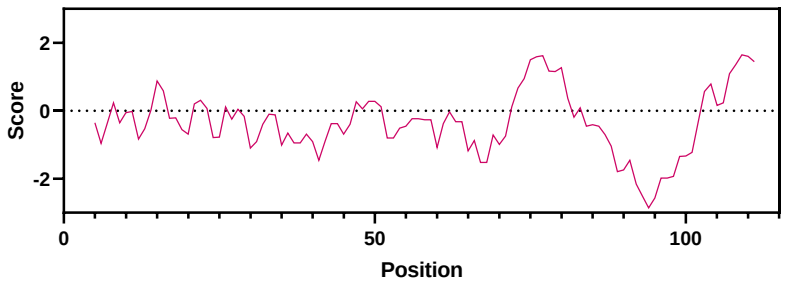

Figure 19. Kyte-Doolittle hydrophilicity plot of the MYXV M029 protein

The plot represents the hydrophilicity profile (Y-axis), with positive values indicating hydrophobic regions and negative values indicating hydrophilic regions, along the 115 amino acid sequence of M029 (X-axis).

M071

M071 is a protein of 324 aa with a theoretical molecular weight of 36.85 kDa, and pI of 7.72 (NP_051785.1). The instability index (II) of 44,58 computed by ProtParam analysis tool (Expasy) classified this protein as unstable. The transmembrane region analysis conducted using TMHMM-v.2.0 (DTU Health Tech) predicted a large extracellular N-terminal region encompassing amino acid residues 1 to 282, a transmembrane helix between residues 283 to 305, and a short cytoplasmic C-terminal region spanning positions 306 to 324. When the hydropathy profile of the M071L protein was predicted, this region showed high putative hydrophobic character (Figure 20). Hence, the nucleotide sequence encoding the amino acid residues from positions 283 to 324 of the M071L protein was omitted in the fragment of the *m071l* ORF cloned into the pET28a(+) vector. The predicted molecular weight of the recombinant M071 protein would be 32.2 kDa.

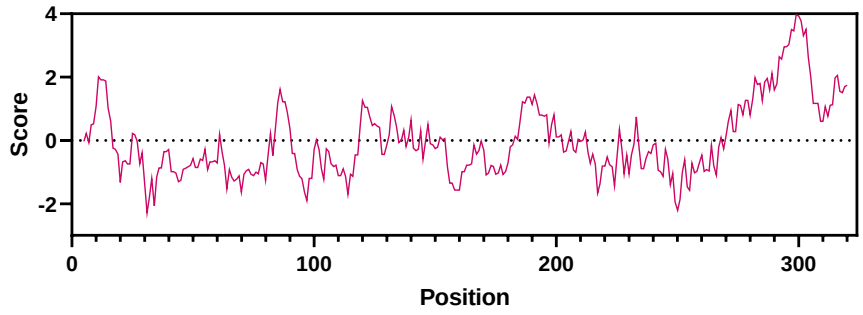

Figure 20. Kyte-Doolittle hydrophilicity plot of the MYXV M071 protein.

The plot represents the hydrophilicity profile (Y-axis), with positive values indicating hydrophobic regions and negative values indicating hydrophilic regions, along the 324 amino acid sequence of M071 (X-axis).

M083

MYXV M083 is a 286 aa protein with a theoretical molecular weight of 32.26 kDa, and with a pI of 9.15 (NP_051797.1). The transmembrane prediction analysis conducted using TMHMM-v.2.0 (DTU Health Tech), suggested that M083 follows a type I transmembrane model, with a large extracellular N-terminal region encompassing amino acid residues 1 to 247, a transmembrane helix between residues 248 to 270, and a short cytoplasmic C-terminal region spanning positions 271 to 286.

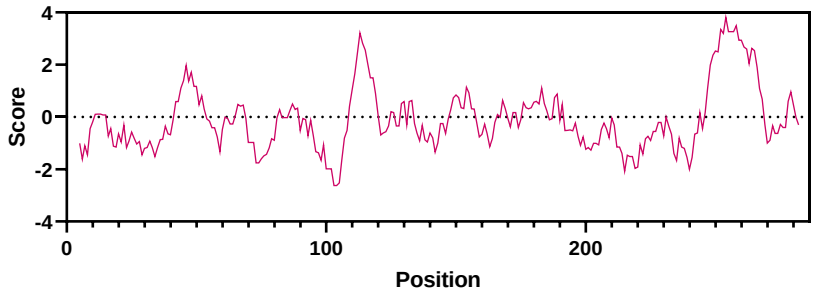

Figure 21. Kyte-Doolittle hydrophilicity plot of the MYXV M083 protein.

The plot represents the hydrophilicity profile (Y-axis), with positive values indicating hydrophobic regions and negative values indicating hydrophilic regions, along the 286 amino acid sequence of M083 (X-axis).

The intra-domain protein analysis of M083L in ScanProsite (SIB) predicted an α-carbonic anhydrase (CA) domain spanning amino acid positions 1 to 229. However, this CA-related protein as well as its homologous in other poxviruses, such as D8 from VACV, lost several CA-characteristic features and conserved residues (Matho et al., 2012). In fact, the CA domain of M083 has 40% identity with the last 232 amino acid from *O. cuniculus* carbonic anhydrase I (NCBI Reference Sequence: XP_051700566.1) but lacks three highly conserved residues involved in the Zn(2+)-binding site and two additional residues belonging to the catalytic site.

Considering the gathered data and with the aim of improving the efficiency and outcomes of soluble protein expression in exogenous expression systems, the nucleotide sequence encoding amino acid residues from positions 248 to 286 was omitted in the sequence cloned into the pET28a(+) vector (see supplementary information) As a result, the 247-amino acid recombinant M083 product expressed from the sequence cloned into pET28a(+) would be missing the TM domain yet retain the CA domain. Therefore, it would have a predicted molecular weight of 27.8 kDa, and a pI of 8.60 (ProtParam tool, Expasy).

M115L

The MYXV *m115l* ORF encodes a 21.58 kDa protein with isoelectric point of 5.49 (NP_051829.1). The hydrophobicity analysis of M115 revealed two relevant hydrophobic regions, the first one spanning residues between positions 42-50 and the second one between 133-149 (Figure 22).

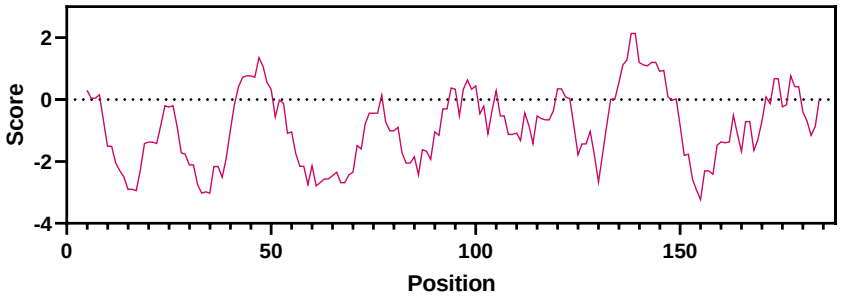

Figure 22. Kyte-Doolittle hydrophilicity plot of the MYXV M115 protein.

The plot represents the hydrophilicity profile (Y-axis), with positive values indicating hydrophobic regions and negative values indicating hydrophilic regions, along the 188 amino acid sequence of M115 (X-axis).

Based on the X-ray structure of VACV A27, M115 amino acid structure modeling predicts conserved structural folding (Chang et al., 2013). However, protein alignment analysis of homologs A27 and M115 revealed notable differences between both proteins. While the HBD is generally highly conserved across Orthopoxviruses, the amino-acid alignment indicated that MYXV M115 lacks the KKPE sequence which is the essential domain for binding to HS on the cell surface (Shih et al., 2009).

The prediction of coiled-coil (CC) motifs within the M115 sequence was performed through the DeepCoil2.0 Bioinformatic took in MPI Toolkit (Ludwiczak et al., 2019). The probability plot revealed a putative CC motif between amino acid positions 137-180, constituted by up to seven heptad repeats (Figure 23, A). All this putative CC domain is predicted to have α-helix secondary structure (residues 132 to 182) by PSIPRED analysis (Jones, 1999). Part of this motif also fits with the hydrophobic peak (133-149 aa) described in the hydropathic analysis (Figure 22).

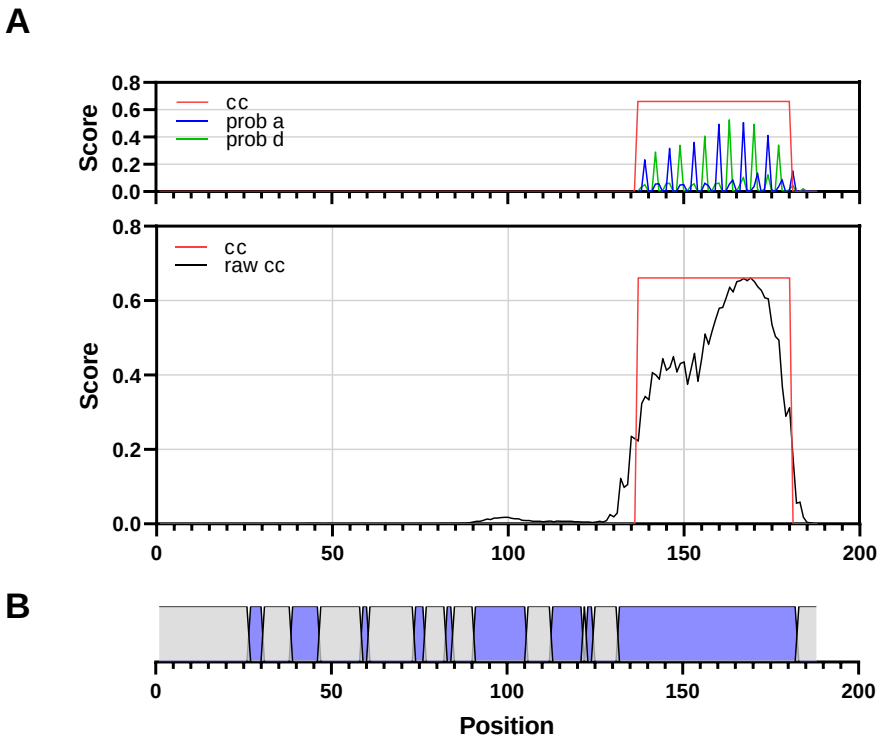

Figure 23. Bioinformatic analysis of M115's secondary structure

A) Coiled-coil domain prediction in 188 amino acid M115 sequence by DeepCoil2.0. Graphical continuous plot of the probability value for each residue to be in a coiled coil domain. A predicted coiled coil domain between amino acid positions 137 and 180 were plotted in red, with a score probability of 0.661. At the top, the prediction of residues at the "a" (*prob a*) and "d" (*prob d*) positions within the heptad repeat of the CC alpha-helix is represented by probability scores, in blue for the "a" position and in green for the "d" position along the sequence. B) Secondary structure prediction of M115 using (PSIPRED). α-helix conformations are represented in purple.

Despite the fact that the two cysteine residues in the A27-CCD (positions 71 and 72), which are crucial for the formation of covalent assembly with A26 protein through disulfide bond formation, are highly conserved in *Orthopoxvirus* (VACV, VAR, MPXV, CPXV, ECTV) and *Parapoxvirus*, there is a notable exception in other poxvirus genera. For instance, viruses within the *Capripoxvirus* (LSDV, GTPV, SPPV) are missing one of these residues, and both *Leporipoxvirus* (MYXV, SFV) and *Suipoxvirus* (SWPV) genera lack both cysteine residues (T. H. Chang et al., 2013). The LZD at the C-termini of A27 is more conserved in MYXV M115 and is predicted to be the region involved in A17 binding (Vázquez et al., 1998). According to what is described in the literature, M115 sequence also lack these two conserved cysteines (Figure..).

M141R

M141 is a 218 aa in length with an expected molecular weight of 23.70 kDa, and with a pI of 9.61 (NP_051855.1). The V-like Ig domain of M141 exhibits an unusually high level of putative N-

glycosylation sites, which would increase the apparent MW during protein expression analysis in heterologous systems. The hydropathicity study of the M141R identified two relatively hydrophobic regions, comprising the 18 first residues at N-terminus and the last 14 at the C-terminal ends (Figure 24). The first 18 amino acid residues correspond to a N-terminal type I signal sequence, predicted by the bioinformatic PSORT analysis tool (Jackson et al., 1999).

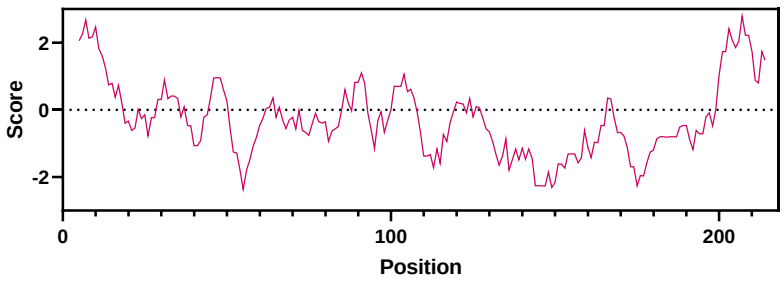

Figure 24. Kyte-Doolittle hydrophilicity plot of the MYXV M141 protein.

The plot represents the hydrophilicity profile (Y-axis), with positive values indicating hydrophobic regions and negative values indicating hydrophilic regions, along the 218 amino acid sequence of M141 (X-axis).

Although orthologous sequences of M141R showed a unique membrane spanning domain in the C-terminal, TMpred showed two possible transmembrane regions at both terminal ends, agreeing with previous hydropathicity information, corresponding with residues 1 to 19 and 196 to 214. Taking all this information into consideration, nucleotides coding for the amino acid residues at positions 1 to 19 and 196 to 218 were removed from the sequence cloned in the pEt28a(+) vector. Therefore, the 178 aa product from the cloned sequence in pEt28a(+) would have a theoretical molecular mass of 19.2 kDa) and pI of 9.4 (ProtParam tool, Expasy).

CHARACTERIZATION OF THE MYXV TARGET GENES IN MULTIPLE EXPRESSION SYSTEMS

Bacterial expression

Generation of bacterial expression vectors for the antigenic candidates

M022L in pGEX-2T

For the bacterial expression of M022, the pTriEx-*m022l* and pGEX-*gst-m022l* recombinant vectors were provided, courtesy of Dr. Kevin P. Dalton from our lab, which have not been published (*see Materials section).*

M029L, M071L, M083L, M115L, M141R in pET-28a(+)

Following the comprehensive review of the literature, along with the corresponding hydropathic analyses and prediction of antigenic regions (see supplementary information). Within the amino acid sequences of all the viral candidates, these genes were designed as full-length or partial fragments and cloned *in silico* between *Nde*I and *Xho*I sites in the bacterial pET-28a(+) expression vector (Figure 25). The resulting sequences (pET-28a(+) expression vectors) were synthesized *in vitro* and purchased from Genscript.

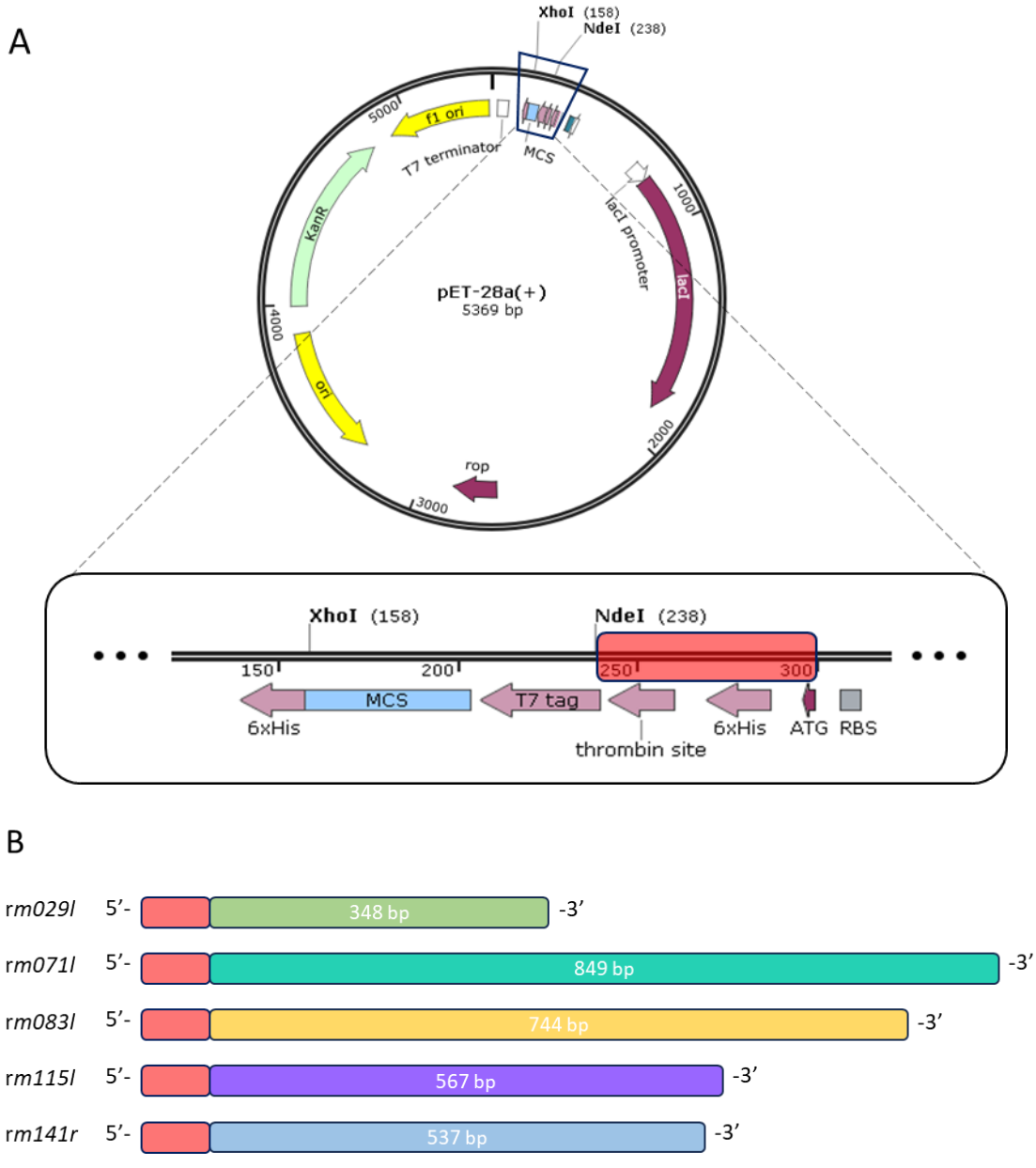

Figure 25. Construction of the expression cassettes in pET-28a(+).

A) Restriction strategy for insertion of the target genes into pET-28a(+) bacteria vector, using *Nde*I and *Xho*I restriction sites. The features included within the 60 bp defined by the red rectangle are the fusion epitope tag and include the translation start (ATG) codon, a polyhistidine tag and a thrombin cleavage site. B) Scheme of the

expected expression cassettes, containing the antigenic candidate genes (full-length or without their hydrophobic terminal domains) fused to the 60 bp N-terminal epitope tag.

Given that no TM regions or highly hydrophobic regions were predicted within the ORFs of *m029l* and *m115l*, their complete nucleotide sequences (352 bp and 567 bp, respectively) were cloned into the vector with a stop codon at the C-terminus to ensure termination of protein synthesis. However, cloning ORFs *m071l, m083l, m141r* involved incorporating_sequence deletions to avoid the presence of predicted hydrophobic regions and putative TM domains to improve their solubility and stability during heterologous expression (see the nucleotide sequences in the supplementary information).

The designs ensured that the resulting recombinant proteins would be fused to an N-terminal polyhistidine (6xHis) tag followed by a thrombin cleavage site (Figure 25, B). This configuration would imply the introduction of an additional 2.1 kDa (approximately) to the recombinant proteins following bacterial expression, in addition to facilitating purification, subsequent processing and detection (Table 7).

Table 8. Comparison of the theoretical gene sizes cloned into the expression vectors and the molecular weight (MW) of the corresponding encoded protein

CANDIDATES	*CLONED GENE SIZE*	*THEORICAL MW*	*ORF SIZE*	*RECOMBINANT PROTEIN*
M029L	348 bp	12.8 kDa	408 bp	14.9 kDa
M071L	849 bp	32.2 kDa	909 bp	34.4 kDa
M083L	744 bp	27.8 kDa	804 bp	30 kDa
M115L	567 bp	21.6 kDa	627 bp	23.8 kDa
M141R	537 bp	19.2 kDa	597 bp	21.4 kDa

Note: Theoretical MW of the constructs was determined by the Translate tool of ExPasy server from the Swiss Institute of Bioinformatics.

Note 2: the ORF sizes include the 60 bp epitope tag and the corresponding recombinant protein size (kDa).

Recombinant proteins expression screening

For the exogenous expression of viral proteins using a bacterial expression system, the *E. coli* BL21(DE3) strain was used. This strain is characterized by encoding the λDE3 gene (T7 phage RNA polymerase) under the control of an IPTG-inducible lacUV5 promoter.

Individual colonies of the BL21(DE3)-pTriEX-*m022l* transformants were screened on LB agar plates containing ampicillin, while BL21(DE3)-pET-28a(+)-*m029l, -m071l, -m083l, -m115l, and -m141r* transformants were screened on LB agar plates containing kanamycin. Several of the individual colonies that grew after an overnight incubation at 37°C under the corresponding

selective conditions were processed to extract the plasmatic DNA and characterize the recombinant plasmid by colony PCR and restriction enzyme digestion.

Upon confirmation of the presence and correct orientation of the insert, the correct expression of recombinant viral proteins was confirmed through induction of small-scale cultures of transformed BL21(DE3) cells (see Materials and Methods) and was confirmed by Western blot analysis using anti-HisTag or anti-GST primary antibodies and anti-mouse labeled secondary antibody.

Solubility screening of target proteins

M022

BL21(DE3)-pTriEX-*m022l* transformed cells cultured in 50 ml of LB-ampicillin culture were induced using 1 mM IPTG for 1h 30 min at 37ºC. Following culture harvest, lysis by freeze-thaw cycles and sonication, and clarification of the induced cultures, soluble (SF) e insoluble (PF) fractions were analyzed by 10% acrylamide SDS-PAGE (Figure 26). A protein with the predicted molecular weight for the target M022 protein, of approximately 42 kDa, was obtained in the induced culture, as expected, while in un-induced cultures, such a band was not detected. These induction conditions led to a significant expression of recombinant M022 protein, yet it was exclusively found in the lysed cell pellet (PF). This indicated that M022 protein was likely misfolded or aggregated into inclusion bodies during the translation process. Despite numerous efforts on trying to enhance the solubility of M022 through the optimization of various parameters, including inducer concentration, incubation times, incubation temperatures, and culture densities (OD_{600} measurements), no improvement in solubility was achieved (Data not shown).

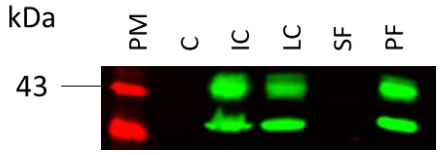

Figure 26. Western blot analysis showing expression of recombinant M022 using anti-HisTag antibodies.

A) Identification of M022 synthesis induced by 1 mM IPTG for 1,5h at 37°C. Lane 1: pre-stained NIR protein marker, Lane C: non-induced cells, Lane IC: induced cells, Lane LC: lysate of induced cells, Lane SF: clarified lysate, Lane PF: insoluble fraction after clarification.

The pGEX-*gst-m022l* vector was used as an alternative approach to produce M022 protein, since GST fusion may enhance the overall solubility of the construct as well as prevent premature or

incorrect folding during synthesis (Harper and Speicher 2011; Costa et al., 2014). In addition, parameters such as incubation temperature and concentration of inducer were varied. The product obtained following translation of the expression cassette of pGEX-*gst-m022l* would result in a 68 kDa fusion protein in which the GST protein (26 kDa), which is a naturally soluble protein, would be expressed at the N-terminal end of the M022 protein. Expression of the recombinant GST-M022 fusion protein was induced in transformed BL21(DE3) cultures with either 0.2 mM or 1 mM IPTG at OD600 < 0.2, which were incubated overnight at 18°C. After cell harvest, lysis, and clarification of the induced cultures, soluble (SF) e insoluble (PF) fractions were analyzed by 10% acrylamide SDS-PAGE (Figure 27). A protein band around 70 kDa, the expected molecular weight of the fusion GST-M022 protein, was detected and clearly recognizable in induced and lysed bacteria cultures (lanes 3, 4, 7 and 8), and was also detectable (although to a lesser extent) in the uninduced cells (lane 2), indicating a basal level of expression.

Under these specific induction and incubation conditions, the GST-M022 fusion protein exhibited a good level of expression, while variations in the inducer concentration appeared to have minimal impact on protein yield. In addition, GST fusion significantly increased the yield of soluble protein, as evidenced by the 70 kDa band present in the SF (lanes 5 and 9) under both induction conditions. Despite this enhancement, GST-M022 was predominantly located in the PF insoluble fraction (lanes 6 to 11) (Figure 27).

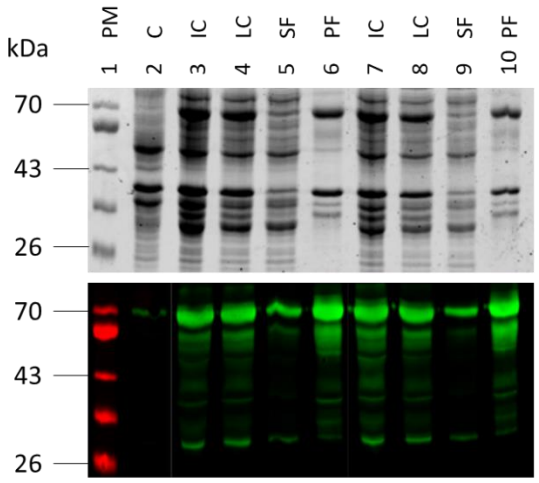

Figure 27. Western blot analysis showing expression of recombinant GST-M022 fusion protein using anti-GST antibodies.

Identification of the fusion GST-M022 synthesis induced by 0.2 (lanes 3-6) and 1 mM (lanes 7-10) of IPTG and overnight incubation at 18°C. PM: pre-stained protein marker, C: non-induced cells, IC: induced cells, LC: lysate of induced cells, SF: cleared lysate, PF: insoluble fraction.

In conclusion, the addition of a fusion tag (GST) to the N-terminal end of the MYXV M022 protein significantly improved its solubility, although most of the recombinant protein produced through this system remained in the insoluble fraction upon clarification.

M029

A selected clone of BL21(DE3)-pET-28a(+)-*m029l* transformed bacteria was cultured in 50 ml LB-kanamycin media, and was subjected to variations in IPTG inducer concentration, incubation temperature, lysis methods, culture media composition, and lysis buffer composition. Despite all the variables that were screened during prokaryotic expression of M029, none of the combinations improved the concentration of the viral protein in the soluble fraction (SF) since the detection of the approximately 15 kDa protein band was consistently found in the insoluble fraction (PF) (data not shown). The best result was obtained with induction of transformed bacteria culture in the log phase (OD600 around 0.5) using 0.2 mM IPTG followed by overnight incubation at 18°C (Panel A, Figure 28).

Considering that these conditions led to a significant amount of M029 recombinant protein, predominantly expressed in the insoluble fraction, a protocol using incubations of these fractions with mild non-ionic detergents (Tween-20, IGEPAL and Triton X-100) was implemented to study their effect on M029 solubilization (See Methods section). S1 and P1 samples were obtained after a first clarification of lysate cultures at low speed. S1 contained around half of the overexpressed M029, and its total volume was equally divided into 4 aliquots that were centrifuged at high-speed generating S2 and P2 (not shown). Since most of the M029 protein was in P2, two sequential washing steps with 1% and 2% final concentration of detergents were carried out, respectively. All fractions collected during the process were examined in a 12% acrylamide SDS-PAGE (Panel B, Figure 28).

A

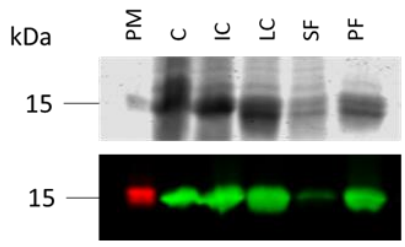

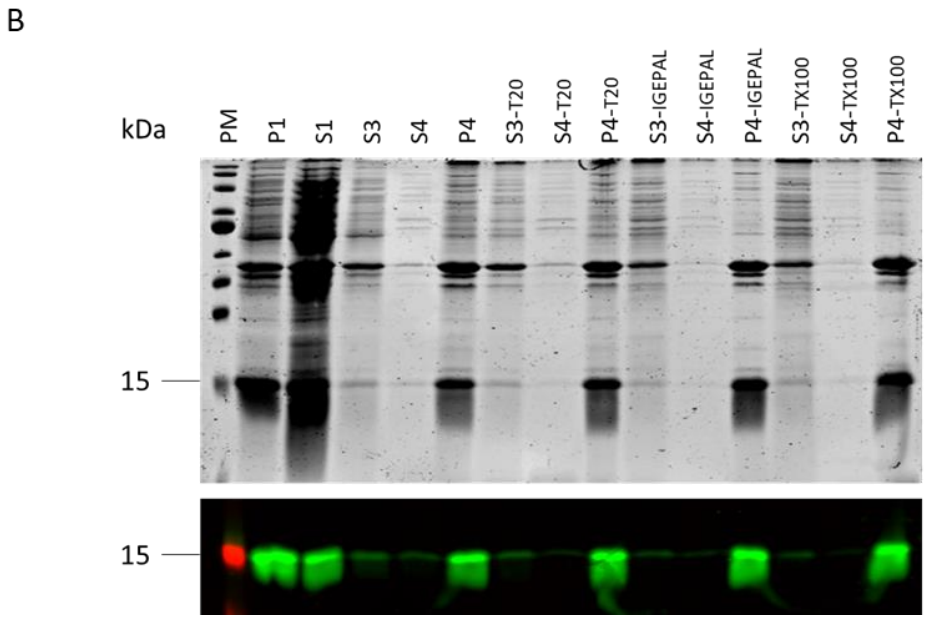

Figure 28. SDS-PAGE (12%) analysis of recombinant M029 protein expression and solubility in induced *E.coli* cultures.

The top image of each panel shows a Coomassie blue stained gel while the bottom shows a Western blot analysis detecting His-tagged proteins. A) Induction and incubation conditions that gave the best solubility for M029: 0.1 mM IPTG induction and ON incubation at 18°C (Lane PM: pre-stained NIR protein marker, Lane C: non-induced bacteria culture, Lane IC: induced culture, Lane LC: lysed culture; Lane SF: soluble fraction, Lane PF: insoluble fraction). B) Evaluation of detergent efficacy in M029 protein solubilization. Supernatant/soluble fractions (S) and pellet/insoluble fractions (P) obtained after each step of the solubilization process, using Tween-20 (T20), IGEPAL (IGEPAL) or Triton X-100 (TX100) non-ionic detergents. S3, S3-T20, S3-IGEPAL and S3-TX100 lanes show the protein fractions solubilized in the first wash; while S4, S4-T20, S4-IGEPAL and S4-TX100 lanes show the proteins solubilized after the second wash. P4, P4-T20, P4-IGEPAL, P4-TX100 lanes indicate the protein fraction that remains insoluble after incubation with detergent.

The addition of non-ionic detergents failed to significatively enhance the solubility of the recombinant M029 protein (rM029). In fact, the control sample that was processed in Tris-HCl buffer pH7.5 without any detergent demonstrated similar or even higher solubility outcomes (S3, S4 in panel B, Figure 28). No obvious differences in solubilization effectiveness were observed among the screened detergents. Indeed, each one displayed a modest solubilizing impact during the first incubation at 1% concentration of Tween-20 (S3-T20), IGEPAL (S3-IGEPAL) or Triton X-100 (S3-TX100) (panel B, Fig…). This effect diminished in the subsequent incubation, despite an increase in Tween-20, IGEPAL and Triton X-100 detergent concentration to 2% (S4-T20, S4-IGEPAL and S4-TX100, respectively) (Panel B, Figure 28).

M083

M083 protein expression was confirmed through the detection of a protein band of slightly less than 34 kDa in size in Western blot analysis of induced BL21(DE3) cultures. The selected transformed clone was cultured in 50 ml LB media containing kanamycin, to study the solubility

of M083 protein under several induction conditions. This viral protein had a good solubility profile since it was produced in native form at physiological incubation temperature, and under standard inducing conditions (Figure 29). About half of the recombinant M083 protein produced within the 0.2 mM IPTG-induced culture is found in the cleared lysate (SF) whilst the other half was produced insoluble in nature (PF). Addition of 1 mM IPTG induced a higher overexpression of M083 protein but instead of being detrimental to its solubility, it even increased the yield of soluble M083 protein in the cleared lysate (SF), compared to its amount found in insoluble form.

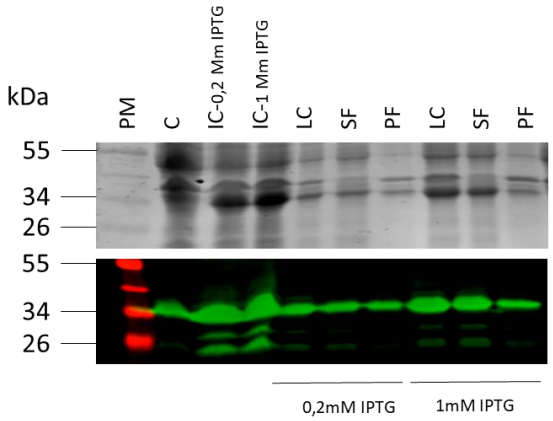

Figure 29. Detection of M083 recombinant protein production and solubility analysis in *E.coli* expression system.

Bacteria cultures induced with 0.2 mM or 1 mM IPTG for 1.5 h at 37°C, lysed and clarified. Protein fractions were resolved on 12% SDS-PAGE gels and stained with Coomassie blue (top image) or transferred to a nitrocellulose membrane and blotted against anti-His tag (bottom image). Lane 1: pre-stained NIR protein marker, Lane 2: uninduced bacteria, Lane 3: 0.2 mM IPTG induced cultures, Lane 4: 1 mM IPTG induced cultures, Lanes 5 to 7 include samples from the 0.2 mM IPTG induced culture whilst Lanes 8 to 10 include samples from 1 mM IPTG induced cultures. Lanes 5 and 8: lysis culture, Lanes 6 and 9: soluble fraction, Lanes 7 and 10: insoluble fraction.

M115

The heterologous expression of M115 protein in induced *E.coli* cultures was confirmed through the detection of a protein band reactive to anti-Histidine tag antibody of approximately 30 kDa in size, in Western blot analysis. The selected clone was cultured in 50 ml LB media containing kanamycin to study the solubility of the M115 recombinant protein under several induction and growth conditions, including variations in IPTG inducer concentration, incubation temperature, lysis method, culture media composition, and lysis buffer composition (Panel A, Figure 30). The best M115 soluble protein yield was achieved through 0.2 mM IPTG induction and overnight incubation at 18°C (Panel B, Figure 30). The pronounced intensity of the protein bands stained with Coomassie blue throughout the SDS-PAGE gel indicated high protein concentrations, reflecting abundant bacteria growth. Compared to the overall protein content, the recombinant viral protein constituted a relatively minor fraction, and its corresponding ~30 kDa Coomassie-

stained protein band was barely distinguishable. While this combination of induction and growth conditions did not lead to a high overexpression of the M115 protein, a substantially good rate of expressed M115 protein was found in the soluble fraction (SF), suitable for further purification under native conditions.

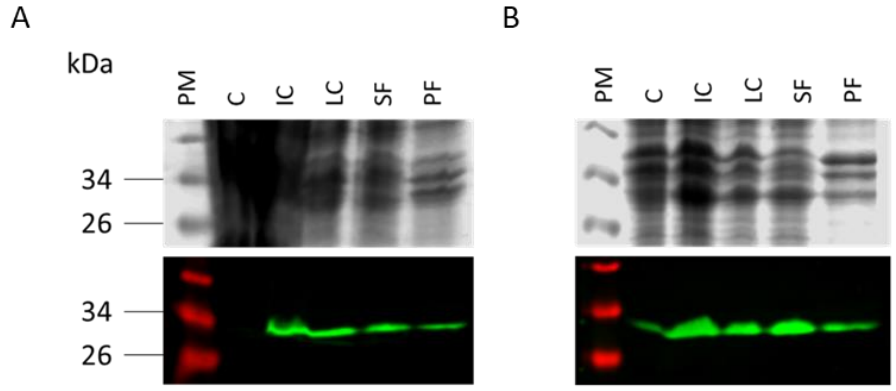

Figure 30. SDS-PAGE (12%) analysis of recombinant M115 protein expression and solubility in induced *E.coli* cultures.

The top image of each panel shows a Coomassie blue stained gel while the bottom shows a Western blot analysis detecting His-tagged proteins. A) Growth of bacteria culture in LB-B/S (LB, 2.5 mM glycyl-betaine, 1M D-sorbitol) and induction at low OD_{600} with 0.2 mM IPTG and incubation for 5 days at 22°C. Lane 1: pre-stained NIR protein marker, Lane 2: non-induced bacteria culture, Lane 3: induced culture, Lane 4: lysed culture; Lane 5: soluble fraction, Lane 6: insoluble fraction. B) Induction with 0.2 mM IPTG and overnight incubation at 18ºC. Lane 1: pre-stained NIR protein marker, Lane 2: non-induced bacteria culture, Lane 3: induced culture, Lane 4: lysed culture; Lane 5: cleared lysate, Lane 6: insoluble fraction.

M071

M071 protein expression was confirmed through the detection of a protein band of approximately 34 kDa in size in induced BL21(DE3) cultures, in Western blot analysis using anti-Histidine tag blotting. The selected transformed clone was cultured in 50 ml LB media containing kanamycin to study the solubility of M071 protein under several conditions. First, bacteria cultures were induced by addition of 1 mM IPTG followed by 1.5 h incubation at 37°C. The intensity of the Coomassie-stained protein bands indicated high concentrations of protein analyzed in the gel, which in turn suggested abundant bacteria growth. However, this induction condition did not lead to a significant overexpression of M071 protein, and the little amount that was produced was found in the insoluble fraction (PF) (Panel A, Figure 31). Several factors may have contributed to the low expression level of the M071 protein, including incorrect folding or low protein stability, which could have resulted in M071 being targeted for degradation.

The expression level of the M071 protein was considerably higher when the incubation temperature during induction was lowered to 18°C, even when the expression was induced by

0.2 mM IPTG (Panel B, Figure 31). The Coomassie-stained protein bands of the induced culture (IC) were lighter compared to the non-induced culture (C), indicating that induction of M071 protein expression could somehow be toxic to the host cells, leading to growth inhibition or certain degree of cell death. Apart from that, the M071 protein overexpressed under these conditions was essentially insoluble (PF).

Despite several variables being considered to enhance the solubility of M071, including media composition (e.g. LB-B/S), induction strategies, cell lysis method, none of these made significant improvements. Given that the expressed protein was predominantly found in the insoluble fraction, three different non-ionic mild detergents (Tween-20, IGEPAL and Triton X-100) were evaluated for their ability to extract M071 potentially associated with cell membranes, particularly from any associated bilipid fragments (See Methods section 1.3.4.) (Panel C, Figure 31). S1 and P1 samples were obtained after a first low-speed clarification of lysate cultures obtained from cultures induced with 1 mM IPTG and incubated overnight at 18°C. S1 contained around half of the overexpressed M071, and its total volume was equally divided into 4 aliquots that were centrifuged at high-speed generating S2 and P2 (not shown). Given that the majority of the M071 protein was located in fraction P2, it was subjected to two sequential washing steps, the first one with 1% and the second with a 2% final concentration of the corresponding detergents. The detergent incubation process did not yield a noticeable transfer of M071 protein into the cleared lysate. This result was consistent across all three detergents tested, indicating that the protein might be forming aggregates or be part of inclusion bodies that are resistant to solubilization by such mild detergents. In addition, increasing the concentration of detergents didn´t improve the overall solubility of the proteins present in the insoluble fraction. This was evidenced in the Coomassie stained gel, in which the number of bands visualized in lanes S4-T20, S4-IGEPAL and S4-TX100, corresponding to the proteins solubilized in the second washing step using 2% detergent, was derisory.

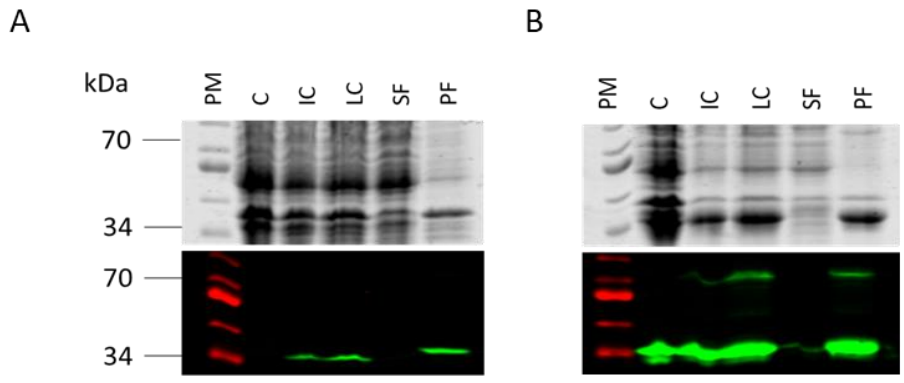

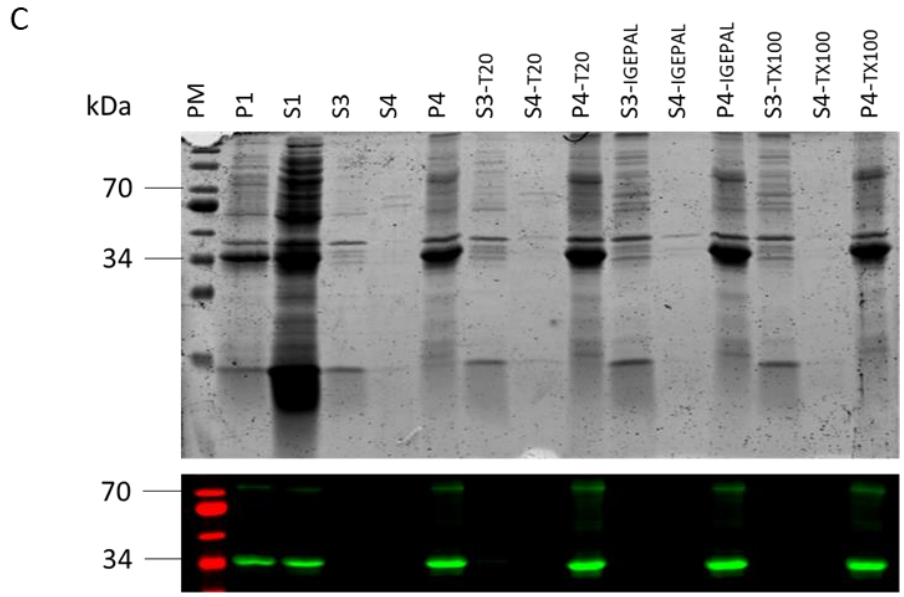

Figure 31. SDS-PAGE (12%) analysis of recombinant M071 protein expression and solubility in induced E.coli cultures.

The top image of each panel shows a Coomassie blue stained gel while the bottom shows a Western blot analysis detecting His-tagged proteins. A) 1 mM IPTG induction for 1.5 h at 37°C. Lane 1: pre-stained NIR protein marker, Lane 2: non-induced bacteria culture, Lane 3: induced culture, Lane 4: lysed culture; Lane 5: soluble fraction, Lane 6: insoluble fraction. B) Overnight 0.2 mM IPTG induction at 18°C. Lane 1: pre-stained NIR protein marker, Lane 2: non-induced bacteria culture, Lane 3: induced culture, Lane 4: lysed culture; Lane 5: soluble fraction, Lane 6: insoluble fraction. C) Evaluation of detergent efficacy on M071 protein solubilization. Supernatant/soluble fractions (S) and pellet/insoluble fractions (P) obtained after each step of the solubilization process, using Tween-20 (T20), IGEPAL (IGEPAL) or Triton X-100 (TX100) non-ionic detergents. S3, S3-T20, S3-IGEPAL and S3-TX100 lanes show the protein fractions solubilized in the first wash; S4, S4-T20, S4-IGEPAL and S4-TX100 lanes show the proteins solubilized after the second wash, and P4, P4-T20, P4-IGEPAL and P4-TX100 lanes indicate the protein fraction that remains insoluble after incubation with detergent.

Besides indicating the need to find an alternative approach for M071 protein solubilization, the previous results showed that a one-step wash of the insoluble fraction with either one of the three detergents, could indeed reduce the amount of membrane proteins, lipids, and other proteins loosely associated with the inclusion bodies. This wash-step could have several benefits when being performed before the solubilization of inclusion bodies by chaotropic agents by improving the purity and yield of the M071 recombinant protein. Therefore, it was included in the isolation and solubilization of bacterial inclusion body recombinant proteins protocol and referred to as buffer W (see methods section). To enhance the efficiency of the inclusion body solubilization process, the buffer S was supplemented with different components: 8 M urea (a), 8 M urea + 10 mM β-mercaptoethanol (b), 8 M urea + 10 mM β-mercaptoethanol + 2% Triton X-100 (c) (Panel A, Figure 32). Notably, all solubilization buffers achieved similar yields of M071 recombinant protein solubilization from the inclusion bodies found in P2, of around half protein

being transferred into the cleared fraction (S3, S3-a, S3-b, S3-c). However, none of them could completely solubilize the protein.

Finally, the use of a washing step of the inclusion bodies (P2) with 2% Triton X-100, and the use of 8 M urea in the solubilizing buffer were found essential steps for the purification and solubilization of M071 recombinant protein from bacterial inclusion bodies generated upon protein induction (Panel B, Figure 32).

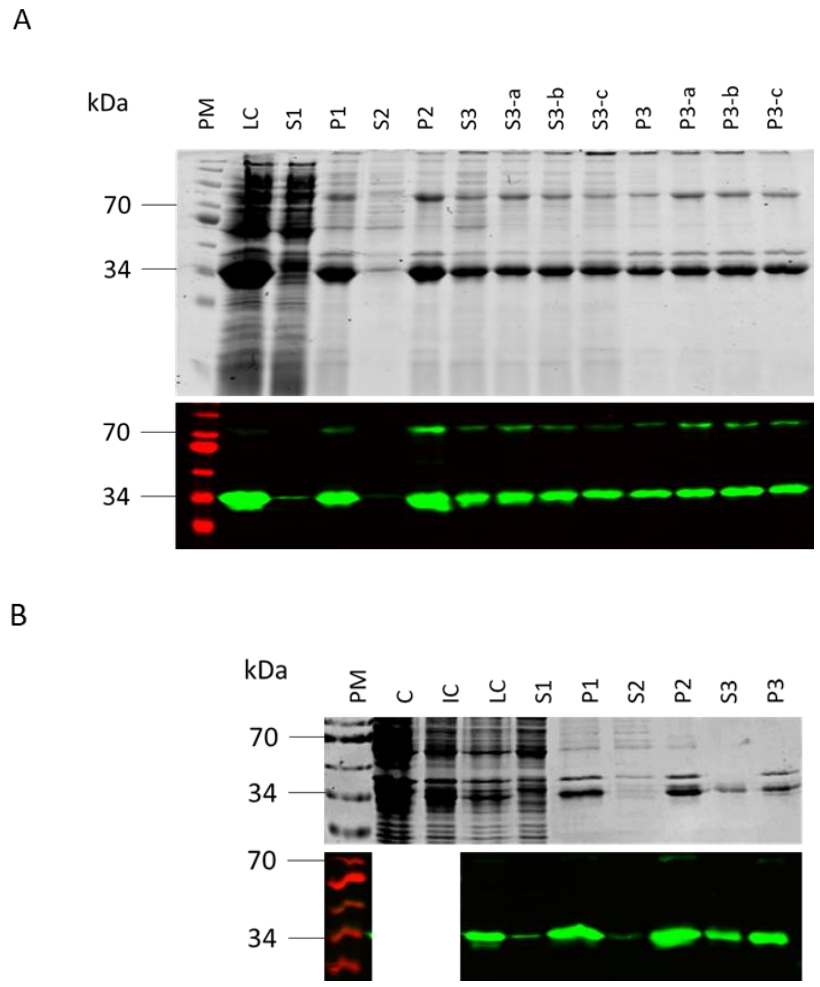

Figure 32. Evaluation of inclusion body purification and solubilization for recombinant M071 protein expressed in induced E.coli cultures

The protein fractions of 1 mM IPTG induced cultures cultivated for 3 hours at 30°C were analyzed using 12% SDS-PAGE, the top image of each panel shows a Coomassie blue stained gel while the bottom shows a Western blot analysis detecting His-tagged proteins. A) Optimization of purification and solubilization of inclusion bodies containing the M071 recombinant protein using different buffer S composition: 8 M urea (a), 8 M urea + 10 mM β-mercaptoethanol (b), 8 M urea + 10 mM β-mercaptoethanol + 2% Triton X-100 (c). B) Analysis of purification and solubilization of inclusion bodies containing the M071 recombinant protein under the ideal conditions. Legend for both panels; Lane PM: pre-stained protein marker, Lane C: uninduced bacteria, Lane IC: induced cultures, Lane LC: lysed cultures, Lane S1: raw cleared lysate, Lane P1: raw pellet containing inclusion bodies, Lane S2: solubilized fraction after incubation with buffer W containing 2% Triton X-100, Lane P2: insolubilized fraction, Lanes S3: solubilized fraction using denaturing conditions, Lanes P4: final insolubilized fraction.

M141

The heterologous expression of M141 protein in induced *E.coli* cultures was confirmed through the detection of a protein band antibody of approximately 22 kDa in size, in Western blot analysis which was reactive to anti-Histidine tag. The selected bacteria clone was cultured in 50 ml LB media containing kanamycin to study the solubility of M141 protein under several conditions. Bacteria induced with 1 mM IPTG and incubated overnight at 18°C and lysed by homogenization, generated a high level of M141 expression, but none of it was found in the cleared lysate (Panel A, Figure 33). Several IPTG inducer concentration, incubation temperature, lysis method, culture media composition, and lysis buffer composition, were screened to improve overexpression and solubility of this recombinant viral protein. Nonetheless, the conditions found to produce the highest solubility rate for M141 still resulted in a low yield of soluble protein (Panel B, Figure 33).

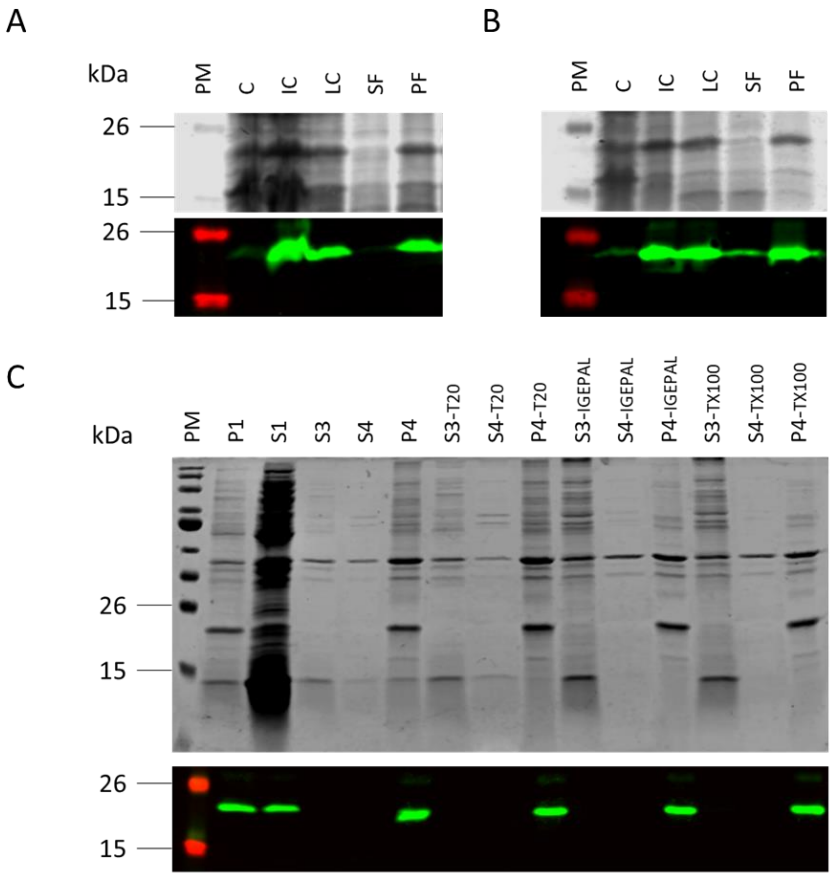

Figure 33. SDS-PAGE (12%) analysis of recombinant M141 protein expression and solubility in induced *E.coli* cultures.

The top image of each panel shows a Coomassie blue stained gel while the bottom shows a Western blot analysis detecting His-tagged proteins. A) Induction with 1 mM IPTG followed by overnight

incubation at 18°C and high-pressure homogenization cell lysis. Lane 1: pre-stained NIR protein marker, Lane 2: non-induced bacteria culture, Lane 3: induced culture, Lane 4: lysed culture; Lane 5: soluble fraction, Lane 6: insoluble fraction. B) Growth of bacteria culture in LB-B/S media and induction at low OD_{600} with 0.2 mM IPTG and incubation for 5 days at 22°C. Lane 1: pre-stained NIR protein marker, Lane 2: non-induced bacteria culture, Lane 3: induced culture, Lane 4: lysed culture; Lane 5: soluble fraction, Lane 6: insoluble fraction. C) Evaluation of detergent efficacy on M141 protein solubilization. Supernatant/soluble fractions (S) and pellet/insoluble fractions (P) obtained after each step of the solubilization process, using Tween-20 (T20), IGEPAL (IGEPAL) or Triton X-100 (TX100) non-ionic detergents.

Since the expressed viral protein was predominantly found in the insoluble fraction, like in the previous case of the M071 protein, three different non-ionic mild detergents (Tween-20, IGEPAL and Triton X-100) were also evaluated for their ability to extract M141 potentially associated with cell membranes (See Methods section 1.3.4.) (Panel C, Figure 33). This process did not achieve a significant transfer of M141 protein into the cleared lysate at any of the three detergents tested. The performance of a second washing step with an increased detergent concentration (2%) did not enhance the overall solubility of proteins within the insoluble fraction, as shown by the minimal number of protein bands stained by Coomassie blue in lanes S4-T20, S4-IGEPAL and S4-TX100.

Despite these findings, the initial wash with 1% IGEPAL or 1% Triton X-100 appeared to have a more effective solubilization effect over the whole proteomic profile of the insoluble fraction. The intensity and number of protein bands on lanes S3-IGEPAL and S3-TX100 in the Coomassie-stained gel is considerably higher than the negative control sample S3 (without washing steps) or S3-T20. This also implied that the recombinant M141 in the final insoluble fraction were less contaminated by other proteins (Panel C, Figure 33). Since the M141 protein might be aggregating or incorporated into inclusion bodies that are resistant to solubilization by mild detergents, it was purified under denaturing conditions from solubilized inclusion bodies using a chaotropic agent (8 M urea). Also, considering the results obtained in the attempts of solubilizing M071 with non-ionic detergents, a washing step with 2% Triton X-100 was included in the isolation and solubilization of bacterial inclusion body recombinant proteins protocol and referred to as buffer W (see methods section*).*

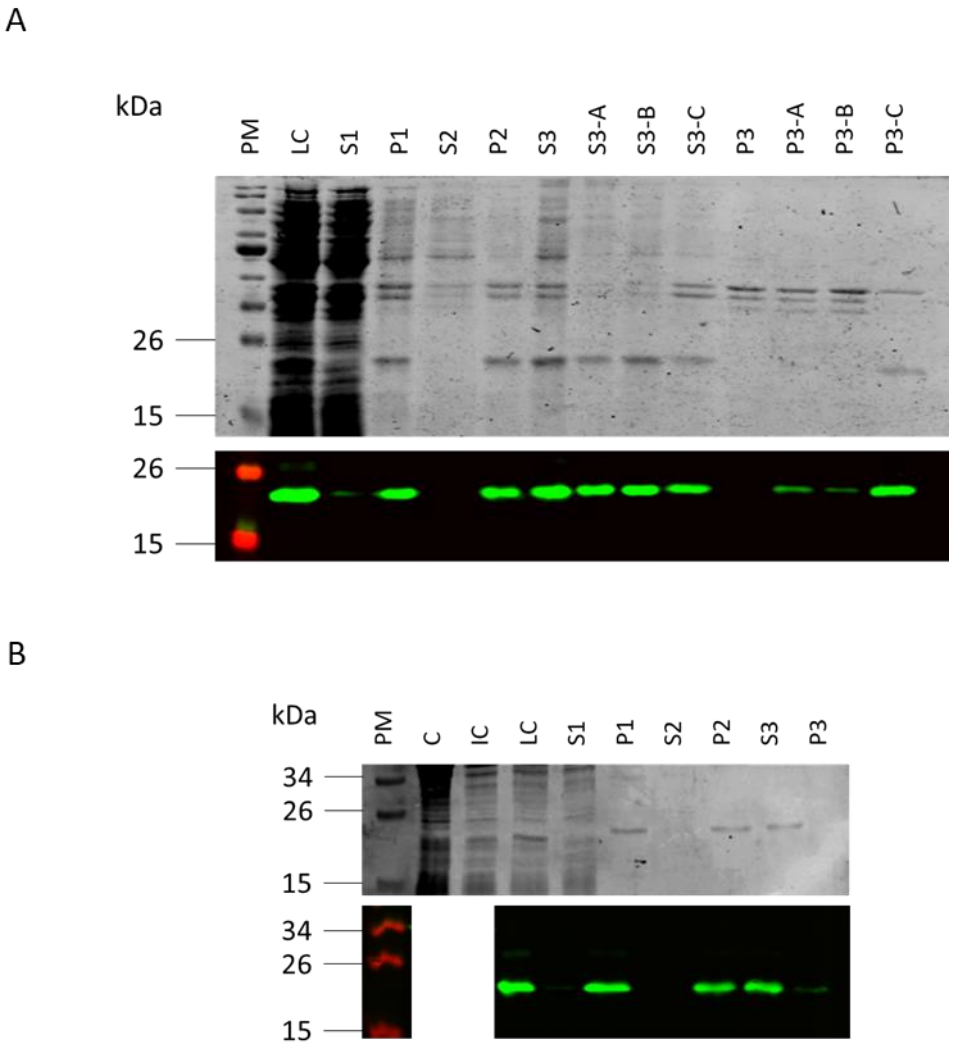

Figure 34. Evaluation of inclusion body purification and solubilization for recombinant M141 protein expressed in induced E.coli cultures

The protein fractions of 1 mM IPTG induced cultures cultivated for 1.5 hours at 37°C were analyzed using 12% SDS-PAGE. The top image of each panel shows a Coomassie blue stained gel while the bottom shows a Western blot analysis detecting His-tagged proteins. A) Optimization of purification and solubilization of inclusion bodies containing the M141 recombinant protein using different buffer S composition: 8 M urea (a), 8 M urea + 10 mM β-mercaptoethanol (b), 8 M urea + 10 mM β-mercaptoethanol + 2% Triton X-100 (c). B) Analysis of purification and solubilization of inclusion bodies containing the M141 recombinant protein under the ideal conditions. Legend for both panels; Lane PM: pre-stained protein marker, Lane C: uninduced bacteria, Lane IC: induced cultures, Lane LC: lysed cultures, Lane S1: raw cleared lysate, Lane P1: raw pellet containing inclusion bodies, Lane S2: solubilized fraction after incubation with buffer W containing 2% Triton X-100, Lane P2: insolubilized fraction, Lanes S3: solubilized fraction using denaturing conditions, Lanes P4: final insolubilized fraction.

Buffer S composition was also optimized by supplementing it with different components: 8 M urea ("a"), 8 M urea + 10 mM β-mercaptoethanol ("b"), 8 M urea + 10 mM β-mercaptoethanol + 2% Triton X-100 ("c") (Panel A, Figure 34). Indeed, the composition of buffer S was found to play a crucial role in the solubilization process of M141 protein; the amount of this recombinant protein extracted from the inclusion bodies in P2 ranged from approximately 50% to the

complete solubilization of the protein. Although buffer composition "c" had the best overall efficiency in solubilizing proteins from the P2 fraction, its M141 protein's recovery rate from the insoluble fraction was the lowest. Solubilization buffers "a" and "b" performance had a higher but similar efficiency on recovering soluble M141 recombinant protein from inclusion bodies, with a recovery rate of around 90% for both buffers. This indicated that the addition of 10 mM β-mercaptoethanol was truly not being of much use. Moreover, straight incubation of inclusion bodies with buffer S, without the washing step, showed a complete solubilization of M141 protein (absence of protein band in WB using anti-Histidine tag in lane P3), although the use of a washing step of the inclusion bodies (P2) with 2% Triton X-100 got rid of contaminant proteins in the cleared fractions. Hence, this step was maintained in the final protocol for the purification and solubilization of M141 recombinant protein from bacterial inclusion bodies generated upon protein induction, together with the use of the solubilizing buffer "a", were found essential steps for the (Panel B, Figure 34).

Baculovirus expression vector system (BEVS)

Generation of multivalent vectors for the characterization of viral genes M022L, M071L and M115L in insect and vertebrate cells

The pTriEX-1.1 expression vector offered a versatile gene expression system across different expression platforms, being able to transcribe the genes cloned in the vector in prokaryotic and eukaryotic cells. The homologous flanking baculovirus sequences *lef2/*603 and ORF 1629 included in pTriEX-1.1 vector allow the generation of recombinant baculovirus. In regards of the recombinant viral proteins exhibited low solubility (M071) or low yield of overexpression (M022, M115) in the *E. coli* expression system, their ORFs were cloned into pTriEX-1.1 using suitable restriction enzyme sites, subsequently tested by restriction mapping and Sanger sequencing to ensure correct assembly (Data not shown).

Generation of recombinant baculovirus (rBV): rBV-M022, rBV-M71, rBV-M115

Sf9 insect cells were co-transfected with 500 ng of a linearized baculoviral genome and 500 ng of the recombinant expression vectors pTriEX-GST-M022, pTriEX-M071 or pTriEX-M0115, using the transfection reagent Cellfectin II (Thermo Fisher). Since the linearization of the AcMNPV viral genome truncated the essential gene ORF 1629, only those genomes that experience

homologous recombination with the transfer plasmids (pTriEX-GST-M022, pTriEX-M071 or pTriEX-M115) would restore it, producing viable rBV.

The recombinant BV stocks rBV-M022, rBV-M071, rBV-M115 were amplified in larger Sf9 cultures, and the number of infectious particles present in each stock was determined by plaque assay. High titers (>10^8 pfu/ml) were reached in all three rBV generation process.

Protein expression in insect cells using rBVs infection

Heterologous gene expression in the generated rBVs is driven by the very late p10 promoter in insect cells (García-Fruitós, 2015). Adherent insect cell cultures were seeded in 6-well plates and infected with the rBVs at different MOI to express the target MYXV proteins and a time course of infection was analyzed at 24h intervals ranging from 24 to 96 hours post infection (hpi). At each time point, infected cells were collected to assess protein expression levels through SDS-PAGE and Western blot analysis, with antibodies targeting their corresponding protein markers (polyhistidine tag or GST tag).

The time-course analysis of the GST-M022 protein revealed differences between the expression profile obtained at an MOI of 1 and the one at an MOI of 10 (Figure 35). Initial expression of the recombinant protein, detected as a protein band around 70 kDa, was observed as early as 24 hpi for the rBV-M022 infected cells with the highest MOI. However, the Western blot analysis revealed a second band of around 30 kDa that gave a more intense signal, presumably corresponding to the GST fusion protein, which was detected until the end of the experiment. This second band was also detected in the samples obtained from the cells infected at a MOI of 1.

GST-M022 protein expression displayed a gradual increase during the rBV-M022 infection at an MOI of 1, reaching a maximum yield between 72 and 96 hpi. However, the peak in GST-M022 protein expression during infection at an MOI of 10 was reached sooner, between 48 and 72 hpi. After this time point, the loss of signal intensity in the 70 kDa band, and increased signal in the 30 kDa band observed in the Western blot analysis, evidenced a significant drop of the GST-M022 protein yield, and increased protein degradation. Cell viability started to dramatically decrease past 72 hpi. Overall, these results suggested that in Sf9 cultures infected with rBV-M022 at an MOI of 10, a harvest window between 48 and 72 hpi would provide a substantial protein production whilst avoid the deleterious effects of infection derived from loss of cell integrity and death.

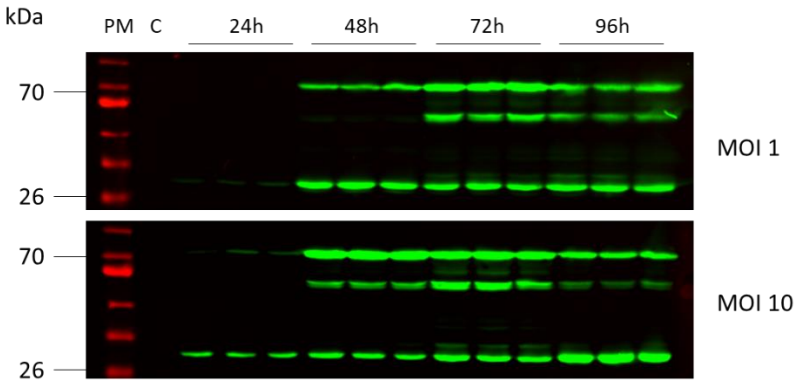

Figure 35. Temporal expression profile of GST-M022 protein produced in rBV-M022 infected Sf9 adherent cell cultures infected at a MOI 1 or MOI 10

Samples were collected in triplicates 24h, 48h, 72h and 96 hpi, and analyzed in a 10% SDS-PAGE gel. Lane 1: pre-stained NIR protein marker, Lane 2: non-infected Sf9 cells, Lanes 3 to 5: infected Sf9 cells collected 24 hpi, Lanes 6 to 8: infected Sf9 cells collected 48 hpi, Lanes 9 to 11: infected Sf9 cells collected 72 hpi, Lanes 12 to 15: infected Sf9 cells collected 96 hpi.

The pET28-M71 contained an incomplete version of the *m071l* gene that resulted in the production of a truncated M071 protein with a molecular weight of 34.4 kDa. Meanwhile, the genome of rBV-M71 incorporated the complete *m071l* ORF from MYXV, leading to an expected molecular weight of 36.8 kDa for the recombinant M071 (plus the additional ~1 kDa corresponding to the addition of the polyhistidine tag) expressed in the baculovirus infected insect cells. This discrepancy in the size of M071 protein expressed via the BEVS compared to the recombinant M071 produced in a prokaryotic expression system, was evidenced in the Western blot analysis (Panel A, Figure 36).

The time-course analysis for the M71 protein revealed a similar expression profile when comparing infections at an MOI of 1 to those at an MOI of 10 (Panel B, Figure 36). In the first infection condition, the peak expression of the M071 protein was distinctly observed at 72 hpi, with the 37 kDa protein band not detectable at any other time points, before or after 72 hpi. In the Sf9 cultures infected at an MOI of 10, the M071 viral protein band was initially detected at 48 hpi in the Western blot analysis and had its peak in expression between 48 and 72 hpi.

The expression of M071 protein in the Sf9 cells infected at an MOI of 10 in suspension started at 48 hpi, 24 hours before than in the culture infected at an MOI of 1, and under both infection conditions, the M71 37 kDa protein band was detected until 96 hpi. However, these bands did not reach high signal intensities at any condition, indicating the recombinant protein had very low yield of production.

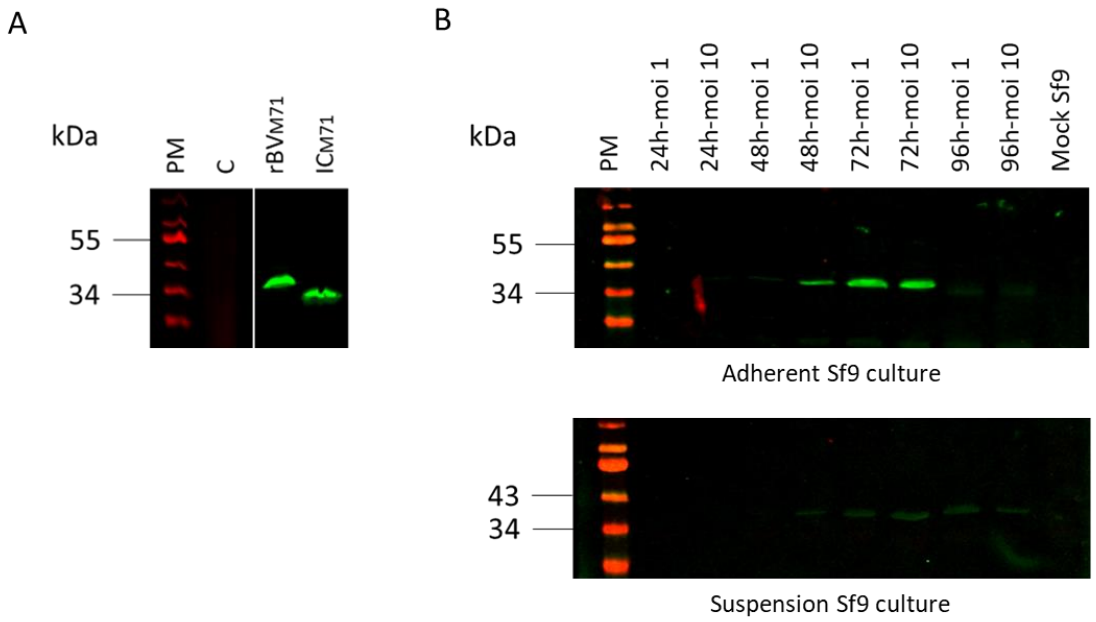

Figure 36. Analysis of the recombinant M071 protein expressed in Sf9 insect cells.

A) Comparative expression of MYXV recombinant M071 protein using either BEVS or *E.coli* expression system. Lane 1: pre-stained NIR protein marker, Lane 2: non-infected Sf9 insect cells, Lane 3: rBV-M71 Sf9 infected cells, Lane 4: induced *E.coli* culture transformed with pEt28-M71. B) Temporal expression profile of M071 protein produced in adherent, and in suspension, Sf9 cell cultures infected with rBV-M71 at MOI of 1 or 10. Infected cell samples were collected at 24h, 42h, 72h and 96 hpi.

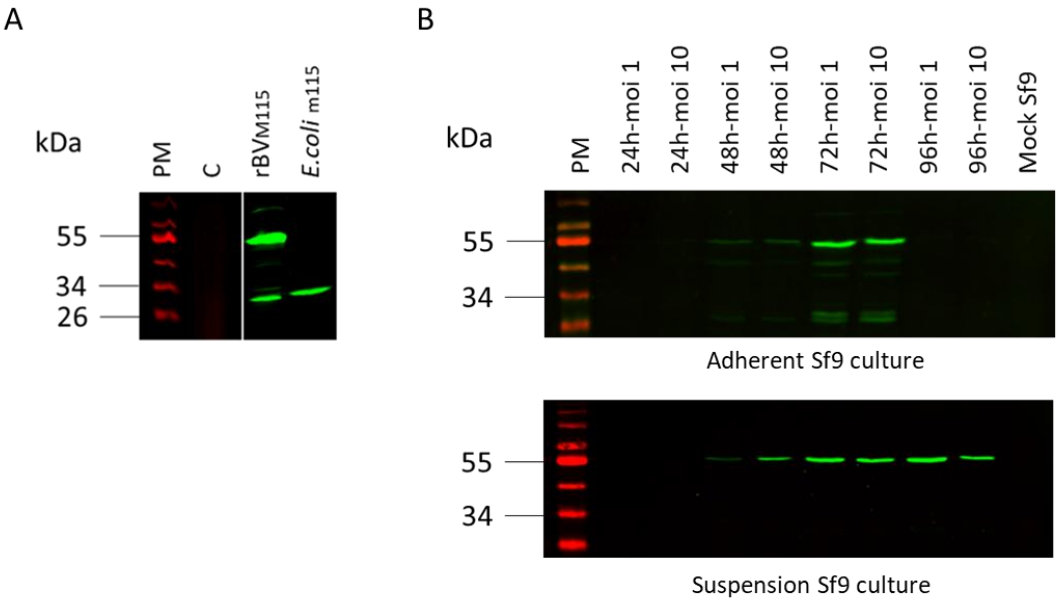

Figure 37. Analysis of the recombinant M115 protein expressed in Sf9 insect cells

A) Comparative expression of MYXV recombinant M115 protein using either BEVS or *E.coli* expression system. Lane 1: pre-stained NIR protein marker, Lane 2: non-infected Sf9 insect cells, Lane 3: rBV-M115 Sf9 infected cells, Lane 4: induced *E.coli* culture transformed with pEt28-M115. B) Temporal expression profile of M115 protein produced in adherent, and in suspension, Sf9 cell cultures infected with rBV-M115 at an MOI of a1 or 10. Infected cell samples were collected at 24h, 42h, 72h and 96 hpi.

The rBV-M115 genome included the complete coding sequence of *m115l* gene from Vac-MYXV, therefore the expected molecular weight of its product expressed in infected cells upon translation was of 21.6 kDa (plus the additional ~1 kDa of the fused C-terminal polyhistidine tag). The M115 protein expression in the BEVS was analyzed in SDS-PAGE and Western blot analysis with anti-histidine tag antibody, revealing two well defined bands, one with apparent molecular weight of ~28 kDa, and another of around ~55 kDa (Panel A, Figure 37). Additionally, a third band of an apparent weight around 90 kDa was roughly visible. In comparison, the M115 protein expressed through the *E.coli* expression system displayed one band with slightly higher apparent molecular weight (around 30 kDa) than the smallest band produced in insect cells upon rBV-M115 infection.

The time-course analysis for the M115 protein showed a practically identical expression profile of the viral protein at both infection conditions, MOI of 1 and of 10 (Panel B, Figure 37). In the adherent rBV-M115 infected cells, the protein was first observed at 48 hpi, but it reached an expression peak at 72 hpi. However, in the infected Sf9 cells cultured in suspension, there was a progressive increase in protein production from 48 to 96 hpi, with the peak of M115 expression reached between 72 and 96 hpi.

Solubility of GST-M022, M71 and M115 recombinant proteins produced in the BEVS

Once the infection conditions for each rBV were determined and the harvest timing for maximizing the production of recombinant proteins were identified, the BEVS protein production was scaled up. Larger Sf9 cells cultured in suspension were infected with the rBVs and harvested at the corresponding conditions. Cell pellets were freeze-thawed and resuspended in 50 mM phosphate buffer at pH 8.0 and lysed by sonication. Samples from the cleared fractions were analyzed in an SDS-PAGE gel and Western blot analysis to determine the solubility profile of every recombinant protein: GST-M022 (Figure 38), M071 (Figure 39), and M115 (Figure 40).

The solubility of GST-M022 produced by the BEVS exhibited notable differences depending on the insect cell line that was infected, despite identical infection conditions were used (Panel B, Figure 38). In HF cells, the overexpression of GST-M022 was significantly higher but only a small proportion was detected in the soluble fraction. In contrast, while the overall viral protein expression in Sf9 cells is lower, approximately 50% of it was soluble. These results were compared to the solubility of GST-M022 produced from a prokaryotic expression system, using the same expression vector that was used for the generation of rBV-M022 (pTriEX-GST-M022).

In this system, protein solubility was significantly lower than in the BEVS, even under optimal induction and growth conditions (Panel A, Figure 38). Thus, considering the solubility yields, the combination of the BEVS with Sf9 cell infection was selected as the method for the GST-M022 fusion protein production.

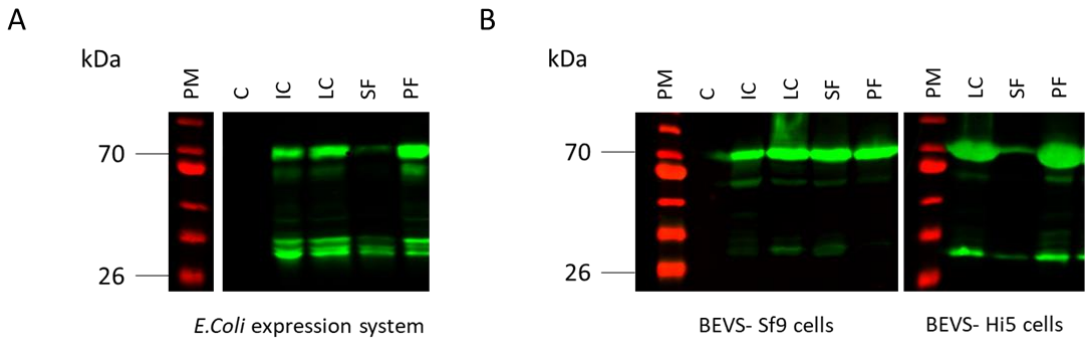

Figure 38. Solubility profile of the GST-M022 protein across different expression systems.

A) Solubility profile of GST-M022 produced in pTriEX-GST-M022 transformed *E.coli* cells, induced with 0.2 mM IPTG and incubated overnight at 18°C. B) Differential expression and solubility profile of the GST-M022 protein across two insect cell lines infected with rBV-M022 at an MOI of 10 in Sf9 (left panel) and Hi5 (right panel). PM: pre-stained NIR protein marker, C: non-induced/non-infected cells, IC: induced/infected cells, LC: lysed induced/infected cultures, SF: soluble fraction, PF: insoluble fraction. Anti-GST blotting

The same approach was used to determine the solubility of M071 in a suspension culture of rBV-M071 infected Sf9 cells. Given the results of the time-course curve of adherent Sf9 cells infected with rBV-M071, two conditions were analyzed for the BEVS expression: an MOI of 10 for 48 hours, and MOI of 1 for 72 hours (Figure 39). The recombinant viral protein showed similar production yields under both infection conditions (Lanes 4 and 9), but the M071 protein seemed to suffer degradation or proteolysis after clarification of cell lysates, specifically in the samples belonging to the cells infected at an MOI of 1 and harvested at 72 hpi.

The solubility of the M115 protein, produced using the BEVS, was determined in a suspension culture of Sf9 cells infected with the rBV-M115 at an MOI of 1, and were incubated for 72 hours (Figure 40). These infection parameters were chosen since they yielded the highest protein production in the previously performed time-course analysis of M115 protein expression. The results in the Western blot analysis showed that the M115 protein is predominantly (and almost exclusively) located in the soluble fraction (SF), indicating that the viral protein produced using the BEVS was efficiently folded.

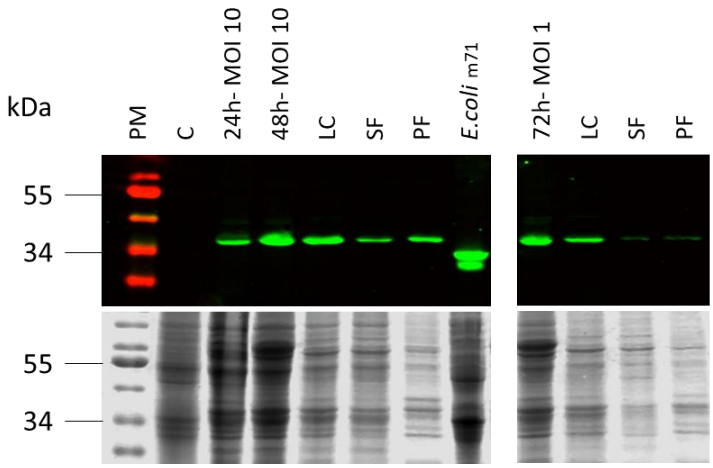

Figure 39. Solubility analysis of the M071 recombinant protein in rBV-M071 infected Sf9 cells.

The M071 recombinant protein produced in 50 ml of suspension Sf9 cultures infected with rBV-M071, using 12% SDS-PAGE and Western blot analysis with anti-Histidine tag antibodies (top), alongside Coomassie blue staining (bottom). Insect cells were infected at an MOI of 10 for 48 hours (Lanes 3 to 7), or an MOI of 1 for 72 hours (Lanes 9 to 12). Upon cell lysis by sonication (LC), clarified lysates (SF) and insoluble fractions (PF) of both cultures were analyzed for the expression of the recombinant M071 protein.

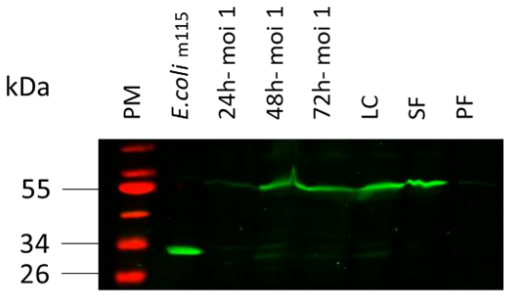

Figure 40. Solubility analysis of the M115 recombinant protein in rBV-M115 infected Sf9 cells.

The M115 recombinant protein produced in 50 ml of suspension Sf9 cultures infected with rBV-M115, using 12% SDS-PAGE and Western blot analysis with anti-Histidine tag antibodies (top). Sf9 were infected at an MOI of 1 and a sample of the culture was collected every 24h until reaching 72 hours after infection. Upon cell lysis by sonication (LC), clarified lysates (SF) and insoluble fractions (PF) were analyzed for the expression of the recombinant M71 protein.

PURIFICATION OF SOLUBLE RECOMBINANT MYXV PROTEINS

Protein purification using Glutathione Sepharose resin under native conditions

The GST-M022 protein found in the soluble fractions obtained from the cell lysates of infected Sf9 cultures were purified under native conditions using elution buffers containing 20 mM GSH and 40 mM GSH at pH 8 (Figure 41). Eluates 1 to 6 were mixed and dialyzed overnight at 4°C in

PBS, removing low molecular weight contaminants and the excess of GSH concentration, for a pH and ionic strength adjustment. The purified GST-M022 protein solution, which from now on will be referred to only as M022, was mixed with glycerol to a final concentration of 20% prior to storage at -20°C.

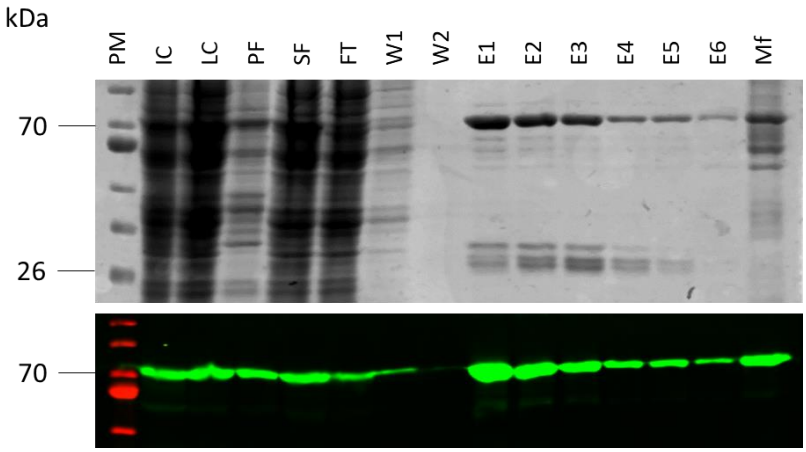

Figure 41. Affinity column purification of the recombinant GST-M022 protein using a Glutathione Sepharose resin under native conditions

The recombinant protein (70 kDa) was produced in the BEVS through the infection of a Sf9 suspension culture with rBV-M022 at an MOI of 10, for 48 hours. Samples were analyzed on a SDS-PAGE (10%) gel. The top image shows a Coomassie blue stained gel, and the bottom one shows a Western blot analysis using anti-histidine tag antibodies. Lane 1: pre-stained NIR molecular weight marker, Lane 2: infected Sf9 cells at an MOI of 10, Lane 3: cell culture lysate, Lane 4: insoluble fraction, Lane 5: cleared soluble fraction, Lane 6: flow-through, Lane 7: first washed fraction, Lane 8: last washed fraction, Lanes 9 to 14: protein eluates, Lane 15: final matrix-bound protein fraction.

Protein purification using IMAC column under native conditions

The recombinant proteins M083 and M115 were also produced in the soluble fraction after clarification of the lysate, either by the prokaryotic expression system or the BEVS. Thus, they were selectively purified under native conditions using Immobilized Metal Affinity Chromatography (IMAC), through the affinity of histidine residues found in both recombinant proteins, for the nickel ions immobilized on the column resin.

During this process, the buffer system that was used preserved the physiological pH and ionic strength that could maintain the protein's native conformation. The buffer that was specifically used for the resuspension of the cell pellets consisted of 50 mM phosphate, 300 mM NaCl, and 10 mM imidazole, with a pH of 8. The washing buffer had a higher concentration of imidazole, at 50 mM, for the removal of non-specifically bound proteins. For the elution of the histidine-

tagged recombinant proteins, the buffer was enriched with 250 mM and 500 mM of imidazole within the same phosphate buffer base, to compete with the histidine-tagged protein for the nickel ions on the column. The efficiency the purification process was evaluated through SDS-PAGE and Coomassie staining, and quantification of the protein concentration.

The purification of the M083 recombinant protein in the soluble fraction performed under the previous conditions had a good efficiency, evidenced by the intensity of the stained band corresponding to the M083 protein. The elution was not fully complete, since the sample corresponding to the matrix-bound proteins still showed an intense M083 signal after the fifth elution. The purity of the process was confirmed through Coomassie blue staining on an SDS-PAGE gel, which revealed a distinct and predominant band at the expected molecular weight of the viral protein in all the eluates. A second abundant protein band was also recognized by the anti-histidine tag antibody, and had a molecular weight of around 55 kDa, thus it could represent an aberrant form of the M083 construct. Besides this exception, no other bands were visible, confirming the high purity of the M083 purified protein (Figure 42).

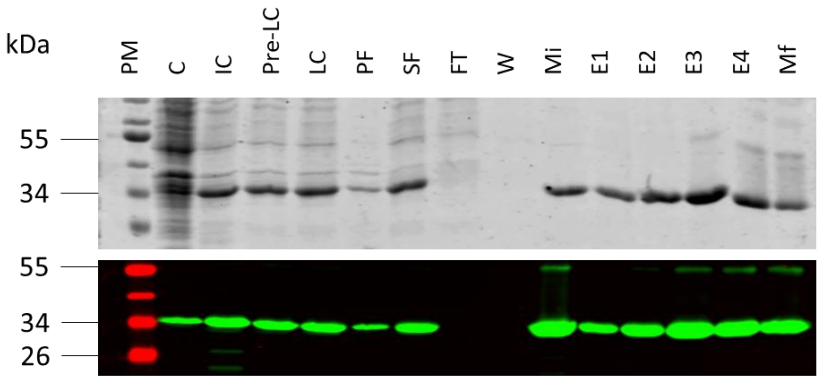

Figure 42. Analysis of IMAC column purification of the viral M083 recombinant protein under native conditions

The M083 protein was expressed in pET-28a-*m083l* transformed *E.coli* cultures, induced using 1 mM IPTG and incubated for 1.5 hours at 37°C. The top image shows a Coomassie blue stained gel and the bottom one shows a Western blot analysis detecting His-tagged proteins. Lane 1: pre-stained NIR protein marker, Lane 2: non-induced cells, Lane 3: induced culture, Lane 4: resuspended induced culture, Lane 5: cell lysate, Lane 6: insoluble fraction, Lane 7: cleared lysate/soluble fraction, Lane 8: flow-through, Lane 9: washed fraction, Lane 10: initial matrix-bound fraction, Lane 11 to 14: protein eluates, Lane 15: final matrix-bound protein fraction.

The M115 recombinant protein was expressed in two heterologous expression systems: *E.coli* expression system and the BEVS, and was found in the soluble fraction in both of them. Since the M115 construct produced through each system did not share the same apparent molecular weight in a 12% SDS-PAGE gel, they were independently purified. The $M115_P$ was produced in a prokaryotic expression system, and its apparent molecular weight was around 30 kDa. The eluates obtained from its purification showed different degrees of M115 purity, with the first

two (E1 and E2) containing multiple non-specific Coomassie stained protein bands of higher and lower molecular weight as the target viral protein. Eluates E2, E3 and E4 showed the more intense anti-histidine signal, correlating to high amounts of the target protein, but given the abundant presence of contaminant proteins in E2, the eluates that were finally selected for dialysis were eluates E3, E4 and E5 (Figure 43).

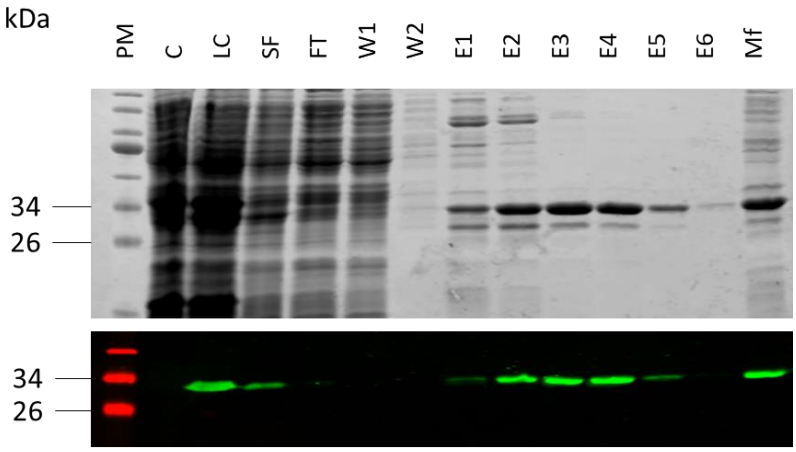

Figure 43. Analysis of IMAC column purification of the viral M115 recombinant protein expressed in a prokaryotic system under native conditions

The M115 protein was expressed in pET-28a-*m115l* transformed *E.coli* cultures, induced using 0.2 mM IPTG and incubated overnight at 18°C. The top image shows a Coomassie blue stained gel, and the bottom one shows a Western blot analysis detecting His-tagged proteins. Lane 1: pre-stained NIR protein marker, Lane 2: non-induced cells, Lane 3: lysate of induced cells, Lane 4: cleared lysate/soluble fraction, Lane 5: flow-through, Lane 6: initial washed fraction, Lane 7: final washed fraction, Lanes 8 to 13: protein eluates, Lane 14: final matrix-bound protein fraction.

$M115_I$ protein was produced using the BEVS in Sf9 cells infected with rBV-M115. The stained band pattern displayed upon $M115_I$ protein expression in a 12% SDS-PAGE gel showed at least two bands recognized by the anti-histidine tag antibody in the Western blot analysis, corresponding with the expressed recombinant protein. The most abundant and predominant one had an apparent molecular weight of around 60 kDa, and the second had an apparent molecular weight close to the one observed for the $M115_P$ protein, of around 28 kDa. The imidazole in the washing buffer did not efficiently eliminate all the contaminant proteins, and like in the previous $M115_P$ protein purification, the first two eluted fractions (E1 and E2) included abundant additional stained protein bands. Hence, elutes E3 and E4 were selected for further dialysis in PBS, which resulted in a practically pure $M115_I$ protein stock (Figure 44). This time the imidazole composition in the elution buffer could effectively displace the recombinant protein and recover the maximum amount of $M115_I$ from the column (minimal amount of $M115_I$ protein is detected in the final matrix-bound fraction).

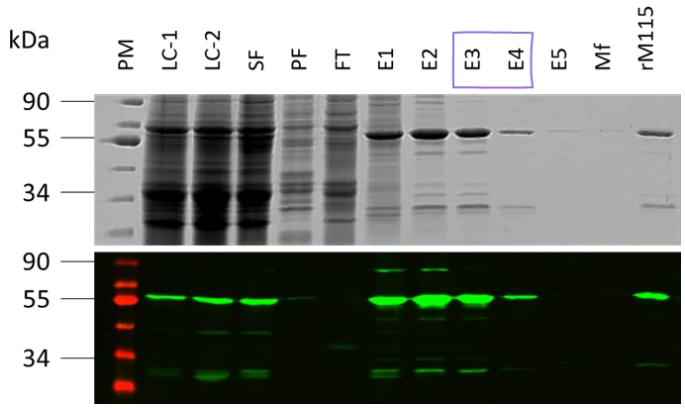

Figure 44. Analysis of IMAC column purification of the viral M115 recombinant protein expressed in rBV-M115 infected Sf9 cells under native conditions.

The M115 protein was expressed and purified from two rBV-M115 infected Sf9 cultures (LC-1 and LC-2) using an MOI of 1 for 72 hours. The top image shows a Coomassie blue stained gel, and the bottom one shows a Western blot analysis detecting His-tagged proteins. Lane 1: pre-stained NIR protein marker, Lane 2: lysate of infected Sf9 culture 1, Lane 3: lysate of infected Sf9 culture 2, Lane 4: cleared lysate/soluble fraction, Lane 5: insoluble fraction, Lane 6: flow-through, Lanes 6 to 10: protein eluates, Lane 11: final matrix-bound protein fraction, Lane 12: post-dialysis pure M115.

The M071 protein was partially detected in the soluble fraction of Sf9 lysates of cultures infected with rBV-M071. However, the production yield obtained through this expression system never showed good overexpression results. On the contrary, when studying the solubility of BEVS produced M071 protein, it seemed to be very unstable and was degraded during the process. In spite of this, the small amount of soluble M071 protein in the cleared lysate was purified through IMAC (Figure 45). The purification process had low efficiency, showing a high rate of unspecific bound proteins, and a very small amount of the target protein in the eluates.

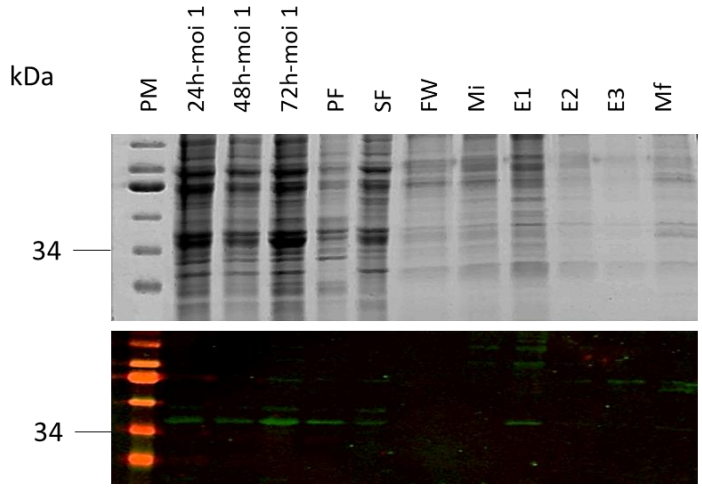

Figure 45. Analysis of IMAC column purification of the viral M071 recombinant protein expressed in rBV-M071 infected Sf9 cells under native conditions.

The M071 protein was expressed and purified from rBV-M071 infected Sf9 cultures using an MOI of 1 for 72 hours. The top image shows a Coomassie blue stained gel, and the bottom one shows a Western blot analysis detecting His-tagged proteins. Lane 1: pre-stained NIR protein marker, Lane 2: infected Sf9

culture 24 hpi, Lane 3: infected Sf9 culture 48 hpi, Lane 4: infected Sf9 culture 72 hpi, Lane 5: insoluble fraction, Lane 6: soluble fraction, Lane 7: flow through, Lane 8: initial matrix-bound fraction, Lanes 9 to 11: protein eluates, Lane 12: final matrix-bound protein fraction.

Protein purification using IMAC column under denaturing conditions

The M071 and M141 proteins that were exclusively isolated in the insoluble fraction of induced bacterial lysates, were effectively solubilized from the inclusion bodies under denaturing conditions by incubating them with a solubilization buffer containing 8 M urea. Since the inclusion bodies were washed with a buffer containing 2% detergent before the solubilization process, many impurities such as membrane fragments, residual DNA, endotoxins, and other loosely associated proteins were removed from the insoluble fraction. This step provided cleaner inclusion bodies and increased the relative yield of the corresponding target recombinant proteins in the final S3 fraction.

The M071 protein in the S3 fraction was not successfully purified under these conditions (Figure 46). The amount of solubilized recombinant protein was high enough to saturate the resin, as evidenced by the initial matrix-bound fraction (Mi) producing a saturating signal at 34 kDa in the Western blot analysis with anti-histidine tag antibodies. Even some of it that was lost in the flow through (FT). In spite of this, the protein was scarcely visible in eluates E3 to E6, which showed a faint double band around 34 kDa in the Western blot analysis. In addition, these eluates displayed a continuous Coomassie-stained band pattern of sizes less than 34 kDa, indicating that there could be indicating a significant level of protein degradation.

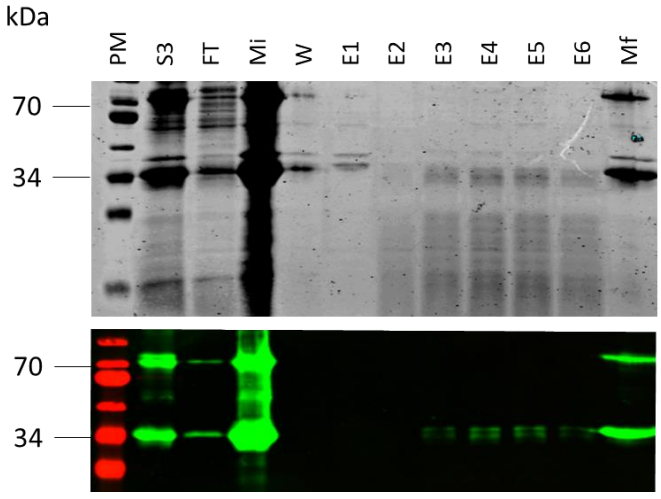

Figure 46. Analysis of IMAC column purification of the viral M071 recombinant protein expressed in a prokaryotic expression system under denaturing conditions

The M071 protein was expressed in pET-28a-*m071l* transformed *E.coli* cultures, induced using 1 mM IPTG and incubated for 3 hours at 30°C. Cells were harvested following the protocol for the purification

and solubilization of proteins in inclusion bodies, and M071 solubilized proteins in S3 were purified under denaturing conditions. The top image shows a Coomassie blue stained gel, and the bottom one shows a Western blot analysis detecting His-tagged proteins. Lane 1: pre-stained NIR protein marker, Lane 2: cleared S3 fraction, Lane 3: flow-through, Lane 4: initial matrix-bound fraction, Lane 5: washed fraction, Lanes 6 to 10: protein eluates, Lane 11: final matrix-bound protein fraction.

The viral M141 protein solubilized in S3 was started to be collected from the IMAC column from the third eluate (E3) and had a progressive detachment effect during the following two consecutives eluates (E4 and E5) (Figure 47). The protein recovered from these eluates had a high purity, and the E5 reached a good yield, however a large proportion of it was still bonded to the resin and was not able to be eluted.

The polyhistidine tag is an oligopeptide that does not require any specific structural conformation for its specificity of binding metal ions. Therefore, an advantage of using denaturing conditions is that the lack of secondary conformation of the his-tagged denatured proteins enhances the exposure of their tag and contributes to increase their binding to the IMAC column. The elution of the target proteins was performed by lowering the pH of the column from pH of 8, to 6.8 with the washing buffer, and a final pH of 4.5 with the elution buffer. In both attempts of his-tagged protein purification under denaturing conditions, the amount of recombinant protein that remained bound to the IMAC resin was significantly high, suggesting that the histidine residues might indeed bind strongly to the metal ions.

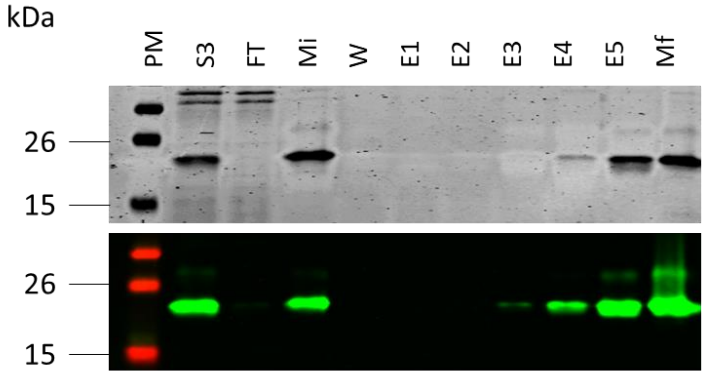

Figure 47. Analysis of IMAC column purification of the viral M141 recombinant protein expressed in a prokaryotic expression system under denaturing conditions

The M141 protein was expressed in pET-28a-*m141r* transformed *E.coli* cultures, induced using 1 mM IPTG and incubated for 1.5 hours at 37°C. Cells were harvested following the protocol for the purification and solubilization of proteins in inclusion bodies, and M141 solubilized proteins in S3 were purified under denaturing conditions. The top image shows a Coomassie blue stained gel, and the bottom one shows a Western blot analysis detecting His-tagged proteins. Lane 1: pre-stained NIR protein marker, Lane 2: cleared S3 fraction, Lane 3: flow-through, Lane 4: initial matrix-bound fraction, Lane 5: washed fraction, Lanes 6 to 10: protein eluates, Lane 11: final matrix-bound protein fraction.

ANTIGENIC PROPERTIES OF THE RECOMBINANT VIRAL PROTEINS

Three of the selected MYXV protein candidates were produced and purified in a soluble and presumably native form: M022, M083 and M115. The other three recombinant proteins, M029, M071, M141, were discarded along the way for various reasons (inability to achieve soluble expression, challenges in their purification, etc.). Nevertheless, they all were subsequently screened for linear epitopes, conformational epitopes, or both.

Linear epitope analysis in recombinant MYXV proteins

Upon purification and quantification of the pure recombinant M022, M083 and M115, different amounts of each protein were analyzed in a 12% SDS-PAGE and Western blot with a pool of two serums obtained from seropositive rabbits (Figure 48). The purity of the protein stocks, as well as the relative amount of each protein was visually evaluated in the Coomassie-stained gel (panel A), while the unequivocal presence of each protein was verified through an analysis with anti-Histidine tag antibodies (panel B). The antigenicity of the three proteins was evaluated in a Western blot with a pool of two rabbit serum samples (positive control) seropositive for MYXV (Panel C). When comparing the intensity of the bands across the blot, the M115 protein was found to be the viral protein with the highest antigenicity, developing an intense protein band corresponding to ~30 kDa. It was followed by the M022 that showed a 70 kDa band on the blot with relatively low intense signal. The M083 protein did not show any immunoreactivity with the antibodies present in the seropositive control.

M115 was cloned in two different expression vectors (pET28a(+) and pTriEX-1.1), and each of them was employed to produce the recombinant protein in a different expression system. The expression of this protein in each system gave two expression products that differed from each other in the 12% SDS-PAGE mobility and apparent molecular weight. Given that both approaches allowed the purification of soluble M115 protein, they were analyzed to compare the intensity of their bands in a Western blot analysis with the positive and negative control sera (Figure 49). Although the amount of each protein was the same (panel A), the reactivity with the anti-Histidine tag antibodies was notably weaker in the case of the M115 protein produced in the prokaryotic system with the pET28a(+)-*m115l* vector (panel B), indicating a possible instability or degradation of the protein in its C-termini. Both M115 proteins displayed a good band intensity and specificity of the immune response, since both were detected by specific antibodies in the positive control sera but not by the negative control serum. The antibodies

present in the seropositive control reacted with the M115 proteins in the blot generating their respective bands around the size determined by the Coomassie stained gel: a primary intense ~30 kDa band and a secondary band around 68 kDa for the pET28a(+) vector, and a single protein band of ~60 kDa for the pTriEX-1.1 vector (Panel C and D, Figure 49). Both protein products had similar behavior overall, but the M115 generated through BEVS seemed to maintain its integrity better, thus was able to be recognized with the anti-Histidine tag antibodies.

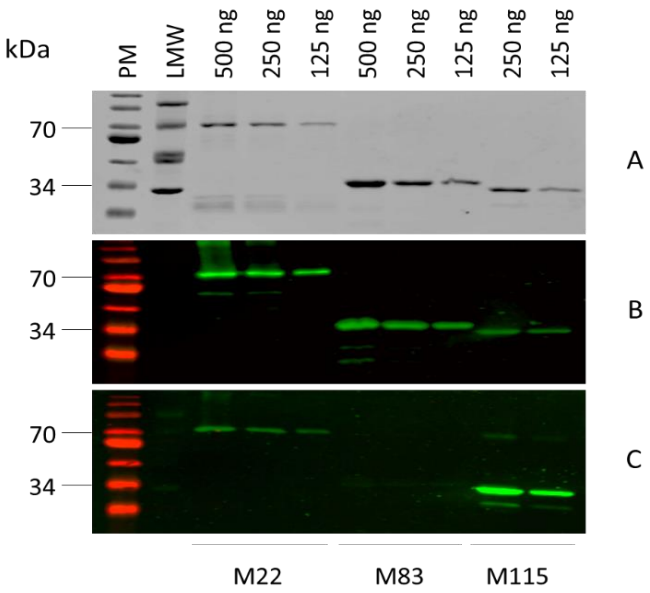

Figure 48. Antigenic characterization of the M022, M083, M115, recombinant proteins purified under native conditions.

A) Coomassie blue staining. B) Reactivity with anti-Histidine tag antibodies. C) Reactivity with the positive serum pool. Lane 1: pre-stained NIR protein marker, Lane 2: LMW protein marker, Lanes 3 to 5: different amount of M022 protein, Lanes 6 to 8: different amount of M083 protein, Lanes 9 and 10: different amount of M115. Samples were analyzed on a SDS-PAGE (12%).

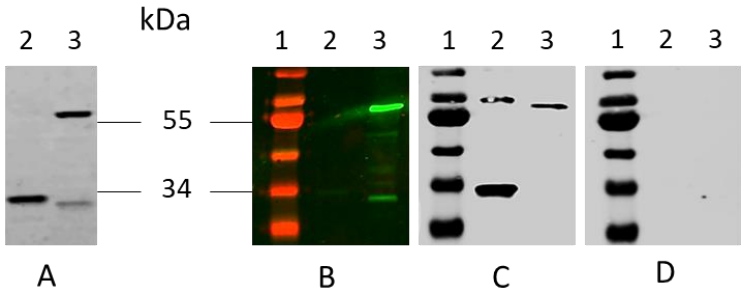

Figure 49. Comparative antigenicity of purified M115 recombinant protein stocks obtained in prokaryotic cells or insect cells

A) Coomassie blue staining. B) Reactivity with anti-Histidine tag antibodies. C) Reactivity with the positive anti-MYXV sera. D) Reactivity with the negative control rabbit serum. Lanes 1: pre-stained NIR protein marker, Lanes 2: M115 protein purified from bacteria transformed with the pET28-*m115l* vector, Lanes 3: M115 protein purified from Sf9 insect cell culture infected with rBV-M115 (generated using the pTriEX-*m115l* expression vector).

The molecular mass of the M115 protein synthetized by BEVS was approximately twice that of the M115 protein produced in the prokaryotic expression system. As a means to describe the reason of the major molecular mass difference found between both M115 proteins, the protein synthetized by BEVS was analyzed on 12% SDS-PAGE under reducing and non-reducing conditions (Figure 50). For that, samples were denatured in presence of various concentrations of β-mercaptoethanol (β-ME) (5%, 0.15%, 0.05%), or without this reducing agent (Lai et al., 1990). The purity of the protein stock was not complete, since non-specific protein bands appear in the Coomassie-stained gel (Panel A), yet the target protein was correctly identified by the anti-Histidine tag (Panel B). All the protein analyzed under reducing conditions, treated with 0.05 to 5% of β-ME, exhibited the same immunoreactivity in the anti-Histidine tag blotting and the anti-MYXV sera (positive control), which displayed one single band with a molecular weight of 60 kDa (Panels B, C). The M115 protein denatured under non-reducing conditions exhibited a distinct pattern characterized by multiple high molecular weight protein bands. They were not only visible with Coomassie blue staining (Panel A) but the same bands were also recognized by the anti-Histidine tag antibodies (Panel B) and antibodies in the positive sera control (Panel C) in Western blot analysis. The presence of these bands suggested potential multimerization or aggregation, since disulfide bonds and other protein-protein interactions are maintained in the non-reducing conditions. The lack of cross-reactivity in all the samples regardless of the reducing or non-reducing processing indicated that the immune recognition of protein bands by the positive sera was specific to the M115 protein (Panel D).

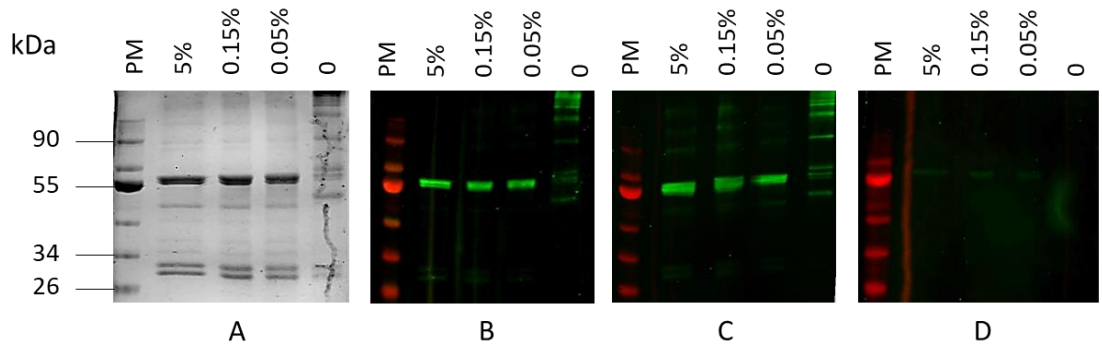

Figure 50. Analysis of the M115 recombinant protein purified from rBV-M115 infected Sf9 cultures, in reducing and non-reducing conditions (treated with 5%, 0.15%, 0.05% and 0% β-ME).

A) Coomassie blue staining. B) Reactivity with the anti-Histidine tag antibody. C) Reactivity with the positive anti-MYXV sera. D) Reactivity with the negative reference control serum. Lanes 1: pre-stained NIR protein marker, Lanes 2: M115 with 5% β-ME, Lanes 3: M115 with 0.15% β-ME, Lanes 4: M115 with 0.05% β-ME, Lanes 5: M115 with no β-ME

Since the linear epitopes are preserved in the denatured form of a protein, even the three recombinant proteins that failed to be expressed and/or purified in a soluble form: M029, M071

and M141, were screened. Insoluble fractions enriched with these proteins were used for the preliminary antigenic characterization analysis of these proteins (Figure 51). The samples were generated by the prokaryotic expression system, and constituted the insoluble fraction obtained prior to the washes with 2% detergent (M029 P4, M71 P4, M141 P4) and two of the insoluble fractions obtained after the washing steps (P4-IGEPAL and P4-TX100). Although there was a fair amount of all recombinant proteins within their corresponding samples (Panel A), the antibodies in the rabbit sera that were used as positive anti-MYXV control had high reactivity with other prokaryotic proteins found in the insoluble fractions analyzed. The unspecific multiple protein bands, which were more abundant in the unwashed insoluble M029 P4, M71 P4, M141 P4 fractions, masked the possible reactivity of specific anti-MYXV with the recombinant viral proteins (Panel B).

The specificity of the signal was enhanced after a step of immunoadsorption performed on the anti-MYXV rabbit sera that was being used as positive control. This step reduced or depleted some non-specific antibodies that were recognizing prokaryotic proteins, thereby reducing background noise, and improving the clarity of specific antibody interactions with the viral recombinant proteins M029, M071 or M141 (Figure 52). The presence of faint protein bands corresponding to the molecular weights of M029, M071 and M141 appeared in the positive anti-MXYV sera blot (signaled by black arrows in Panel C).

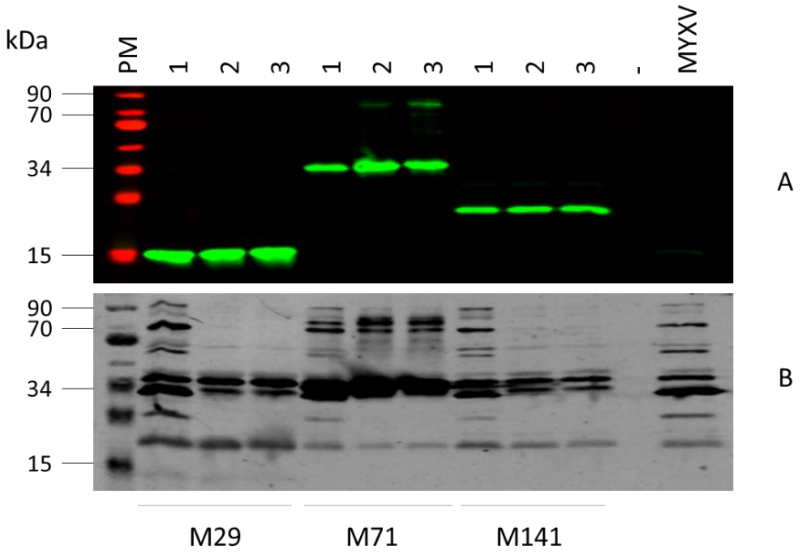

Figure 51. Antigenic characterization of the recombinant proteins M029, M071, M141 obtained from the prokaryotic expression system

A) Western blot analysis with anti-Histidine tag antibodies. B) Western blot with anti-MYXV seropositive control. Lane PM: pre-stained NIR protein marker, Lanes 1: insoluble fraction, Lanes 2: insoluble fraction resulting from consecutive washes with 2% of IGEPAL, Lanes 3: insoluble fraction resulting from consecutive washes with 2% of Triton X-100. Lane MYXV: pure MYXV lysate.

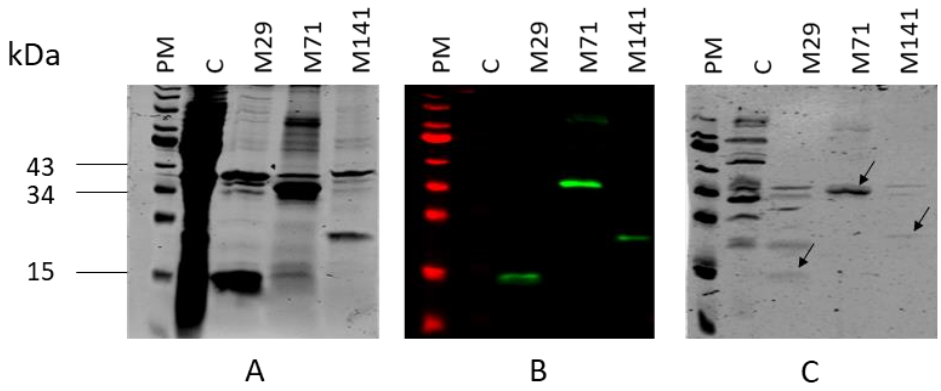

Figure 52. Antigenic characterization of the recombinant proteins M029, M071, M141 obtained from the prokaryotic expression system, after depletion of anti-*E.coli* antibodies from rabbit sera

A) Coomassie blue staining. B) Reactivity with anti-Histidine tag. C) Reactivity with the anti-MYXV seropositive control sera depleted in antibodies binding to bacteria proteins. Lanes 1: pre-stained NIR protein marker, Lanes 2: bacteria lysate, Lanes 3: M029 P4 after 2% Triton X-100 washes, Lanes 4: M071 P4 after 2% Triton X-100 washes, Lanes 5: M141 P4 after 2% Triton X-100 washes. Black arrows indicate the band corresponding to the theoretical size of each protein.

The antibody profiles in rabbits after vaccination against MYXV often show a broad variability regarding the titers of total antibodies and neutralizing antibodies in particular, ranging from high titers to lower or non-neutralizing responses. This broad range in antibody response highlighted the importance of incorporating a greater number of individual serum samples to the positive anti-MYXV control, to ensure a more representative picture of the rabbit immune response. Thus, to enhance the reliability of the results, the antigenicity of each viral protein candidate was characterized in a Western blot analysis conducted using a new positive anti-MYXV control that comprised a pooled collection of individual seropositive samples to increase the reliability of the results (Panel C, Figure 53). This new positive anti-MYXV control consisted of nineteen rabbit serum, pooled in equal volumes, that were collected from rabbits that successfully seroconverted following immunization with a homologous Myxoma virus vaccine.

In addition, a commercial rabbit serum that did not contain antibodies specific for MYXV, was used as a negative control for reactivity against MYXV for identification of nonspecific binding (Panel D, Figure 53). Blotting with the negative control serum was crucial for evaluating the specificity of the rabbit antibodies against the different recombinant MYXV proteins and helped identify baseline signals, generated either by the main target recombinant protein, or by the presence of contaminant proteins (e.g. in impure samples M071, M029).

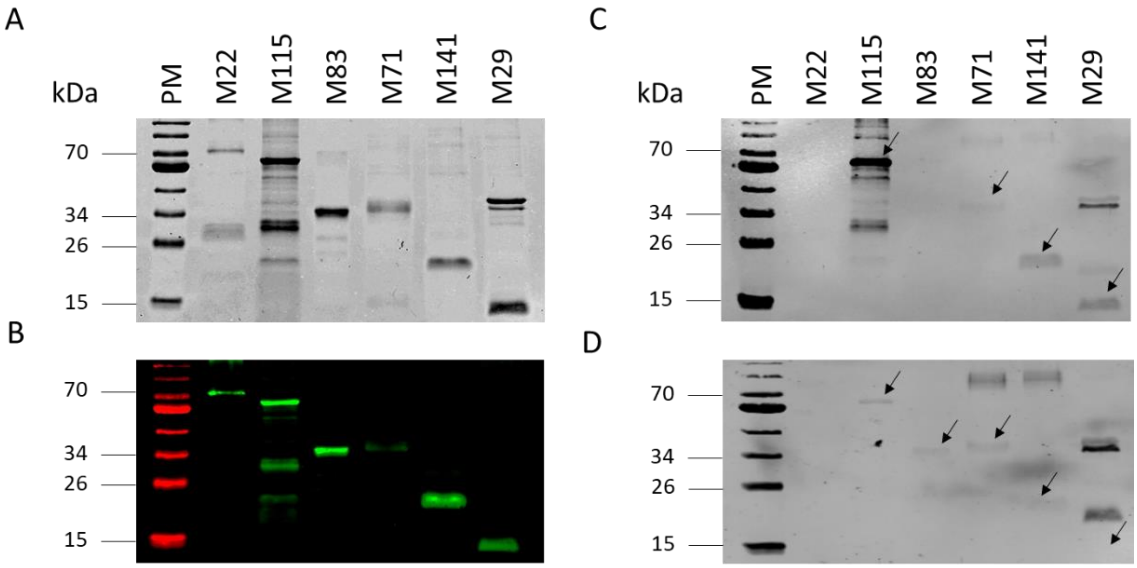

Figure 53. Characterization of linear epitopes in the whole viral recombinant protein panel

Reactivity analysis of the recombinant M022, M115, M083, M071, M141 and M029 MYXV proteins in 12% SDS-PAGE stained with Coomassie blue (panel A) and Western blot analysis with anti-histidine tag antibodies (panel B), positive anti-myxoma sera pool (panel C) and negative control rabbit serum (panel D). Some viral proteins were purified under native (M022, M115, M083) or denaturing (M141) conditions, while others were overexpressed and enriched in the soluble fraction under denaturing conditions (M071) or in the insoluble fraction after detergent washes (M029). The proteins were analyzed following the same disposition in all panels. Lane 1: pre-stained NIR protein marker, Lane 2: M022 pure protein, Lane 3: M115 pure protein, Lane 4: Samples corresponding to each protein were loaded in a different lane. Black arrows indicate the protein bands of each recombinant protein, according to their expected size.

Among the proteins purified under native conditions (M022, M115 and M083), the strongest antibody response was directed against the sample in lane 3, which corresponded to the pure M115 protein (Panel C, Figure 53). Although several bands were visible, the two most intense bands corresponded to protein sizes also recognized by the anti-Histidine tag antibodies (~30 and ~60 kDa), indicating the presence of antibodies that were specific to the M115 protein within the sera constituting the positive control. The highly immunogenic character of the M115 protein was corroborated by the negative control blot, since the pure sample showed a residual reactivity with the 60 kDa band.

Conversely, the anti-MYXV positive serum failed to detect bands for the recombinant M022 (GST-M022) and M083 proteins, suggesting that these viral proteins may lack antigenic epitopes recognizable by the antibodies present in the seropositive control. This reason could be a valid explanation for the absence of the 36 kDa band, corresponding to the M083 protein, but not for the M022 protein, since the 70 kDa protein band was already detected in the preliminary screening in which a mixture of two seropositive rabbit serum samples was used as the positive control (Panel C, Figure 53). Instead, the negative results obtained for the M022 protein in the

positive serum blot, might imply that the overall immune response induced by this specific protein in the vaccinated rabbits is significantly weak. The M083 protein, also had certain but limited basal reactivity with the negative control serum, possibly due to its high protein concentration (Panel D, Figure 53).

The M141 protein that had been finally purified under denaturing conditions without further reconstitution, showed certain degree of immunogenicity and barely non background signal. The remaining two recombinant proteins, M071 and M029, were not completely isolated from other bacterial contaminants in the analyzed samples, but they still constituted the majority of their composition. M071 was faintly recognized across both blots, by rabbit antibodies from the positive and the negative control sera. However, M029 was only recognized by antibodies in the positive control sera, indicating a higher potential for eliciting a specific immune response.

Conformational epitope analysis in recombinant MYXV proteins

The Western blot analysis only considered the linear antigenic epitopes of each recombinant protein. To evaluate the full immune reactivity of the recombinant proteins (adding the contribution of conformational antigenic epitopes), equal quantities of the protein samples analyzed in Figure 53 were also for a dot immunoassay (Figure 54). The same positive (+) pool (upper panel) and negative (-) sera (lower panel) controls were used in the determination of specific immunogenic activity.

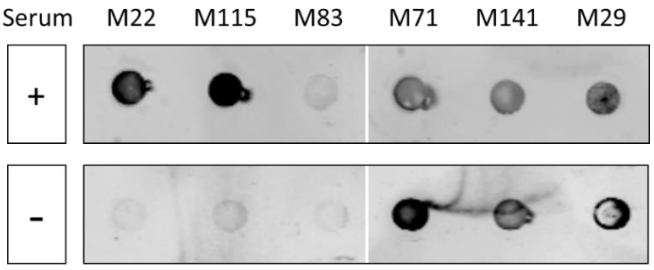

Figure 54. Dot immunoassay displaying the reactivity of the viral proteins with the positive (+) and the negative (-) control samples

The upper panel shows the reactivity of each sample when incubated with the + rabbit serum control, whilst the lower panel used the – serum control. Each dot represents a distinct viral protein. Protein samples M022, M115 and M083 were purified under native conditions, M071 was overexpressed and enriched in the soluble fraction under denaturing conditions, M141 was purified under denaturing conditions, and M029 was enriched in the insoluble fraction after detergent washes.

The presence of an intense dot for M022 protein in the upper panel, but its absence in the lower panel, resulted from a strong reaction between the recombinant protein and the antibodies

found within the positive control, but not with those in the negative control serum. This pattern strongly indicated that M022 did have antigenic determinants that allowed its recognition by the rabbit immune system. The M022 dot immunoassay result contrasts with the results previously displayed in Figure 53 (Panel C and D). Antibodies within the positive control failed to recognize any linear epitopes of protein M022 in Western blot analysis yet reacted strongly to the native, or semi-native conformation of the M022. This finding highlighted the crucial role of M022 native conformation for its immunogenic potential and suggested that the tridimensional structure of the protein is essential for eliciting a specific antibody response, highlighting its significance as an immunogen.

In addition to demonstrating the presence of antigenic linear epitopes, evidenced by the strong reactivity of the denaturized M115 protein with the antibodies in the positive control (Panel C, Figure 53), the tertiary structure of this viral protein also exhibited high immunoreactivity, as indicated by the intense dot for M115 in the upper serum panel. The recognition of the recombinant M115 protein by the positive control anti-MYXV antibodies might indicate that the protein was exposed to the immune system during immunization of the rabbits. Since it was immunoreactive in both Western blot and dot immunoassay analysis, M115 stood out as a good and robust antigen with potential utility in the development of diagnostic tests.

The absence of M083 protein dots in both panels indicated a lack of conformational antigenic epitopes within this recombinant viral protein. Together with the findings from the Western blot analysis, this evidence led to the exclusion of the M083 protein as a viable candidate for further studies.

The presence of M071, M141 and M029 dots in the upper and lower panel indicated non-specific binding or background reactivity. Since both M071 and M141 proteins are found in denaturing buffers containing 8 M urea, it was expected that the dot immunoassay would display similar results than those obtained in the Western blots. The inability to express and purify the native forms of M071 and M141 restricts the analysis of potential conformational epitopes, which are essential for conducting a thorough investigation into the antigenic properties of these proteins.

Antigenicity analysis of native MYXV proteins expressed in Mammalian cells

The transient expression of M022, M71 and M115 viral proteins in the RK13 cell line, an established epithelial rabbit cell line, provided the specific enzymatic pathways and environment that mimicked more closely the modification events that occur during natural

MYXV infection. This method was useful in providing information on the antigenicity of the viral proteins supposedly in their native conformation and cellular context.

None of the three proteins showed significant variation in the apparent molecular weight. Despite the transfection process being optimized for this cell line, each protein differed in the levels of expression, with M115 produced in significantly higher levels than M071 and M022 (Panel A, Figure 55). In fact, despite the efforts in increasing M022 expression, it was consistently detected very faintly by the anti-Histidine tag antibodies (data not shown). This fact was supported by the results of the immunofluorescence assay, which showed a lower rate of cells expressing M022 compared to those transfected with the eGFP (positive transfection control), as well as cells expressing proteins M071 and M115 (Figure 55).

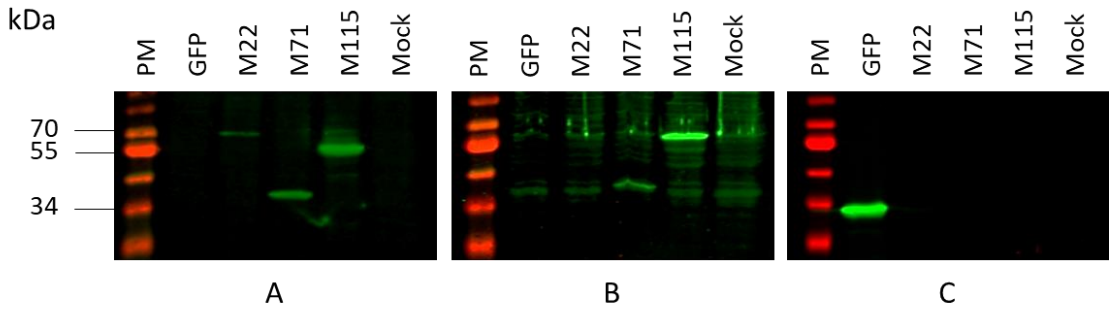

Figure 55. Analysis of recombinant protein transient expression in transfected RK13 cultures.

Cells were harvested 48 hours post-transfection. Lysates were analyzed in 12% SDS-PAGE and Western blot analysis with: A) anti-Histidine tag antibodies. B) positive anti-MYXV sera. C) anti-GFP antibodies.

The antigenic characterization of the M022 and M115 proteins produced through this mammalian system rendered the same results as those that were previously seen for the proteins produced in the BEVS. Moreover, the characterization of the M071 protein gave clearer results due to the reduced background signal that facilitated determining the presence of antigenic linear epitopes. The M071 protein exhibited a limited degree of immunoreactivity with the seropositive anti-MYXV sera, yet it was still higher than that observed for M022 (Panel B, Figure 55).

In the immunofluorescence assay, the recombinant proteins were simultaneously targeted by two primary antibodies: anti-Histidine tag antibody produced in mouse (red staining), and the anti-MYXV antibodies present in the positive control rabbit sera (green staining) (Figure 56). The secondary antibodies were conjugated with differential fluorescence dyes, anti-mouse with Alexa-Fluor 633 and anti-rabbit with Alexa-Fluor 488. This assay allowed the verification of the recombinant proteins' expression and tag accessibility (red staining), and whether the expressed proteins maintain their native epitopes (green staining).

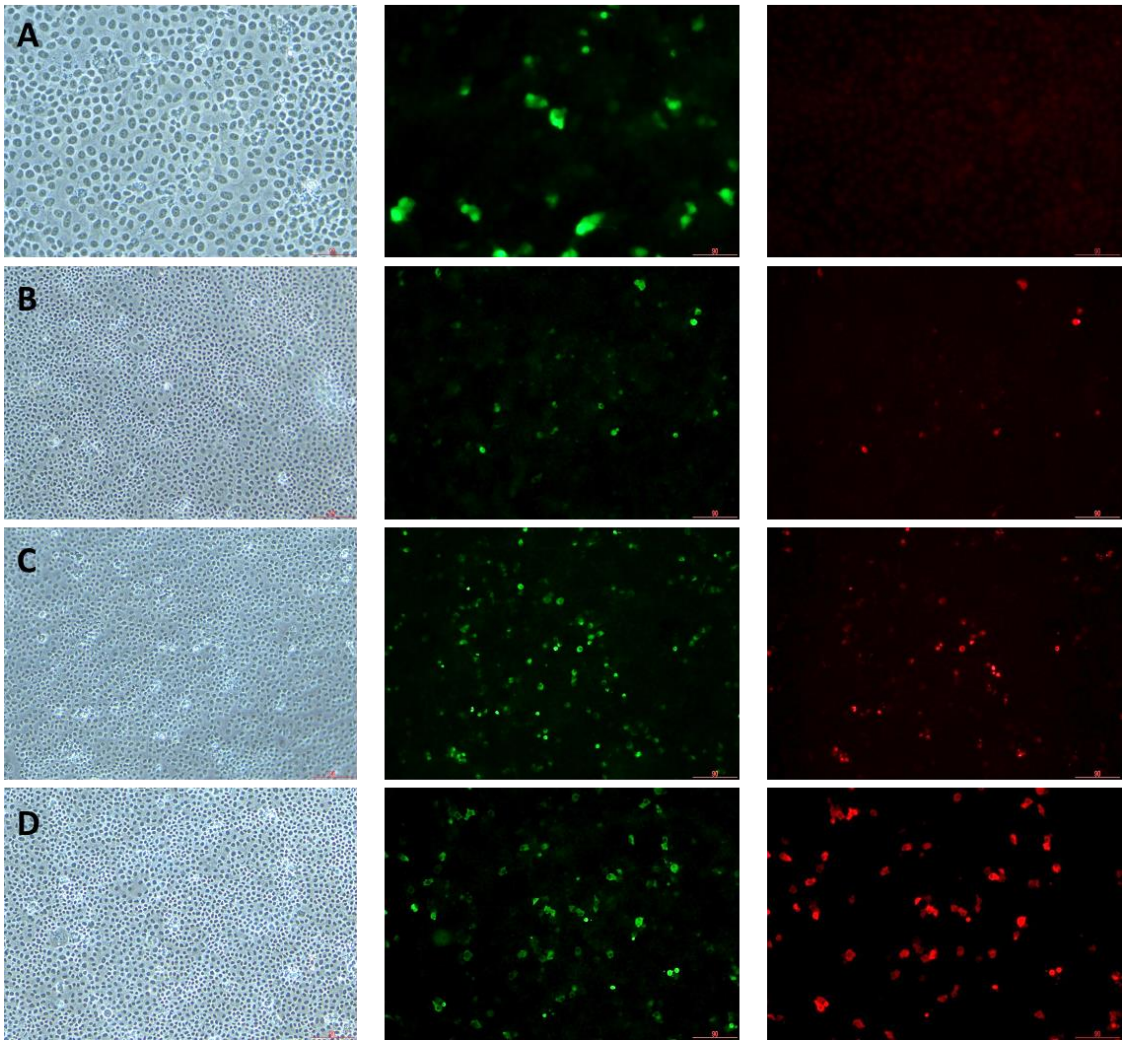

Figure 56. IF staining microscopy images of RK13 cultures transfected with the viral proteins M022, M071 and M115, captured 48 hours after transfection.

Transfection was performed with A) pcDNA-*eGFP*, B) pTriEX-*m022l,* C) pTriEX-*m071l,* D) pTriEX-*m115l* expression vectors. Images from A were collected at 40x, images from B, C and D were collected at 10x. Left panel- bright light, middle panel- green channel displaying anti-MYXV reactivity, right panel- red channel displaying anti-Histidine tag reactivity.

All three viral proteins were tagged by the anti-Histidine antibodies, and by the antibodies in the anti-MYXV seropositive serum. All transfected cells expressing M071 recognized by the anti-Histidine tag antibodies (conjugated with AF644, red) also immunoreacted with the seropositive serum (conjugated with AF488, green). The number of RK13 cells recognized by these anti-MYXV antibodies surpassed the one of cells tagged by the anti-Histidine tag antibodies (Panel B). The same phenomenon was observed for the transfected RK13 cells expressing M115 (Panel C).

The fact that the recombinant M022, M071 and M115 were tagged by both antibodies cross-validated the results of the immunoassay, suggesting the presence of antigenic epitopes that were successfully recognized by antibodies that would naturally target MYXV in the immune response following vaccination.

CHAPTER 6: OPTIMIZATION AND DIAGNOSTIC EVALUATION OF SEROLOGIC ASSAYS BASED ON ANTIGENIC MYXV PROTEINS

CHARACTERIZATION OF RABBIT SERA SAMPLES BY THE "GOLD STANDARD" SEROLOGICAL TEST

The method acknowledged as the most accurate and reliable for diagnosing a disease is known as "gold standard". The results obtained from this test serve as the benchmark for evaluating the performance of other diagnostic tests for the same disease.

In this regard, the evaluation and validation of the in-house indirect ELISA tests developed in this Doctoral Thesis, which use the whole MYXV virus (iELISA-Lu) or the antigenic viral proteins M022 (iELISA-rM022) and M115 (iELISA-rM115) as antigens, was performed using the commercial indirect ELISA test INgezim Mixomatosis (Ingenasa S.A) as the "gold standard". This assay is the only commercially available assay for detecting anti-MYXV antibodies in rabbit serum and has a DSe of 98% and DSp of >99%.

Reference standard diagnosis

A collection of 259 rabbit sera, obtained from three distinct panels (PANEL 1, *n*= 161; PANEL 2, *n*= 64 and PANEL 3, *n*= 34) (Table ...), which are described in the Materials section, were analyzed by the reference diagnostic test and categorized into positive or negative samples based on the cut off of the ELISA (levels of specific anti-MYXV antibodies). In brief, PANELS 1 and 2 were composed of rabbit sera obtained from animals that participated in two independent vaccination/challenge experiments, in which some rabbits were vaccinated SC or ID with a homologous MYXV vaccine, and others were not. In addition, the protective effect of the vaccine and the impact of different administration routes were evaluated by challenging the subjects with a virulent MYXV strain. Sera from PANEL 3 were obtained from 2-months old rabbits, non-exposed to the virus, nor vaccinated.

While 24.2% (*n*= 39) of samples in PANEL 1 tested seronegative, 75.8% (*n*=122) gave a positive result when analysed with this ELISA test. Samples from PANEL 2, had a similar outcome of negative and positive results, with seronegatives accounting for 48.4% (*n*=31) and seropositives for 51.6% (*n*=33). The OD_{450nm} values obtained for these 229 sera samples were represented in Figure… according to their negative (*n*= 70) or positive (*n*= 155) outcome, representing the strong discriminating ability of the reference ELISA test. All 34 samples from PANEL 3 were seronegative, as could be expected given the fact that they were obtained from naïve young rabbits presumably non-exposed to the virus. However, these results were not included in the plot from Figure…, since the samples were analyzed using a different ELISA kit (CIVTEST®Cuni

Mixomatosis, Laboratorios HIPRA, S.A.). At that moment, the CIVTEST was used for serological diagnosis of myxomatosis in the *Instituto Nacional de Investigação Agrária e Veterinária* (INIAV), the institution where I did the international research stay, but now its manufacture is discontinued and thus, it is no longer available.

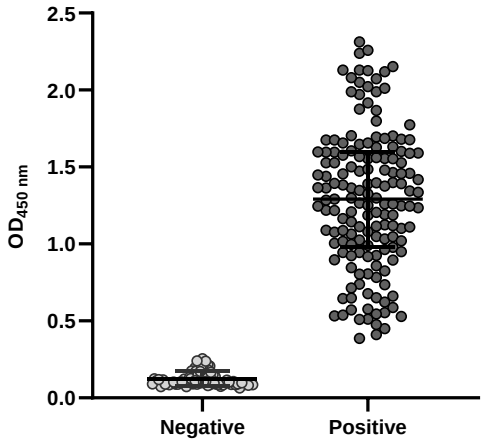

Figure 57. Characterization of rabbit sera samples by the reference ELISA test.

Characterization of rabbit sera samples from PANEL 1 (*n*= 161) and PANEL 2 (*n*= 64) by the commercial ELISA kit, categorized into two diagnostic groups depending on the absence (Negative, *n*= 70) or presence (Positive, *n*= 155) of specific antibodies against MYXV. The OD_{450} readings for each serum from both groups are displayed along the Y axis, as well as the mean and SEM for each group.

Sera samples categorized as negative in the iELISA results showed a low mean OD_{450} value of 0.1241 (95% CI: 0.1128 to 0.1354) with a SEM ± 0.0056, indicating that the measurements were closely clustered around the low mean. This data set distribution showed high skewness (1.149), indicating long tail in the distribution towards higher OD_{450} values. Consistent with the skewness, the distribution also had slightly heavier tails than a normal distribution (excess kurtosis value of 0.2580), as there were few samples with higher readings (Figure 57).

In contrast, samples within the positive category displayed a higher mean OD_{450} value of 1.288 (95% CI: 1.216 to 1.360) with a SEM ± 0.03636. The dispersion of individual data points within the positive group is considerably higher (SD ± 0.4526), which can be expected in positive samples due to the greater variation of the individual immune response intensity. This category exhibited a more symmetric distribution (skewness of 0.07427), and lighter tails since there are fewer extreme values or outliers compared to a normal distribution (excess kurtosis of -0.5394).

Considering the unequal variances between the two categories (F test, p value <0.0001), the comparison of the means of the negative (0.1241) and positive (1.288) groups were significantly different (unpaired t test with Welch's correction, P value <0.0001).

In summary, out of the 259 sera samples, 104 were categorized as negative and 155 were categorized as positive for anti-MYXV antibodies (Table 8).

Table 9. Serological test results from sera PANELS 1, 2 and 3 analyzed by the commercial ELISA INgezim.

	NEGATIVE	*POSITIVE*	*TOTAL*
PANEL 1	39	122	161
PANEL 2	31	33	64
PANEL 3	34	0	34
TOTAL	104	155	259

Comparative serological study

All 259 sera samples included in the analysis were divided into three categories, depending on the status of the rabbit they were obtained from. The samples obtained from non-vaccinated animals (NV, *n*= 89) represented around 34.4% of the total sera, while the 170 remaining (65.6% of the total) were obtained from rabbits vaccinated against myxomatosis. From those, 132 sera were obtained from rabbits vaccinated subcutaneously (SC) (comprising 50.9% of the total sera) and the 38 remaining were obtained from intradermally vaccinated (ID) rabbits (14.7% of the total). All 89 NV sera gave negative results in the commercial reference ELISA, all 38 ID sera gave positive results, 117 out of 132 SC sera were categorized as positives, and the 15 SC remaining were negatives. The Kruskal-Wallis test indicated significant differences among the groups (p value < 0.0001), and all pairwise comparisons of the group's distribution a showed highly significant differences between all of them (Dunn's multiple comparison test, all p values < 0.0001) (Figure 58).

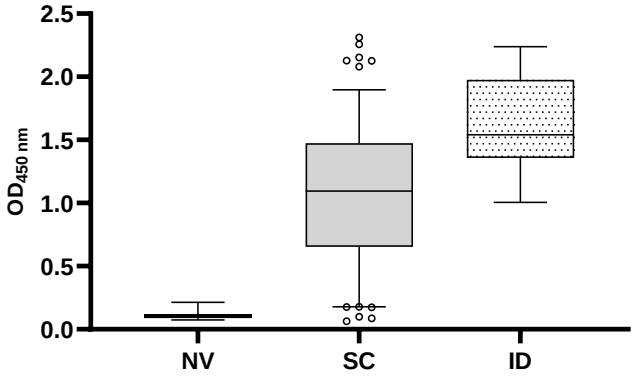

Figure 58. Reactivity of the 259 rabbit sera grouped by the vaccination status of the animal they were extracted from.

Box and whiskers plot of the reference diagnostic test absorbance level obtained for serum samples from non-vaccinated (NV) and vaccinated (SC, ID) animals, expressed as OD_{450} values. Each box represented the IQR of absorbance for the corresponding sera group with its median absorbance showed by a horizontal line, and the whiskers representing the 5-95 range of the group. Outliers are represented by empty dots, outside the whiskers.

DEVELOPMENT OF AN IELISA TEST BASED ON WHOLE LU-MYXV (IELISA-LU)

Optimization of the iELISA-Lu test

An in-house serological assay for broad-spectrum detection of anti-MYXV antibodies was developed, mirroring the design from the commercial ELISA, as an attempt to replicate its diagnostic performance. For that, whole viral particles from the virulent Lu-MYXV and an attenuated MYXV homologous vaccine (Vac2-MYXV) strains were produced and purified by ultracentrifugation (as specified in Methods). The purified stocks were used to prepare a solution containing 1 ng/µl in 0.05M C-B buffer (pH 9.5). Ninety-six well plates were coated with 100 µl of either Lu-MYXV or Vac2-MYXV solutions per well and used in a preliminary iELISA reaction.

Three rabbit sera samples previously categorized as seronegative (N, OD_{450nm} 0.134), weak seropositive (P, OD_{450nm} 0.890) and strong seropositive (PP, OD_{450nm} 2.954) with the discontinued commercial ELISA CIVTEST® Cuni Mixomatosis, were used. Two-fold serial dilutions of all sera were tested with the in-house Lu-MYXV and Vac2-MYXV based indirect ELISAs using the following protocol: overnight coating at 4°C, followed by 30 minutes incubation at 37°C with a 1% yeast-PBST blocking solution, 1 hour incubation at 37°C with rabbit serum, 1 hour incubation at 37°C with the HRP-conjugated secondary antibody diluted 1:3000 in blocking solution, 5 minutes incubation with TMB and addition of the same volume of H_2SO_4 3N to stop the enzymatic reaction. A PBS+T washing step was performed five times between each stage of the protocol (except after TMB addition) (Figure 59).

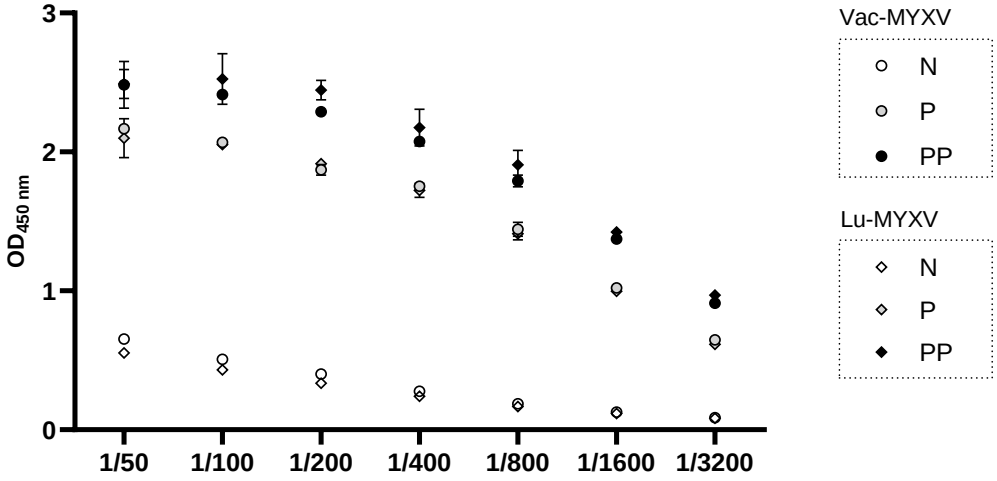

Figure 59. Reactivity of rabbit serum in the in-house iELISA coated with the attenuated vaccine strain Vac2-MYXV (o) or the virulent reference strain Lu-MYXV (◊).

The plot displays the raw OD_{450nm} measurements for three distinct serum samples subjected to a two-fold serial dilution ranging from 1:50 to 1:3200, where N represents a seronegative sample (white shapes); P a weakly seropositive sample (grey shapes); and PP a strongly seropositive sample (black shapes). Mean ± SD absorbance results were plotted against their corresponding dilution factor.

The absorbance values obtained from the same serum samples showed minimal differences regardless of whether they were analysed using the Lu-MYXV based iELISA or the Vac2-MYXV based iELISA tests. The strongly positive serum (PP) and the weakly positive (P) serum displayed similar performances in both tests, generating curves with sigmoidal shape and similar slope. Nevertheless, they showed a consistent difference in the magnitude of the OD_{450nm} measurements throughout the entire range of dilutions, with PP exhibiting higher values than P, as anticipated. In fact, the PP curve reached a plateau stage with an absorbance value around 2.5 in both iELISA tests, indicating the saturation conditions of the assay for PP were reached at the 1/100 dilution. The P curve also seemed to reach saturation between dilutions 1/50 and 1/100, with a peak absorbance around 2. The seronegative (N) sample displayed absorbance values relatively high at those same dilutions, of around 0.5, which could indicate certain contribution of non-specific reactivity at low dilutions.

Considering that cross-reactive antibodies in rabbit's serum target antigenic determinants present in the MYXV strains screened, the Lu strain was chosen for the further optimization of the iELISA protocol, since it is the reference strain. Also, only the N and PP serums were used for the optimization process as negative and positive controls, respectively.

The optimization process design was structured into two sequential CB titrations (CB1 and CB2). The first stage consisted of the optimization of the amount of antigen (Lu-MYXV) used in the coating phase which involved two parallel CB1 titrations (CB1-PP and CB1-N). In this reaction,

different antigen concentrations (from 4 ng/µl to 0.0625 ng/µl) diluted in carbonate-bicarbonate buffer were systematically combined with two-fold serial dilutions of the control serum (PP and N). The HRP-conjugated secondary Ab was used at 1:3000 (Figure 60).

Control sera were diluted in 1% yeast-PBST blocking buffer from 1/50 to 1/1600. The fact that PP serum displayed incomplete sigmoidal curves, suggested that there was not a point within the range of antigen concentrations tested at which all available antibody binding sites were consistently saturated across all serum dilutions. In contrast, the lowest Lu-MYXV concentrations (0.25 to 0.0625 ng/µl) showed a saturation signal across the PP dilutions, where the OD_{450nm} measurements seemed to converge to each other, indicating that all antigen was recognized at PP dilutions as low as 1/400.

The N control analysis unveiled an interference of the serum concentration itself on non-specific binding, which did not seem to be affected by changes in the antigen concentration, since the absorbance signal remained constant across the antigen concentration for the same N serum dilution. Higher reactivity was observed at lower serum dilutions, and this reactivity diminished progressively with increasing levels of serum dilution. The marks on the Y-axis indicate the background value obtained for each serum dilution, in absence of the antigen (Figure 60). This high background signal was concerning and highlighted the presence of non-specific binding events or contaminants interfering in the assay, independently from the antigen's presence.

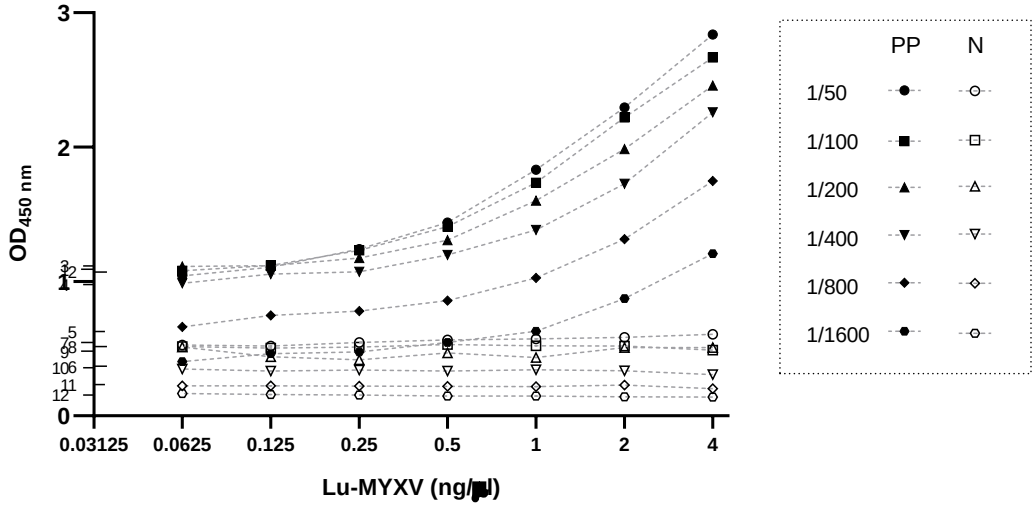

Figure 60. CB1 titration for the optimization of the in-house Lu-MYXV iELISA test

Serial dilutions of the seropositive reference serum (PP, represented by black filled shapes) and the seronegative reference serum (N, represented by empty shapes) across a gradient of antigen concentrations ranging from 0.0625 ng/µl to 4 ng/µl per well. The absorbance at 450 nm obtained for the reference control sera at each dilution in the Lu-MYXV iELISA (Y-axis) was plotted against each antigen concentration (X-axis in log_2 scale). *Marks on the Y-axis represent the absorbance of each

serum dilution in absence of antigen (numbers 1-6 correspond to PC serum dilutions 1/50 to 1/1600, and numbers 7-12 correspond to NC serum dilutions 1/50 to 1/1600).

As part of the optimization process, a range of blocking agents were screened to investigate their effect on reducing the background signals. Blocking agents were selected regarding availability in our laboratory and their utility in other studies: yeast extract, skimmed milk, and BSA. Since high absorbance signals were obtained after performing the iELISA test were apparently independent from the Lu-MYXV concentration, the three blocking solutions were first tested in the absence of antigen (Figure 61, A). Unexpectedly, the blocking solution initially used in the iELISA protocol, composed of 1% yeast extract in PBST, generated the highest absorbance readings for both control sera (PP and N). In contrast, the other two blocking buffers displayed very low absorbance throughout the assessed conditions.

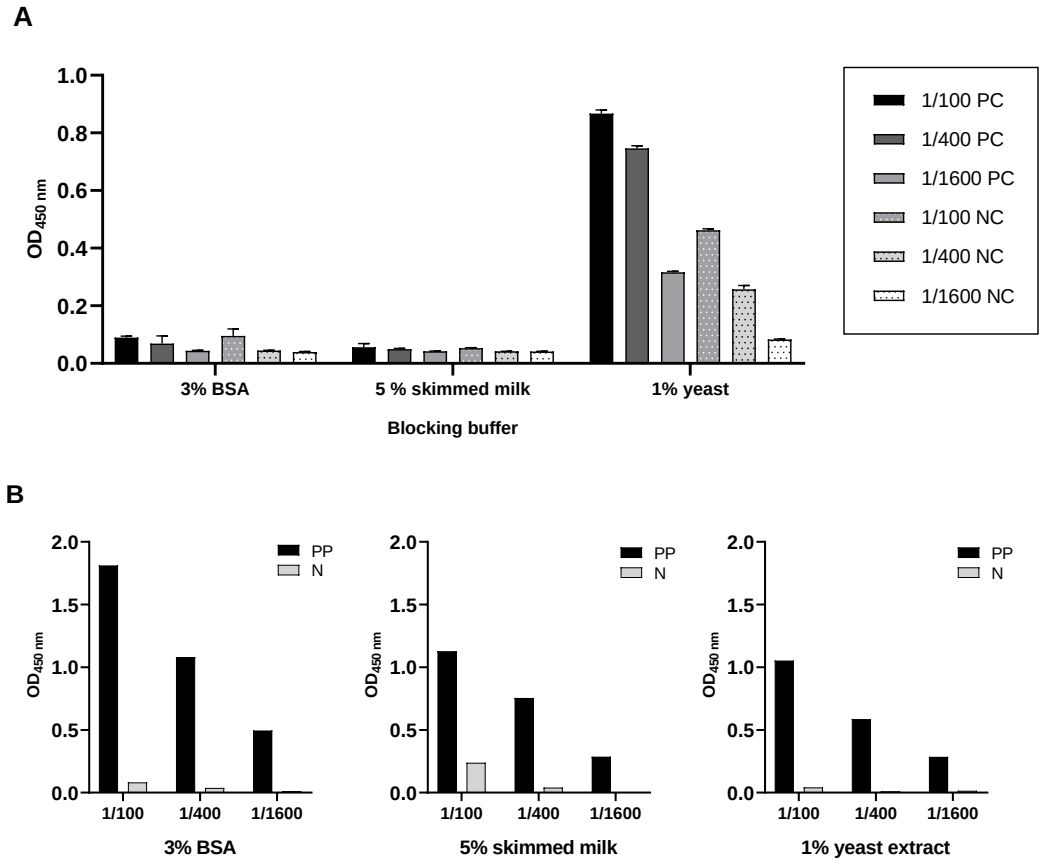

Figure 61. Optimization of the blocking buffer composition for the iELISA-Lu test

A) Comparative analysis of the background reactivity for the in-house iELISA using 3% BSA, 5% skimmed milk or 1% yeast, in PBST as blocking buffers. The background absorbance signal, being obtained from wells with no antigen on it, were measured across three 1:4 serial dilutions (1/100, 1/400 and 1/1600) using a positive (PC) and negative (NC) serum for myxoma virus. B) Reactivity obtained in the in-house iELISA after subtracting the background signal from each blocking buffer from the absorbance obtained for three different PC and NC serum dilutions, against 100 ng of antigen (Lu-MYXV).

Then, the three blocking buffers were screened in the Lu-ELISA protocol, and the discriminating power was studied after extracting the corresponding background values associated to each blocking buffer (Figure 61, B). Despite 1% yeast extract showing low reactivity in negative controls and high Positive/Negative (P/N) ratios after background extraction, the positive values were insufficiently high. A similar pattern emerged with the 5% skimmed milk-PBST buffer, though it yielded higher reactivities in negative controls compared to yeast extract. Overall, the 3% BSA-PBST blocking buffer displayed the most consistent results across the three tested dilutions, balancing a high P/N ratio (22.05 for 1/100, 28.45 for 1/400 and 38.21 for 1/1600), good $OD_{450\ nm}$ values of the positive control serum, and low background.

In light of these results, CB1 was repeated using the same protocol, but using the 3% BSA-PBST buffer for blocking the wells and to prepare the serum and the conjugated secondary antibody dilutions (Figure 62). After running the CB1 assay, the combination of antigen that gave the highest P/N ratio throughout the serum dilutions with minimal background noise, and without compromising the OD_{450} signal was determined to be 1 ng/µl.

In the second CB titration (CB2), the secondary Ab (anti-rabbit IgG conjugated with HRP) was titrated against 4-fold serial dilutions of the positive and negative control sera, starting from 1/50 to 1/12800 (Figure 63). The background noise showed values around zero across all secondary antibody dilutions, which indicated the absence of enzyme activity without the presence of specific primary antibodies, and also that the blocking adaptation performed on the assay took account of non-specific binding. The dilution effect of the PP serum is noticeable across the absorbance curves, none of which seemed to plateau within the examined dilution range, except for the highest secondary Ab dilutions (1/24000 and 1/48000). All curves converged at higher PP serum dilutions, after 1/3200, suggesting that beyond this point the concentration of secondary antibody would not significantly affect the readings, but the antibody concentration present in the serum would constitute the limiting factor.

The absorbance readings of all secondary Ab dilutions tested against N serum dilutions had practically negligible OD_{450} values from 1/800 N dilution. However, there was an increase in absorbance at the lowest serum dilutions 1/50 and 1/200, in which the iELISA results showed increased reactivity at the highest concentrations of secondary Ab in particular. This could be attributed to an amplification effect on the absorbance signal resulting from some unspecific binding between an excess of primary rabbit antibodies and the antigen, added to an excess of secondary Ab (Figure 63, B). The combination that gave a good P/N ratio throughout the serum

dilutions with minimal background noise, and without compromising the OD_{450} signal was the serum dilution 1/200 and secondary Ab dilution of 1/6000.

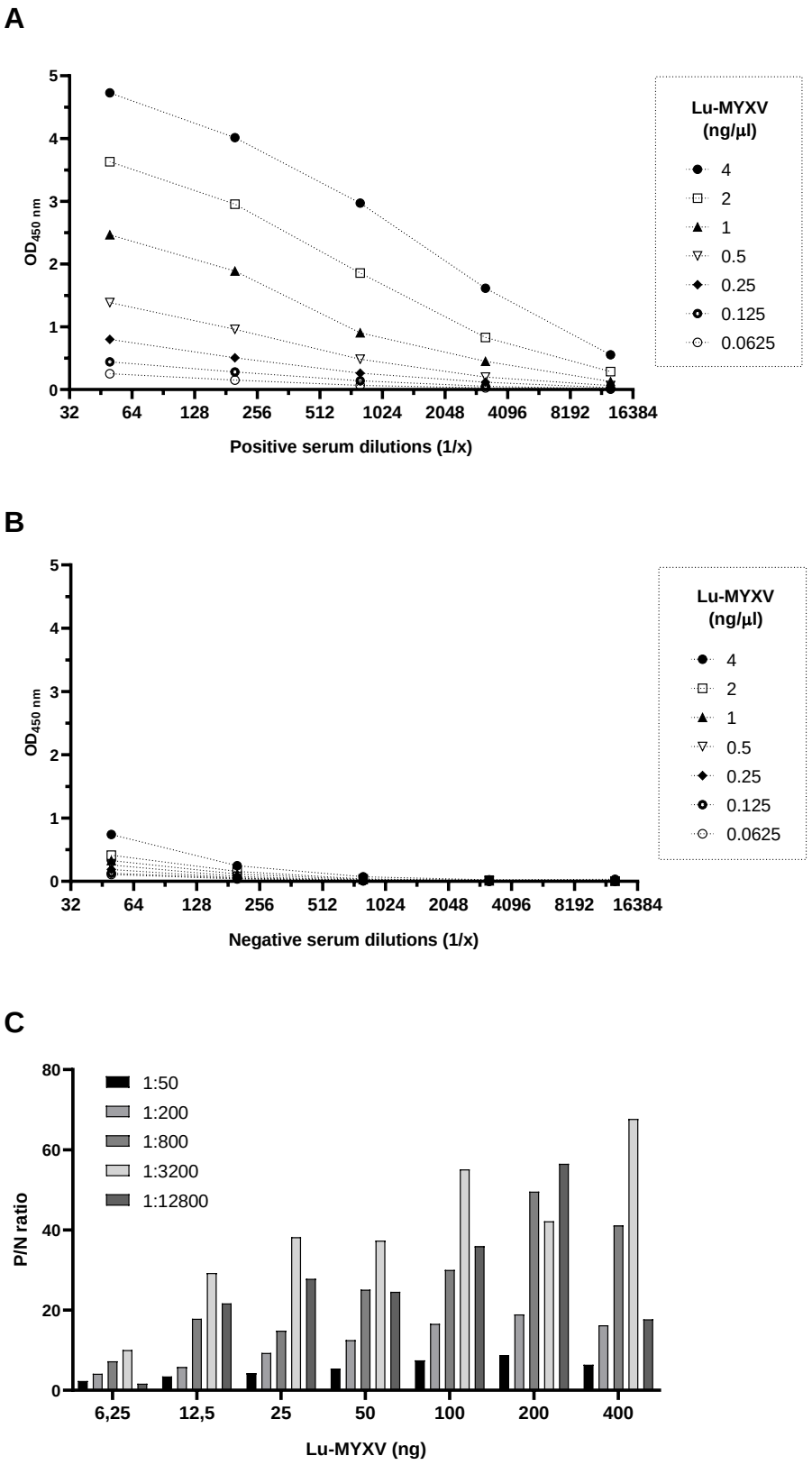

Figure 62. CB1 results for the Lu-MYXV based iELISA using a suitable blocking buffer

(A) OD_{450} readings from five 4-fold serial dilutions of the positive control (PP) serum, starting from 1:50, against different concentrations of the Lu-MYXV antigen that were used to coat the 96-well plate, ranging from 0.0625 ng/µl to 4 ng/µl. (B) OD_{450} readings for five 4-fold serial dilutions of the negative control (N) serum, starting from 1:50, against same antigen concentrations. (C) P/N ratio of each sera dilution, for every amount of Lu-MYXV.

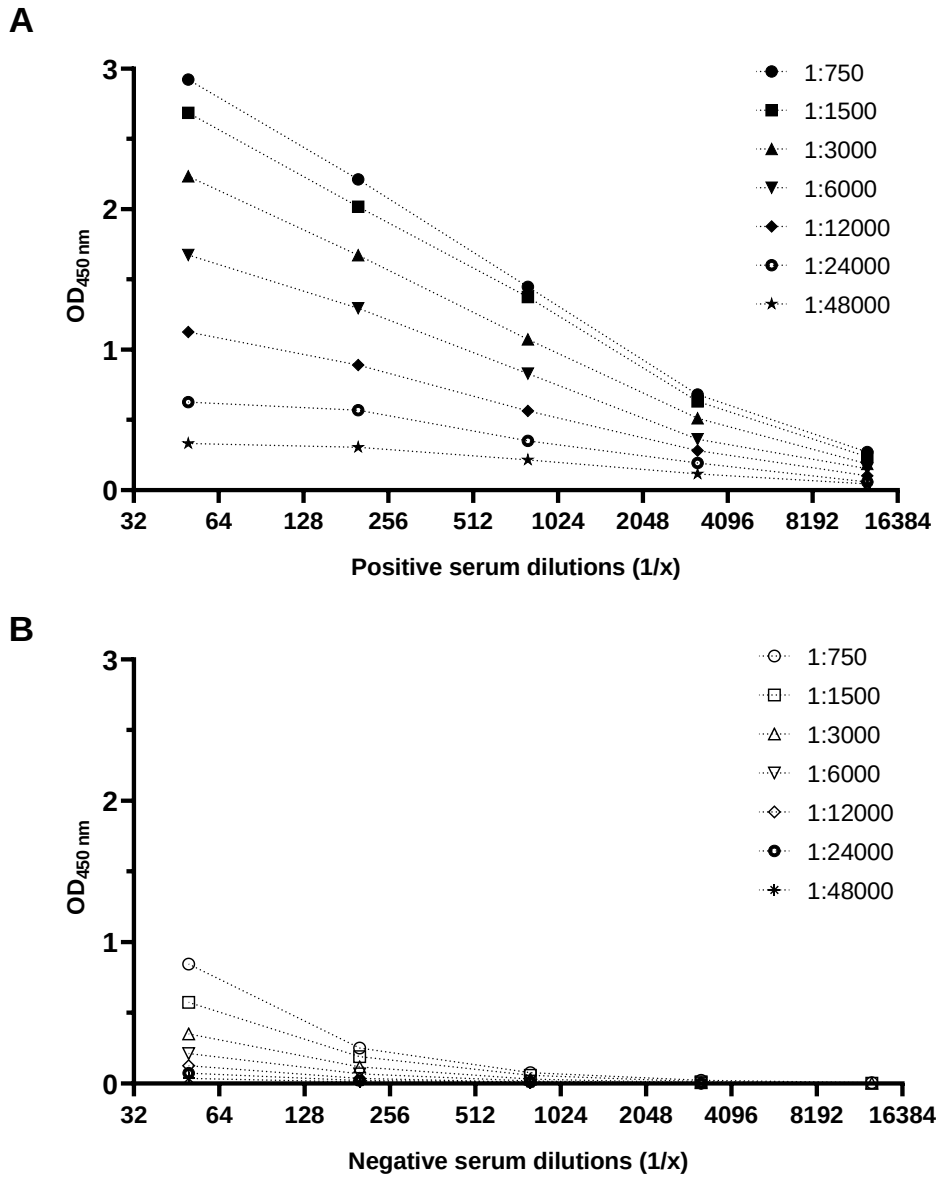

Figure 63. CB2 results for the iELISA-Lu test.

(A) OD_{450} readings of 2-fold serial dilutions of the secondary Ab, starting from 1:750, combined with different positive serum dilutions. (B) OD_{450} readings for five 4-fold serial dilutions of the secondary Ab, combined with different negative serum dilutions. Note: The amount of antigen used for coating each well was 100 ng/well.

Antigenicity of heat-inactivated Lu-MYXV in iELISA

This iELISA protocol was based on whole viral particles of viable MYXV, an infectious agent that even though it is not considered a direct threat to humans, its handling requires implementation of several biosafety measures according to the specific biosafety level (BSL)-2 containment. To improve the safety profile of the serological test, as well as understanding the antigenic stability of the virion, the iELISA was coated with 1 ng/µl viable Lu-MYXV particles and the same concentration of heat inactivated Lu-MYXV. The inactivation process consisted of incubating the viral particles that were already diluted in 0.05M C-B pH 9.5 buffer at its working concentration, in a water bath at 60°C for 30 minutes. The untreated aliquot was prepared simultaneously and incubated on ice for the same amount of time. Both samples were added to a RK13 cell culture to confirm the thermal inactivation was completed successfully. An interesting finding observed on the infection assay was that the virus stability started dropping in the aliquot of viable Lu-MYXV diluted in the C-B buffer, despite being kept cool. The 60°C water bath incubation inactivated the viral particles diluted either in PBS or C-B buffer, after just 5 minutes of incubation (Figure 64).

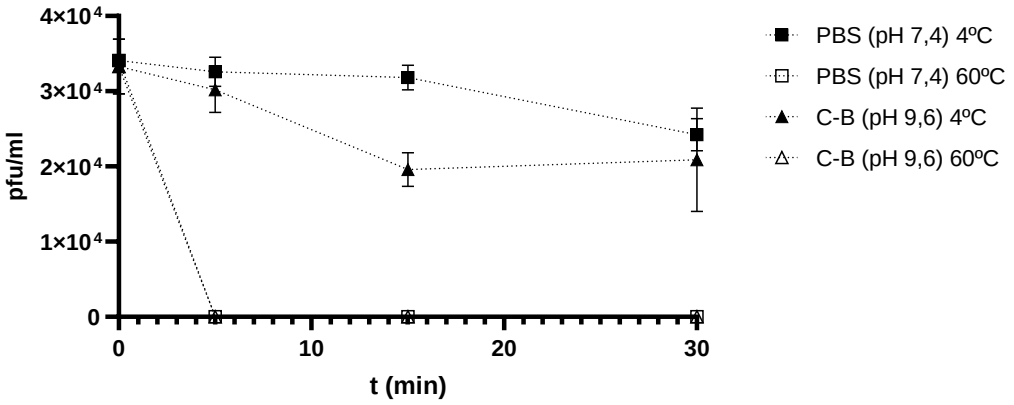

Figure 64. Titration of Lu-MYXV viral aliquots treated and untreated by heat-inactivation.

Viral dilutions were prepared in PBS and C-B buffer, and virus was inactivated by heat treatment. Samples were collected before starting the treatment (0 minutes), and 5, 15 and 30 minutes of incubation either at 60°C or on ice (untreated control) and titrated in RK13 culture. Mean and SD are plotted.

Absorbance values of the thermally inactivated virus were compared with those of the untreated control. Overall, the heat treatment caused a significant reduction on the OD_{450nm} measurement on both PP and N control serums (Table 9). The diminished reactivity of rabbit antibodies to Lu-MYXV particles indicated a substantial loss of critical antigenic determinants

within the virion's structure, attributed to structural changes and protein denaturation resulting from heat exposure. Although the P/N ratio also suffered an important decrease, it was still above the commonly accepted threshold value, and the test was still able to distinguish between positive and negative results.

Table 10. Antigenic comparison between reactivity of positive and negative rabbit sera to heat-inactivated Lu-MYXV and untreated virus in iELISA.

	Positive serum OD_{450nm}	**Negative serum OD_{450nm}**	**P/N ratio**
Untreated Lu-MYXV	1.334 ± 0.052	0.032 ± 0.005	41.976
Heat-inactivated Lu-MYXV	0.524 ± 0.013	0.029 ± 0.010	17.955

Note: Corrected OD_{450nm} measurements ± SD and P/N ratios are shown.

Performance evaluation of the iELISA-Lu test

For the evaluation of intra-plate variability of the Lu-MYXV iELISA, the mean $OD_{450\ nm}$ values of 4 replicas from each control sera (PC and NC), SD and CV% were calculated in two independent experiments (Table...). For the inter-assay variability, absorbance data of control serums from a total of 7 independent experiments were used for the between-run variability assessment. The Lu-MYXV iELISA's inter-assay CV% for the positive serum was 16.12% and for the negative serum was 21.90%. Both values could be considered within the acceptable ≤ 25% CV. Given that it consistently produces results with small variations relative to the mean under the same conditions, the Lu-MYXV iELISA assay could be considered reproducible.

Table 11. Within-plate mean OD450 nm and CV% between seropositive (PP) and seronegative (N) quadruplicates.

	PLATE 1		**PLATE 2**	
SERUM SAMPLE	Mean	CV (%)	Mean	CV (%)
PP	1.7424	2.75	1.3524	2.73
N	0.1013	8.41	0.071	11.23

DEVELOPMENT OF AN IELISA TEST BASED ON ANTIGENIC RECOMBINANT MYXV PROTEINS

Following the serological analysis of the 259-rabbit serum by the commercial iELISA, a total of 9 samples from panel 1 were selected based on their high OD_{450} values. They were proportionally pooled to create a homogenous serum pool with a high presence of antibodies against MYXV. Considering the substantial variability observed in rabbits mounting an immune response against the MYXV and the lack of positive reference control serum, this pooled mixture was established to be used as the positive control (PC) serum during the iELISAs protocol optimization. Such approach aimed to ensure consistent high values for the recombinant protein-based iELISAs.

The optimization process designed for the iELISA-rM022 and iELISA-rM115 tests was also structured into two sequential CB titrations (CB1 and CB2). The first stage consisted of the optimization of the amount of antigen (M022 or M115 proteins) used in the coating phase, and involved two parallel CB1 titrations, one for the positive serum control, and one for the negative serum control (CB1-PC and CB1-NC). In the CB1 titration, the secondary Ab (anti-rabbit IgG conjugated with HRP) was used at 1:6000. In the CB2 titration, different PC and NC serum dilutions were tested against three different secondary Ab concentrations (1:3000, 1:6000 and 1:12000).

The specific assay conditions that provided the best signal-to-noise measured by the P/N ratio were established as the optimal conditions for the corresponding iELISA assay.

Development of the iELISA-rM022 test

Optimization of the iELISA-rM022 test protocol

The PC serum curves showed a dose-dependent behaviour of the antigen concentration, according to the antigen-antibody specific interactions, displaying a sigmoidal shape (Figure 65, A). At the beginning of the curve, the readings were close to the baseline indicating that the antigen concentration was too low to be detected by the antibodies in the serum dilutions, even in the lowest dilution (1:50). As the antigen concentration increased, the antibodies present in the serum bonded proportionally, and the curve acquired a linear behaviour which is the range where the assay is most sensitive to changes in antigen concentration. In this case, this range would comprise 0.25 to 2 ng/µl. Towards the highest M022 protein concentrations, the curves seemed to be arriving to the plateau phase, where the antibody binding sites seemed to get

saturated and despite increasing antigen concentration, the rise in OD_{450} values was not significant.

The CB1 titration of the NC serum and the M022 protein concentration was decisive for the analysis of the non-specific binding and background noise corresponding to the inherent nature of the rabbit serum and variables other than the rM022 antigen itself interferences. This titration allowed the identification of the antigen concentrations that still produced a signal above the background, such as 2 ng/µl and 4 ng/µl especially in the lowest serum dilutions (Figure 65, B).

The optimal antigen concentration for the assay was determined to be 100 ng, as it displayed the highest P/N ratio across all sera dilutions, and therefore a clear differentiation between positive and negative samples (Figure 65, C). This amount of M022 protein also yielded absorbance readings within the assay's linear detection range for every PC serum dilution, avoiding potential accuracy issues associated with the measurement process. Hence, this concentration would also grant the acquisition of more accurate and reproducible results.

After setting the amount of protein, the secondary Ab was titrated against serial dilutions of the PC and NC sera in the CB2. Overall, the OD_{450} readings corresponding to this second stage gave remarkably high values. The curves for dilutions 1:6000 and 1:12000 had logarithmic shape, seeming to reach a plateau phase at the 1:50 dilution, with an absorbance 2.55 and 1.83, respectively. However, the 1:3000 dilution curve's shape had a linear tendency in combination with the PC serum, reaching OD_{450} values > 3. As the PC serum dilution increased, the resulting absorbance signal was reduced in an apparently linear way. A similar behavior was observed with the NC serum, which had considerably high absorbance for the three secondary Ab concentrations at 1:50 and 1:100 dilutions. From dilution 1:400 onwards, the OD_{450} is practically negligible (Figure 66, A). The P/N ratio was calculated for all the combinations, but it was only represented for the sera dilutions between 1:50 and 1:6400. Higher dilutions showed heterogeneous values unsuitable for the desired working conditions (negative ratios, and 0< P/N <1). The P/N ratio increased with higher serum dilutions, enhancing test specificity by reducing non-specific binding. Additionally, within each serum dilution group, the P/N ratio increased with higher secondary antibody dilutions, though the variation among the three dilutions was consistent for sera dilutions ranging from 1:50 to 1:400 (Figure 66, B).

Combining the OD_{450} values observed in the titration curves with the P/N ratio data, the optimal working dilutions for the serum and the secondary antibody were determined to be 1:400 and 1:12000, respectively. This combination displayed the highest P/N ratio, and the best iELISA-

rM022 assay performance by extension, without compromising the OD_{450} value obtained for the PC serum.

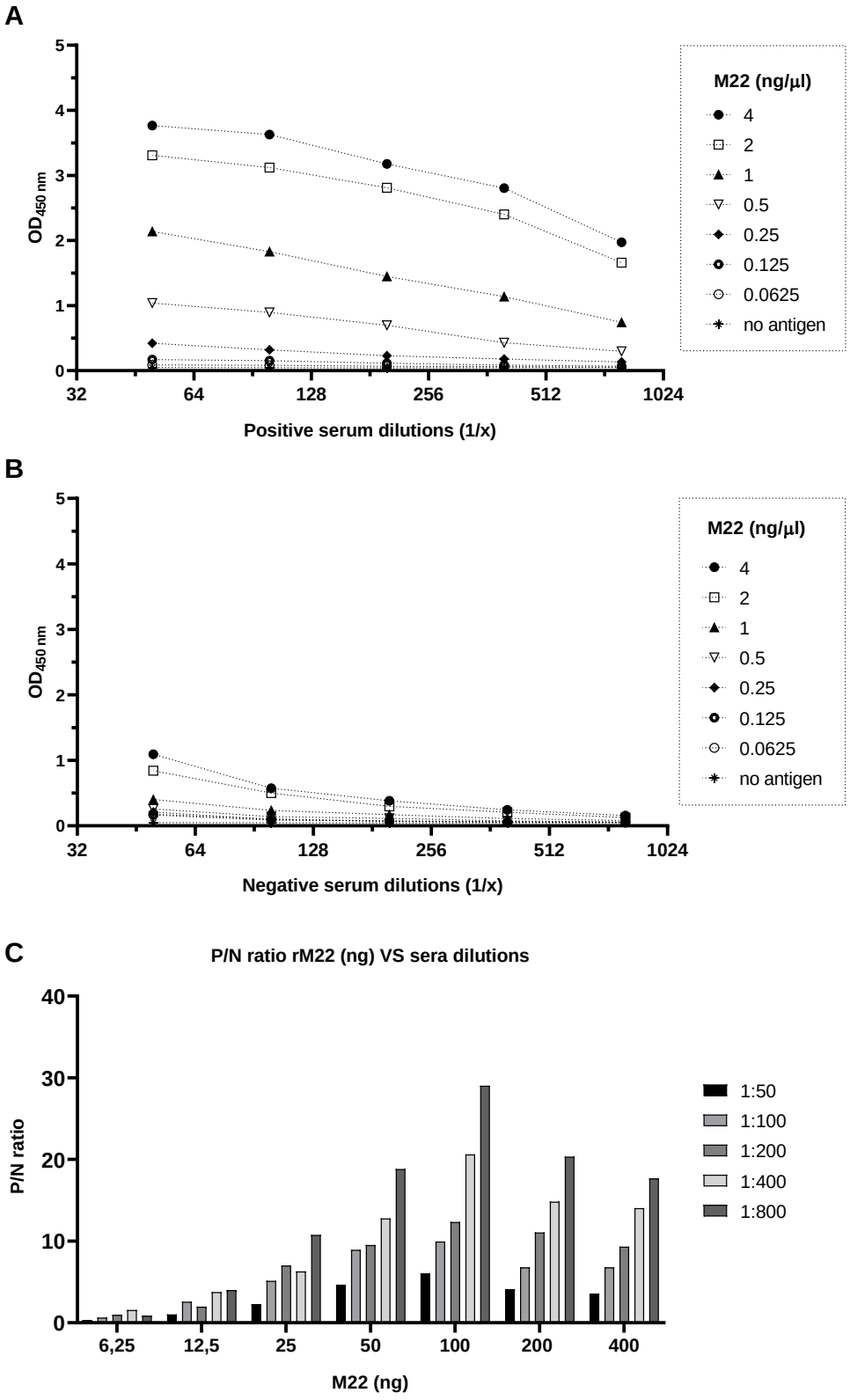

Figure 65. CB1 titration results for iELISA-rM022 test.

(A) CB1-P: OD_{450} readings from five two-fold serial dilutions of the positive control (PC) serum, starting from 1:50, against different concentrations of the rM022 antigen that were used to coat the 96-well plate, ranging from 0.0625 ng/µl to 4 ng/µl. (B) CB1-N: OD_{450} readings for five two-fold serial dilutions of the negative control (NC) serum, starting from 1:50, combined with 0.0625 ng/µl to 4 ng/µl of the antigen rM022. (C) P/N ratio of each sera dilution, for every amount of antigen rM022 coating each well. Note: The X-axis in A and B is plotted in a log_2 scale; the values are shown as antilog.

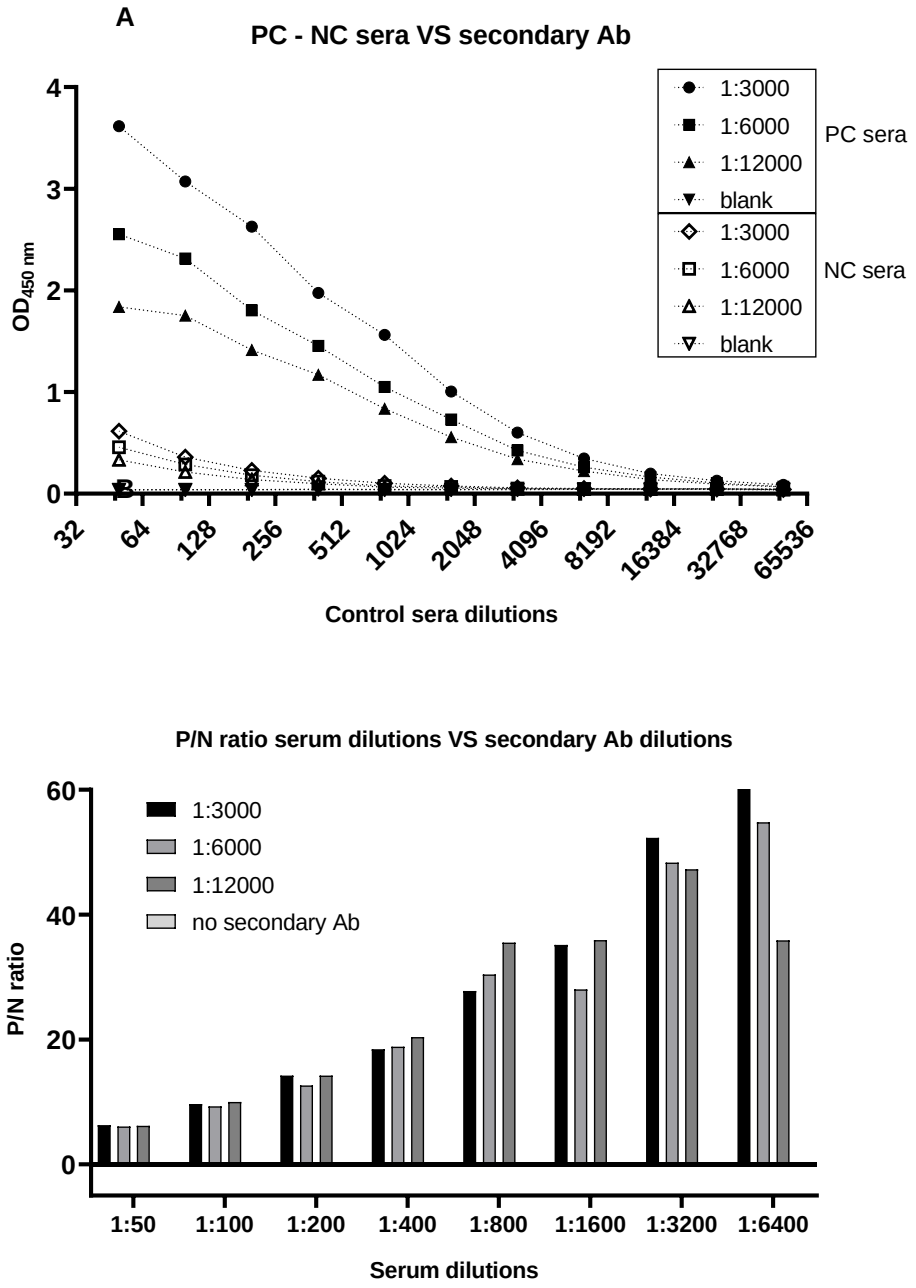

Figure 66. CB2 titration results for iELISA-rM022 test

Control sera dilutions were titrated with different secondary antibody dilutions. A) OD_{450} readings from three different secondary Ab dilutions for different PC serum (filled figures) and NC serum (empty figures) dilutions. B) P/N ratios obtained at varying two-fold serum dilutions (1:50 to 1:6400) and secondary Ab dilutions (1:3000, 1:6000 and 1:12000). A "no secondary antibody" control was included to confirm that the variation in P/N is influenced by the secondary Ab concentration. Note: The X-axis in A and B is plotted on a log_2 scale; the values are shown as antilog.

Given that the M022 protein was expressed as a fusion protein with GST, the cross-reactivity of this tag was assessed by coating the ELISA plates with two different concentrations of GST pure stock protein, one considerably higher than the approximate working amount used when coating with M022 (25 ng/µl) and the other being 100 times lower (0.25 ng/µl). The iELISA assay was performed using the optimal conditions described for the iELISA-rM022 test. Results of this analysis indicate negligible absorbance values when the PC serum was used in search for reactivity against either GST concentrations (Figure 67). Surprisingly, although NC serum also displayed low reactivity, it displayed higher absorbance values than the ones obtained for PC at both GST amounts tested: 2500 ng (difference of OD_{450}: 0.0075) and 25 ng (difference of OD_{450}: 0.024). The NC serum's apparent higher cross-reactivity could help to explain the slight background signal associated with this serum that was observed in previous optimization processes.

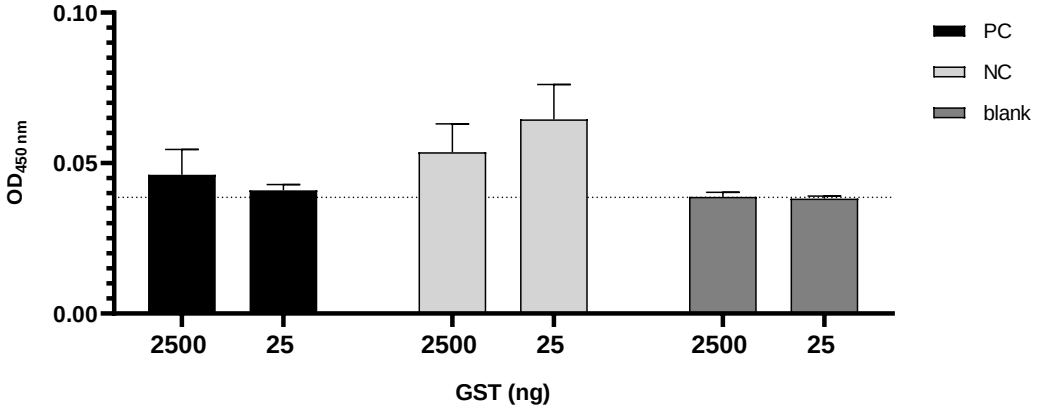

Figure 67. Cross-reactivity analysis of rabbit sera in iELISA-rM022 with pure GST protein.

Either 2500 ng or 25 ng of GST protein were used in the coating process, and the assay was performed using the optimal sera and secondary Ab dilutions, incubation times, incubation temperature, etc. Mean and SD of the replicas are shown in the bar plot for each condition.

Performance validation of the iELISA-rM022 test

Intra-plate assay variation was determined by performing 8 replicates of the positive (PC) and negative (NC) controls in the same 96-well plate, keeping all variables constant. Inter-assay repeatability was checked by testing positive and negative controls in 3 independent plates (Figure 68).

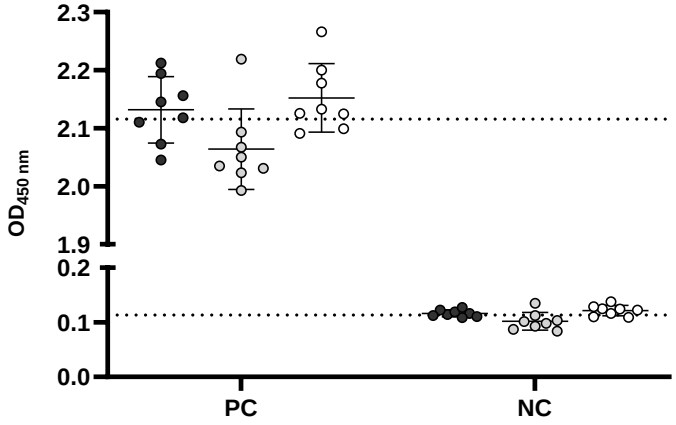

Figure 68. Evaluation of within-run and between-runs consistency of control samples (PC and NC) in the iELISA-rM022.

Absorbance values from eight individual replicates of the PC and NC, performed across three different plates (each represented by black, grey, or white dots) are plotted along with their mean and ± SD. The PC and NC mean OD_{450} values of the three plates were represented by a dashed line in the Y-axis.

The within-run variabilities expressed as CV% are shown in Table 11. The intra-assay CV% of the PC at the working dilution was very low in all three plates, ranging from 2.68% to 3.37%. The intra-assay CV% of the NC ranged from 5.42% in PLATE 1, to 15.99% in PLATE 2. Such high value could be explained by the presence of an outlier within the replicas that gave an absorbance at 450 nm of 0.135 (Table…). The inter assay CV was calculated using the SD and mean of the three intra-plate CVs, resulting in a CV% of 2.18% for the PC, and 9.10% for the NC. These results are somehow expected, since the negative control ODs are close to the limit of detection thus small variations in the measurement can result in relatively larger CV changes (Trottier et al., 1992).

Table 12. Evaluation of the iELISA-rM022 test intra-plate variability among PC and NC replicates.

	PLATE 1		PLATE 2		PLATE 3	
	Mean	CV (%)	Mean	CV (%)	Mean	CV (%)
PC	2.1318	2.68	2.0639	3.37	2.1522	2.74
NC	0.1164	5.42	0.1018	15.99	0.1217	7.87

Note: Mean $OD_{450\ nm}$ values of 8 replicas for each control sera (PC and NC), and each plate (1, 2 and 3) are displayed. CV% of the PC and NC was calculated for each plate.

The consistency of the P/N ratio was also studied as an alternative measure of quality control to inspect the performing reliability of the test and its ability to provide reproducible results (Table 12). The CV% among the three P/N ratio replicates was 7.22%, within the acceptable range indeed, which indicated good precision and consistency in the results.

Table 13.P/N ratio consistency in the iELISA-rM022 test.

P/N PLATE 1	P/N PLATE 2	P/N PLATE 3	P/N MEAN (95% CI)	SD	CV (%)
18.32	20.28	17.69	18.76 (15.41-22.12)	1.35	7.22

Note: P/N ratio of each plate (1, 2 and 3) were calculated with the mean values obtained from their PC and NC. The arithmetic mean, SD and CV (%) are also shown.

To ensure the consistency and reliability of the iELISA-rM022 test results, additional factors that could affect the accuracy and robustness of the test were characterized. For instance, the impact of the temperature at which the enzyme substrate TMB is added to the ELISA plate, and the condition of the secondary antibody stock were simultaneously analyzed.

Two secondary antibody stocks diluted at the working concentration were prepared: one fresh (new aliquot) and one that had undergone multiple freeze-thaw cycles (old aliquot). In the same run, three different TMB temperatures were tested: lower (16°C), the recommended (room temperature, or 25°C) and higher (37°C) temperatures. The TMB temperature variations did not impact the assay, within the tested range, which indeed is a wide range for being considered "room temperature". Although there were slight variations in the OD_{450} measured values across the different temperatures in both PC and NC sera, the P/N ratio was consistent (Figure...).

The repeatedly freeze-thawed second antibody aliquot (old) had a great impact in the assay reactivity and performance. The significant loss of reactivity (p value < 0.01) of the PC serum when the old aliquot was used, regardless of the TMB temperature, underscored the importance of proper handling and storage of secondary antibodies (Panel A, Figure...). Although the P/N ratios were consistent within the three TMB temperatures tested for each antibody stock, there was a considerable decrease in the average P/N ratios between each antibody aliquot: from a mean of 19.53 for the New, to a mean of 12.25 for the Old (Panel C, Figure...).

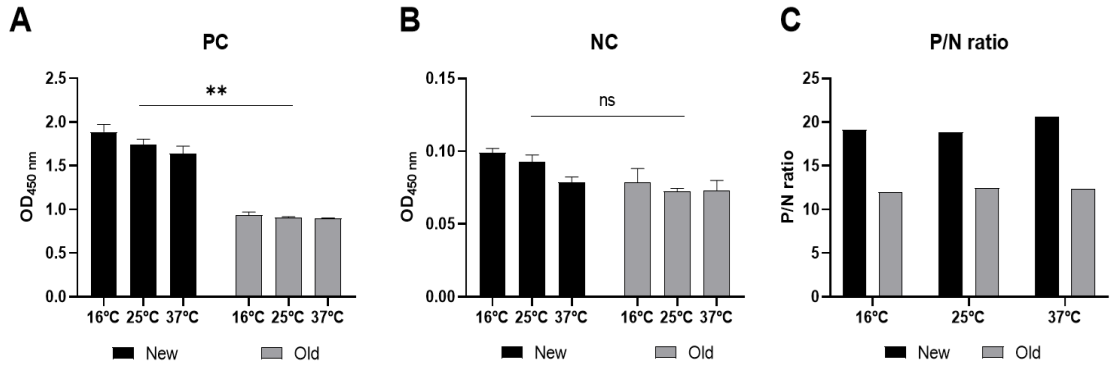

Figure 69. Effect of TMB temperature and the condition of the secondar antibody stock on the reactivity of the iELISA-rM022 test.

A) Raw OD_{450} values obtained for the PC serum. B) Raw OD_{450} values obtained for the NC serum. C) P/N ratios from the tested conditions. Mean ± SD were displayed in A and B. Statistical significance (**) indicates p value < 0.01.

To study the stability of surface-bound M022 antigen, plates were coated overnight at 4°C and blocked the next day and oven dried at 37°C, and then sealed and stored at 4°C until further use. PC and NC sera were analyzed at three different time points after storage: 1 day, 7 days and 30 days. The CV% of the positive control showed a value within the acceptable range, of 8.59%, but the negative control showed more variability across the OD_{450nm} measurements obtained at the three different time points, with a CV% of 28%. Antigen adsorbed onto the plates was stable at least up to one month after preparation (Figure…).

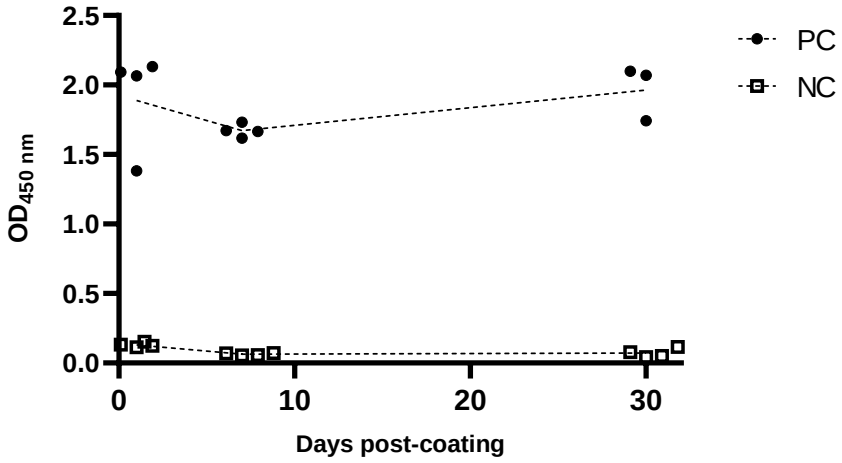

Figure 70. Stability profile of the M022 coated plates tested with replicates of the positive (PC) and negative controls (NC).

Individual replicates of PC and NC analysed 1, 7 and 30 days after coating the plates are staggered plotted in the Y-axis and connected with their means by a discontinuous line.

DEVELOPMENT OF THE IELISA-RM115 TEST

Optimization of the iELISA-rM115 test protocol

The optimization process for the iELISA-rM115 test was identical to the one that was followed for the iELISA-rM022 test, but with particular differences. Considering that M115 has a higher immunogenicity compared to the M022 protein, the concentration of the coating M115 antigen used for the CB1 titration started from 2 ng/µl, instead of 4 ng/µl.

The dilution curves resulting from different antigen-PC serum combinations reached high absorbance values and showed the expected dilution effect as antigen or primary antibodies (serum) concentration decrease (Figure 71, A). The plateau height of the curves decreased sharply from antigen concentration 0.25 ng/µl, indicating that upon this concentration, the limited antigen availability strongly restricts the antigen-antibody complex formation. The shape of the curves also indicated a good antigenic strength for the M155 protein since there was a robust binding response across all the range of antigen concentrations. In addition, there was a significant binding even at high serum dilutions (e.g. 1:800), which could suggest that the primary antibody availability would be the limiting agent for the rM155-antibody complex formation.

Titration of the negative serum resulted in a much lower reactivity in the iELISA-rM115, as would be expected when there is no antibody binding to the antigen. There was, however, some substantial absorbance across all antigen concentrations at the lowest NC serum dilution of 1:50, most likely owing to background and unspecific interactions (Figure 71, B). The P/N ratio profile for a given rM155 concentration at large rose in correspondence with higher sera dilution. The P/N ratio also exhibited higher values with increased M115 antigen concentrations, ranging from 3.125 ng to 25 ng. Beyond this point, it remained relatively stable at 25 ng and 50 ng, showing a slight decrease at 100 ng and even a more noticeable decline at 200 ng (Figure 71, C). Thus, the addition of more than 25 ng rM115 would not improve the resolution capacity of the assay.

The optimal rM155 concentration for the iELISA was determined to be 25 ng, as it displayed the highest P/N ratio across all sera dilutions, maintaining both reasonable OD_{450} readings for the PC serum, and a low background signal.

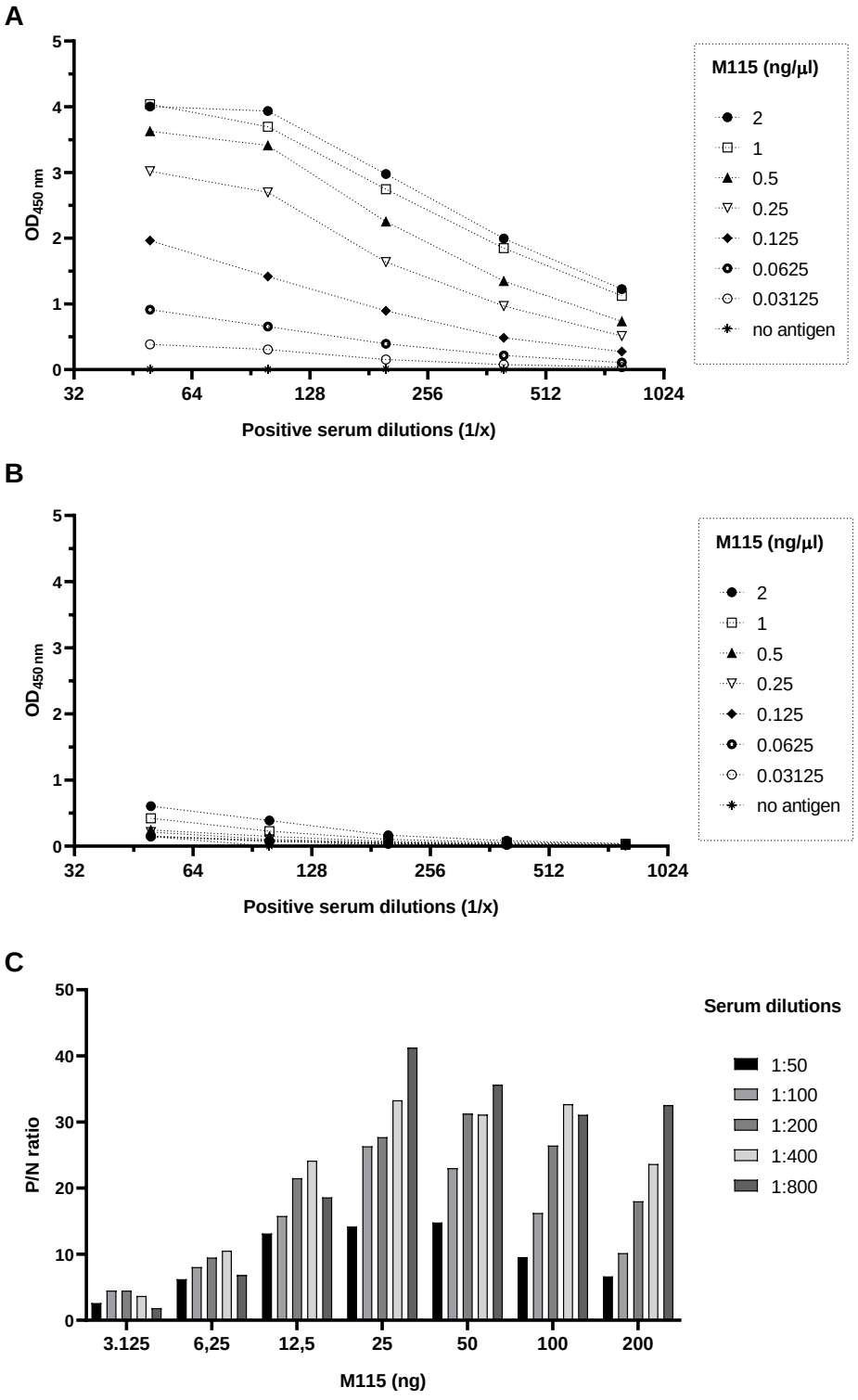

Figure 71. CB1 titration results for iELISA-rM115 test.

A) CB1-PC: OD_{450} readings from five two-fold serial dilutions of the positive control (PC) serum, starting from 1:50, for each concentration of the rM115 antigen, ranging from 0.03125 ng/µl to 2 ng/µl. B) OD_{450} readings for five two-fold serial dilutions of the negative control (NC) serum, starting from 1:50, for each rM115 concentration, ranging from 0.03125 ng/µl to 2 ng/µl. C) P/N ratio of every serum dilution-rM115 antigen concentration. Note: In A and B, the X-axis is plotted on a $\log_2$ scale; the values are shown as antilog.

The secondary Ab (anti-rabbit IgG conjugated with HRP) titrated in the CB2 against two-fold serial dilutions of the PC and NC serum, ranging from 1:50 to 1:51200, used a coating M115 antigen concentration of 0.25 ng/µl. The curves for PC serum dilutions displayed logarithmic shapes but none seemed to reach the plateau phase in the tested conditions, which could indicate that the primary antibody did not reach a saturating concentration. As the PC serum dilution increased, the resulting absorbance signal of the three curves was reduced in a linear way until reaching the lower plateau around 1:12800 dilution. In fact, the endpoint dilution of the PC serum remained consistently similar, regardless of the variation in the secondary Ab dilution.

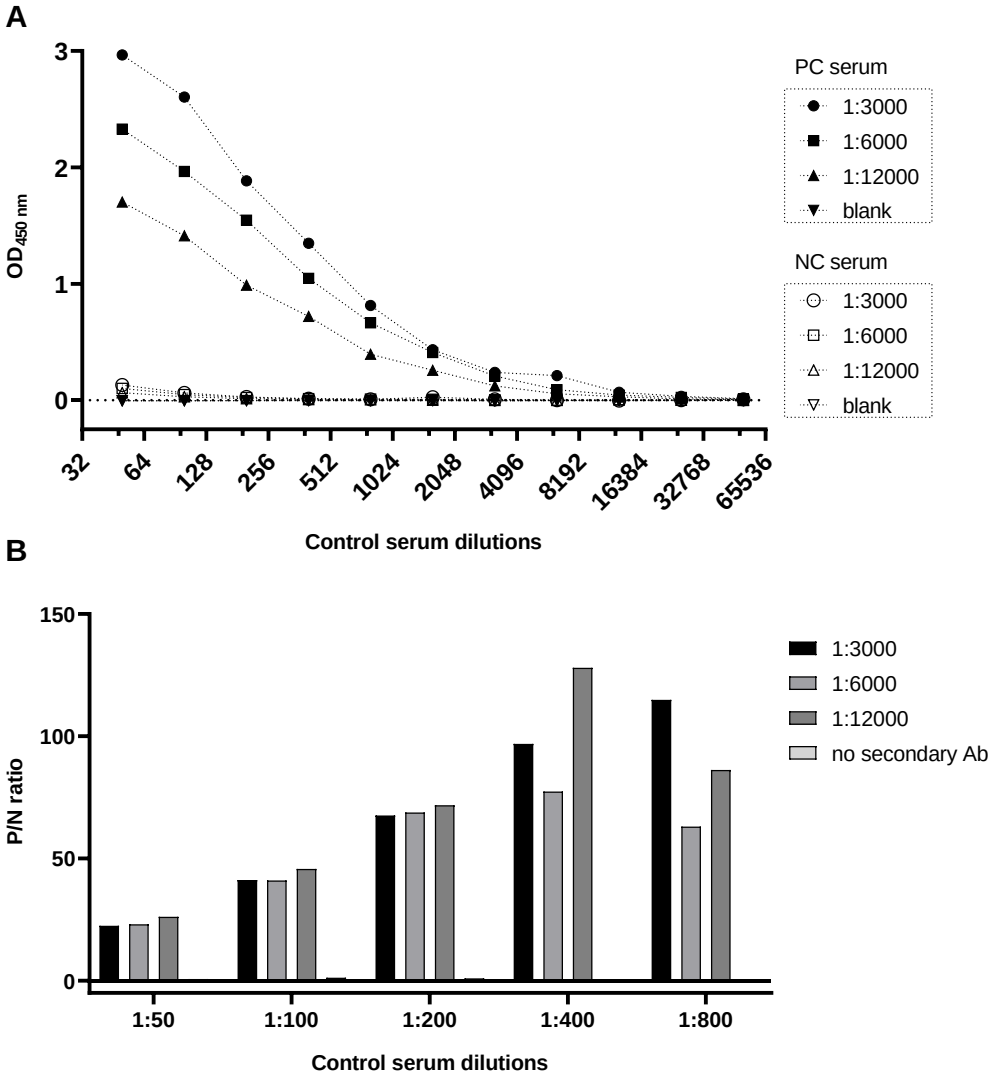

Figure 72. CB2 titration results for the iELISA-rM115 test.

PC and NC serum dilutions were titrated against secondary antibody dilutions. A) OD_{450} readings from three different secondary Ab dilutions for different PC serum (filled figures) and NC serum (empty figures) dilutions. B) P/N ratios obtained at varying two-fold serum dilutions (1:50 to 1:6400) and

secondary Ab dilutions (1:3000, 1:6000 and 1:12000). A "no secondary antibody" control was included to confirm that the variation in P/N is influenced by the secondary Ab concentration. Note: The X-axis in A and B is plotted on a log_2 scale; the values are shown as antilog.

The absorbance curves for the NC also exhibited slightly higher values at a 1:50 dilution when combined with each of the three secondary Ab concentrations, but the OD_{450} is practically negligible across the remaining combinations, indicating a very low background signal associated to the NC serum (Figure 72, A).

The P/N ratio was only represented for the sera dilutions comprised between 1:50 and 1:800, because higher dilutions showed heterogeneous values not suitable for the desired working conditions (negative P/N ratios, low PC serum absorbance, etc). As the serum dilution increased, the P/N ratio tended to rise, enhancing the test's specificity by minimizing non-specific binding. The ratio within each serum dilution group further increased with higher secondary Ab dilutions, although the difference was not relevant (Figure 72, B).

Combining the OD_{450} values observed in the titration curves with the P/N ratio data, the optimal working dilutions for the serum and the secondary antibody were determined to be 1:100 and 1:6000, respectively.

Performance evaluation of the iELISA-rM115 test

Intra-plate assay variation was determined by performing 8 replicates of the positive (PC) and negative (NC) controls in the same 96-well plate, keeping all variables constant. Inter-assay repeatability was checked by testing positive and negative controls in 3 independent plates (Figure 73).

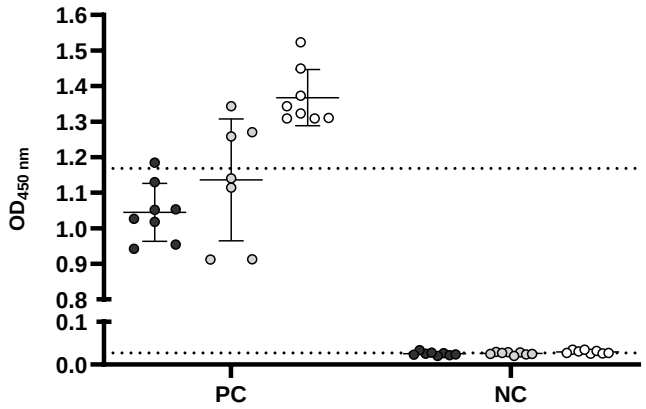

Figure 73. Evaluation of within-run and between-runs consistency of control samples (PC and NC) in the iELISA-rM115 test.

Absorbance values from eight individual replicates of the PC and NC, performed across three different plates (each represented by black, grey, or white dots) are plotted along with their mean and ± SD. The PC and NC mean OD_{450} values of the three plates were represented by a dashed line in the Y-axis.

The within-run (intra-plate assay) variabilities of PC and NC analysed in the iELISA-rM115 were expressed as CV% (Table). The intra-assay CV% of the PC at the working dilution differ amongst the three plates, ranging from 5.77% CV in PLATE 3, to 18.13% in PLATE 2, whereas the intra-assay CV% of the NC gave variability values between 12.57 and 16.34%. The relatively high variability described by the CV% for the NC serum was not graphically observed in Figure … , since it was more likely a consequence of the low nature of their OD_{450} readings. The inter-assay CV% was calculated using the SD and mean of the three intra-plate mean OD_{450} readings, resulting in a CV% of 14.87% for the PC, and 9.02% for the NC.

Table 14. Evaluation of intra-plate variability among replicates of the PC and NC in iELISA-rM115.

	PLATE 1		**PLATE 2**		**PLATE 3**	
	Mean	CV (%)	Mean	CV (%)	Mean	CV (%)
PC	1.0449	7.81	1.0939	18.13	1.3674	5.77
NC	0.0253	16.34	0.0259	12.57	0.0298	12.65

Note: Mean $OD_{450\ nm}$ values of the 8 replicas for each control sera (PC and NC), and each plate (1, 2 and 3) are displayed along with their CV%.

The consistency of the P/N ratio was also studied as an alternative measure of quality control to inspect the performing reliability of the test and its ability to provide reproducible results. The CV% among the three P/N ratio values was 5.63%, which indicated a good precision and consistency of the iELISA-rM115 performance (Table 14).

Table 15. P/N ratio consistency analysis of the iELISA-rM115 test

P/N PLATE 1	**P/N PLATE 2**	**P/N PLATE 3**	**P/N MEAN (95% CI)**	**SD**	**CV (%)**
41.37	42.24	45.95	43.18 (15.41-22.12)	2.43	5.64

The mean, SD and CV (%) of the P/N ratio across the three runs were calculated using the P/N ratios from each plate (1, 2 and 3).

To study the stability of surface-bound rM115 antigen, plates were coated at 4°C overnight at 0.25 ng/µl, blocked the next day, oven dried at 37°C and then sealed and stored at 4°C until further use. Positive and negative control samples were analyzed at three different time points after storage: 1 day, 7 days and 30 days. The PC serum demonstrated higher variability than the

NC across the three time points: CV% for the PC serum was 25.45%, whilst the CV% for the NC serum was 11.6%. Although the rM115 antigen seemed to lose some degree of antigenicity, regarding that the PC serum reactivity decreased within a week of storage, the variability appears to be within the acceptable range (CV% < 30%). Since the discriminatory power of the iELISA-rM115 test given by the P/N ratio had an acceptable stable behavior with a mean of 20.80, and CV% of 14.98%, the performance of the test seemed to remain reliable.

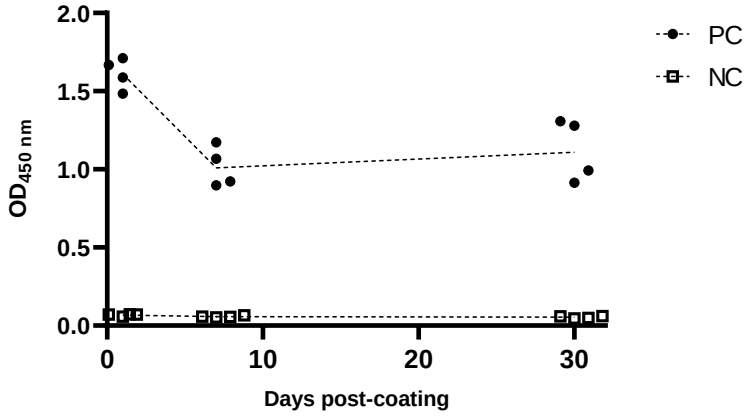

Figure 74. Stability profile of the M022 coated plates tested with replicates of the positive (PC) and negative (NC) sera controls.

Individual replicates of PC and NC analyzed 1, 7 and 30 days after coating the plates are staggered plotted in the Y-axis and connected with their means by a discontinuous line.

EVALUATION OF THE DIAGNOSTIC PERFORMANCE OF THE SEROLOGICAL TESTS

Once specific steps of the assay were established independently for each ELISA test, they were subjected to a validation process in which the diagnostic performance was evaluated. The assessment of metrics such as diagnostic sensitivity and specificity were crucial for determining the credibility and reliability of such assays as a diagnostic tool.

Diagnostic power of the iELISA-Lu test

Although the overall sera panel described in Materials comprised 259 samples, only 188 of them were used in the validation of the iELISA-Lu test. The exclusion of some samples from this analysis was mainly because they were obtained after having performed the validation of this iELISA-Lu assay (e.g. all samples from the PANEL 3), or because of practical constraints such as reagent limitation or insufficient volume (some samples from PANEL 1 and 2).

Threshold determination for the iELISA-Lu test by ROC analysis

The first step was to establish the threshold or cut-off value which could best differentiate between positive and negative test results. This was performed through a ROC analysis. The AUC calculated with a 95% CI for the ROC analysis using the % ROD results of the positive and negative sera samples analyzed in the Lu-MYXV iELISA was 0.9816 (0.9679-0.9953), with a standard error of 0.00698 (Figure 75).

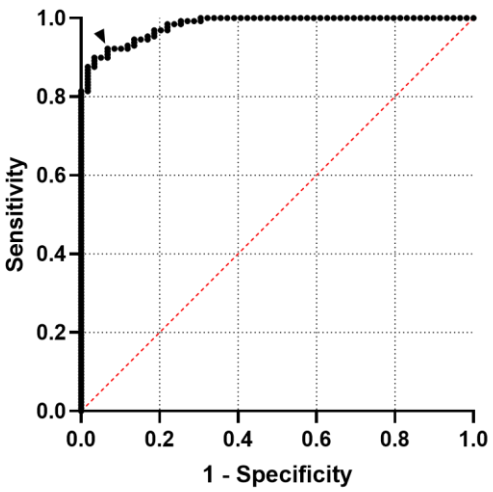

Area under the ROC curve	
Area	0,9816
Std. Error	0,00698
95% CI	0,9679 to 0,9953
P value	<0,0001

	Lu-MYXV iELISA
AUC	0,9816 (0,9679-0,9953)
Cut-off	25,28%
Se (%)	92,25 (86,32-95,74)
Sp (%)	93,22 (83,82-97,33)
P value	<0,001

Figure 75. ROC analysis and diagnostic performance of the in house iELISA test based on the Lu-MYXV as antigen.

ROC plot constructed with Se (*Y* axis) and 1- Sp (*X* axis) paired values for each decision threshold value (*cut-off*) of the Lu-MYXV iELISA. The AUC was 0,9816. A black arrow pointed the threshold set by the Youden's Index that gave the best Se/Sp compromise: 92,25% DSe and 93,22% DSp. The cut-off value was 25,28% ROD.

The diagnostic Se and Sp of this test were determined after defining the optimum cut-off value by the Youden's Index, which maximized both parameters. In graphical terms, these values were given by the point on the ROC curve closest to the upper-left corner (black arrow points to the cut-off in Figure 75). The optimal threshold for the Lu-MYXV iELISA test was established at 25,28% ROD, achieving a diagnostic Se 92.25% and a Sp 93.22%. Its performance was slightly worse when compared to the reference diagnostic iELISA test results (INgezim MIXOMATOSIS, R.17.MIX.K1, Ingenasa), which has 98% DSe and >99% DSp.

Comparison of the iELISA-Lu performance with the Gold Standard

The cut-off value for MYXV-directed IgGs antibody positivity determined by the ROC curve analysis (25.28%) was used to categorize 188 serum samples in the in-house iELISA-Lu into positives or negatives (Figure 76). Data were not normally distributed within any group, although the positive dataset (Shapiro-Wilk test, W= 0.9756, p-value=0.0251) showed less deviation to normality than the negative one (Shapiro-Wilk test, W=0.8595, p-value<0.0001). The median %ROD of the negative samples was 4.442% ROD and the median of the positive ones was 84.42%, with the Mann Whitney U test determining a significant difference in the distribution of both datasets, without any overlap (U value = 0, p value<0.0001).

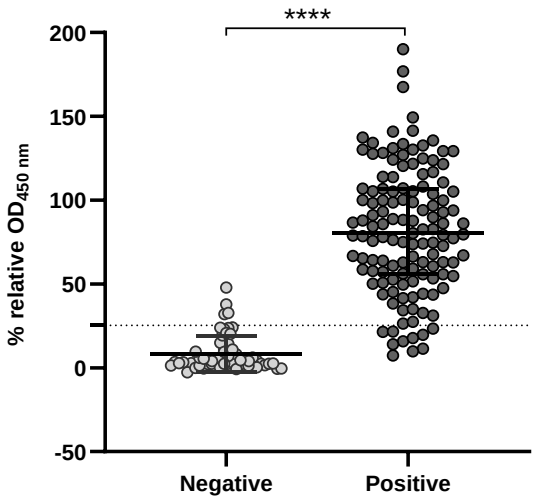

Figure 76. Individual reactivity (% ROD) in the iELISA-Lu test of sera samples categorized by the reference ELISA test.

Individual reactivity (% ROD) of positive (*n*= 129) and negative (*n*= 59). The threshold determined by ROC analysis for the Lu-MYXV iELISA test (25.28%) was represented by a dashed line on the Y-axis. Median and IQR of each group were included in all datasets.

The in-house iELISA of 123 (65.43%) samples tested positive and 65 (34.57%) samples tested negative, compared to the 129 (68.62%) ones that were classified as seropositive by the reference iELISA test, and the 59 (31.38%) that were classified as seronegative, showing similar positive and negative frequencies for the 188 sera tested.

Evaluation of the diagnostic performance and the classification power of the Lu-MYXV iELISA test were conducted by the Fisher's exact test (Table 15). The results showed a strong and statistically significant concordance between the outcomes from both tests (Odds Ratio of 163.62, P value < 0.0001). DSe, DSp, PPV and NPV frequencies associated to the performance of the iELISA-Lu test were calculated from the counts displayed in the contingency table, including a 95% CI computed using the hybrid Wilson-Brown method. The results matched with the ones defined by the ROC analysis during the cut-off determination: DSe of 0.9225 (95% CI from 0.8632 to 0.9574), DSp of 0.9322 (95% CI from 0.8382 to 0.9733), PPV of 0.9675 (95% CI from 0.9194 to 0.9873), NPV of 0.8462 (95% CI from 0.7394 to 0.9142).

Table 16. Comparative overview of the performance of the in-house Lu-MYXV iELISA test (in rows) with the reference iELISA test (in columns).

		Ref. test		
		Positive	**Negative**	**Total**
iELISA-Lu	**Positive**	119	4	123
	Negative	10	55	65
	Total	129	59	188

Note: The contingency table shows frequency counts of samples corresponding to each combination of outcomes.

The Cohen's kappa value of 0.831 (95% CI from 0.747 to 0.916) indicated an almost perfect agreement. In fact, there was an agreement on 92.51% of the observations between both test's outcomes. Therefore, only a discrepancy of 7.49%, accounting for 14 samples, of which 4 were seronegative that tested positive in the in-house iELISA test, and 10 seropositive samples that were misclassified as seronegatives with the iELISA-Lu test.

Since Likelihood Ratios (LRs) are not influenced by the prevalence of the disease or condition, they are a useful measure for the interpretation of the usefulness of a test. The LR+ for the diagnostic test was 13.60, and the (LR-) was 0.083. This combination of LRs results was indicative of a high reliability on the diagnostic outcomes of the in-house iELISA test. The high LR+ (13.60) indicated that positive test results would strongly support a diagnosis of the "disease", or in this case, the exposure either to virulent virus or MYXV vaccine strains, while the low LR- (0.083) would decrease the probability that the subject would have been exposed.

Comparative analysis of rabbit sera performance in iELISA-Lu test based on different vaccination administration routes

Given the known vaccination status of the rabbits from which the 188 samples were collected, the samples were divided into non-vaccinated (NV, *n*= 47) and vaccinated (V, *n*= 142) groups. Samples within the V group was further divided depending on the administration route into subcutaneous (SC, *n*= 109) and intradermal categories (ID, *n*= 32).

When the outcomes from the in-house iELISA-Lu were analysed considering the vaccination status, it was notable that the SC group was responsible for 100% of FN results (10/10) and 75% of FP results (3/4), with the 25% remaining belonging to 1 NV serum (Table 16).

Table 17. Frequency counts of serum samples categorized by the iELISA-Lu test into negative or positive, based on vaccination routes.

	***Negative* (*n*= 65)**		***Positive* (*n*= 123)**		***Total***
	True negative	***False negative***	***True Positive***	***False positive***	
Non vaccinated	46	0	0	1	47
Subcutaneous	9	10	87	3	109
Intradermic	0	0	32	0	32
Total	55	10	119	4	188

The NV group showed a unanimous outcome of negative results, except for an outlier corresponding to a false positive that had a higher reactivity of 47.87% ROD in the Lu-MYXV iELISA test. The NV group median was 3.258% ROD (95% CI 2.387 to 4.442), and the skewness (2.840) and excess kurtosis (10.63) indicated a highly asymmetric and heavy-tailed distribution of the values.

Serum samples from vaccinated rabbits were compared based on the route of vaccine administration: the ID group showed higher accuracy in the absorbance values amongst the samples, with a range of 84.45 (from 49.71% to 134.2% ROD), relatively low compared to the 187.5 (from 2.43% to 190% ROD) of the SC group. However, the highest registered % ROD values belonged to the SC group. ID group also had significantly highest % ROD median (91.34%, 95% CI 85.77 to 105.3) than the SC group (67.12%, 95% CI 55.86 to 78.96) (Figure 77).

Regarding the difference in sample size for each categoric group (NV, SC and ID), the Shapiro-Wilk test was used to assess the normality of each dataset (with a significance level of 0.05). The NV group (W= 0.7026, p-value <0.0001) and the SC group (W= 0.9720, p-value= 0.0214) failed to pass the normality test, indicating some, and substantial deviation from a normal distribution,

for SC and NV respectively. Only the distribution of data belonging to the ID group met the assumptions of normality (W= 0.9532, p value= 0.1774) and equal variances (Bartlett test, p value < 0.001).

The three groups (NV, SC, and ID) showed a statistically significant difference in its %ROD distribution (Kruskal-Wallis statistic (H-statistic) = 100.4, p value < 0.0001). The ranks of each pair of groups were compared by the Dunn's post-hoc test, finding that all groups were significantly different when compared to each other. The highest and more significant mean rank difference was observed in the comparison of NV-ID groups (-110.5, p value < 0.0001), followed by NV-SC groups (-82.37, p-value < 0.0001) and finally by SC-ID groups (-28.13, p-value = 0.0304) (Figure 77).

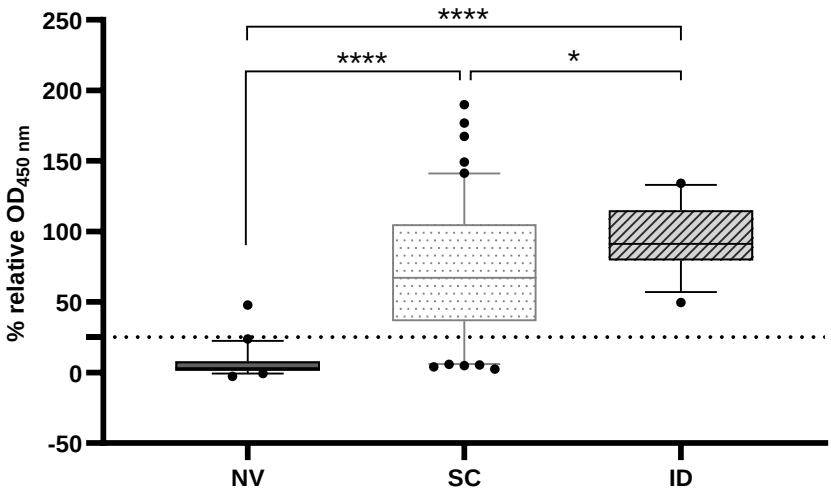

Figure 77. Reactivity (% ROD) of serum samples in iELISA-Lu test, grouped by vaccination status: non-vaccinated (NV), subcutaneously vaccinated (SC) and intradermally vaccinated (ID) rabbits.

Distribution of data across the groups was illustrated by a box-and-whisker plot, where the box shoed the interquartile range (IQR), the median (line within the box), and the whiskers representing the 5-95 percentile. Outliers were represented by individual spots. Cut-off value is displayed at Y= 25.28%.

Diagnostic power of the iELISA-rM022 test

Threshold determination for the iELISA-rM022 test by ROC analysis

The optimized iELISA-rM022 was evaluated for the ability to perform an accurate MYXV's M022 protein antibody detection. All 259 rabbit sera samples, previously characterized for the presence of MYXV antibodies using the reference test, were used to determine the performance of the iELISA-rM022 test through ROC analysis. The % ROD results from the iELISA-rM022 test were analyzed, with each serum sample categorized as positive or negative based on the reference ELISA test results. The resulting curve showed an AUC of 0.9359 (95% CI from 0.9083 to 0.9634), with a standard error of 0,014. The optimum cut-off value was determined maximizing the Youden's Index, resulted in a % ROD value of -0.894% (Indicated by a black arrow in Figure 78). At this threshold, the iELISA-rM022 assay showed its best performance, with a 90.97% DSe and 83.65% DSp.

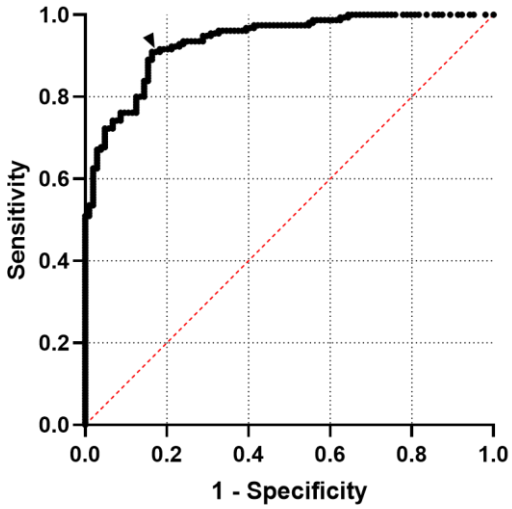

Area under the ROC curve	
Area	0,9359
Std. Error	0,01408
95% CI	0,9083 to 0,9634
P value	<0,0001

	iELISA-rM22
AUC	0,936 (0,906-0,963)
Cut-off	-0,894
Se (%)	90,97
Sp (%)	83,65
P value	<0,001

Figure 78. ROC analysis and diagnostic performance of the in house iELISA test based on the antigenic M022 recombinant protein.

The ROC plot was constructed with Se (*Y* axis) and 1- Sp (*X* axis) paired values for each decision threshold value (*cut-off*) of the iELISA-rM022. The AUC was 0.9359. The black arrow points at the threshold set by the Youden's Index -0.894% ROD, which gave the best compromise between the DSe (90.97%) and DSp (83.65%).

Comparison of the iELISA-rM022 performance with the Gold Standard

The DSe of a test is also known as the TP rate and refers to the ability of a test to correctly identify the actual positive samples as such. A DSe > 90% is typically defined as high, so the 90.97% DSe estimated for the iELISA-rM022 indicated a good discrimination ability. However, there still was a 9.03% of FN rate, that were graphically represented by the samples categorized as positive with the reference test but which %ROD is below the -0.894% ROD cut-off value

defined for the iELISA-rM022 test. The 83.65% DSp could also be considered moderately high, but the FP rate in this case would be of 18.35%. These FP could be graphically identified by the samples in the negative category group which % ROD was above the cut-off value of the iELISA-rM022 assay (Figure 79).

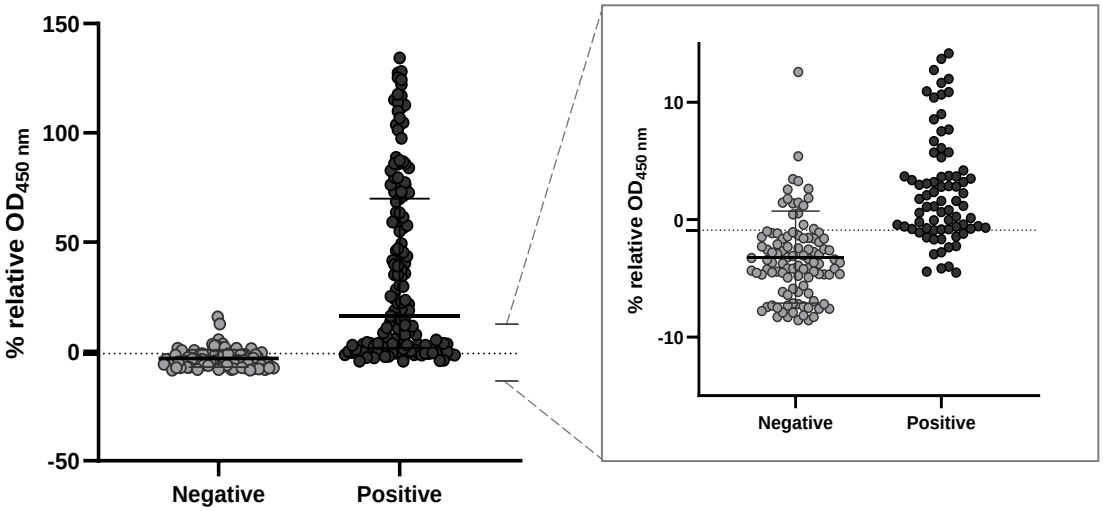

Figure 79. Individual reactivity (% ROD) in the iELISA-rM022 test of sera samples categorized by the reference ELISA test.

Positive (*n*= 155) and negative (*n*= 104) sera samples characterised by the reference iELISA test, evaluated in the iELISA-rM022. Median and IQR of each group were included in the plot. The horizontal dashed line indicates the cut-off value obtained for the iELISA-rM022 test in the ROC curve analysis (-0.894%). A magnification of the region near the threshold value was boxed adjoining the main graph.

According to the discriminatory cut-off value set for the iELISA-rM022, the 259 rabbit sera samples were re-distributed into the positive (*n*= 158) and negative (*n*= 101) categories using the iELISA-rM022 % ROD of -0.894, previously established as the optimum cut-off value for sera discrimination.

When only the number of positive and negative results were considered, the almost identical counts in each category suggested that both tests could exhibit a comparable overall performance: the new categorization of the 259 samples by the iELISA-rM022 closely aligned with the results obtained using the commercial ELISA test, which identified 155 positives and 104 negatives. The positive frequency result was 61%, very close to the 60% frequency observed using the reference test, while the negative frequencies were 39% and 40%, respectively (Figure 80).

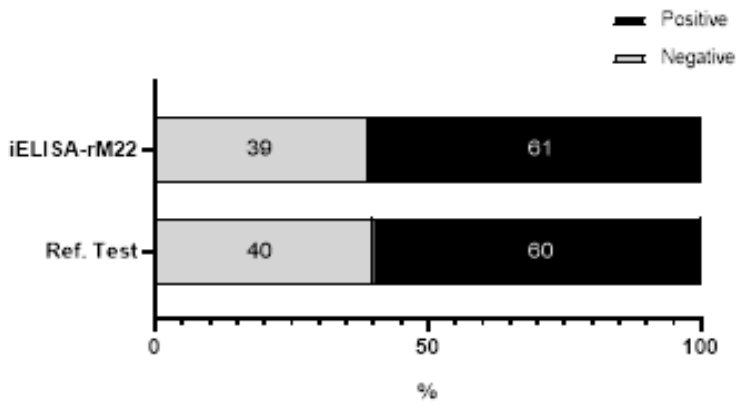

Figure 80. Diagnostic frequency from the 259 rabbit sera samples classified into positive or negative by the iELISA-rM022 or the reference ELISA tests.

Bar chart representation of the diagnostic frequency from the 259 rabbit sera samples classified into positive or negative by both serological tests: the recombinant protein based iELISA-rM022 and the reference commercial test (Ref. test).

Nonetheless, some discrepancies were observed regarding the classification of particular samples: 17 samples identified as positive by the iELISA-rM022 test were actually negative according to the reference ELISA test (FP), whilst 14 samples classified as negative in the iELISA-rM022 were positive in the commercial test (FN).

The frequency counts of the iELISA-rM022 test categorization were compared to those of reference test in a 2×2 contingency table in which the counts for every combination were displayed (Table 17). The high deviation of the observed frequencies from the expected frequencies if the variables were independent indicated a significant statistical association between the two serological diagnostic tests (Chi-square statistic of 142.57, p value < 0.0001). However, there was an evident presence of presence of FP (*n* = 17) and FN (*n*= 14) results.

Table 18. Comparative overview of the performance of the in-house iELISA-rM022 test (in rows) with the reference iELISA test (in columns).

		Ref. test		
		Positive	**Negative**	**Total**
iELISA-rM022	**Positive**	141	17	158
	Negative	14	87	101
	Total	155	104	259

Note: The table contains the frequency counts of samples corresponding to each combination of outcomes.

The evaluation of the agreement between both serological tests was evaluated using Cohen's Kappa statistic. The total agreements observed by both methods (true positives and true negatives) accounted for 88.03% of the total observations, while the number of agreements expected by random guessing was of 52.17%. The Kappa value (κ) was 0.75 with a SE ± 0.042 and a 95% CI of 0.667 to 0.832, indicating a precise estimation of κ, which itself reflected a substantial agreement between both raters (Landis & Koch, 1977).

Performance frequency metrics DSe, DSp, PPV and NPV of the iELISA-rM022 test were calculated from the counts displayed in the contingency table, including 95% CI computed using the hybrid Wilson/Brown method. The DSe and DSp values matched those defined by the ROC analysis during the cut-off determination: DSe of 0.9097 (95% CI from 0.8541 to 0.9454) and DSp of 0.8365 (95% CI 0.7537 to 0.8954). The PPV of 0.8924 (95% CI from 0.8345 to 0.9317) and a NPV of 0.8614 (95% CI from 0.7807 to 0.9156), indicated a good reliability on both positive and negative diagnostic results. Hence, the chance that a positive iELISA-rM022 test result identified an individual that truly had the condition there was 89.24% (PPV), and the chance that an individual that got a negative result did not have the condition was approximately 86.12% (NPV).

The LR+ for the iELISA-rM022 test was 5.565, which although was high it did not have enough power to evidence the presence of a disease (which is possible when LR+ > 10). The LR- was 0.1092, indicating a great diagnostic usefulness for "ruling out the disease", considering that this rate means that a negative test result would reduce the likelihood of the disease (or in this case, the chance of being a true positive) more than 9 times compared to its pre-test likelihood.

Comparative analysis of rabbit sera performance in iELISA-rM022 test based on different vaccination administration routes

Samples were categorized into the groups based on the vaccination status of the animal from which were collected, into NV (*n*= 89), SC (*n*= 132) and ID (*n*= 38), and the % ROD distribution of each dataset was represented independently (Figure 81). The Shapiro-Wilk and Bartlett tests revealed non-normality and unequal variances among the NV, SC, and ID groups. Consequently, the Kruskal-Wallis U test demonstrated significant differences in % ROD distributions among the groups ($H = 143.3$, $p < 0.05$). Post-hoc Dunn's test indicated highly significant differences between NV and both SC (mean rank difference = -98.67, $p < 0.0001$) and ID (mean rank difference = -153.0, $p < 0.0001$), as well as a significant difference between SC and ID (mean rank difference = -54.30, $p = 0.0002$).

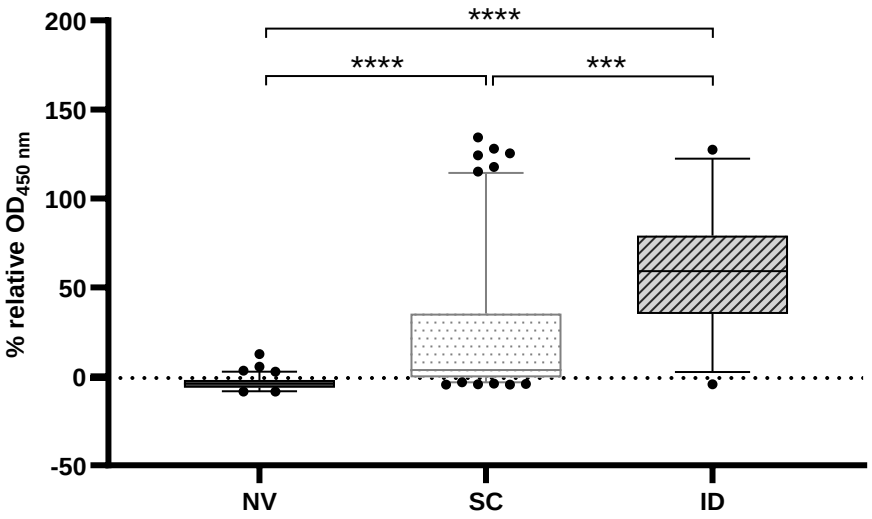

Figure 81. Reactivity (% ROD) of serum samples in iELISA-rM022, grouped by vaccination status: non-vaccinated (NV), subcutaneously vaccinated (SC) and intradermally vaccinated (ID) rabbits.

Differentiation of NV (*n*=89), SC (*n*=132) and ID (*n*=38) sera groups by iELISA-rM022, represented in a box and whiskers plot of the % relative $OD_{450\ nm}$ obtained for each group. The median is represented as a horizontal line within the box, whilst the upper and lower error bar correspond to the 5-95% percentiles, and outliers are represented as empty dots. The dashed line in the plot indicates the -0.894% ROD *cut-off* value for the iELISA-rM022, determined in the ROC analysis.

Table 19. Frequency counts of serum samples categorized by the iELISA-rM022 test into negative or positive, based on vaccination routes.

	Negative		***Positive***		***Total***
	True negative	***False negative***	***True Positive***	***False positive***	
Non vaccinated	77	0	0	12	89
Subcutaneous	10	13	104	5	132
Intradermic	0	1	37	0	38
Total	87	14	141	17	259

The 89 NV samples, which were categorized as negative by the reference test, represented 85.6% of the total negative samples, with the remaining 14.4% being SC samples. The iELISA-rM022 analysis classified 77 out of the 89 NV samples (86.5%) as negative, indicating a notable proportion of false positives (12 out of 89, 13.5%). The NV group contributed the most to the misclassification of negative samples as positive, accounting for 70.6% of the total false positives detected in the serum panel (Table 18).

The ID group was characterized by a high positive count in the iELISA-rM022 test results, with 37 out of 38 sera giving a positive outcome for anti-M022 antibodies. Since all ID samples were characterized as positive with the reference test, the remaining sample that had a negative outcome in the iELISA-rM022 corresponded to a FN (Figure 82, C).

The iELISA-rM022 outcomes revealed a predominance of positive reactivity within the SC group, out of the 132 samples, 107 had % ROD values higher than the -0.894% ROD cut-off, indicating the presence of antibodies against M022. However, 5 of these samples were FP compared to the reference test, accounting for 29.5% of the total FP detected in the 259-sample panel. Conversely, 23 SC samples had negative anti-M022 outcomes, and more than half of these (13 out of 23) were FN results.

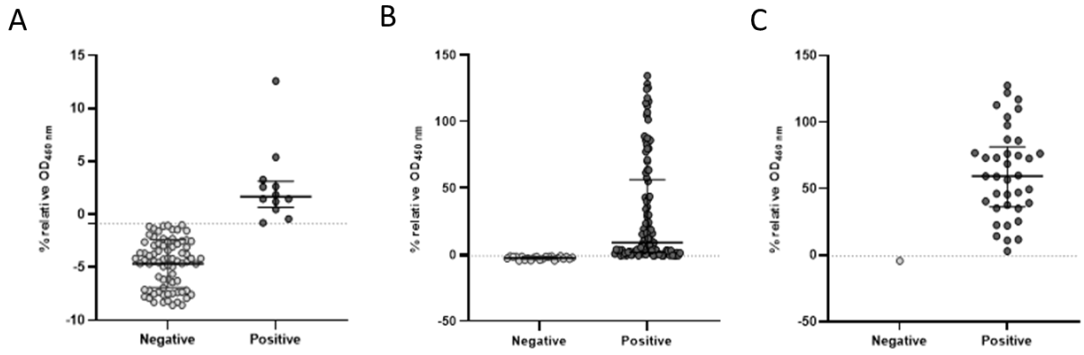

Figure 82. Individual reactivity (% ROD) of rabbit serum samples divided by the vaccination status of the subjects.

A) NV (*n*= 88) sera categorized into negative (*n*= 77) and positive (*n*= 12) with the iELISA-rM022 test analysis, B) SC sera (*n*= 132) categorized into negative (*n*= 23) and positive (*n*= 109) with the iELISA-rM022 test analysis. C) ID sera (*n* = 38) categorized into negative (*n*= 1) and positive (*n*= 37) with the iELISA-rM022 test analysis. The -0.894% ROD test cut-off was represented by a spotted line on the *Y*-axis. Median and IQR were showed.

Diagnostic power of the iELISA-rM115 test

Threshold determination for the iELISA-rM115 test by ROC analysis

These same 259 serum samples previously used in finding the diagnostic threshold of the iELISA-rM022 test, were analyzed with the iELISA-rM115 test. Absorbance values were normalized against the absorbance levels of the PC and NC serums analyzed in the same run. Their % ROD, combined with their known outcomes (categorized as positive or negative) determined by the results of the commercial iELISA, were used to construct the ROC curve (Figure 83). The AUC of

0.9392 (with 95% CI, 0.9133-0.9651 and standard error of 0.0132) indicated a good accuracy of the test's discriminative power. To define the diagnostic Se and Sp of the iELISA-rM115 test, the optimum cut-off value was determined maximizing the Youden's Index: -0.559% ROD. Considering a diagnostic threshold of -0.559% ROD, the assay was found to have a 96.77% DSe and 75% DSp.

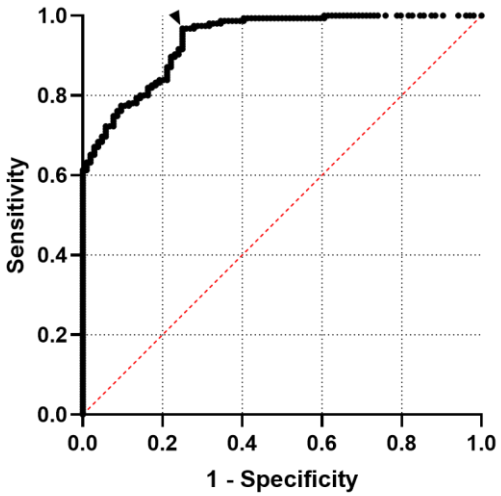

Area under the ROC curve	
Area	0,9392
Std. Error	0,01322
95% CI	0,9133 to 0,9651
P value	<0,0001

	iELISA-rM115
AUC	0,939 (0,913-0,965)
Cut-off	-0,559
Se (%)	96,77 (92,67 to 98,61)
Sp (%)	75 (65,89 to 82,33)
P value	<0,001

Figure 83. ROC analysis and diagnostic performance of the in house iELISA test based on the antigenic M115 recombinant protein.

Diagnostic performance of the rM115-based iELISA test assessed by the ROC analysis. A ROC plot was constructed with Se (*Y* axis) and 1- Sp (*X* axis) paired values for each decision threshold value (*cut-off*) of the iELISA-rM022. The AUC was 0.9359. A black arrow pointed the threshold set by the Youden's Index that gave the best DSe/DSp compromise: 96.77% DSe and 75% DSp. The cut-off value was -0.559 %ROD.

Comparison of the iELISA-rM022 performance with the Gold Standard

The 96.77% DSe estimated for the iELISA-rM115 indicated a good discrimination ability of the test to correctly identify the seropositive samples as such. The FN rate of the test was only of 3.23%, and it could be graphically visualized by the samples categorized as positives by the reference test, which %ROD is below the -0.559 %ROD threshold value defined for the iELISA-rM115 test (Figure….). A 75% DSp could also be considered moderately high, but the FP rate in this case would be of 25%. These FP could be graphically identified by the samples in the negative category group which % ROD was above the cut-off value (Figure 83).

The 259 rabbit serum samples were re-distributed into the positive (*n*= 176) and negative (*n*= 83) categories using the -0.559% ROD cut off value, established as the threshold for optimum sera discrimination by the iELISA-rM115 test (Figure 84).

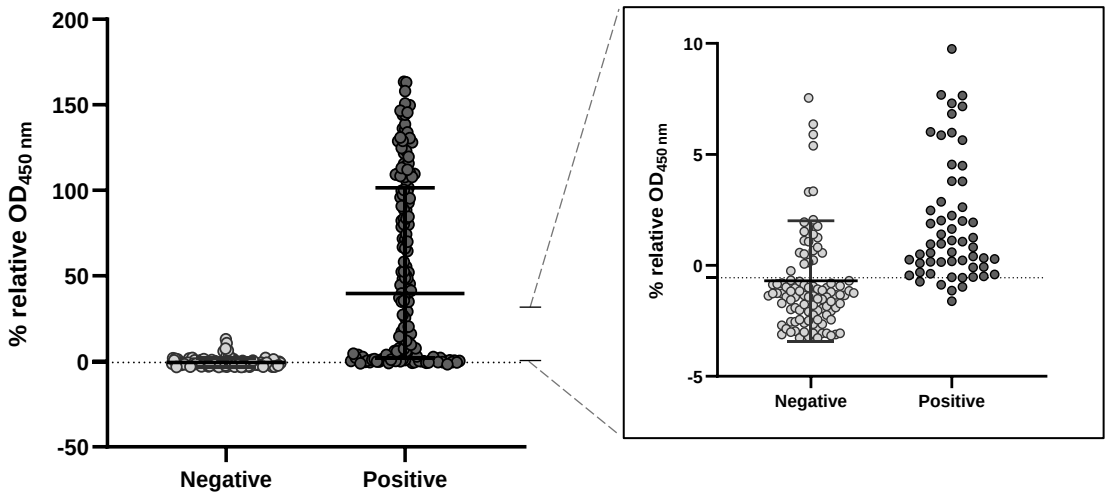

Figure 84. Individual reactivity (% ROD) in the iELISA-rM115 test of sera samples categorized by the reference ELISA test.

Reactivity (% ROD) of individual rabbit positive (*n*= 155) and negative (*n*= 104) sera samples characterised by the reference iELISA test, evaluated in the iELISA-rM115. Median and IQR of each group were included in the plot. The horizontal dashed line represents the cut-off value obtained in the ROC curve analysis (-0.559% ROD). A magnification of the region near the threshold value was boxed adjoining the main graph.

Considering the threshold determined for the iELISA-rM115 test, 176 (68%) sera samples tested positive for anti-M115 reactivity, and 83 (32%) samples tested negative. These results, compared to the 155 (60%) positive counts determined by the reference iELISA test, and the 104 (40%) that were classified as seronegative, indicate an 88% agreement between both test's outcomes.

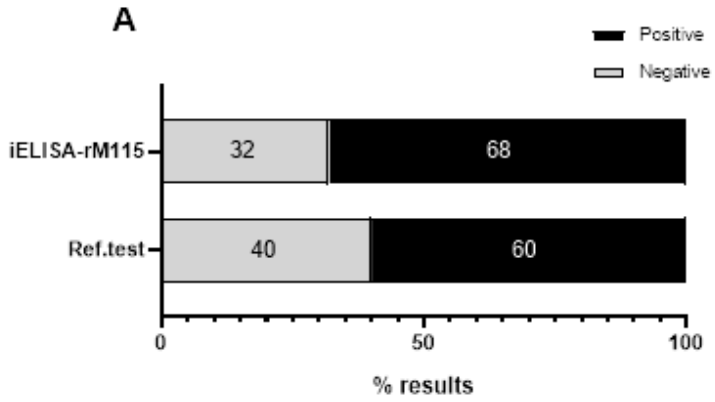

Figure 85. Diagnostic frequency from the 259 rabbit sera samples classified into positive or negative by the iELISA-rM115 or the reference ELISA tests.

Bar chart representation of the diagnostic frequency from the 259 rabbit sera samples classified into positive or negative by both serological tests: the recombinant protein based iELISA-rM115 and the reference commercial test (Ref. test).

The diagnostic performance of the iELISA-rM115 test was evaluated by the Fisher's exact test, showing a strong and statistically significant concordance between the outcomes from both tests (Odds Ratio of 90, P value <0.0001).

Table 20. Comparative overview of the performance of the in-house iELISA-rM115 test (in rows) with the reference ELISA test (in columns).

		Ref. test		
		Positive	**Negative**	**Total**
iELISA-rM115	**Positive**	150	26	176
	Negative	5	78	83
	Total	155	104	259

Note: The contingency table shows frequency counts of samples corresponding to each combination of outcomes.

The -0.559% ROD cut-off value for the iELISA-rM115 established a PPV of 85.23% (95% CI 79.23% to 93.17%) and a NPV of 93.98% (95% CI 86.66% to 97.40%). These predictive values indicated good reliability on both positive and negative diagnostic results. The chance that a positive iELISA-rM115 test result accurately identified a subject with the condition was 85.25%, whilst the chance that a subject receiving a negative result did not have the condition was approximately 93.98%.

A positive result on the test would make it around 3.87 times more likely that the sample was collected from a truly infected or vaccinated animal (LR+ of 3.87). On the other hand, a negative test result would reduce the likelihood of being a true positive more than 9 times compared to its pre-test likelihood (LR- of 0.081). Therefore, the iELISA-rM115 test would have a good diagnostic usefulness for "ruling out the disease", or in this case, ruling out the exposition of an animal to the virus.

The evaluation of the agreement between the reference test and the iELISA-rM115 tests was evaluated using Cohen's Kappa statistic. The distribution of true positives and true negatives displayed by the comparison of the iELISA-rM022 and iELISA-rM115 with the gold-standard were different, but the total agreements observed in both comparisons matched: 288, which made up to 88.03% of the total observations. The number of agreements expected by random guessing was of 53.54%. The Kappa value (κ) was 0.742 with a SE ± 0.043 and a 95% CI of 0.659 to 0.826, indicating a precise estimation of κ, reflecting a substantial agreement between both raters (Landis & Koch, 1977).

Comparative analysis of rabbit sera performance in iELISA-rM022 test based on different vaccination administration routes

The Shapiro-Wilk test indicated non-normality in all groups: NV (W = 0.7575, p value < 0.0001); SC (W = 0.7800, p value < 0.0001); ID (W = 0.9250, p value= 0.014), and the Bartlett test confirmed unequal variances (p < 0.001) (Figure 86). The Kruskal-Wallis test was conducted to compare the distribution of the % ROD in the three datasets. The test results showed a significant difference in % ROD distributions among the NV, SC, and ID groups (H = 138.8, p < 0.0001). Post-hoc analysis using Dunn's test demonstrated highly significant differences between the NV group and the other groups. Specifically, the mean rank difference between NV and SC was -99.61 (p < 0.0001) and between NV and ID was -147.6 (p < 0.0001). Additionally, a significant difference, though to a lesser degree, was observed between the SC and ID groups, with a mean rank difference of -47.97 (p = 0.0015). These findings underscore significant variations in % relative $OD_{450\,nm}$ among the NV, SC, and ID groups.

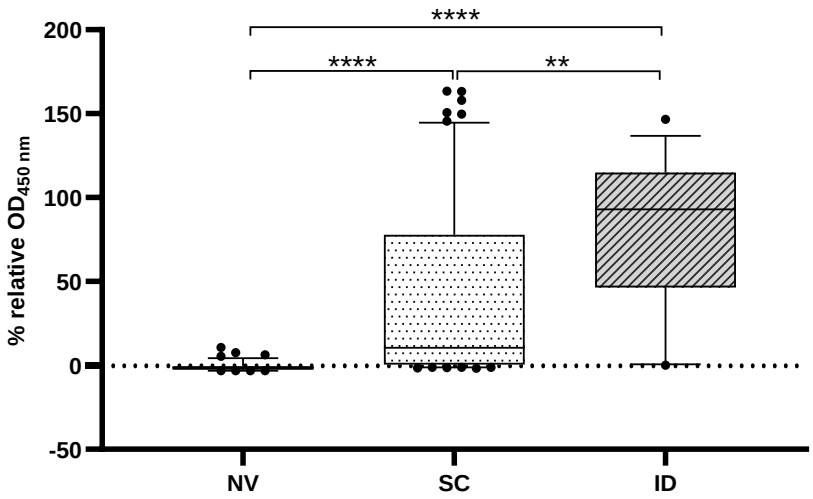

Figure 86. Reactivity (% ROD) of serum samples in iELISA-rM022, grouped by vaccination status: non-vaccinated (NV), subcutaneously vaccinated (SC) and intradermally vaccinated (ID) rabbits.

Differentiation of NV (*n*=89), SC (*n*=132) and ID (*n*=38) sera groups by iELISA-rM115, represented in a box and whiskers plot of the % relative $OD_{450\,nm}$ obtained for each group. The median is represented as a horizontal line within the box, whilst the upper and lower error bar correspond to the 5-95% percentiles, and outliers are represented as empty dots. The dashed line in the plot indicates the -0.559% ROD *cut-off* value for the iELISA-rM115, determined in the ROC analysis.

In the evaluation of the 89 NV serum samples with the iELISA-rM115 test, only 68 samples were accurately classified as negative, which highlighted a significant frequent occurrence of FP samples, with 21 out of the 89 NV samples (23.60%) being incorrectly classified as positive. In

fact, the NV group had the largest contribution in the misclassification rate, constituting over 80% of the total FP detected across the serum panel (Table 20).

All 38 ID samples that were characterized as positive by the reference test, also had positive anti-M115 reactivity in the iELISA-rM115 test, showing 100% agreement.

Finally, the analysis of 132 samples from the SC group with the iELISA-rM115 test revealed 117 samples with positive anti-M115 reactivity. However, 5 of these were FP, representing 20% of the total FPs identified in the serum panel analysed with this test. Of the remaining 15 samples that tested negative, 5 were later identified as FN when compared to the reference test results.

Table 21. Frequency counts of serum samples categorized by the iELISA-rM022 test into negative or positive, based on vaccination routes.

	Negative		***Positive***		***Total***
	True negative	***False negative***	***True Positive***	***False positive***	
Non vaccinated	68	0	0	21	89
Subcutaneous	10	5	112	5	132
Intradermic	0	0	38	0	38
Total	78	5	141	26	259

Correlation between antigen- specific serological reactivity and immune protection

To determine if a certain level of antigen-specific reactivity could predict the outcome of the vaccinated subjects, the study aimed to investigate whether there was a correlation between the iELISA-rM022 and/or iELISA-rM115 test results and an effective protection against MYXV infection. This involved analyzing the serological data outcomes obtained in both tests, in order to identify a certain level of reactivity with good association with higher likelihood of successful immunoprotection.

For this purpose, a total of 34 samples from the 166 sera in PANEL 1 were used, which included serum from animals involved in a vaccination/challenge experimentation. Specifically, 23 of these samples were obtained from rabbits vaccinated SC, 2 from ID vaccinated, and 8 from NV controls. These samples were extracted from these 34 rabbits on the day before they were subjected to a challenge with lethal dose of MYXV strain Gran05/09. The 8 NV rabbits served as

a control group and were needed for representing the natural response to the virus, without any prior immunization.

Correlation between iELISA-rM022 results and immune and survival to challenge

As expected, the NV subjects displayed low % ROD values in the iELISA-rM022 test prior to the virus challenge, and upon infection, they all developed the classic clinical signs of myxomatosis and died. Both rabbits that were ID-vaccinated developed high anti-M022 response prior to challenge and survived the infection with the virulent MYXV. The SC-vaccinated rabbits showed a wide range of immune responses against the M022 antigen, and while 13 rabbits succumbed to the challenge, the remaining 10 survived.

Samples were divided into two categories depending on the outcome of the rabbits subjected to the challenge: survivors (*n*=12) and deceased (*n*=22), or in other words, negative and positive for mortality post-challenge, respectively (Figure 87, A). The representation of the individual % ROD measurements of both groups showed a normal distribution (Shapiro-Wilk test, p value > 0.05), with unequal variances (F test, p value < 0.0001). With a mean %ROD of 39.38 for the survivor group (negative), and a mean of -1.722 %ROD, the groups showed a significant difference between their means of 41.10 ± 10.18.

The anti-M022 antibody levels in the survivor's group were significantly higher than those in the deceased animals, the 95% CI for the difference between means (Negative-Positive) ranged from 18.70 to 63.50 (Welch's t-test, t= 4.038, df= 11.01, p value = 0.002). The η^2 of 0.5969, indicated that nearly 60% of the variance in antibody levels could be attributed to group differences, which is considered a strong although not perfect association between the anti-M022 antibody levels and the outcome upon challenge.

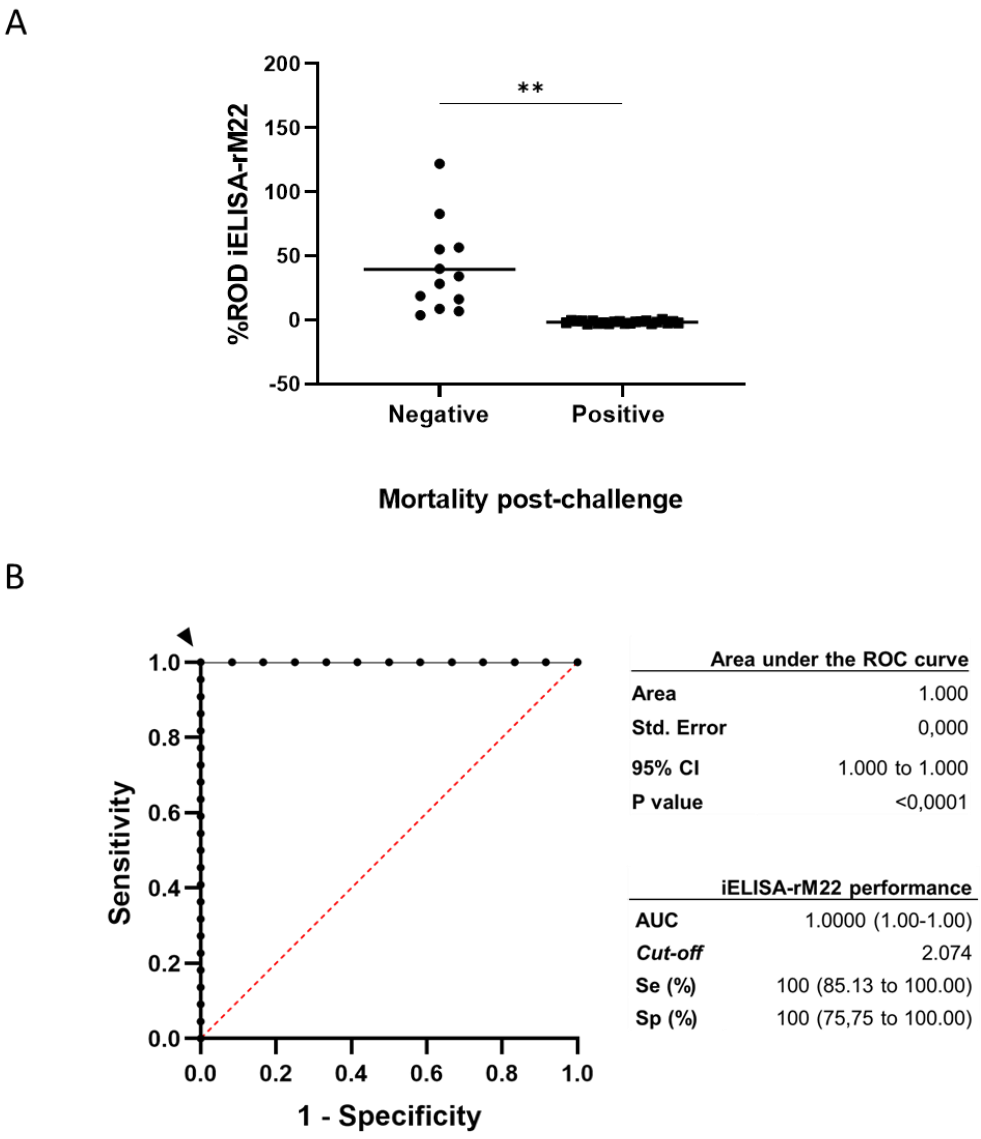

Figure 87. Correlation of anti-M022 antibodies with protection against MYXV challenge.

34 rabbit sera samples were obtained from vaccinated and non-vaccinated animals, one day before challenging them with a virulent MYXV strain. A) Comparison of the anti-M022 reactivity with the iELISA-rM022 test of the samples grouped depending on the outcome of the rabbits to the challenge, into Positive (n=12) and Negative (n=22) for mortality post-challenge. Individual %ROD values from each group were plotted, together with their mean. Statistical analysis was performed using Welch's t-test (p value = 0.002). B) ROC analysis plot showcasing the predictive power of the antibody levels against the MYXV protein represented by the %ROD values obtained with the iELISA-rM022 test analysis, on an effective immune protection. The plot displays the Se (Y axis) and 1- Sp (X axis) paired values for each decision threshold value. The black arrow points out the cut-off value that maximizes the Youden's Index: 2.074 %ROD.

Besides finding a statistically significant difference between the two groups, a ROC analysis was used to evaluate how well the anti-M022 response, corresponding to antibody levels, can predict the outcome of the animal upon challenge with a virus. For that, the % ROD values of these 34 sera samples, and the outcomes of those rabbits were used for the construction of the ROC curve (Panel B, Figure 87). The AUC reached its maximum value of 1, indicating the

diagnostic test model showed perfect discrimination between the two groups. Indeed, the maximization of the Youden's Index found the threshold at which the test achieved 100% DSe and 100% DSp, simultaneously: 2.074 % ROD. This value corresponded to the plot coordinates X (1-Sp) = 0, Y (Se) = 1. Every positive test result, that is, showing higher values than the cut-off (2.074 % ROD) corresponds to a true positive, defined by the when the rabbit serum reactivity to M022, measured in the iELISA-rM022 is higher than 2.074 % ROD.

Correlation between iELISA-rM022 results and immune and survival to challenge

Two out of 8 of the NV rabbits showed a positive anti-M115 reactivity in the iELISA-rM115, showing %ROD values slightly higher than the threshold. However, none of the 8 NV survived the challenge. From the two ID-vaccinated rabbits, one showed a strong anti-M115 response, but the other one barely developed anti-M115 reactivity. The SC-vaccinated rabbits, consistent with what was seen for the M022 protein, showed a wide range of intensities regarding the immune responses against the M115 antigen.

The samples were again divided into survivors or Negative for mortality post-challenge (n=12), and deceased or Positive for mortality post-challenge (n=22) (Panel A, Figure…). Neither group's data passed the normality Shapiro-Wilk test (p value = 0.0093 for the Negative, and p value < 0.0001 for the Positive). The sera from rabbits that survived the challenge showed a median of 22.62 %ROD with the iELISA-rM115 test, while in the group of deceased animals, the median was of -0.7112 % ROD. This difference between the groups' % ROD measurements was statistically significant (Mann-Whitney test, p value = 0.0004).

A ROC analysis was also used to evaluate the predictive power of the anti-M115 response, corresponding to antibody levels, in determining the outcome of animals challenged with MYXV. The % ROD values obtained with the iELISA-rM115 for these 34 sera samples, and the outcomes of those rabbits were used for the construction of the ROC curve. In this situation, the animals that survived were categorized as Positive for protection, and the animals that did not survive, were categorized as Negative for protection (Panel B, Figure...). The AUC of 0.8561 indicated an overall good but not perfect performance across all possible thresholds, hence a trade-off between sensitivity and specificity needed to be pursued. The maximization of the Youden's Index found that 0.082 % ROD was the threshold value at which the test had the best balance between DSe and DSp, being 83.33%, and 72.73% respectively. Considering that animals that

survive and display sufficient anti-M115 antibody levels are considered as true positives, the test correctly identifies 83.33% of the rabbits that survived the challenge. This means that some of the survivors (and thus, the protected) did not show iELISA-rM115 results above the threshold. Specifically, 2 out of the 12 rabbits that survived had lower % ROD values. While the test correctly identifies 72.73% of the non-protected animals, which are those who did not survive the challenge and had low levels of anti-M115 reactivity. Although fewer protected animals were incorrectly classified as non-protected (false negatives), there was a higher rate of false positives (Table 21). For instance, 6 rabbits that died showed iELISA-rM115 values above the threshold but did in the end, indicating that the presence of anti-M115 is not sufficient to predict protection.

Table 22. Contingency table showing the performance of the iELISA-rM115 test (in rows) in predicting the protection degree of animals based on their anti-M115 antibody reactivity.

		Protection post-challenge		
		Protected	**Non-protected**	**Total**
iELISA-rM115	**> 0.082 % ROD**	10	6	16
	< 0.082 % ROD	2	16	18
	Total	12	22	34

Note: Frequency counts of samples corresponding to each combination of outcomes are shown.

The test correctly predicted the protection status in 78.79% of the observations analyzed, while 51.24% agreement would be expected by chance. Although the observed agreement could seem high, the Cohen's kappa (κ) of 0.565 (SE ± 0.143) actually reflected a moderate agreement between the test outcomes or power of protection prediction, and the actual protection status. The wide 95% CI of 0.285 to 0.845 showed high variability in the κ estimate, that the true value could eventually describe a range from fair to substantial agreements.

A

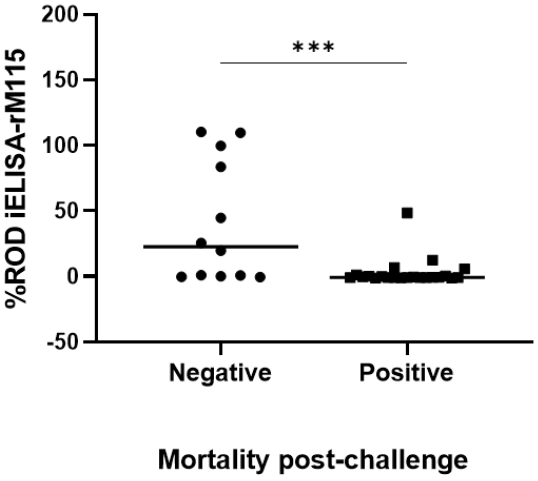

B

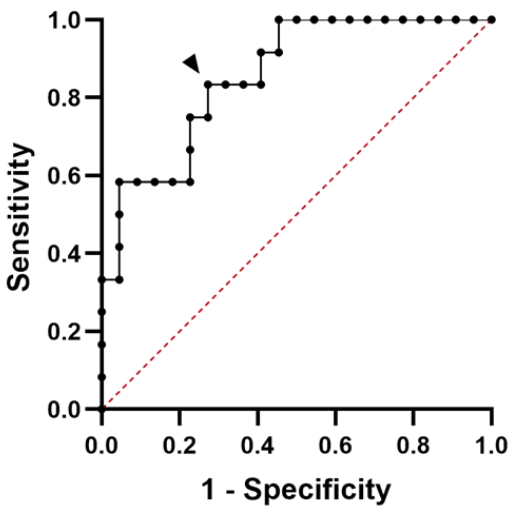

Area under the ROC curve	
Area	0.8561
Std. Error	0,06403
95% CI	0.7306 to 0,9816
P value	0,0007

iELISA-rM115 performance	
AUC	0.8561 (0.7306 to 0.9816)
Cut-off	0.08203
Se (%)	83.33 (55.20 to 97,04)
Sp (%)	72.73 (51.85 to 86.85)

Figure 88. Correlation of anti-M115 antibodies with protection against MYXV challenge.

34 sera samples were obtained from vaccinated and non-vaccinated animals, one day before challenging them with a virulent MYXV strain. A) Reactivity with the iELISA-rM115 test of the samples grouped depending on the outcome of the rabbits to the challenge, into Positive (n=12) and Negative (n=22) for mortality post-challenge. Individual %ROD values from each group were plotted, together with their median. Statistical analysis was performed using the Mann-Whitney U test (p value = 0.0004). B) ROC analysis plot showcasing the predictive power of the antibody levels against the MYXV protein represented by the %ROD values obtained with the iELISA-rM115 test analysis, on an effective immune protection. The plot displays the Se (Y axis) and 1- Sp (X axis) paired values for each decision threshold value. The black arrow points out the cut-off value that maximizes the Youden's Index: 0.08203% ROD.

EVALUATION OF HARE SERA IN THE IELISA-RM022 AND IELISA-RM115 TESTS

Due to the recent appearance of ha-MYXV in the Iberian Peninsula, it was of interest to test the differential capacity of the iELISA tests developed along this Doctoral Thesis in detecting anti-MYXV antibodies in hare sera. It was particularly valuable to investigate the possible antigen-specific reactivity of hare sera to the MYXV M022 and M115 antigens. With this in mind, a total of 20 sera samples obtained from wild Iberian hares (*Lepus granatensis*) and provided by the Instituto Nacional de Investigação Agrária e Veterinária (INIAV), in Portugal, were analyzed with the iELISA-rM022 and iELISA-rM115 tests.

First, the 20 hare sera were analyzed by the commercial iELISA and categorized into 9 positives and 11 negatives for the presence of anti-MYXV antibodies. Then, the same 20 hare sera were analyzed in search of M022- and M115-specific reactivity with the iELISA-rM022 and iELISA-rM115 tests, respectively. All 9 samples categorized as positive by the commercial iELISA showed consistent positive results in both tests, showing reactivity towards the M022 and M115 proteins (Panel A, Figure 89). This positive reactivity suggested that all individuals that were exposed to the pathogen (either by a virulent infection or through vaccination), developed antigen-specific antibodies towards M022 and M115. The hare samples that were categorized as negative by the commercial iELISA, consistently displayed very low % ROD in both tests (Panel B, Figure 89). However, two samples had slight anti-M022 reactivity that surpassed threshold for the iELISA-rM022, as opposed to the result obtained from the analysis with iELISA-rM115.

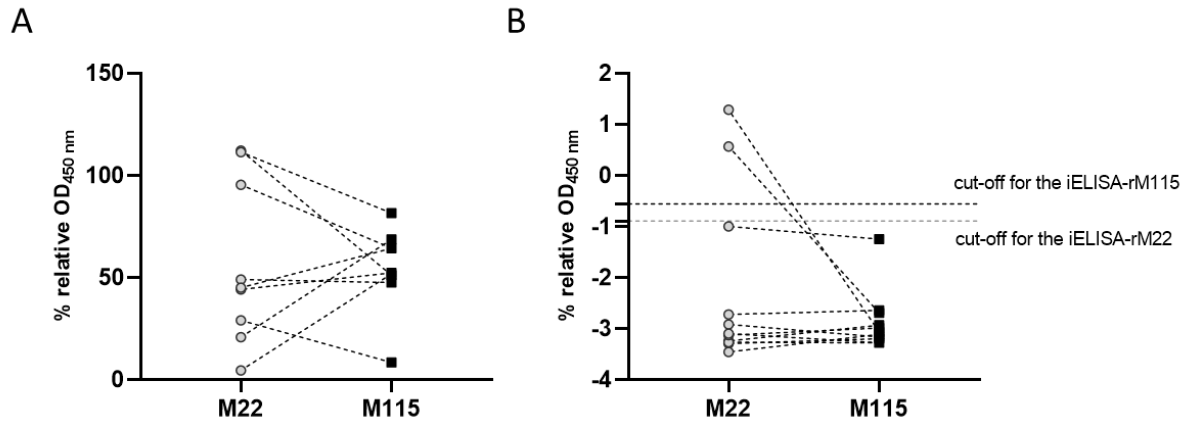

Figure 89. Hare sera reactivity measured to assess the presence of specific antibodies against antigenic MYXV proteins M022 and M115 in the samples categorized as positive (panel A) and negative (panel B) by the reference iELISA test.

The cut-off values determined for the optimization of the iELISA-rM022 test performance is displayed as a grey horizontal dashed line at Y= -0.864 % ROD; the cut-off value determined for the iELISA-rM115 is displayed as a black horizontal dashed line at Y= -0.559 % ROD.

Regarding the non-normal distribution of the %ROD data obtained from the iELISA-rM022 (Shapiro-Wilk test, p value < 0.0001) and iELISA-rM115 (Shapiro-Wilk test, p value = 0.0002), the strength and significance of the relationship between the results obtained from both tests was analysed using Spearman correlation.

The correlation coefficient of 0.847 (approximate p value of 2.52×10^{-6}) indicated a strong and statistically significant positive monotonic relationship between the results of the two tests. This indicated that the results from the two tests change in a consistent way, although not necessarily lineal, relative to each other. For instance, if one test showed higher values, the other did likely the same.

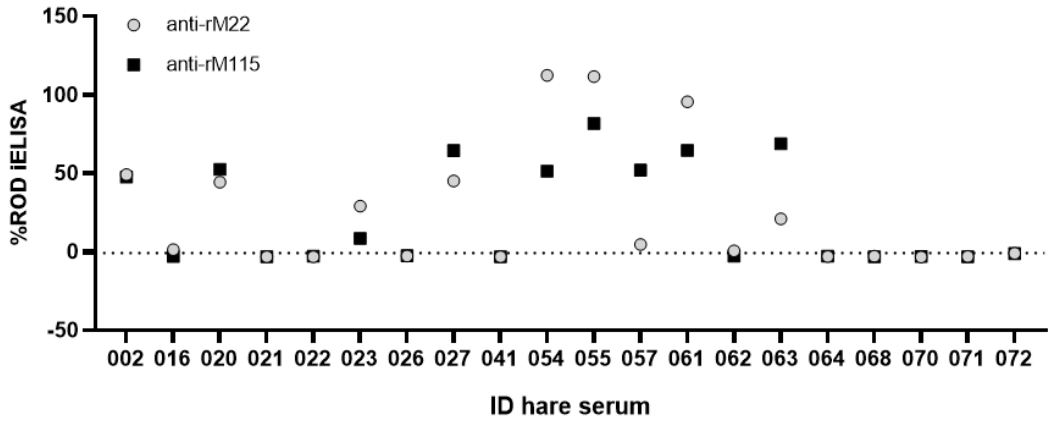

Figure 90. Comparison of the M022 and M115 antigen-specific reactivity (% ROD) of the 20 hare serum analysed with the iELISA tests based on the recombinant proteins.

Reactivity of hare antibodies against rM022 is showed by grey circles and against rM115 is showed by black squares. The dashed lines across the Y-axis represent the *cut off* values for the iELISA-rM022 and -rM115 tests, determined for rabbit sera.

A Bland-Altman plot was generated to analyse the agreement between the measurements obtained with both serologic tests for each hare serum sample (Figure 90). The bias, or mean difference of 1.44, indicated that iELISA-rM022 %ROD values are slightly higher on average than the ones obtained with iELISA-rM115 test. The relative wide 95% upper and lower limits of agreement (ULA, LLA) indicated a substantial variability in the differences between the values obtained with each test across the samples, that the extent of agreement varies significantly from one sample to another.

Data points scattered above and below the mean difference line revealed individual variability in serological responses to the antigenic viral proteins rM022 and rM115, without showing a proportional bias towards either test. The plot underscores the diverse antibody ratios developed against rM022 and rM115, with some samples deviating significantly from the mean, highlighting the importance of considering individual serological patterns in interpreting these tests. For instance, all 11 negative serum samples that were described by low %ROD values, clustered around the mean difference line (blue) in the region close to the origin of coordinates indicating low differences.

Whilst the positive serum samples, with higher average %RODs, also displayed the highest differences, corresponding with more deviation from the mean difference line. Moreover, three of these positive serum samples lied outside the limits of agreement, indicating high disagreements between both test measurements: one of them demonstrated a significantly higher %ROD using the iELISA-rM022 test, while the remaining two samples exhibited the opposite, a higher %RODs with the iELISA-rM115 test. Although difference of serum %RODs increased (Y-axis) and deviated from the mean line as the mean of the values obtained for the same sample increased (X-axis), there was not an evident trend indicating a bias towards either of the iELISA tests (Figure 91). Instead, the highest mean values randomly scattered around the mean difference line highlights the individual variability in serological responses against MYXV, where the ratio of antibodies developed in seropositive animals against each of the two antigenic viral proteins (rM022 and rM115) is not always equal.

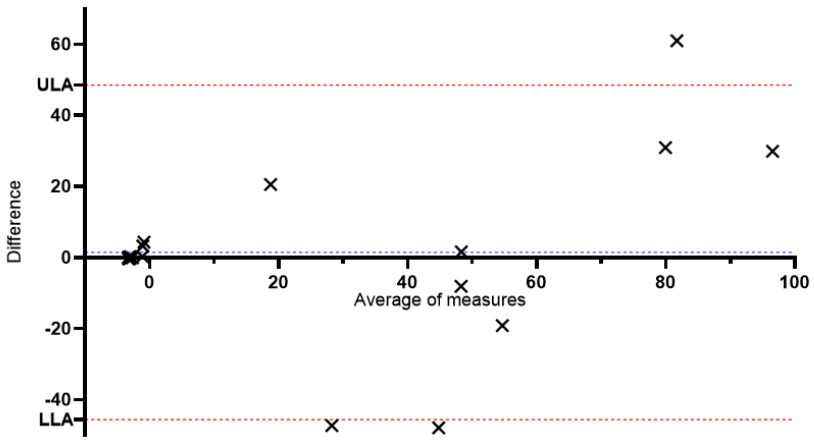

Figure 91. Bland-Altman plot illustrating the level of agreement between iELISA-rM022 and –M115 tests across a range of hare serum samples.

The Y-axis represents the differences in %RODs between the two tests, while the X-axis shows the mean %ROD of each sample as measured by both tests. The central blue dashed line at Y = 1.44 indicates the average difference between the tests (mean difference line). The red dashed lines denote the upper (ULA) and lower limits (LLA) of agreement, calculated by the mean difference ± 1.96 SD.

EVALUATION OF DISCORDANT RABBIT SERA SAMPLES IN INDIRECT IMMUNOFLUORESCENCE TITRATION

A subset of rabbit sera tested in the 3 iELISA tests, that were previously categorized as positive or negative by the commercial (reference) ELISA, were selected and analyzed using a different serologic technique. In this case, they were titrated by indirect immunofluorescence test (IFT). Results are displayed in Table 22. Of the 17 rabbit sera selected for IFT: 4 were obtained from SC vaccinated animals, 10 from ID vaccinated animals and 3 from NV rabbits. The samples were assigned specific codes (IDs) for easier identification. Each code reflects the vaccination route or immune status, followed by a sequential number.

Sera samples were selected for having discordant iELISAs result profiles: positive outcomes in iELISA-rM022, iELISA-rM115 and reference iELISA (ID-1, ID-2, ID-3, SC-1, SC-2, S-3); positive in iELISA-rM022 and reference iELISA tests, but negative in iELISA-rM115 (SC-4, ID-4, ID-5); positives in iELISA-rM115 and reference iELISA tests, but negatives in iELISA-rM022 test (ID-6, ID-7, ID-8, NV-1); negatives in the recombinant protein-based iELISAs but positives in reference iELISA tests (ID-9); or negatives in the reference iELISA test but positives in any recombinant protein-based iELISA test (ID-10, NV-2, NV-3). The seropositive pool used as PC for the iELISA-rM022 and iELISA-rM115, as well as the NC, were also included in the IF titration assay (Figure 92).

The non-specificity of the secondary antibody was accounted for by analyzing it against a monolayer of ha-MYXV-infected cells incubated with PBS in place of serum dilutions. The potential basal fluorescence of each serum was also considered by incubating the lowest dilution (1:8) on the uninfected cell monolayer. In both cases, the background signal was low.

The IFT titration results showed an almost perfect agreement with the outcomes of the reference iELISA test (Cohen's κ value of 0.821±0.171). The uncertainty in the estimate (95% CI from 0.486 to 1.000) may be due to the size of the sample set, since there was only one single disagreement. Sample NV-1 was categorized as (weak) positive by the iELISA test, but no fluorescence was detected in the IFT at the lowest dilution (1:8) (Figure…). This sample also tested positive for anti-M115 reactivity (Table 22). Regarding that it was obtained from non-vaccinated 8-week-old rabbits, the discordant results could be due to the interference with

remaining maternal antibodies, which could more likely be only detected by an iELISA test due to the lower detection limits compared to IFT titration (P. J. Kerr, 1997).

Seropositive rabbit serums ID-4 and ID-7 in the reference iELISA test, had inconsonant results in the iELISA-rM022 and iELISA-rM115 test analysis. Despite ID-4 did not have a positive antigen-specific reactivity against M115 and ID-7 did not have anti-M022, they both displayed a high titer by the IF assay (Figure 92).

Table 23. Serological characterization and comparison of IFAT titers and iELISA results.

SAMPLE ID	IF TITER	REFERENCE IELISA TEST RESULT	%ROD IN IELISA-rM022	%ROD IN IELISA-rM115
ID-1	2048	***POS***	**84.90**	**89.60**
ID-2	2048	***POS***	**94.14**	**6.62**
ID-3	>4096	***POS***	**20.08**	**69.04**
SC-1	>4096	***POS***	**105.49**	**123.73**
SC-2	>4096	***POS***	**5.38**	**98.34**
SC-3	>4096	***POS***	**3.85**	**5.42**
SC-4	>4096	***POS***	**32.29**	-4.18
ID-4	>4096	***POS***	**57.04**	-5.68
ID-5	2048	***POS***	**1.81**	-6.27
ID-6	2048	***POS***	-4.35	**51.67**
ID-7	2048	***POS***	-2.94	**84.63**
ID-8	1024	***POS***	-2.92	**0.67**
ID-9	1024	***POS***	-4.67	-7.01
ID-10	0	*NEG*	-4.47	**8.13**
NV-1	0	***POS***	-5.63	**23.63**
NV-2	0	*NEG*	-7.78	**10.70**
NV-3	0	*NEG*	-7.20	-3.12
PC	>4096	***POS***	**100**	**100**
NC	0	*NEG*	0	0

Results in bold indicate a positive outcome in the corresponding serologic diagnosis test

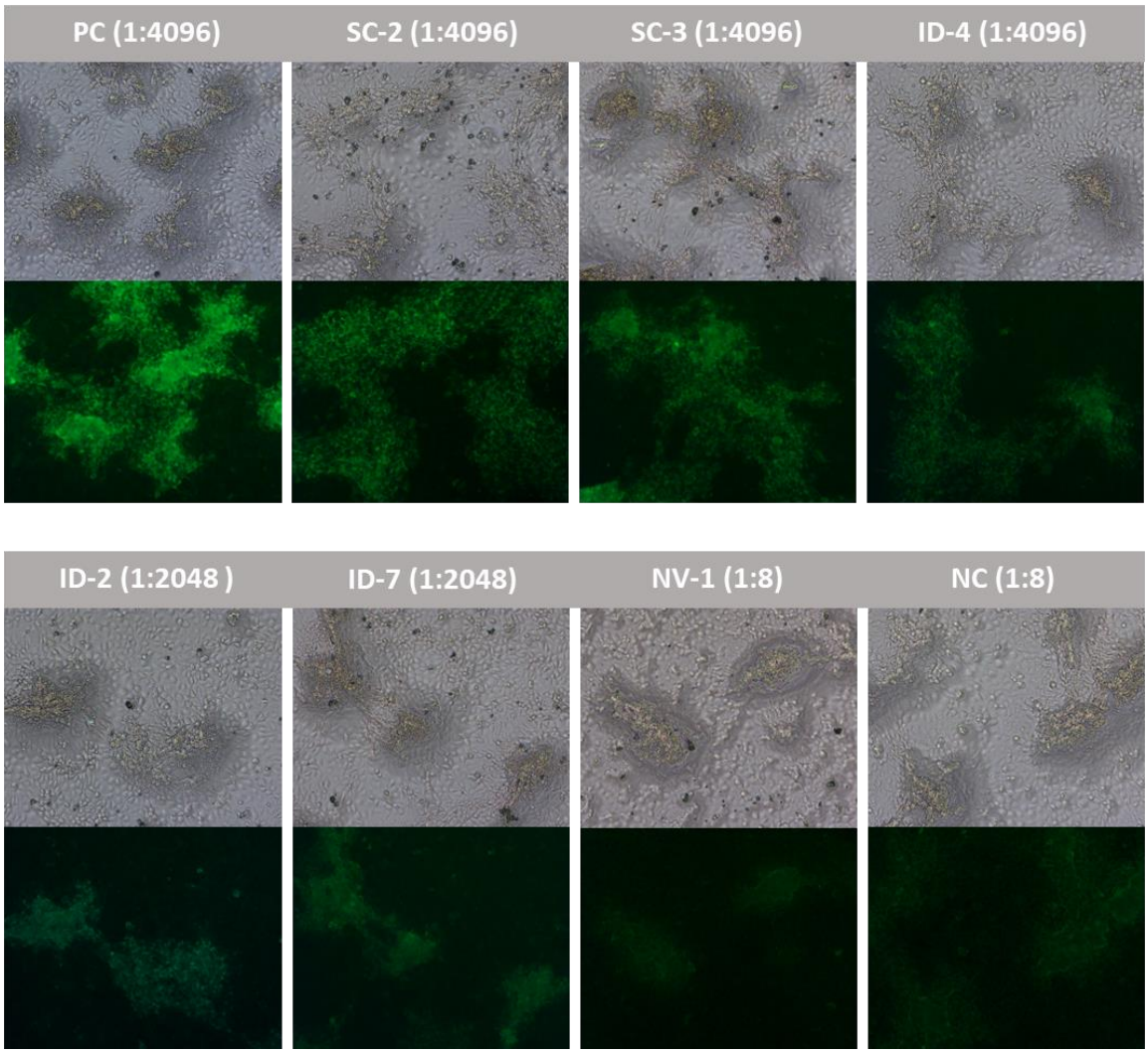

Figure 92. Immunofluorescence titration results using a subset of discordant rabbit sera.

RK13 cultures infected at a MOI of 0.001 ha-MYXV were fixed at 72 hpi. Rabbit sera samples were titrated in 2-fold serial dilutions, from 1/8 to 1/40. The secondary antibody (anti-rabbit IgG, whole molecule) was labelled with FITC. Brightfield microscopy images and the corresponding fluorescence image, indicating the last dilution with positive and specific fluorescent reactivity in both replicates, are displayed at 100X. Six of the discordant rabbit sera are shown, together with the PC and NC.

CHAPTER 7: CONSTRUCTION AND CHARACTERIZATION OF ATTENUATED MARKED MYXV

GENERATION OF RECOMBINANT MYXV KNOCKOUTS

Transient dominant selection of recombinant MYXV produced by homologous recombination

The generation of recombinant virus through homologous recombination using the transfer vectors pΔM071*dTmt* and pΔM115*dTmt* demonstrated low recombination yield results, as was evidenced by the scarce production of fluorescent progeny foci. This failure indicated the suboptimal design of the process and suggested the implementation of adjustments to the selection system to enhance the efficiency of recombinant virus production and recovery.

Transient dominant selection (TDS) is a strategy that benefits from the presence of a dominant selection marker that will not be stably integrated into the viral genome, cloned in a plasmid under the control of a poxvirus promoter (Falknert & Moss, 1990; Scheiflinger et al., 1998). A plasmid designed for each deletion of *m022l, m071l* and *m115l* ORFs from MYXV by TDS was constructed using the plasmid pHiFi3 (*generated in the lab by Dr. Dalton*) as the generic transfer vector for recombinant MYXV generation (See vector description in materials' section). The vector includes three different selectable markers controlled by strong poxvirus promoters: *gusA* and *eGFP* genes, under the synthetic pE/L promoter, and the *E.coli gpt* gene, under the $p_{7.5}$ promoter (Chakrabarti et al., 1997). Each marker gene is surrounded by spacer regions designed to contain multiple cloning sites (MCS) for subsequent cloning strategies.

To produce recombinant viruses, RK13 cells were infected with the parental Vac-MYXV strain at a MOI of 0.2, and 2 h later viral inoculum was removed. Cells were then transfected with 0.5 µg of the corresponding transfer plasmids (pHiFiΔM022*gfp*, pHiFiΔM071*tdTmt* or pHiFiΔM115*gfp*) using Lipofectamine 2000 (Invitrogen) according to manufacturer's instructions. Following an overnight incubation at 37°C in a 5% CO_2 atmosphere, GPT selection media was added to the cell cultures (Falknert & Moss, 1988). The GPT selection media's composition consisted of 25 µg/ml mycophenolic acid (MPA) (Millipore®) and aminopterin solution (Millipore®), containing 250 µg/ml xanthine, 15 µg/ml hypoxanthine, 2 µg/ml aminopterin, and 10 µg/ml thymidine in complete DMEM supplemented with 2.5% FBS.

In cells that had simultaneously suffered both events of transfection and infection, a single and infrequent crossover event between one of the two flanking regions from the transfer vector, and the parental MYXV genome, led in the integration of the circular plasmid into the corresponding homologous region of the viral genome. The recombinant progeny produced as a result of this event carry the selection marker genes *gpt,* along with the fluorescence reporter

gene (either *gfp* or *tdTomato*) and *GUS,* in addition to the corresponding target ORF (Figure 94). Consequently, only those recombinant viruses would successfully complete their infection cycle when subjected to the selective pressure of MPA in the culture media. The expression of GPT exclusively by the single cross-over recombinant viruses provide substantial enrichment of these genotypes over the parental virus (Figure…).

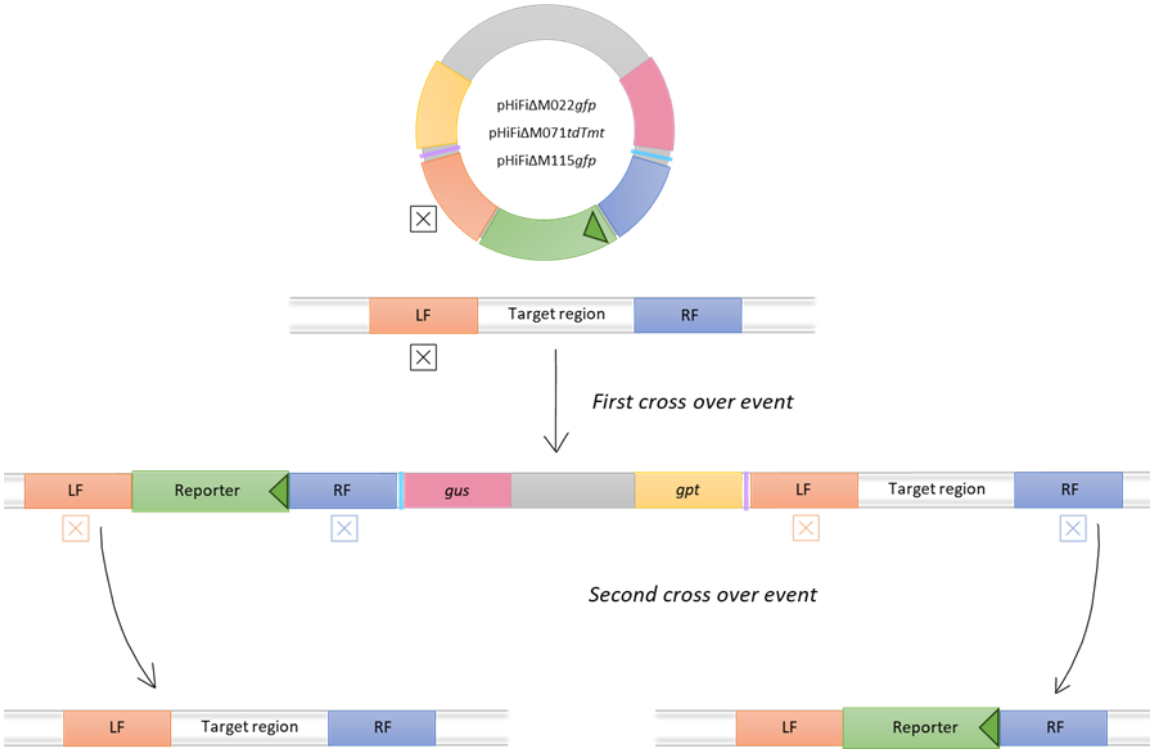

Figure 93. Schematic outline of homologous recombination events for the generation of recombinant myxoma viruses using transient dominant selection (TDS).

The circular plasmid contains the reporter genes *gfp* or *tdTomato* and ~500 bp left (LF) and right (RF) flanking sequences of the ORFs to be deleted: *m022l, m071l* or *m115l*. First, a single crossover event results in the integration of the full-length plasmid into the parental genome in one of the two flanking homologous regions (LF or RF). This provides MPA-resistance to the viral progeny that incorporates the modified genome sequence, allowing the selection of this phenotype. In the next step a subsequent crossover event occurs, resulting in the creation of either the parental MYXV, or the targeted deletion recombinant virus (MYXV-ΔM022*gfp,* MYXV-ΔM71*tdTmt,* MYXV-ΔM115*gfp*) in which the reporter gene takes the place of the deleted viral ORF (*m022l, m071l* or *m115l*). The recombination events are marked with different colors indicating the specific region involved in the crossover event.

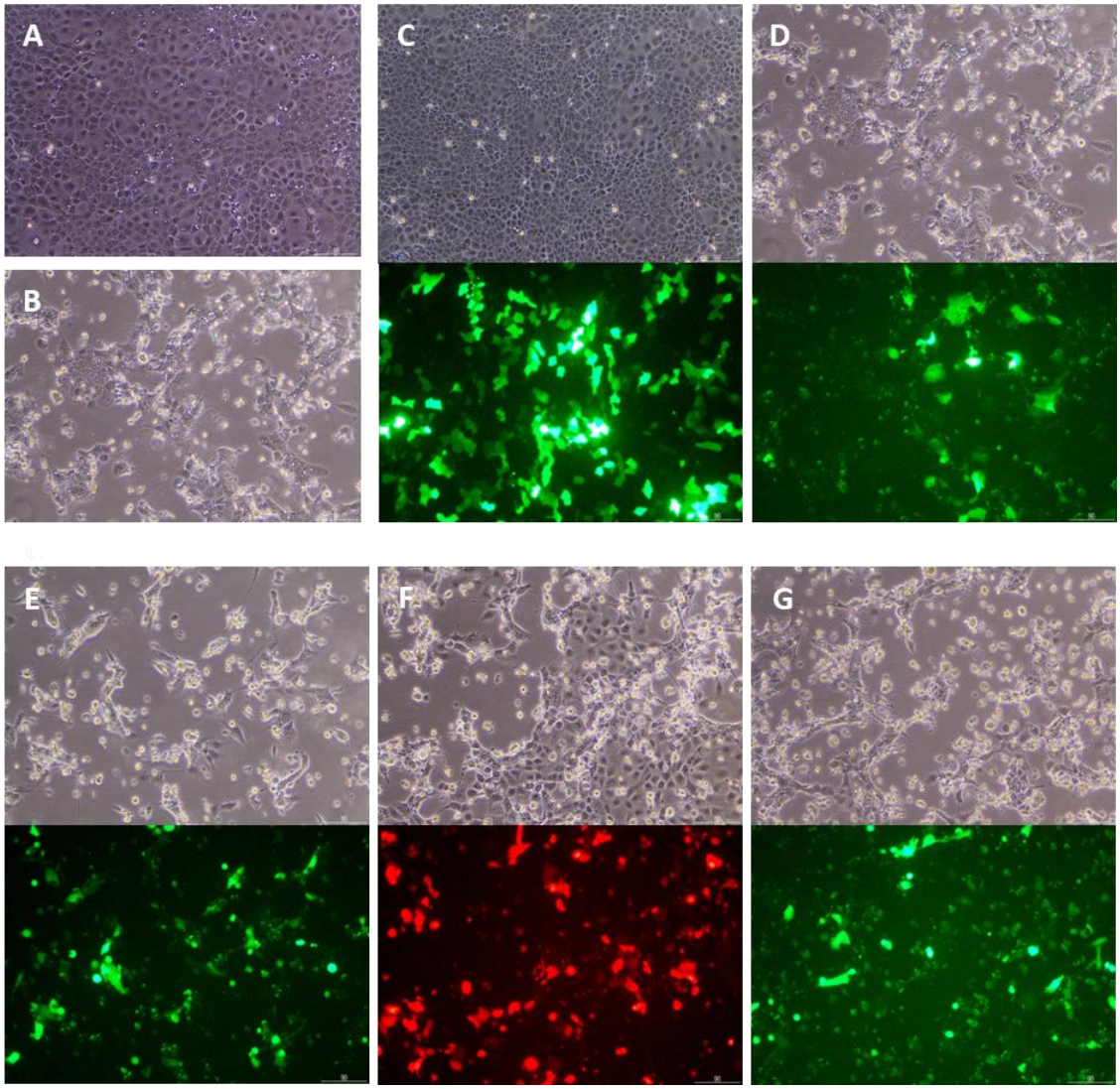

Figure 94. Generation of recombinant Vac-MYXV.

(A) RK13 mock-infected cells, (B) RK13 cells infected with Vac-MYXV at MOI 0.2, (C) RK13 transfected with pcDNA-eGFP, (D) RK13 first infected at MOI 0.2 with Vac-MYXV and then transfected with pcDNA-eGFP. In the lower 6 panels RK13 cells co-infected / transfected with the following transfer vectors are show (E) pHiFiΔM022*gfp*, (F) pHiFiΔM071*Tmt*, and (G) pHiFiΔM115*gfp*, Images were obtained 72-hour post infection. Brightfield and the corresponding relevant fluorescent images of eGFP or dTmt are shown.

Selection and isolation of the desired recombinant Vac-MYXV (Vac-ΔM022gfp, Vac-ΔM71tdTmt, Vac-ΔM115gfp)

Using the *gpt* gene as a transient selectable marker, recombinant viruses were first selected for resistance to mycophenolic acid (MPA). Given the rarity of spontaneous MPA-resistant mutations, only viruses that successfully incorporate the vector through homologous DNA crossovers can replicate and form plaques (Broder & Earl, 1999). Viral progeny was harvested after an additional incubation of 72h in selection media (P_0) (Figure 94, E, F, G). For that, the

infected-transfected RK13 cultures were collected and freeze-thawed 3 consecutive times to disrupt the integrity of cell membranes.

The recombinant viruses within the viral progeny, released from inside the harvested cells, were amplified through a subsequent round of MPA selection in RK13 cells cultured in liquid selection medium (P_1) (Figure 95, A). This was followed by one additional round of foci isolation under this selection pressure (P_2), where RK13 monolayers were infected in duplicate with aliquots of serial dilutions prepared by the amplified P_1 viral stock (10^{-2}, 10^{-3}, 10^{-4}), overlayed with sterile 1.5%-low-melting point agarose in MEM supplemented with GPT selection media (Figure 95, B).

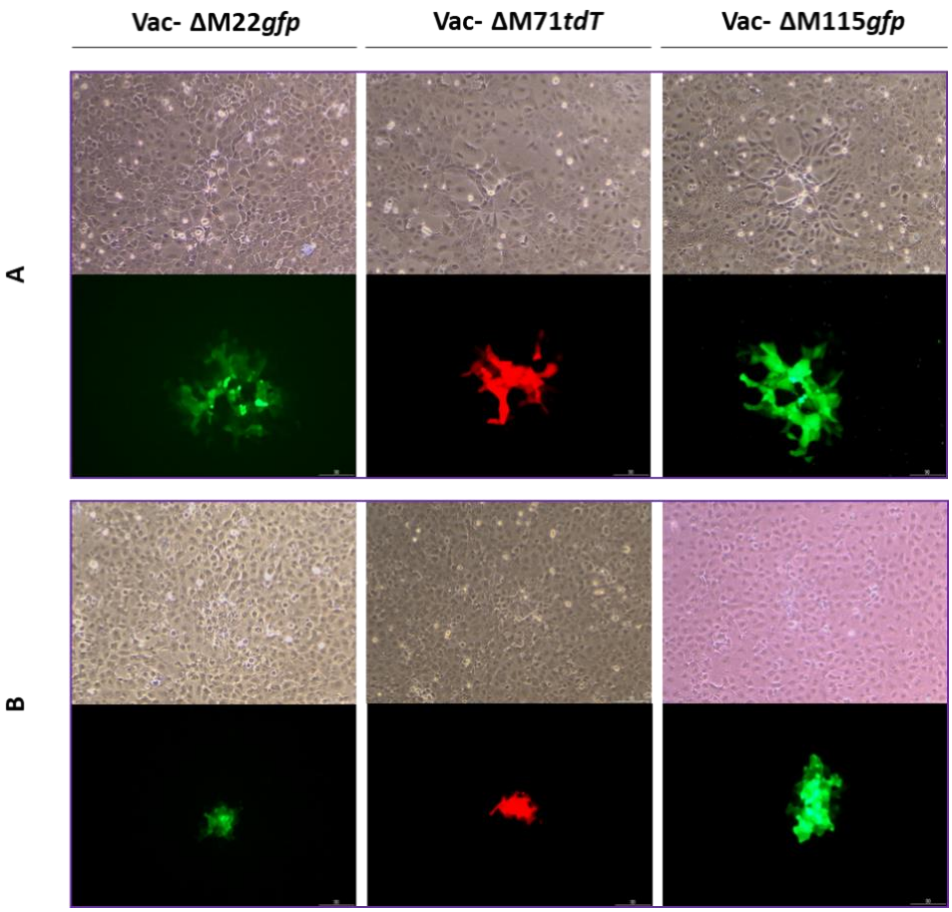

Figure 95. MPA selection for recombinant Vac-MYXVs.

A) Amplification of recombinant Vac-ΔM022*gfp*, Vac-ΔM71*tdTmt*, Vac-ΔM115*gfp* progeny in liquid selection medium (P_1 samples), at 96 hpi. B) Focus forming assay of P_1 samples of all recombinants under agarose overlay selection media, 48 hpi (for Vac-ΔM022*gfp*, Vac-ΔM71*tdTmt*) and 96 hpi (for Vac-ΔM115*gfp*). Fluorescent foci are selected as P_2. Brightfield and fluorescent images of single isolated virus foci are shown.

During the infection of susceptible cells under a semi-solid agarose overlay, each productively infected cell gave rise to an infected area on the monolayer known as viral focus, as a result of cell-to-cell transmission. The dilutions aided in the estimation of the recombinant viral titer as

well as increasing the chance of obtaining well-separated viral foci: 2,45 × 10^3 FFU/ml for Vac-ΔM022gfp, 3 × 10^4 FFU/ml for Vac-ΔM71*tdTmt*, and 3,5 × 10^4 FFU/ml for Vac-ΔM115*gfp*.

Each viral focus originated from a single MPA-resistant virus particle, therefore collection of cells from one individual focus allowed the isolation of pure recombinant MYXV clones. A sterile pipet tip was used to remove infected cells from the foci and placed in culture medium supplemented with 2.5% FBS. Viral clones were vortexed briefly and released by freeze-thaw cycling and sonication in ice-water. Then, each isolate was amplified on fresh RK13 monolayers without MPA-selection pressure (DMEM-2.5%FBS).

As long as selective pressure is maintained, foci harboring the virus with the selectable marker genes could be consistently isolated. However, the configuration of the selectable markers (*gpt* and *GUS*), between two direct repeats, predisposes them to being lost by a second crossover event upon removal of selection, given the high frequency of intramolecular recombination in cells infected by poxviruses (e.g. VACV)(Ball, 1987). This second cross-over recombination can lead to two different outcomes, each with approximately 50% likelihood of occurring (Figure 93): either the original DNA segment is preserved, and the vector is expelled, leading to a return to the parental DNA sequence; or the desired recombinant is obtained, resulting in the loss of both the selection marker genes and the targeted DNA sequence (Falknert & Moss, 1990).

Recombinant clones that were amplified without selective media, maintained the fluorescent marker gene, and were further identified by focus fluorescence, in contrast to the fluorescent-less foci produced by the parental MYXV phenotype (Figure 96, Images A, B, C, J). Recombinant MYXV clones were purified by additional three rounds of single focus selection and screening, until all isolates yielded exclusively recombinant progeny.

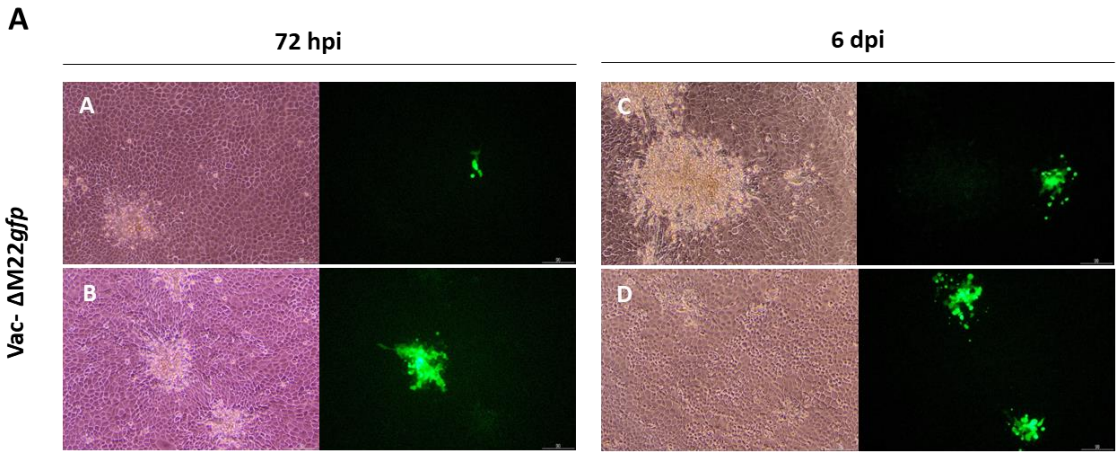

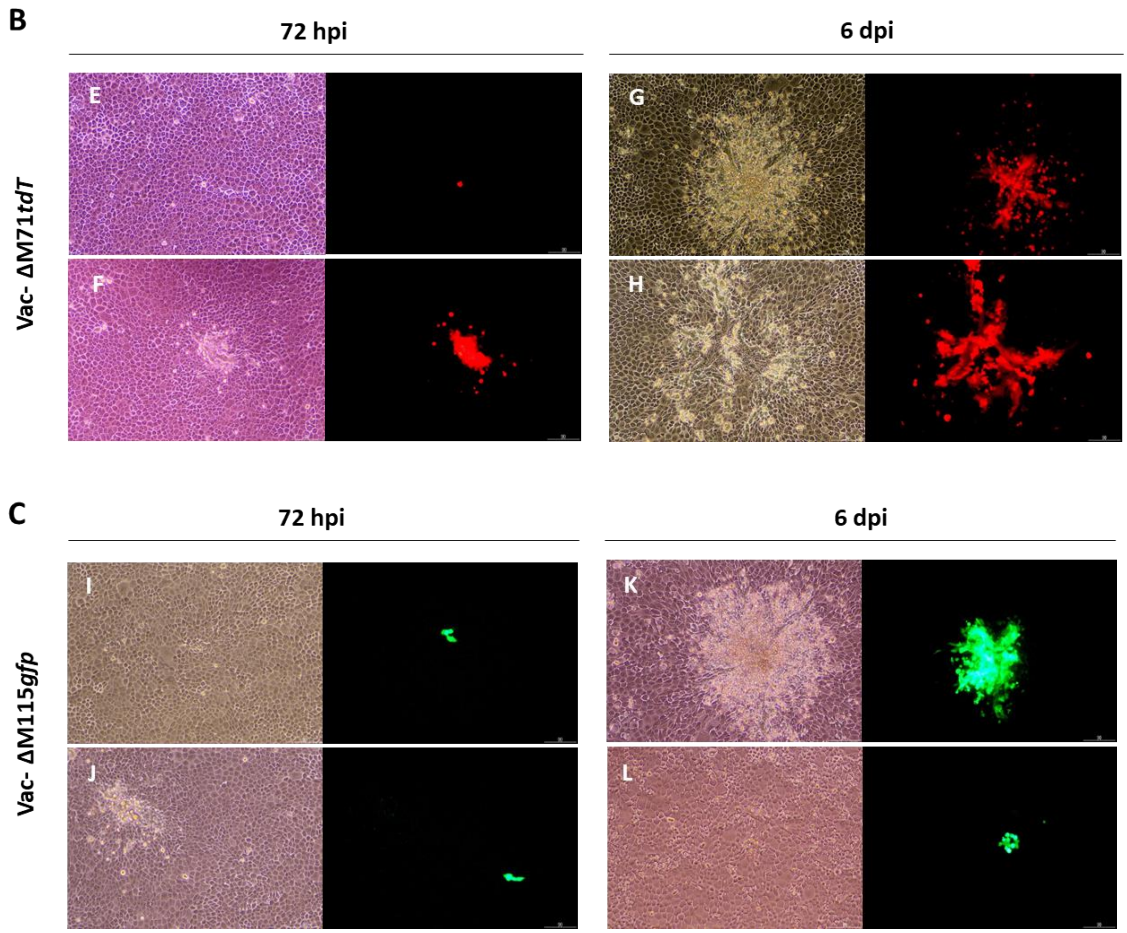

Figure 96. Screening of recombinant Vac-MYXVs amplified in cell culture without selective media.

(A) Vac-ΔM022*gfp,* (B) Vac-ΔM71*tdTmt*, (C) and Vac-ΔM115*gfp.* Brightfield and fluorescent images of virus foci formed at 72 hpi and 6 dpi are displayed for each MYXV mutant. The three different outcomes for the viral progeny following homologous recombination and elimination of selective media are displayed in the set of images from each panel (images A to L): wild-type virus resulting from the reversion of the first cross-over event forming foci with no fluorescence; progeny with insertion, resulting from a single cross-over event, displaying fluorescence without the corresponding gene deletion, and the recombinant Vac-MYXV mutant that results from the second cross-over event, displaying fluorescence and unable to form viral foci until 6 dpi.

Generation of recombinant knockouts in Lu-MYXV

Deleting the specific genes (*m022l* and *m115l)* that encode antigenic viral proteins in a virulent strain (Lu-MYXV) was proposed as a supplementary study to provide a comprehensive understanding of the potential role of these genes in viral attenuation. Since neither of these mutations were previously characterized for MYXV, this was seen as a relevant gap to be filled.

Only the mutant lacking the *m022l* gene was generated (Figure 97). Due to time and technical constraints, it was prioritized to create only one of the two recombinant Lu-MYXV strains. The

same protocol that was used for the generation of Vac-MYXV mutants, was applied in this occasion, resulting in a straightforward process that led to a high titer stock of Lu-ΔM022*gfp.*

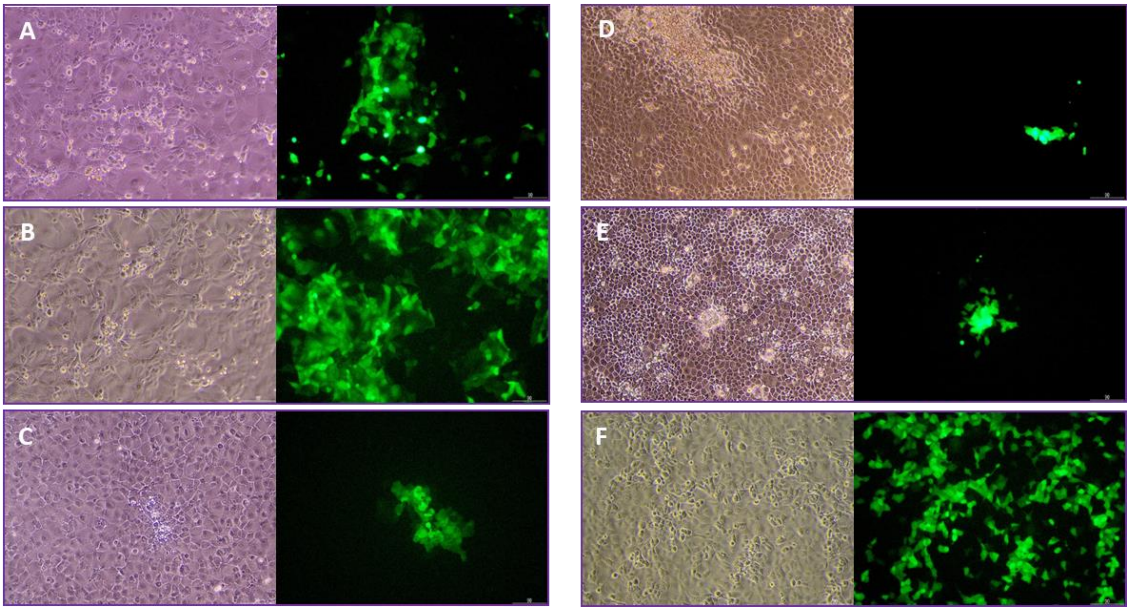

Figure 97. Comprehensive overview of the recombinant Lu-ΔM022gfp mutant generation process.

A) RK13 infected at MOI 0.2 with Lu-MYXV and transfected with the pHiFiΔM022gfp vector, 72 hpi. B) Amplification of recombinant MYXV progeny in liquid selection medium (P_1 samples), 96 hpi. C) Focus forming assay of P_1 samples for selection of the recombinant virus under agarose overlay selection media, 72 hpi. D) Amplification of the progeny without selective media, 72 hpi. E) Purification of Lu-ΔM022gfp mutants, and F) Amplification of the viral Lu-ΔM022gfp stock. Brightfield and fluorescence microscopy images are shown.

Screening and stock amplification of the recombinant MYXV isolates

The purity of recombinant viruses was verified through PCR analysis and subsequently confirmed by DNA sequencing (Broder & Earl, 1999). First, each isolate was amplified on RK13 monolayers until an evident cytopathic effect was noted, then cells were harvested and lysed, and processed for DNA extraction using the QIAamp® DNA mini kit as described in the Materials and Methods section.

The loci of the targeted MYXV genes that were deleted for the generation of the mutant virus (*m022l* and *m115l*) were studied by PCR using two amplification strategies. First, a PCR reaction was designed for the differential amplification of a 890 bp fragment using a forward primer flanking the corresponding ORFs (see Materials and Methods). The viral genome of the mutant recombinants Lu-ΔM022*gfp,* Lu-ΔM022*gfp,* and Vac-ΔM115*gfp* generated the corresponding ~900 bp amplicon, whereas the parental genome of both Lu-MYXV and Vac-MYXV did not yield any PCR product due to the reverse primer's inability to hybridize with the DNA template (Figure

98, A). The second PCR reaction was performed to compare the *m022l* and *m115l* locus between the mutant virus and their parental genomes (Figure 97, B). Amplicons generated from the deletion mutants showed different size than their corresponding parental genomes. For the *m022l* locus, the parental Lu- and Vac-MYXV showed higher molecular size of the amplified fragment than their corresponding ΔM022 mutants, given that the *m022l* gene is larger than the *gfp* gene. Opposite results were found in the *m115l* locus, since the viral gene is around 160 nucleotides shorter than the *gfp* gene.

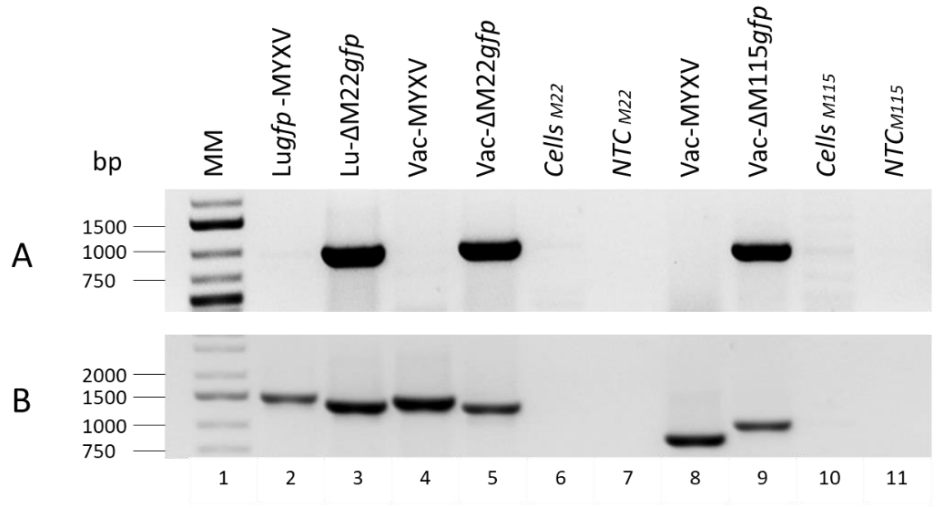

Figure 98. PCR analysis design for ΔM022gfp and ΔM115gfp mutants' screening.

A) Amplification products using primers that hybridized in a region 5' upstream the target gene, and within the *gfp* gene. B) Amplification of the *m022l* locus (lanes 2-7) or the *m115l* locus (lanes 8-11). A negative control of amplification consisting of genomic DNA of uninfected RK13 cells (lanes 6 and 10) was added, as well as a no-template control of the reaction (lanes 7 and 11).

Once it was demonstrated that recombinant viruses were pure, hence free of parental virus DNA by PCR analysis, the amplicons were sequenced to confirm the recombinant constructs, as described in the section Materials and Methods.

A single isolate with the validated expected genomic sequence for each desired MYXV mutant was chosen for further viral amplification. The generation of high titer stocks was achieved by progressively increasing the number of RK13 cells infected in successive rounds until an acceptable titer (> 10^6 pfu/ml) was reached (3 amplification rounds for Vac-ΔM115*gfp* and 2 for Vac-ΔM022*gfp* and Lu-ΔM022*gfp*). Final recombinant MYXV isolates were aliquoted and stored at -20°C.

Characterization of MYXV deletion recombinants

The comparison of virus fitness between the deletion mutants and the parental virus stock is essential for the successful characterization of these potential vaccine candidates. Plaque or focus size is often used to determine the capacity of a particular viruses for cell-to-cell spread and acts as a good indicator of viral fitness *in vitro*. For a viral infection to successfully result in virus production, host cells must be susceptible, allowing them to be infected, and permissive, enabling them to support viral replication once the virus is inside. When the infection spreads to adjacent cells, clusters of infected cells are generated. The size of these foci can provide valuable information about several aspects of the viral infection, influenced by the characteristics of the virus itself and its interactions with host cells.

Size of MYXV foci

To study the size and foci dynamics of the mutant MYXV strains, cell cultures in 6-well plates were infected at low MOI (50 to 100 FFU/well) with the parental MYXV strains (Lu and Vac), and the mutants lacking M022 (Lu-ΔM022*gfp* and Vac-ΔM022*gfp*) or M115 (Vac-ΔM115*gfp*) in serum-free DMEM media. Following one hour of incubation, the viral inoculums were removed, DMEM-10 was added to the cells, and plates were incubated at 37°C, 5% CO_2. The diameter and area of randomized virus foci developed in the RK13 monolayers were measured at different time points (24-, 48-, 72-hpi and 6 dpi).

Virus foci formed by the Vac-ΔM022*gfp* and Vac-ΔM115*gfp* recombinants in RK13 cell monolayers were evaluated at different time points and compared with the size of their parental Vac-MYXV, while the foci formed by the Lu- ΔM022*gfp* virus was evaluated and compared with the size of the foci generated during the Lu strain infection. The experiment was performed in duplicate, with one of the replicates for each virus strain being incubated in semi-solid medium containing 1.5% agarose (from now on referred to as semi-solid medium), and the other in DMEM with 5% FBS culture media (from now on referred to as culture medium).

After a six-day incubation period, the RK13 infected cells were fixed with formaldehyde and stained with Crystal violet. The parental MYXV strains, Vac-MYXV and Lu *gfp*-MYXV exhibited large foci, consisting of dense clusters of infected cells that were recognizable for being distinctly stained areas on a background monolayer of non-infected cells (Figure 99). The size of these viral foci was considerably larger in the monolayers incubated in semi-solid medium (panel B) compared to the size of foci formed on the monolayers incubated in culture medium (panel A). Unlike their corresponding parental strains, the virus foci formed by the recombinant strains

Vac-ΔM022*gfp* and Vac-ΔM115*gfp* and Lu- ΔM022*gfp* after 6 days of incubation could not be detected with crystal violet staining.

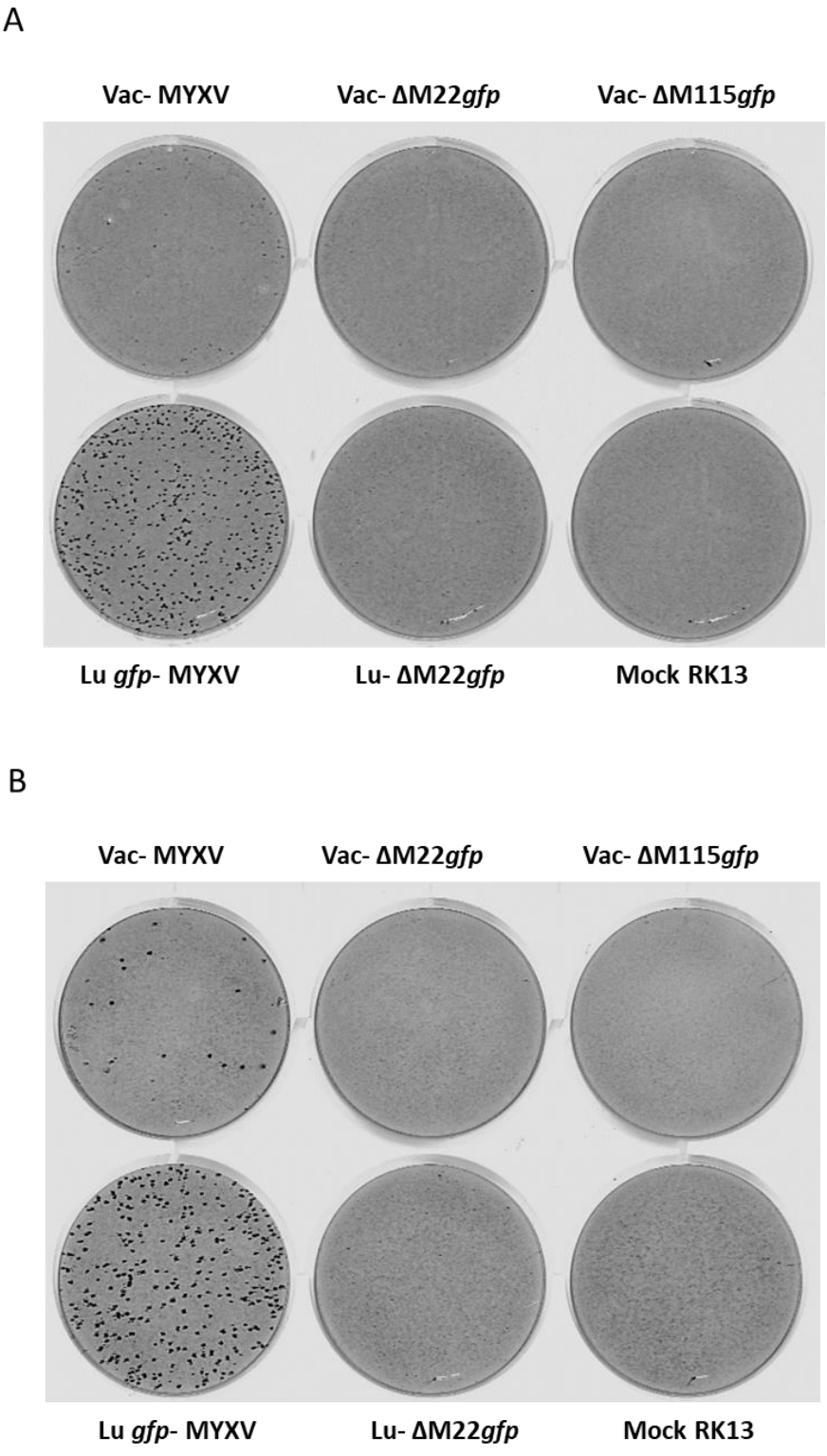

Figure 99. Foci formation by the parental strains (Vac-MYXV and Lu gfp-MYXV) and the deletion MYXV recombinants (Vac-ΔM022gfp, Vac-ΔM115gfp and Lu-ΔM022gfp) on RK13 cell monolayers.

Cells were infected with 50-100 FFU and incubated in liquid medium (complete DMEM, 5% FBS) (A) or in semi-solid medium (MEM-1.5% agarose) (B). The cell monolayers were fixed with formaldehyde and stained with crystal violet 6 days post-infection.

The difference in foci sizes that was determined upon staining the infected monolayers was also quantitatively analyzed by measuring their diameter and area. Randomized measurements of the diameter and area were determined for 6 to 15 representative fluorescent foci in RK13 cultures infected with each of these recombinants at four time points (24 hpi, 48 hpi, 72 hpi and 6 dpi). Infected cells and viral foci were directly identified by detecting the fluorescence emitted by cells infected by the recombinant viruses or the GFP expressing Lu-MYXV strain (Lu *gfp*), using a fluorescence microscope. Since the Vac-MYXV strain lacked a reporter gene that allowed the infection development to be followed, virus foci generated upon Vac-MYXV infection at the different time points were identified through indirect immunofluorescence using seropositive antibodies in a positive anti-MYXV rabbit serum to tag the viral antigens produced during MYXV infection, followed by secondary anti-rabbit IgG conjugated with Alexa Fluor 350.

These area measurements were obtained in arbitrary units (a.u.) and the corresponding comparisons of foci size among the five MYXV strains analyzed (Figure 99). The absence of bars representing the measurements for some of the viruses at 24 hpi was due to the inability to form detectable viral foci. In fact, they were only formed in the cell monolayers infected with the virulent Lu-MYXV, in both culture conditions. For the three deletion recombinant strains (Lu-ΔM022*gfp*, Vac-ΔM022*gfp* and Vac-ΔM115*gfp*) the infection was limited to single cells. For the Vac-MYXV infection in semi-solid medium, where the virus lacked a fluorescent reporter gene, any single infected cell or developing foci were indistinct from the rest of non-infected cells.

All tested MYXV strains displayed smaller area sizes in the cultures incubated in culture medium (panel A, B) compared to those that developed in cultures incubated with a semi-solid medium (panel C, D) (Figure 100). The influence of medium composition on foci's size was more pronounced at late times of infection (72 hpi and 6 dpi) and the largest discordance within these time points were observed for the recombinant viruses Vac-ΔM022*gfp*, Vac-ΔM115*gfp*. In contrast, foci generated from cells infected by the recombinant Lu-ΔM022*gfp* strain showed the smallest difference in area between both culture conditions. The normalization of the area values for the mutants to the measurements obtained for the parental strains (Lu or Vac-MYXV) at each time point showed a significant overall difference in the formation, growth, and resolution of de MYXV deletion mutants, compared to their respective parental strains (Table 23).

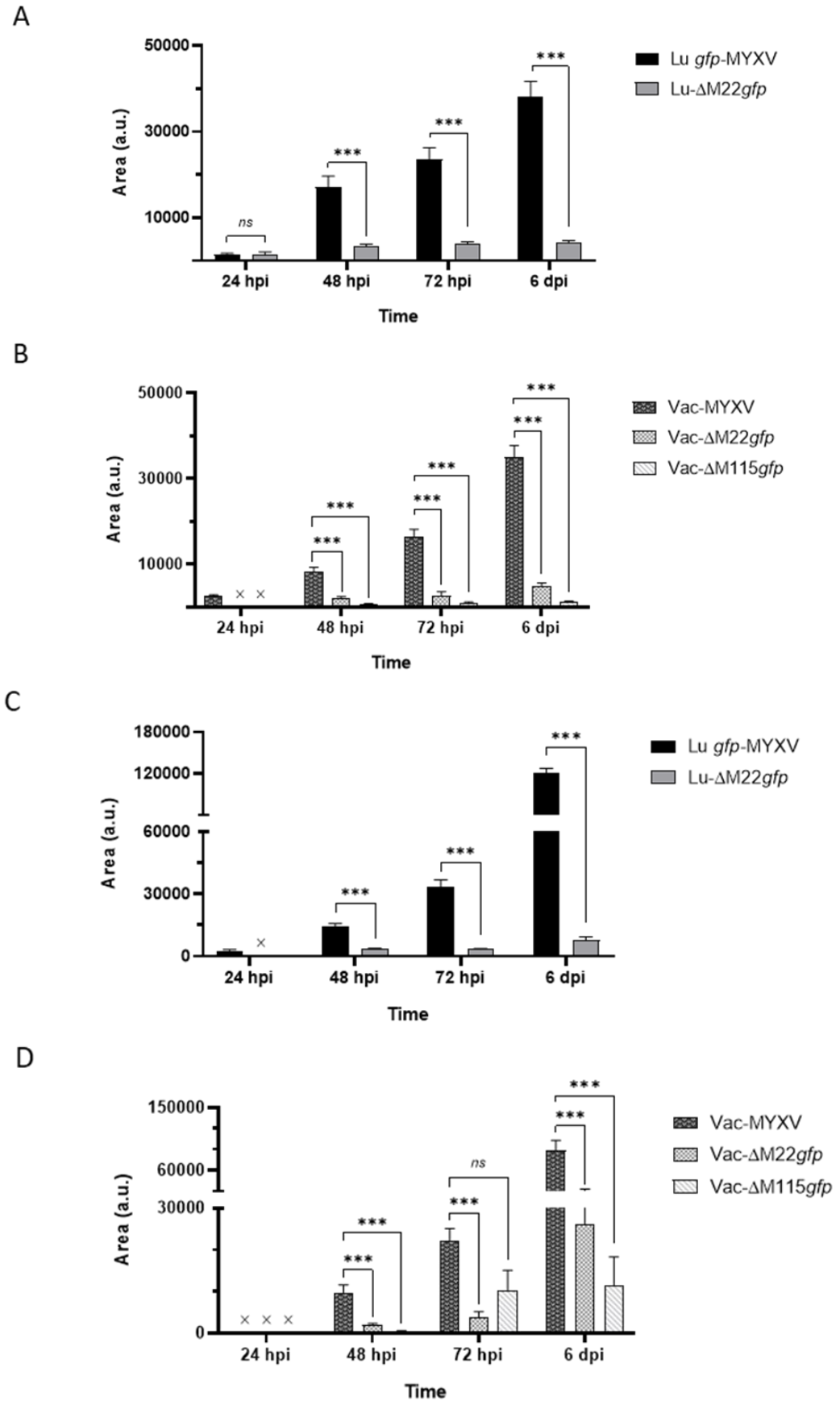

Figure 100. Area measurements of the viral foci developed by different viruses in RK13 monolayers in culture medium (Panels A and B) or in semi-solid overlay (Panels C and D), infected at low MOI.

Measures of foci grown Foci size (area) of the recombinant MYXVs were compared to those of the parental strains: the deletion mutant Lu-ΔM022*gfp* to the Lu *gfp*-MYXV strain (Panels A and C), and the deletion recombinants Vac-ΔM022*gfp* and Vac-ΔM115*gfp* to the Vac-MYXV strain (Panels B and D). The Y-axis represents the foci area, expressed in arbitrary units (a.u.). Data represents the mean ± SEM of the area measured for 6 to 15 randomly selected foci. Non-available area data are indicated by a cross.

The study of foci dynamics for the parental Lu-MYXV virus showed a consistent increase in their size over time, although the expansion rate differed whether the infection was carried out in culture medium (panel A) or semi-solid medium (panel C). The lack of M022 in the mutant virus resulted in a significative reduction in the Lu-ΔM022*gfp* foci measured at all time points, except for the 24 hpi (Panels A and C, Figure 100). The difference in the area of the viral foci became more pronounced as the infection progressed, but also when the infected cultures were incubated with the semi-solid overlay (Table 23).

Table 24. Relative area (in %) of the viral foci generated in RK13 cultures infected with 50-100 f.f.u with the recombinant MYXV strains measured at different time points.

CULTURE MEDIA	*24 HPI*	*48 HPI*	*72 HPI*	*6 DPI*
Lu-ΔM022gfp	102.51 (±77.87)	19.76 (±7.68)	16.11 (±9.07)	10.86 (±5.24)
Vac-ΔM022gfp	*NA*	26.20 (±11.04)	16.23 (±20.48)	14.18 (±7.22)
Vac-ΔM115gfp	*NA*	9.04 (±1.16)	6.39 (±2.84)	3.67 (±1.71)
SEMI-SOLID MEDIA	*24 HPI*	*48 HPI*	*72 HPI*	*6 DPI*
Lu-ΔM022gfp	*NA*	23.74 (±10.09)	9.78 (±4.31)	6.46 (±3.48)
Vac-ΔM022gfp	*NA*	21.01 (±8.91)	17.00 (±23.33)	29.45 (±28.10)
Vac-ΔM115gfp	*NA*	5.21 (±1.70)	45.72 (±62.31)	12.88 (±23.80)

Note: NA are not available values. Area measurements of the recombinant strains are expressed as a percentage of the area size determined at each time point, for their respective parental MYXV strain. Mean (±SD) are shown in %.

The Vac-MYXV strain showed a similar pattern of foci dynamics than the virulent Lu-MYXV, with slightly smaller foci size, not significative in all the time points with the exception of 72 hpi in the infections in culture media (p value of 0.0974), indicating a slower ability for initial propagation than Lu-MYXV. According to what was discerned for the virulent strain, the lack of M022 had a detrimental effect on the fitness of the virus, affecting foci development and propagation regardless of the virus that was used as parental strain. The multiple t-test demonstrated a statistical significance in all the time points (panel B and D, Figure 100). This restriction appeared to be less severe for Vac-ΔM022*gfp* when the mutation was performed in the vaccine background. As a matter of fact, infection with this mutant under a semi-solid overlay resulted in higher relative areas indicating that the Vac-ΔM022*gfp* virus was coping better with the limiting effects of M022 loss when the virions had a restricted spread within the media (Table 23).

The M115 knockout mutation on the Vac-MYXV strain compromised their foci development in culture medium to an even greater extent than the lack of M022 did. The outcome in the t-test analysis confirmed significant differences between the parental Vac-MYXV and the ΔM115 mutant strain at all time points considered (Panel B, Figure 100). The foci size of Vac-ΔM115*gfp* foci's relative area (%) diminished as the infection progressed, down to only 3.67% at 6 dpi (Table 23). The growth dynamics pattern of viral foci developed in cells incubated in the semi-solid medium at 48 hpi showed a significant difference to the parental Vac-MYXV, but at later stages of infection, Vac-ΔM115*gfp'*s foci experienced a sudden size expansion, which was inconsistent with the earlier results observed for infections in culture medium. Notably, the foci area difference outcome of this expansion was non-significant at 72 hpi, whereas despite the larger foci area sizes at 6 dpi, the t-test yielded significant differences at this point (Panel D Figure 100).

Besides the different range of the area measurements, Lu-ΔM022*gfp* constructed in a virulent genomic background displayed the same behavior in both incubation conditions (upper panel in A and B), showing an increasing difference of its relative foci area compared to the Lu-MYXV, with the increase of the incubation times. This suggested that the results obtained are due to the absence of M022 protein, compared to the parental Lu *gfp*-MYXV strain. In turn, deletion of M022 had a similar impact over the dynamics of foci generated on the genetic background of the vaccine strain (Vac-MYXV), in cultures incubated in liquid medium. In this same regard, the absence of M115 had an even more severe impact on the development of viral foci for Vac-ΔM115*gfp*, since the relative area observed for this strain did not even reach 10% compared to its parental area (panel A, Figure 100). These two recombinants, Vac-ΔM022*gfp* and Vac-ΔM115*gfp,* showed a different pattern and higher variability concerning the dynamics of the viral foci area when infections were conducted under a semi-solid overlay (panel B).

Cell cultures infected with Lu *gfp*-MYXV developed virus foci consisting of a low number of infected cells as early as 24 hpi. Their area expanded tenfold over the following 24 hours of incubation, and although the foci continued to increase its size, their rate slowed down from 48 hpi to 6 dpi. In contrast, foci measured in the Lu *gfp*-MYXV infected monolayers overlayed with semi-solid medium showed larger foci sizes already at 24 hpi and seemed to have higher an overall spreading within the cell monolayer, as showed by the significantly large foci areas at 6 dpi (Figure 101, A).

Regarding the assessment of the evolution of foci generated by the recombinant strain lacking the M022 protein, the area measurements of the foci developed during the first 24 hours of infection under the same conditions resulted in the same size as those of the parental strain. As

the infection progressed, the virus foci of Lu-ΔM022*gfp* strain exhibited a very limited expansion rate. Notably, between 72 hpi and 6 dpi, there was no significant overall increase in foci size. The progression of foci size developed by the recombinant strain Lu-ΔM022*gfp* during the first 72 hours of infection with a semi-solid overlay had a similar pattern than the ones without. However, during the incubation period from 72 hpi to 6 dpi, the foci of the Lu- ΔM022*gfp* strain experienced significant enlargement, similar to what was observed in its parental Lu strain (Panel B, Figure 101). Yet, the overall increase in foci areas at 6 dpi was accompanied by greater variability in the area measurements, resulting from the presence of a broad range of foci sizes.

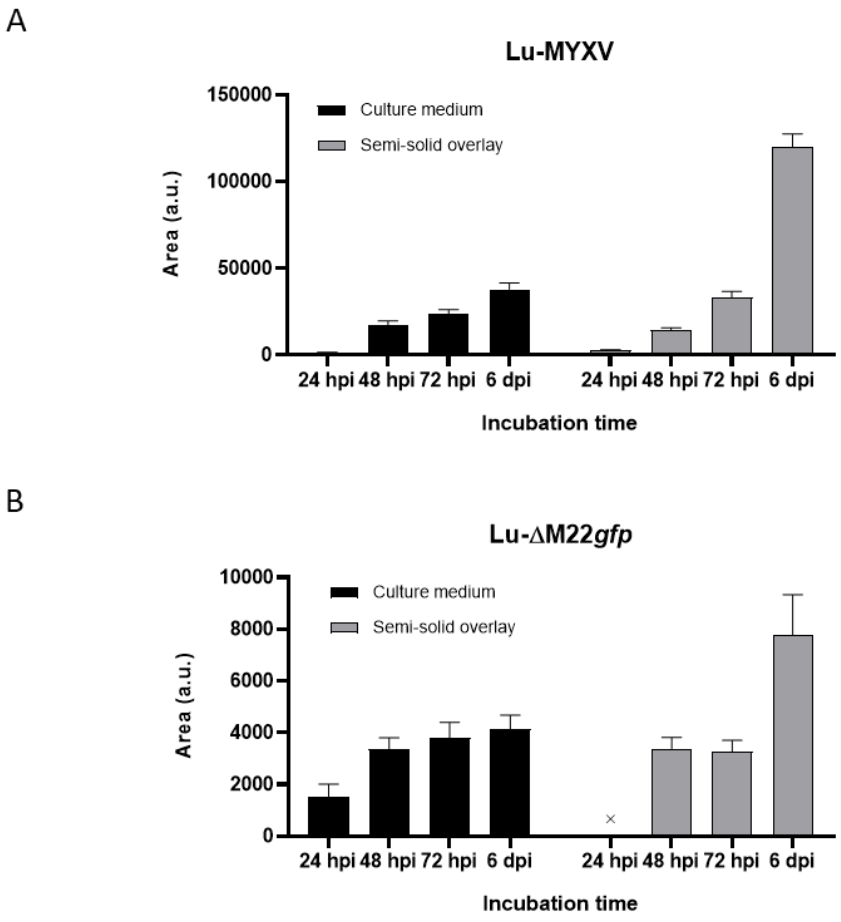

Figure 101. Temporal progression of the size of viral foci during infection of RK13 cultures by the Lu gfp-MYXV parental strain (panel A) and the recombinant deletion Lu-ΔM022gfp strain (panel B).

Each graph illustrates the growth dynamics of viral foci for the respective strain, in RK13 cultures incubated in liquid culture medium (black) or within a semi-solid overlay (grey). Bars represent the mean foci area at each time point ±SEM. Unavailable area measurements are marked by a cross.

Complementing the quantitative analysis, fluorescent microscopy images of viral foci generated in cultures infected with Lu *gfp*-MYXV and Lu-ΔM022*gfp* strains were also captured to provide visual confirmation to these observations (Figures 102). The images were captured at the same

time points and offered clear evidence of the impact that the absence of M022 had on the size of the foci, regarding the reported variation in the temporal progression of each MYXV strain.

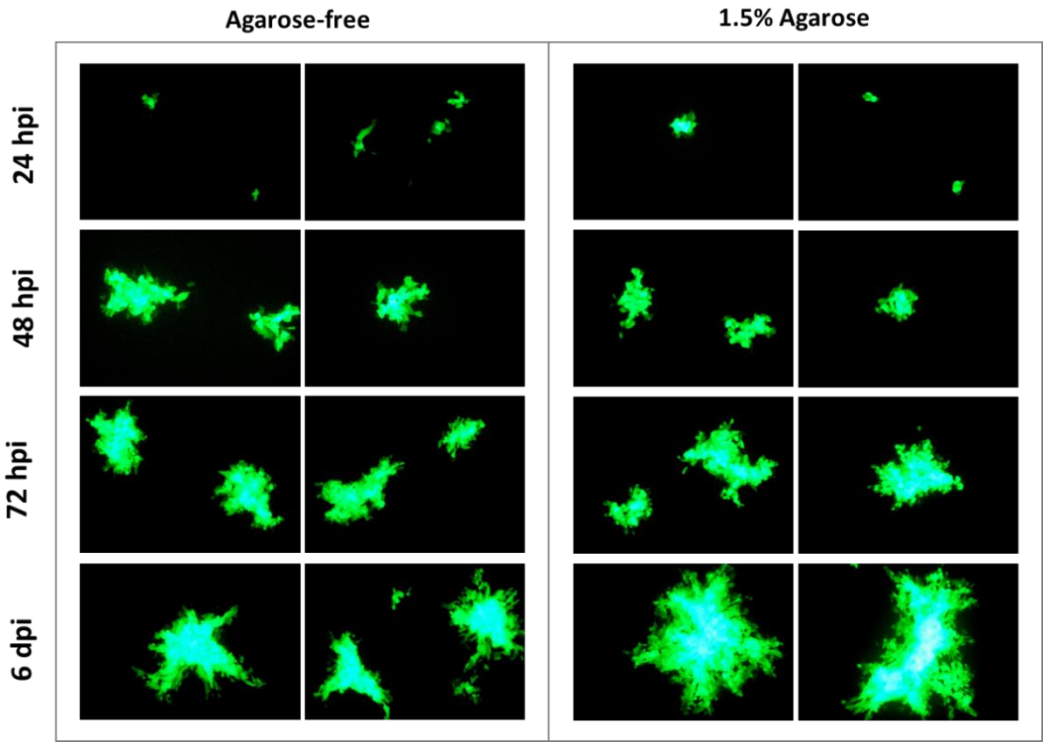

Figure 102. Fluorescent microscopy images of the temporal progression of two Lu gfp-MYXV foci sizes in RK13 cell cultures infected in culture media (left panel) or semi-solid medium (right panel).

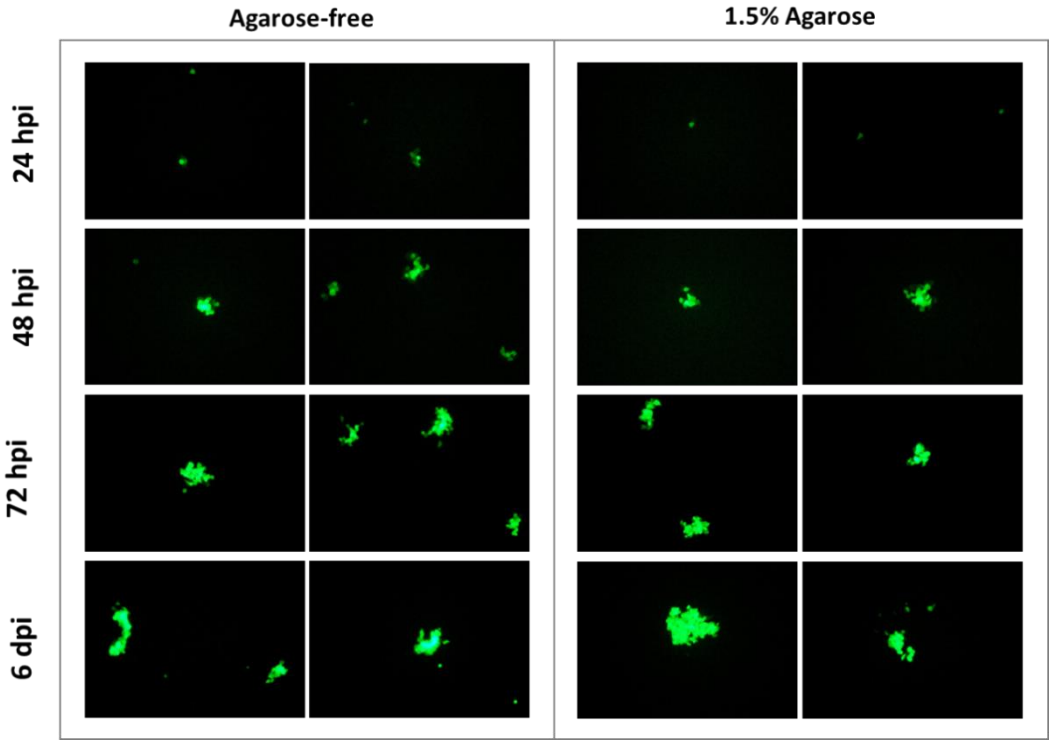

Figure 103. Fluorescent microscopy images of the temporal progression of two Lu-ΔM022gfp foci sizes in RK13 cell cultures infected in culture media (left panel) or semi-solid medium (right panel).

Developing Vac-MYXV foci were detected by immunofluorescence in the infected monolayers incubated in culture medium as early as 24 hpi. The absence of measurements in the semi-solid overlay was due to the inability to identify the single infected cells and/or developing foci from the rest of cell monolayer without an infection reporter (Figure 104).

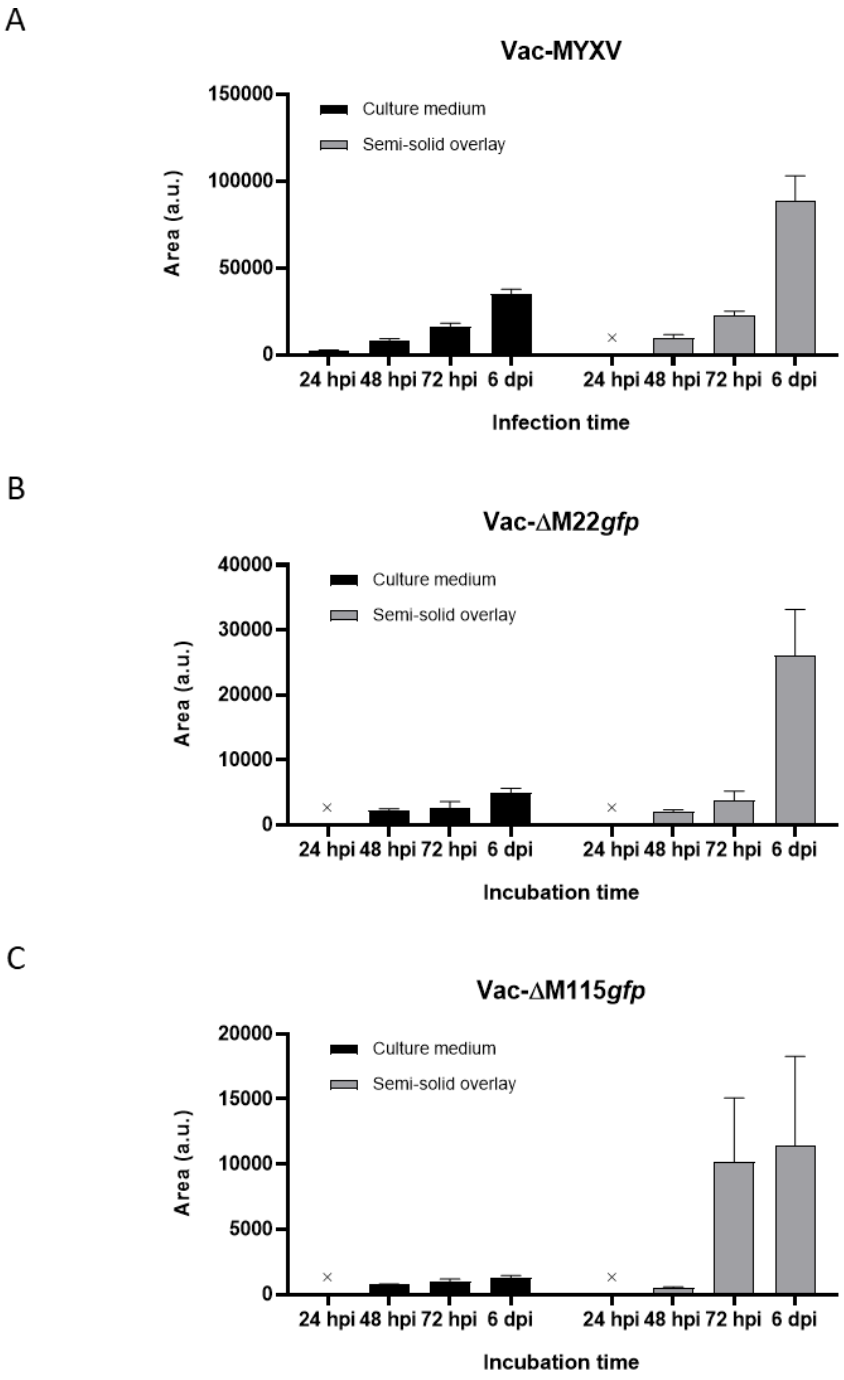

Figure 104. Temporal progression of the size of viral foci during infection of RK13 cultures by the Vac-MYXV parental strain (panel A) and the recombinant deletion strains Vac-ΔM022gfp (panel B), and Vac-ΔM115gfp (panel C).

Each graph illustrates the growth dynamics of viral foci, measured by area, for the respective MYXV strain, in RK13 cultures incubated in liquid culture medium (black) or within a semi-solid overlay (grey).

Individual bars represent the mean foci area at each time point ±SEM. Unavailable area measurements are marked by a cross.

The Vac-MYXV foci displayed a similar growth rate up to 72 hpi, yet the areas that were measured in the infected monolayers overlayed with semi-solid medium doubled the size of the foci generated in culture medium at 6 dpi (Panel A, Figure 105). This phenomenon was described for both parental MYXV strains, Lu and Vac, indicating an apparent advantage for the foci expansion at progressed stages of the infection.

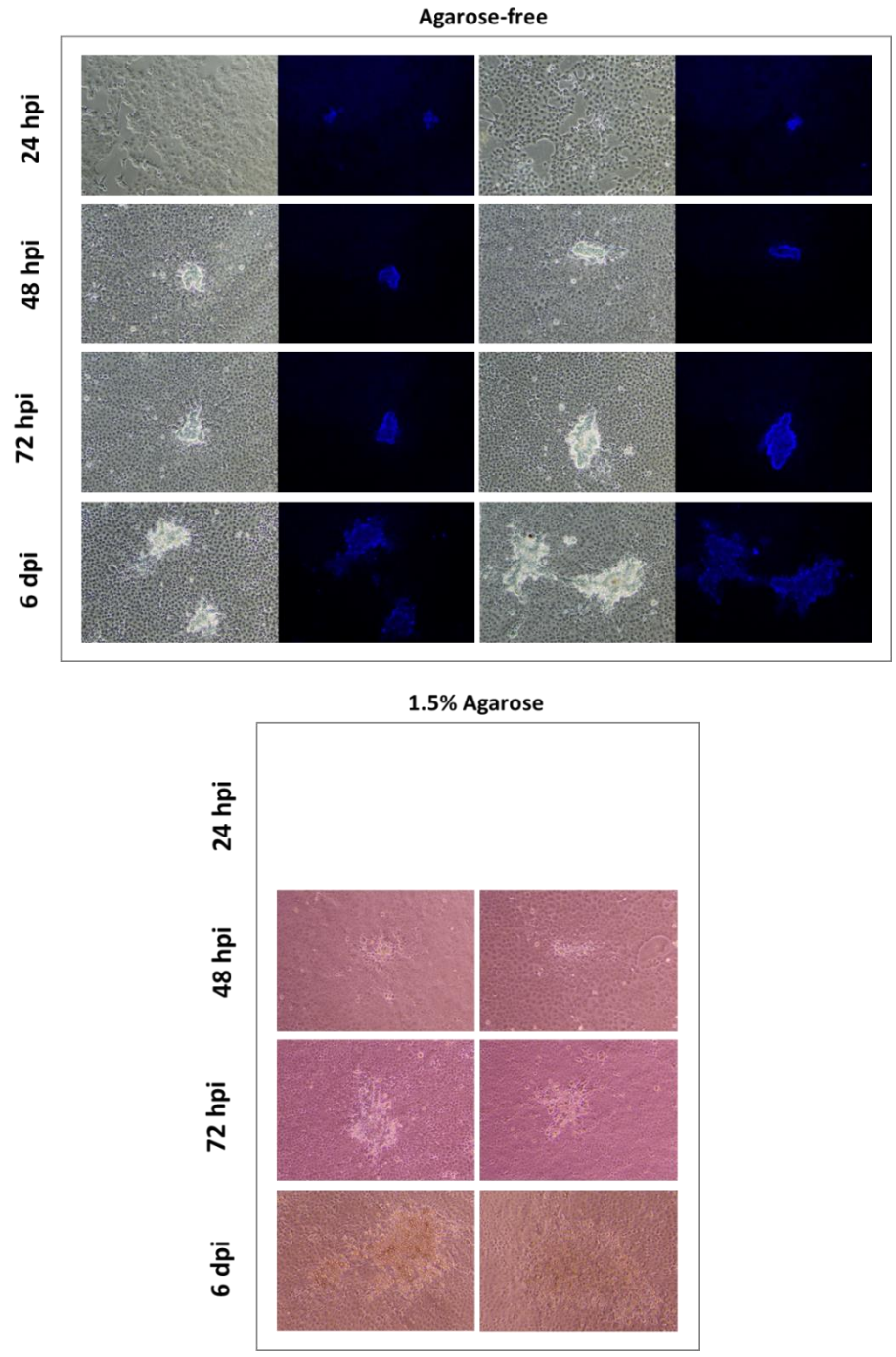

Figure 105. Microscopy images of the temporal progression of Vac-MYXV foci size in RK13 cell cultures infected in culture media (upper panel) or semi-solid medium (lower panel).

The upper panel shows two fluorescence images resulted from immunostaining using a seropositive sample and an AF350 secondary anti-rabbit antibody, together with their brightfield microscopy image. The lower panel exclusively shows two brightfield images per time point, but since infected cells or developing foci were indistinguishable at 24 hpi without a fluorescent reporter, images corresponding to that time point are missing in the panel.

The first stages of foci development were dramatically affected in the two mutant viruses, lacking M022 or M115, which only displayed individual infected cells at 24 dpi (Figure 104, B and C). Despite foci growth being compromised in Vac-ΔM022*gfp*, the area measurements on monolayers in culture medium reflected a progressive increase in foci size (Panel B, Figure). Again, the average area measured for the viral foci was larger when they were developed in monolayers incubated in semi-solid medium, especially at 6 dpi. At this time point, the average foci area for Vac-ΔM022*gfp* was significantly higher, yet the data set displayed a broad range. The SD also being high indicated considerable variability among the measurements, and therefore, less consistency of the individual areas (Table 23). The fluorescent microscopy images of cell cultures infected with Vac-ΔM022*gfp* in Figure 106 provided visual evidence and exemplification of the quantitative findings displayed in panel B, Figure 104. The microscopy images in the left panel showed smaller and more defined foci, and some of them displayed a comet-shaped morphology, with a denser "head" and an elongated "tail" resulting from the unidirectional cell-to-cell viral spread. In VACV, comet-shaped plaque phenotype is indicative of the production of EEVs.

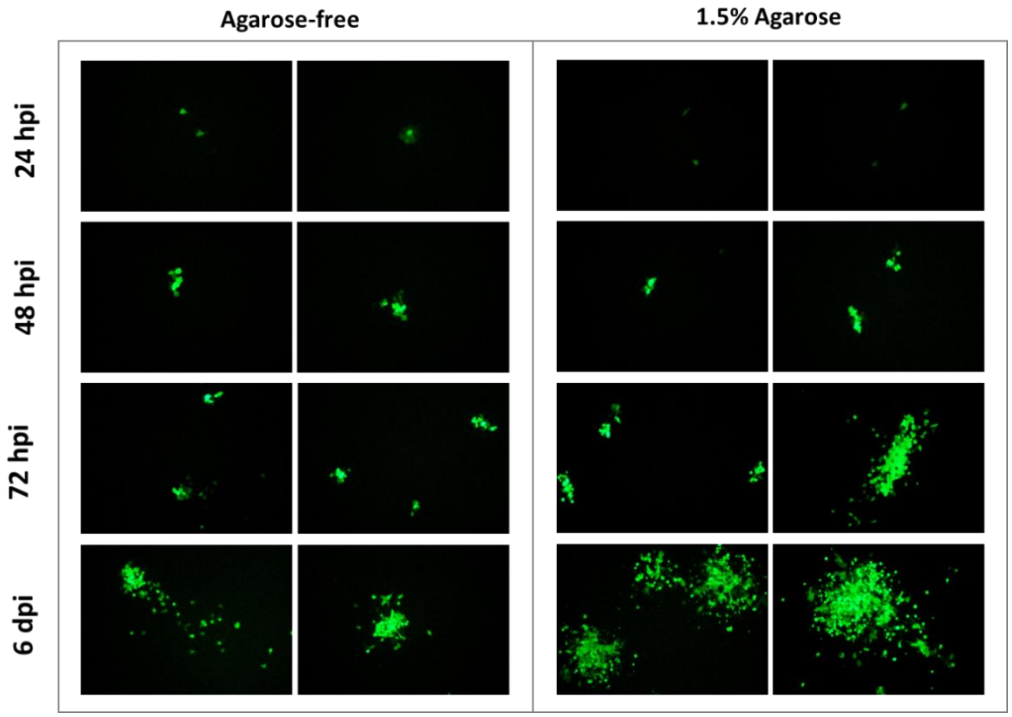

Figure 106. Fluorescent microscopy images of the temporal progression of Vac-ΔM022gfp foci size in RK13 cell cultures infected in culture media (left panel) or semi-solid medium (right panel).

The lack of M115 had even a greater negative impact than lack of M022, on the development and propagation of viral foci. The maximum foci growth reached at 6 dpi by the mutant virus Vac-ΔM115*gfp* in culture medium was limited to few infected and grouped cells (Figure 107). In contrast, virus foci of a broad range of areas were measured in semi-solid medium (panel C, Figure 105). A wide range of foci morphologies was found from 72 hpi, some with small areas, similar to the type of foci described for the culture medium, and others with big areas, constituted by dozens of infected cells. The largest foci were consistently developed at the edges of the well, while the smallest were scattered in the middle of the well. The morphology of these Vac-ΔM115*gfp* foci was unique since they showed a non-compact, dispersed pattern, instead of the usual well defined and tight viral focus. In fact, non-infected cells were interspersed among the infected ones, creating a mosaic-like appearance. Such arrangement was more evident for the small foci (right panel, Figure 107).

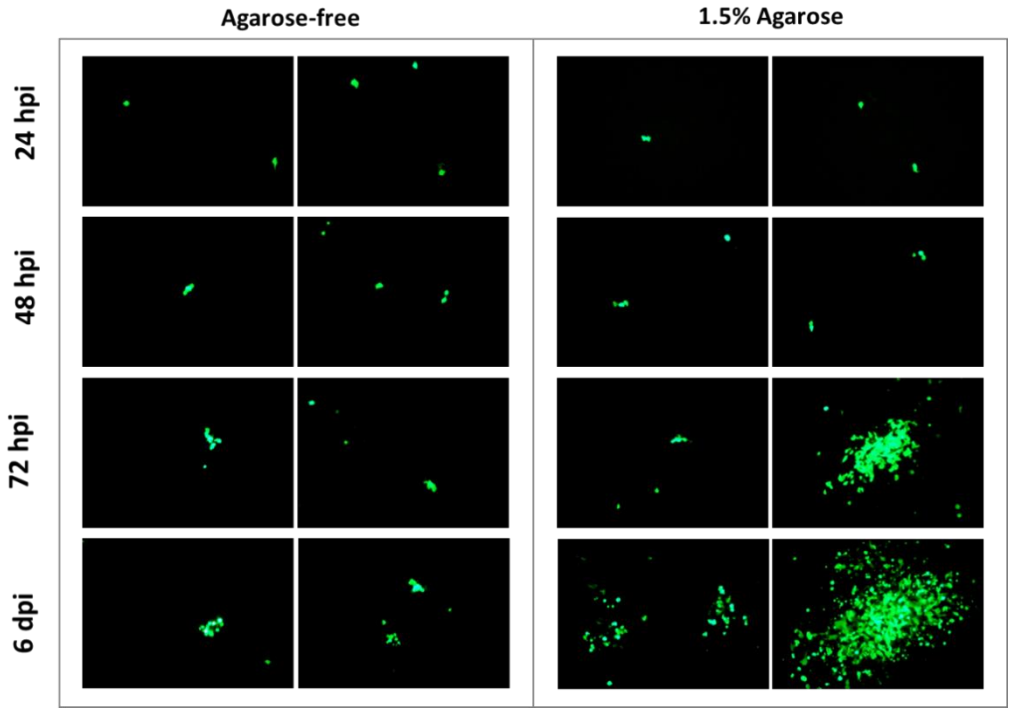

Figure 107. Fluorescent microscopy images of the temporal progression of Vac-ΔM115gfp foci size in RK13 cell cultures infected in culture media (left panel) or semi-solid medium (right panel).

Ultimately, *m022l* and *m115l* deletions on the MYXV genome resulted in a significant change in viral focus size and spread.

Transmission electronic microscopy (TEM) analysis

Virions isolated from infected RK13 cultures and purified by ultracentrifugation were analyzed on whole mount preparations using negative staining electron microscopy. Examination of these purified particles on TEM revealed that practically all virions, regardless of the MYXV type (parental or mutant), displayed what looked like surface elements randomly arranged throughout their surface, which are typically known as *mulberry* like appearance. This is the typical form by which intact IMV particles are visualized using negative staining (Figure 108).

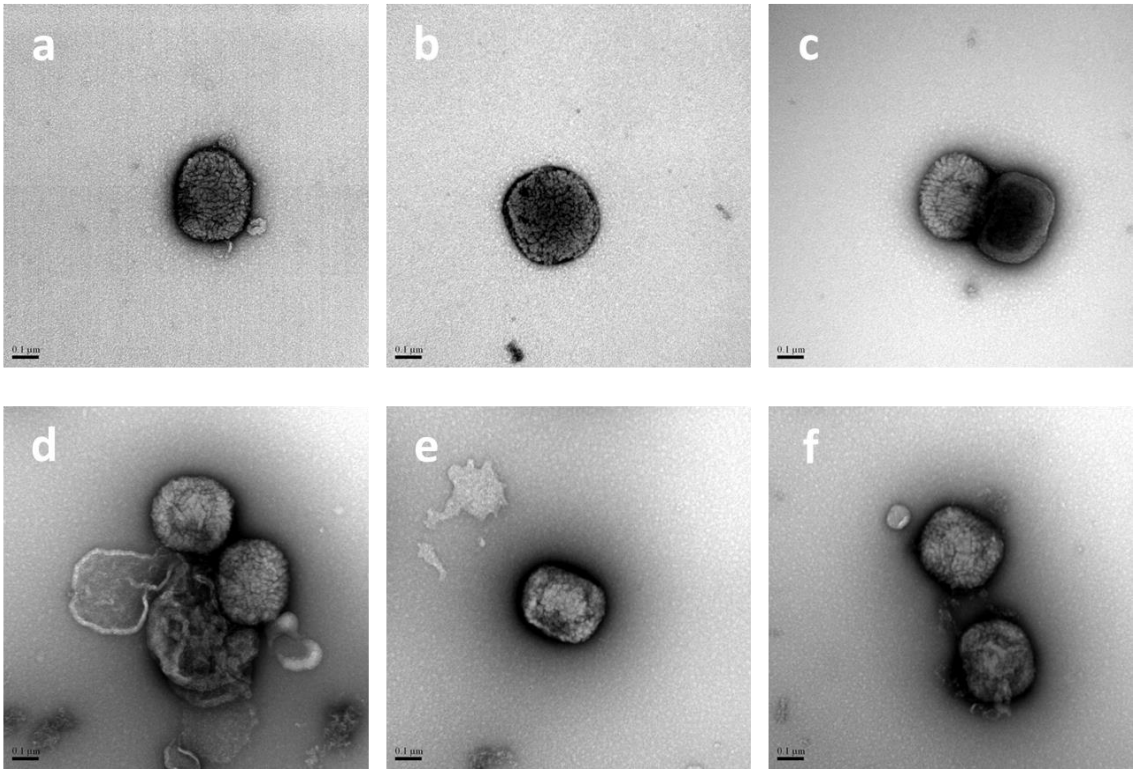

Figure 108. Transmission electron microscopy (TEM) images.

Negative staining TEM images depicting the morphological characteristics of purified MYXV virions at magnification x100,000. Virus particles were released by homogenization from a RK13 culture infected with either Vac-MYXV (a, b, c) or the mutant Vac-ΔM022*gfp* (d, e, f), and purified by ultracentrifugation on a sucrose cushion. Virions were examined by electron microscopy after uranyl acetate negative staining. Scale bars represent 0.1 µm.

TEM images were used to measure the length and width of individual Vac-MYXV (*n* = 13) and Vac-ΔM022*gfp* virions (*n* = 18), defined as the long and short axis perpendicular to it, respectively, using Image J software (Panel D, Figure 109). The mean (± SD) size analysis of the Vac-MYXV virions yielded 337.7 nm (± 22.21) nm for the long axis, and 290.6 nm (± 34.44) for the short axis. By contrast, the dimensions of the ΔM022 mutant virions were 300.1 nm (± 10.84) for the long axis, and 253.5 nm (± 19.44) for the short axis. The difference in size between the two virus was statistically significant for both length (Welch's t-test, p value < 0.0001) (Panel A, Figure...) and width (Welch's t-test, p value = 0.0027) (Panel B, Figure 109).

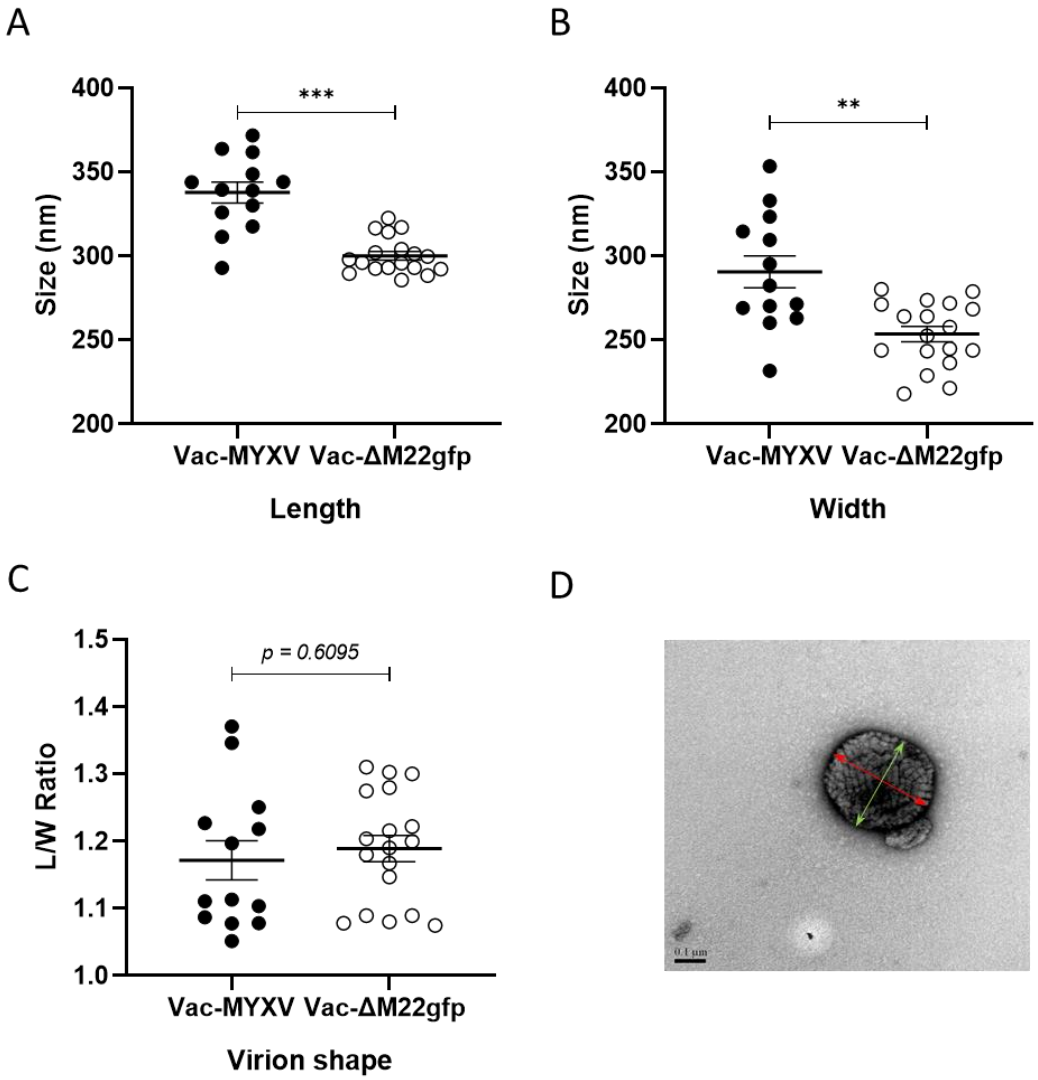

Figure 109. Comparative analysis of the size and morphological characteristics of the parental Vac-MYXV (n = 13) and mutant (n = 18) virions.

Length (A) and width (B) of the virions were measured using TEM images. The L/W ratio (C) was calculated using paired length (red arrow in D) and width (green arrow in D) values of each virion. The distribution of individual measurements provided insights into the structural differences between both strains. Mean ± SEM are also shown.

The length/width (L/W) ratio was calculated to understand the shape of the virions, and to analyze if besides the different size, the two forms showed potential structural integrity differences. The mean (± SD) of the L/W ratio was 1.172 (± 0.1053) for the parental strain and 1.189 (± 0.08301) for the mutant, indicating that both strains displayed similar morphology, with slightly elongated shape. The mean L/W ratio values for the parental Vac-MYXV and the ΔM022 mutant were not statistically significantly different (Student t-test, p value = 0.6095).

Growth curves in cell culture

The *in vitro* infectious cycle of MYXV is typically around 18 hours. Although this duration might be subjected to variation based on specific conditions or viral strains, it represents the average time required for the virus to enter a host cell, replicate its genome, and produce a whole new generation of virus particles.

Virus growth was assessed by infecting RK13 cell monolayers at a MOI of 1 (one-step-growth curve) or 0.1 (multiple-step-growth curve) either with the Vac-MYXV strain or the mutant ΔM022*gfp* strain. One and a half hours after infection, cultures were washed and replaced with pre-warmed DMEM-10 medium. Culture samples, including media and cells, were harvested at the indicated time points (0, 6-, 24-, 48-, 72- and 96-hpi) in triplicate, and frozen at -80°C. After three cycles of freezing and thawing, samples were sonicated, and virus titers were determined by serial dilution and focus forming assays on RK13 cell monolayers. Virus foci were identified by fixing the infected monolayer with 37% formaldehyde followed by staining with crystal violet (for the Vac-MYXV) or by fluorescent microscopy (for the Vac-ΔM022*gfp*).

The Vac-ΔM022*gfp* recombinant was characterized for growth in permissive cell culture and compared to the control Vac-MYXV. The multiple-step-growth curves constitute an approach to investigate viral spread. For that, RK13 cell cultures were infected at MOI 0.1 and the relative difference in viral titer between the recombinant Vac-ΔM022*gfp* and its parental strain was quantitatively assessed at various time points. On average at this low-MOI infection, each cell is infected with less than one virus particle, meaning not all cells are initially infected, and those that are infected are less likely to be co-infected with multiple virions. This enabled the temporal monitoring of viral replication and dissemination over time, offering in a more accurate representation of the replication dynamics observed in a natural infection (Figure 110). Microscopy images of the infected RK13 cultures were also captured at the same incubation time points, the rate of cells infected with the mutant Vac-ΔM022*gfp* was apparently constant with individual infected cells scattered throughout the monolayer (Figure 106).

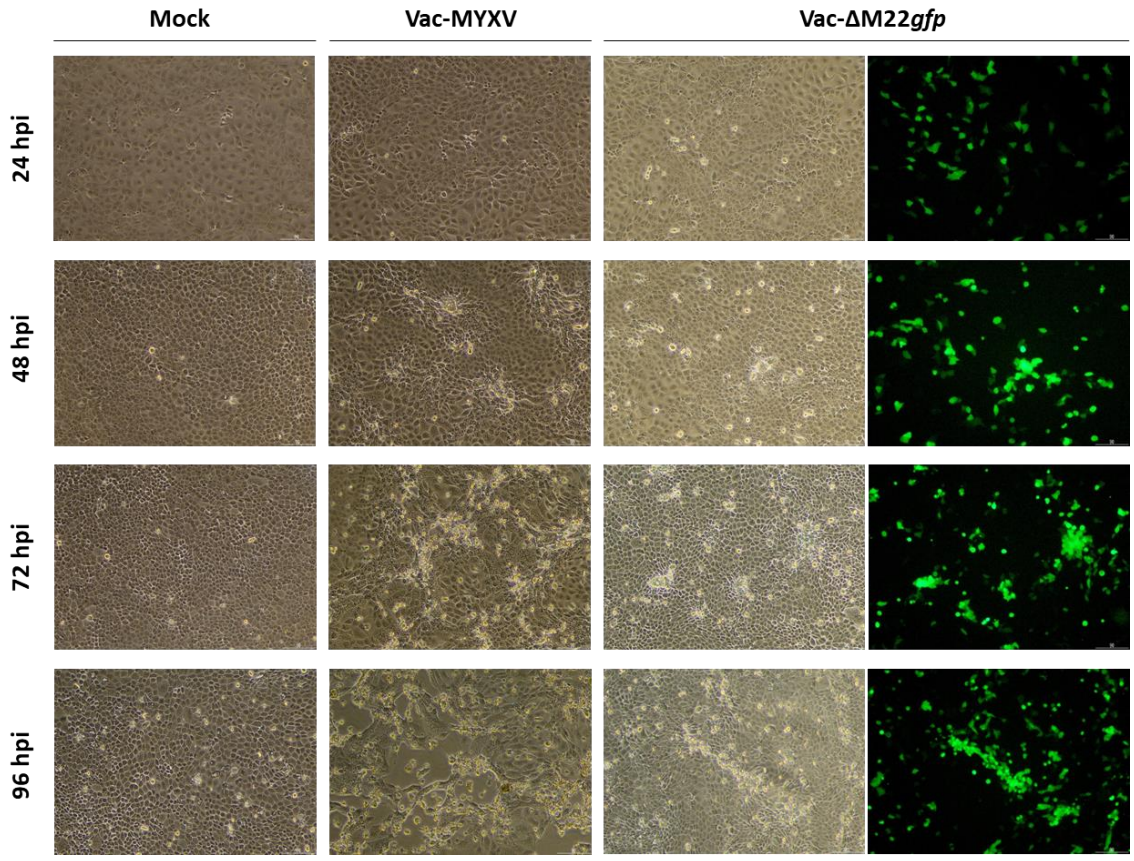

Figure 110. Monolayers of RK13 cells infected with Vac-MYXV and Vac-ΔM022gfp using a low multiplicity of infection (MOI of 0.1).

From all the cells infected at 24 hpi, only a few developed viral foci that could be detected from the 72 hpi onwards (Figure 110). Although the parental strain lacked a reporter gene, the microscopy images reflected the trends that were detected by the titer determination. The extent of cytopathic effects and the level of disruption of the cell monolayer that were observed in the Vac-MYXV infected cultures, which were more pronounced at 72 hpi and 96 hpi, suggested a higher spreading rate of the parental virus over the mutant ΔM022*gfp.*

During the period comprising the immediate hours following infection, known as eclipse and latent phases, the infectious particles entered cells, uncoated, and began their genome replication. The multiple-step growth curves of both Vac-MYXV and the Vac-ΔM022*gfp* recombinant were characterized by a slight loss of titer by 6 hpi, compared to the initial titer (0 hpi). The release of newly synthesized virions from initially infected cells corresponded to the exponential phase of the growth curve, which is detected from 24 hpi (Figure 111, A). At this time point, the titer of Vac-MYXV strain increased 37.38-fold relative to its level at 6 hpi, while the ΔM022*gfp* mutant strain showed even a larger increase, with its titer rising 291-fold compared to its own titer at 6 hpi. The deletion mutant exhibited a titer that was 5.82 times higher than that of the parental strain at 24 hpi.

From 24 hpi onwards, the ΔM022*gfp* curve showed a change of shape, and the growth rate slowed down in the following time points; its titer increased 2.2 times between 24- and 48 hpi, 1.29 times between 48- and 72 hpi, and 2.53 times between 72- and 96 hpi. Instead, the titer of the parental Vac-MYXV increased at a higher rate until the last period analyzed (72 to 96 hpi). Vac-MYXV showed the following relative titers: 23.87-fold increase from 24 to 48 hpi, 4.64-fold increase from 48 to 72 hpi, and a 1.87-fold increase from 72 to 96 hpi. Despite the early replication or release advantage that the mutation seemed to confer at the early phase of the infection dynamics, the lack of M022 supposed a significant disadvantage in the later stages of infection. In the subsequent time points (48-, 72- and 96-hpi) the recombinant ΔM022*gfp* titer was about 46%, 85% and 80% lower than the titer obtained for the Vac-MYXV infection at the same time points, respectively.

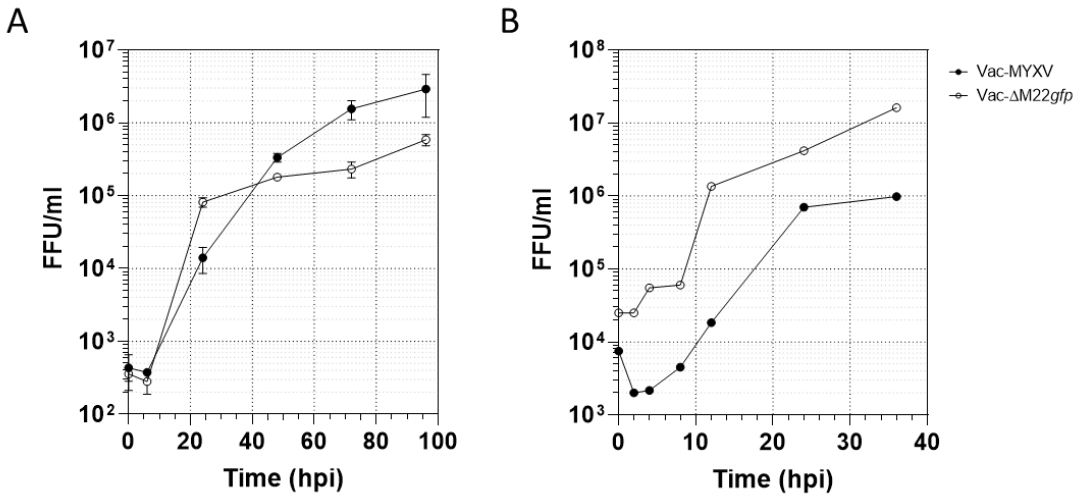

Figure 111. Growth curves of the parental Vac-MYXV (black) and ΔM022gfp recombinant (white) viruses.

A) Multiple-step growth curve of myxoma viruses in RK13 cultures that were infected at MOI 0.1 and incubated up to 96 hours. Cell monolayers and supernatant were harvested in triplicate at the indicated time points and viral titers were determined by focus forming assay in triplicated. Each data point represents the mean ± SEM of the triplicate titer measurements for all the replicates. B) One-step-growth curve of myxoma viruses in RK13 cultures that were infected at MOI 1 and incubated up to 36 hours. Cell monolayers and supernatant were harvested in triplicate at the indicated time points, and the viral titers of one of each replicate was analyzed by focus forming assay.

The one-step-growth curve was designed to investigate the kinetics of virion production for each virus. The infection was performed at an MOI of 1 to ensure that, ideally, all cells of the semiconfluent monolayer were infected simultaneously. Despite the fact that Vac-MYXV lacked a reporter marker, the microscopy images of the RK13 culture infected by the mutant Vac-ΔM022*gfp* at 32 hpi provided visual confirmation of the simultaneous infected status of the RK13 monolayer (Figure 112).

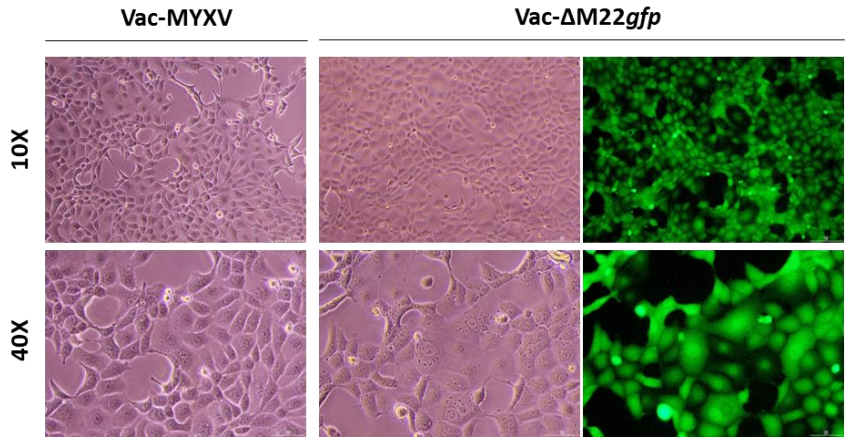

Figure 112. Microscopy images of semiconfluent RK13 cells infected with Vac-MYXV (left) and Vac-ΔM022gfp (right), using a high multiplicity of infection (MOI of 1).

Cells infected with Vac-ΔM022gfp were identifiable by green fluorescence. Images captured at 10X and 40X magnifications are presented.

After 2 hours of incubation to allow virus attachment to the cells, complete DMEM-10 was added and cells were incubated at 37°C, 5% CO_2. At the indicated time points (0, 2-, 4-, 8-, 12-, 24-, and 32 hpi), infected cultures were harvested in triplicate, collecting simultaneously the infected monolayer and the culture media. Then, virions within the cells were released by three freeze-thaw cycles and sonication. The total amount of viral load was determined by focus forming assay since no distinction was made between intracellular and extracellular virions (Figure 111, B).

The concentration of the initial inoculum was not identical for both viruses, indeed the amount of mutant virus that was used for the infection was 3.55 times higher than the parental Vac-MYXV strain. This fact could explain the noted titer difference at the initial time point (0 hpi), which corresponds to a 3.34-times higher titer for the Vac-ΔM022*gfp* titer, over the parental. Therefore, to analyze the true effect of the genetic differences on viral growth dynamics, these values were set as the reference point (or baseline measurement), and the viral titers obtained for each time point were normalized to their corresponding initial value. The resulting values, referred to as “titer fold change” were plotted and used for comparison of the growth dynamics of the viruses (Figure 113).

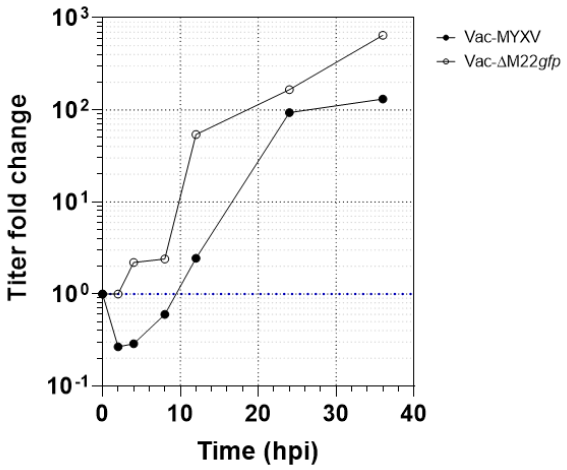

Figure 113. Normalized one-step growth curve of the parental Vac-MYXV (black) and ΔM022gfp recombinant (white) viruses.

Viral titers determined at different time points for each virus were normalized to their baseline (initial viral titer at 0 hpi) to minimize the impact of the variations in inoculum titer, ensuring that any observed differences in viral growth dynamics reflect the true effects of genetic variations. Titer values are represented as fold change over the respective initial values. The blue-dashed line indicates the fold change value of 1, corresponding to the baseline viral titer.

Due to limited availability of time, one of the replicates was analyzed for each time point, therefore the results obtained in this assay, and discussed below, are still preliminary and need to be complemented at least with the other two replicates that were not titrated yet. The increased growth rate of the mutant Vac-ΔM022*gfp* over the parental Vac-MYXV that was seen after a low MOI during the first 24 hpi, was also detected at a MOI of 1. During the lag phase, spanning the first few hours of incubation, viral titers remained relatively stable: Vac-MYXV showed a slight decrease in viral titer, but the mutant virus viral titer remained constant and even increased minimally.

Both viruses seemed to need about the same time, 8 hours, to establish themselves within the host cells and start productive replication. The onset of the exponential phase started right after this, when the viral titer of both viruses started to increase exponentially, reflecting the presence of the newly produced progeny. The largest increase in viral titers, corresponding to the burst or release phase of the progeny, was observed between 8 and 24 hpi for both viruses. However, the timing and magnitude of these increases differed between the strains. The parental virus, Vac-MYXV, showed a 4.07-fold rise in titer from 8 to 12 hpi but it displayed the highest increase, with a 38-fold rise in titer, from 12 to 24 hpi. In contrast, the mutant virus exhibited its major increase earlier, achieving a 22.5-fold rise in titer between the 8 and 12 hpi, followed by a 3.09 increase between 12 and 24 hpi. Indeed, the relative titers of both strains showed the largest difference at 12 hpi, of almost 1.5 $\log_{10}$, with the relative titer of the ΔM022*gfp* mutant being

22-times higher than the parental. At 24 hpi, after the burst release of Vac-MYXV virions, this difference narrowed to only 1.79-times higher for the mutant. Finally, in the period of time from 24 to the 32 hpi, both viruses had a rise in relative titer, but although the parental strain seemed to decrease its growth rate, the mutant showed a significant increase again, with an almost 5-fold compared to its relative titer at 24 hpi (Figure 113).

Production of EEVs

There was no distinction made between IMVs and EEVs within the total viral titer that was measured in the previous experiments. To study the impact that the deletion mutations had on the virion wrapping and release, RK13 cultures were infected at a MOI of 0.1 and incubated for 96 hours. At that time, culture media was collected and infected cells were harvested independently for the characterization of EEV and IMV, respectively. It was assumed that all the virions detected in the media by the focus forming assay titrations belonged to the EEVs released from the infected cells. A total of six different MYXV strains were evaluated in this experiment: the virulent Lu-MYXV and its mutant lacking the M022 (Lu-ΔM022*gfp*), the vaccine strain Vac-MYXV and its mutants Vac-ΔM022*gfp* and Vac-ΔM115*gfp,* and a second homologous vaccine strain Vac2-MYXV (Figure 114, A).

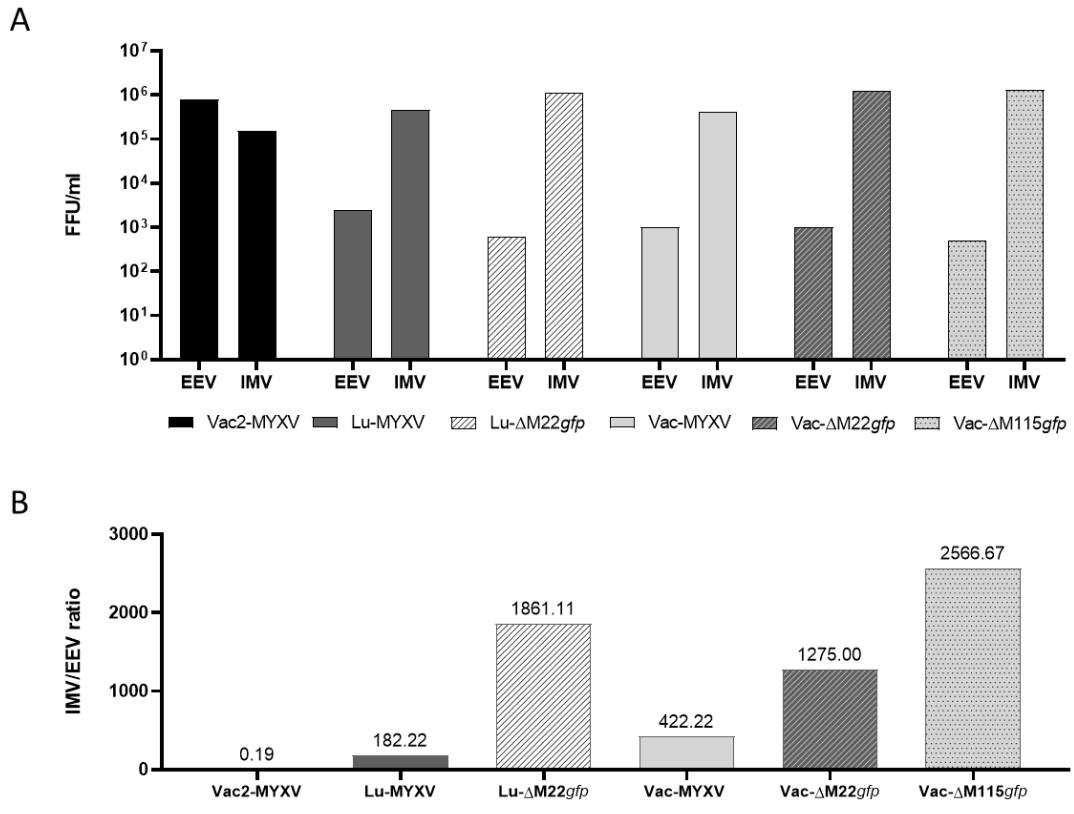

Figure 114. Comparative IMV and EEV production by the mutant MYXV.

RK13 cultures were infected at an MOI of 0.1 and incubated for 96 h. Cells and culture media were collected separately and each fraction was titrated by focus forming assay. A) Viral titer of culture media (EEV) and cell fractions (IMV) of the infected RK13 cultures at 96 hpi. B) IMV/EEV ratio of different MYXV at 96 hpi. The value is added above each bar.

This latter showed the highest titers of EEV at 96 hpi by far, with more than 3 × $\log_{10}$ difference with the rest of MYXV strains. Indeed, Vac2-MYXV had higher production of EEV than IMV at 96 hpi, as it was also indicated by the low IMV/EEV ratio (Panel B, Figure 114, B). The virulent virus Lu-MYXV had 182.22-times more IMV concentration than EEV, but the deletion of M022 increased that difference in 1 $\log_{10}$. This mutation had a milder effect on the vaccine strain Vac-MYXV, since the IMV/EEV ratio only increased three times compared to the parental one. The M115 deletion doubled this difference, the IMV/EEV ratio of Vac-ΔM115*gfp* was 6 times higher than that of the parental Vac-MYXV. This mutant showed the lowest production of EEV amongst all the analyzed strains.

Besides the vaccine strain Vac2-MYXV, which exhibited a significantly high release of EEV, accounting for 83.83% of the total virions detected at 96 hpi, the other strains released a markedly lower proportion of EEV into the media. The virulent strain Lu-MYXV released a 0.55% of EEV, while the vaccine strain Vac-MYXV released an even smaller percentage, 0.24% of the total progeny. The deletion of M022 had an impact on this rate, decreasing the production of EEV in both mutants Lu-ΔM022gfp and Vac-ΔM022gfp, to the 9.83% and 33.17%, respectively, of the already small amount of EEV generated by the parental strains. Hence, the lack of M022 seemed to be more detrimental for the virulent strain. In addition, the deletion of M115 also led to a significant reduction in the production and release of EEV for the Vac-ΔM115gfp, which accounted for only 16.48% of the EEV produced by the Vac-MYXV.

CHAPTER 8: DISCUSSION

To be considered for inclusion in a DIVA design, a suitable candidate needs to meet several criteria. In the first place, it must elicit a strong and specific immune response in the infected animals, facilitating easy detection through antigen-specific serological assays. Also, it is desirable that it is conserved across different strains of the virulent organism, ensuring that the DIVA test would be reliable across any possible field condition. However, since a deletion mutant would be used as a candidate marker vaccine for the immunization of rabbits, a good candidate protein should not be essential for the virus replication, ensuring that its deletion does not compromise its overall viability. The disruption of genes that encode proteins with roles in pathogenesis and host-range are well described (reviewed in Kerr, 2012; Stanford et al., 2007), but numerous other MYXV proteins remain unexplored both structurally and functionally.

Considering the above, the selection of antigenic protein candidates of MYXV was a crucial step for this study. The primary objective of the first experimental chapter was to identify potential DIVA candidate proteins from the existing literature and findings from other members of the poxvirus family. While many MYXV proteins have not been thoroughly characterized, they share significant homology with well described homologous proteins in other poxviruses, particularly VACV. Due to its historical significance, VACV has been extensively studied and serves as the model organism to study poxvirus biology and host interactions (Smith et al., 2013). Although VACV belongs to a different genus to MYXV (orthopoxvirus genus versus leporipoxvirus genus), the functions of some MYXV proteins are inferred from the knowledge mainly generated in VACV research. While homologous proteins often retain similar functions, there can be a significant functional divergence due to evolutionary pressures given by differences in host-virus specific interactions (Villa et al., 2010b). This underscores the relevance of experimental validation in the confirmation of such inferred functions of MYXV proteins detailed biologic functions and structure are not well characterized.

To determine the specific antigenic properties of each candidate, the viral proteins first needed to be isolated and obtained in high concentration. Chemical synthesis was not the ideal system to produce proteins, due to their high molecular complexity and size. *In vivo* biologic production systems were considered for this task instead. Given that every heterologous protein expression system has its own advantages and disadvantages; we considered the prokaryotic expression system first, regarding its high yield, easily scalable and cost-effective process. On this basis, the genes encoding the six MYXV candidates (*m022l, m029l, m071l, m083l, m115l, m141r*) were cloned into different expression vectors, that were used afterwards for transforming competent bacteria cells. The reason M022 protein expression was screened using different and more expression vectors than the rest is that it was the initial and, at that time, only candidate chosen

for investigation. At a later stage, the other five protein candidates were additionally included in the study.

One of the main challenges in producing soluble and functional proteins via heterologous expression systems, encountered specifically in the *E.coli* expression system, is the tendency of proteins to incorrect folding and aggregation into inclusion bodies. This issue significantly hindered the progress of our project, and it was one of the challenges that we most struggled with. In fact, despite all genes (except *m022l*) being codon-optimized for prokaryotic expression, out of the six protein candidates, only the recombinant M083 protein was successfully produced in soluble form without complications.

Reducing the hydrophobic interactions of newly synthetized polypeptides and improving their access to the folding machinery improve proper folding. Several strategies were explored to improve solubility yields of the other proteins, from reducing the inductor concentration, reducing the growth temperature, changing cellular density during induction, to trying different culture media compositions. Slight improvements were only observed in the production and solubility of M115 and M022 recombinant proteins. The M029, M071 and M141 recombinant proteins were practically entirely found in the insoluble fraction (PF) upon clarification of the bacteria lysates.

Considering possible hydrophobic interactions of those proteins with the lipid membrane, several detergents were used to wash the insoluble fraction and try to improve their solubility. However, these washes did not help in any case. At this point, it was of interest to do a tight evaluation regarding their physicochemical properties, and to review other studies conducted on the heterologous expression of some of their homologous proteins. For instance, the C-terminal hydrophobic TM domain that mediates the post-translational insertion of the homologous M071 protein in VACV, H3L, into membranes during IV maturation was not cloned into the expression vector, the recombinant M071 still had a high hydrophobic profile (da Fonseca et al., 2000a; Zinovieva et al., 1994).

Heine et al. (1999) demonstrated that this TM domain showed toxicity to transformed cells, and that although truncated proteins yielded higher amounts, they were more prone to insolubility: the full-length P32 protein was more soluble. Our findings stand in contrast to those reported in previous studies, where soluble homologous of M071 protein in capripoxvirus (P32 protein) (Heine et al., 1999) and VACV (H3L protein) (Lin et al., 2000) lacking the C-terminal domain were successfully produced in prokaryote cells when they were treated with 0.5% Triton X-100. Our

results indicate that neither Triton X-100 nor truncation affected M071's solubility, since this recombinant protein was completely insoluble under all conditions tested.

Indeed, the recombinant proteins M029, and more significantly M071, M141, were enriched in the insoluble fraction after two serial incubations with a wash buffer containing detergents, which led us consider the fact that they could be misfolded and aggregated by hydrophobic interactions into inclusion bodies (IB) (Singh et al., 2015). Due to the low molecular weight of the M029 protein and the challenges associated with its overexpression and stability, it was excluded from the study. In contrast, the promising antigenic properties of M071 and M141, justified further efforts to obtain and study these proteins. Although a high density of recombinant protein can often be isolated from other components by purifying the IBs, additional steps are required to solubilize and refold the proteins into their native state, which is a tricky process. The chaotropic agent selected for the solubilization of IB was a freshly prepared buffer containing 8 M urea. The efficiency of the solubilization was not improved by the addition of reducing agents (β-ME) or detergents (Triton X-100). Washing the insoluble pellet with buffer containing detergents, before the solubilization step, removed possible contaminants that could have been absorbed onto the hydrophobic IBs during cell lysis and sample processing (A. Kumar et al., 2012). The solubilization treatment was successful for both viral proteins, and since they were marked with a polyhistidine tag, attempts were made to purify them directly using affinity columns under denaturing conditions.

The recombinant protein purification process in IMAC columns performed under denaturing conditions was partially successful for M141, but the protein in the eluate buffer had to be refolded to recover its native conformation, or at least a partial secondary structure. The high technical challenges of the refolding step, and the lack of enough concentration of M141 in the eluate prevented the successful obtainment of a native protein. The purification of M071 was also unsuccessful, but this time no protein was obtained in the eluates. In fact, there were unspecific low molecular bands across all eluates, suggesting a possible degradation of the protein sample during the elution process. It seemed that most of the protein remained attached to the chromatographic matrix, probably precipitated.

Hundreds of recombinant proteins have been produced by the BEVS, including recombinant vaccines (Cox, 2012; Van Oers et al., 2015). A relevant feature of the BEVS is that insect cells have a similar post-translational processing capacity as mammalian cells, including the formation of disulfide bonds, cleavage of the signal peptide, and proteolytic processing. While both insect and mammalian cells share the initial steps of N-glycosylation, mammalian cells can

incorporate complex sugar groups with sialic acids, whereas proteins translated in insect cells only incorporate simple oligo-mannose sugar chains (Kubelka et al., 1994). Maturation is an important process in which many of the translated proteins acquire the necessary modifications for developing their biological role in the cell. Since the glycan pattern of a recombinant protein is essential for its structure, heterologous insect expression might affect their main solubility, half-life, and biological properties like activity, interactions, and immunogenicity (Altmann et al., 1999). PTM during maturation may also be relevant for replicating the structural determinants found in the native proteins, which in case of the structural proteins of the IMV and EEV, such as M071, M115, and M022, can be recognized by the immune system.

The gst-*m022l, m071l* and *m115l* ORFs were cloned in an expression vector under the control of a very late promoter, with which recombinant baculovirus (rBV) were generated. Once inserted within the viral genome, rBVs are used for the infection of insect cells where high levels of heterologous protein expression are achieved. Each recombinant protein showed their own expression kinetics and stability within insect cells (Kollewe & Vilcinskas, 2013). In this case, the full-length M071 protein produced through this system was scarce and also remained highly insoluble, in contrast to finds of Heine et al. (1999). M022 and M115 were predominantly expressed in soluble form, and sufficient amounts of both proteins were purified to perform subsequent antigenic determination. Although all recombinant proteins had a polyhistidine fusion tag, M022 was also fused to GST in its N-terminal domain, using the same strategy that worked for the homologous p37 protein expression (F13L ORF) of VACV (Baek et al., 1997). In our case, M022 (GST-M022) was purified as a fusion protein using a Glutathione resin chromatography column without thrombin proteolytic cleavage in the elution process, since according to Baek et al. (1997) results, a GST-free p37 the process failed to release enough protein to work with.

Three recombinant proteins could be isolated and purified in a stable soluble form: M083 obtained in the prokaryotic *E.coli* expression system, M115 and M022 (fused to GST) obtained in the BEVS. The remaining 3 viral proteins were not soluble or stable, which led to analyzing their antigenicity within a heterologous sample.

Just as D8L's ectodomain has significant sequence and conformational homology to human carbonic anhydrases, the M083 protein in MYXV also revealed high sequence identity with the *O. cuniculus* carbonic anhydrase I although lacked several key residues involved in the catalytic activity. The D8L protein is dispensable for VACV's viability, but a deletion mutant displays an attenuated profile *in vivo* (Niles & Seto, 1988; Rodríguez et al., 1992). In concordance to these

results, a deletion MYXV mutant lacking the putative D8L VACV homologous protein, M083, generated virions with normal morphogenesis with an unaltered replication cycle *in vitro.* However, the mutant showed a significant cell-to-cell spread defect that was translated into decreased viral dissemination *in vivo.* This MYXV mutant lacking M083 already showed an attenuated pathogenic profile accompanied by improved host immune responses (Wolfe et al., 2018). Confirming the antigenic profile of the M083 protein was essential for establishing its suitability as a component in developing the marker vaccine and DIVA serologic system.

Under nonreducing conditions, the D8 protein mostly exists as a tetramer, but also as octamers and dimers. Oligomerization is mediated through the C-terminal region of its ectodomain (Matho et al., 2012). The M083 construct that was used in this work included the whole ectodomain, but since it was exclusively analyzed under reducing conditions, a possible multimeric state in MYXV could not be determined.

The D8L VACV protein homologous to M083 has been identified as a highly antigenic determinant, that elicits an intense and consistent immune response in human and mice (Davies et al., 2005; Frey et al., 2021). It is also a relevant target for neutralizing antibodies, and the administration of this a D8L DNA plasmid as part of polyvalent subunit vaccine is able to improve the immune response against lethal OTPV challenge (Sakhatskyy et al., 2006). D8L has a role in VACV's infectivity in cell culture and is responsible for IMVs binding to cell surface CS (Hsiao et al., 1999; Pokorny et al., 2024).

Although the recombinant M083 protein was produced in a prokaryotic expression system it is not likely that the lack of reactivity with the hyperimmune positive anti-MYXV sera in the Western blot analysis or the dot-blot assay, is due to lack of key posttranslational modifications that affect its antigenicity. In fact, D8L produced in *E.coli* is effectively used as part of multisubunit vaccine composed of A27L and D8L, and B5R VACV proteins in mice (Berhanu et al., 2008). Overall, our results indicated that the recombinant M083 protein is not a relevant antigen in MYXV, and therefore it was dismissed for developing the DIVA system.

The additional membrane of EEV particles provides additional viral components that enhance resistance to neutralization. Neutralizing antibodies that target VACV EEV-specific proteins, such as B5 and A33, that can neutralize the virus in cooperation to the complement system (Law & Smith, 2001; Meseda et al., 2013). But F13, the putative homologous to M022, which is located in the inner side of the CEV- and EEV-membranes was not identified as target of antibody recognition or neutralizing activity even though it is the most abundant protein of these virions (Duke-Cohan et al., 2009; Hirt et al., 1986; Schmutz et al., 1995).

F13L is a target for some antiviral compounds (Kato et al., 1969; G. Yang et al., 2005). IMCBH and ST-246 are two compounds with divergent chemical structure with antiviral activity that target a highly conserved region of F13L in orthopoxvirus. ST-246 was approved by the FDA for human oral treatment of smallpox disease and is commercially available under the name Tecovirimat (TPOXX®) (Hoy, 2018). The target sequence of these two specific drugs is only slightly conserved in the F13L orthologue in MYXV, M022L. In fact, the degree of divergence between the putative homologous is sufficient for ST-246 to be ineffective against MYXV (G. McFadden, Personal communication, 2009). This low conservation between homologous proteins across different poxviruses could partially explain the discrepancies observed between studies on the antigenicity of these proteins and our findings on M022.

The recombinant M022 protein (expressed as a fusion protein with GST) showed a differential recognition by the hyperimmune PC sera in Western blot versus dot blot assays. The protein showed minimal specific reactivity in Western blot, whereas it was highly reactive in the dot-blot assay. This difference underscores the importance of the native or partially folded state of the M022 protein in immune recognition, indicating a higher relevance of conformational epitopes over linear ones.

The second viral protein candidate in showing a highly antigenic profile was M115, which displayed a high sensibility in both analytic assays, Western blot and dot-blot. This result strongly agrees with those described in other poxviruses such as VACV, buffalopoxvirus, or capripoxvirus (A. Kumar et al., 2015; Pütz et al., 2006). M115's homolog, A27L, is highly conserved among orthopoxviruses, suggesting that this protein performs essential functions for the virus's biology and survival (Rodriguez et al., 1985). A27 oligomerizes in non-reducing conditions, forming trimers and higher-order structures that enhance its stability and immunogenicity (Dashprakash et al., 2019). This oligomerization is driven by hydrophobic and ionic interactions rather than disulfide bonds (Rodriguez et al., 1993; Vázquez & Esteban, 1999). The ability to elicit neutralizing antibodies and induce strong immune protection depends significantly on maintaining the native oligomeric state of the protein (Lai et al., 1990, 1991). Immunization with A27L induces neutralizing antibodies and provides protection against VACV challenge (Demkowicz et al., 1992).

Despite the significant challenges encountered with the expression and solubility of the MYXV M071 protein produced through various heterologous expression systems, its potential as a key antigen justified all the (unsuccessful) efforts invested in optimizing the conditions for its production, since achieving high yields of soluble M071 protein was crucial for characterizing its

antigenicity and for its possible application in diagnostic assays. In fact, the cELISA used as the routine serological test in the OIE reference laboratory for myxomatosis employs a monoclonal antibody specifically targeting the M071 protein (OIE, 2018).

Its putative homologous, H3L is a VACV immunodominant antibody target in mice and human humoral immune response, and a major target for the neutralizing antibody response (Benhnia et al., 2008), that also induces T-cell immune responses (Ostrout et al., 2007). Anti-H3L response can neutralize VACV *in vitro* infection and provide partial protection from lethal challenges *in vivo* (Davies et al., 2005; Demkowicz et al., 1992).

We were unable to purify soluble recombinant M071 produced in bacteria, or full-length M71 produced in the BEVS. Besides that, the study of its antigenicity using a heterologous sample containing denatured M071 protein did not demonstrate specific anti-M071 reactivity with the PC sera in Western blot or dot-blot. However, its antigenic potential was confirmed when the full-length M071 recombinant protein was expressed in RK13 cells through transfection. These results align with all those previously mentioned, that were reported for other poxviruses, further validating the use of M071 in serological diagnostics.

Transient expression of these recombinant proteins in mammalian cells, specifically in the rabbit cell line RK13, was done for analytical purposes, and not to yield high protein production. The IF staining of transfected cells revealed that M022, M071 and M115 were correctly expressed within the host cell and had a conformation antigenically equivalent to the native viral proteins, since the three proteins were reactive to a seropositive anti-MYXV control. Given that the three proteins were detected in the transfected cultures, confocal microscopy could provide relevant information in the future. For instance, determining their exact location in a virus-free system, allowing to compare its location in a culture infected with MYXV and transfected with the recombinant proteins.

Like in other poxvirus, inactive vaccines are not able to protect the host against a lethal MYXV infection (F. Fenner & Ratcliffe, 1965). The induction of an antigen-specific humoral immune response, or the passive immunization through the administration of high titers of neutralizing antibodies to myxoma virus, are not enough to efficiently provide complete protection to rabbits upon challenge (Adams et al., 2004; F. Fenner & Marshall, 1954). The large array of immunomodulatory mechanisms that MYXV displays, manifests the complexity of the host-pathogen interactions that take place in a natural infection (Jeklova et al., 2008b; Nash, Barrett, Cao, et al., 1999). Live vaccines are the only ones that have proven to be effective in providing rabbits with a full protection from myxomatosis and thus, commercially available. They are

divided into two groups, the first one consists of heterologous vaccines based on the antigenically related leporipoxvirus SFV, and the second one consists of homologous attenuated MYXV. Although heterologous vaccines provide cross-protection against MYXV, they induce a limited or short-term protective immunity (P. Fenner & Woodroofe, 1954; Willer et al., 1999). Homologous vaccines induce a stronger protective immune response but may cause cutaneous lesions and side effects on young rabbits or immunosuppressed animals (McKercher & Saito, 1964; Saito et al., 1964b). SFV vaccination, despite being less effective than homologous vaccines, is still regularly applied as the first shot in rabbit farms and pets, followed by a boost with the homologous vaccines (Marlier et al., 2000).

Maternal antibodies that have been passively transferred to kittens remain detectable up to 6 to 9 weeks after birth and have a relevant role in maintaining high immunity levels within wild rabbit populations. (F. Fenner & Marshall, 1954; P. J. Kerr, 1997). The exposure to MYXV in wild young rabbits that are still protected by maternal antibodies induces milder clinical signs and boosts their immune system (Marchandeau et al., 2014).

Poxvirus infections are characterized by significant individual variability in clinical outcomes and immune responses. Differences in the activation of the adaptive immune response such as the generation of T cell immunity and the neutralization antibodies can generate heterogeneous outcomes. Besides the physiological status and genetic factors intrinsically determined by the host, and its previous exposure to the virus (immune status), vaccine formulations and the administration routes used in vaccination can influence the intensity of the humoral response and the serologic response kinetics (Arenas et al., 2012). The administration of the homologous vaccine intradermally in farm animals results in higher seroconversion rates compared to subcutaneous administration. This enhanced humoral response could be likely due to the tighter and more efficient interaction between the delivered antigen and the antigen-presenting cells located in the dermis (Dalton et al., 2015; Levin et al., 2015; Manev et al., 2018). In contrast, no differences were found between the serological response induced between the two administration systems in healthy seronegative rabbits. Care must be taken for a proper handling and use of the vaccination device (Dermojet®), to avoid variability on the serological response when using the intradermal route (Alfonso & Pagés-Mantè, 2003).

Seroconversion rates in vaccination campaigns involving wild rabbits are highly variable from 69% (Calvete et al., 2005), 81% (Cabezas et al., 2006) for subcutaneous administration of a heterologous vaccine, and 72.7% or 97.2% for intradermal administration of a homologous vaccine or a bivalent vaccine, respectively (Arenas et al., 2012). When vaccination is performed

in field conditions, several immune-depressing factors involved in these vaccination process, such as the capture, handling, and quarantine of wild rabbits, could negatively affect the immune response triggered upon vaccination (Calvete et al., 2004). Vaccination of immunocompetent animals might not completely prevent the infection pathogenesis against a highly virulent MYXV strain (Kritas et al., 2008).

The OIE reference laboratory routinely employs a competition ELISA (cELISA) for diagnosing myxomatosis, utilizing a monoclonal antibody targeting the M071 protein. Reagents for this test are available upon request from the laboratory (OIE, 2018). Additionally, veterinarians have access to a commercial iELISA test (INgezim Mixomatosis R.17.MIX.K1t, Ingenasa), which have a good diagnostic performance (98% sensitivity and > 99% specificity) that can be used in the success evaluation of the humoral responses induced on farm rabbits during the vaccination campaigns.

Moreover, rabbits that survive the disease develop detectable antibodies, complicating the differentiation between infected and vaccinated farmed rabbits, since both groups may test positive in serologic assays (Marlier et al., 1999). In this context, the discrimination can be done at the genomic level through the identification of genetic markers by a PCR strategy (Cavadini et al., 2010). While this method is highly sensitive and gives evidence of active infections, the extraction and isolation of DNA is usually a more invasive process since it requires biologic and tissue samples. The development of a differentiating infected from vaccinated animals (DIVA) test are often considered for serologic diagnostic tests (Barros et al., 2009).

The antigenic screening in ELISA of the virulent Lu strain and the homologous MYXV vaccine strain (VacB) displayed good consistency. Since this was observed across all dilutions, the absence of relevant differences in binding affinity of the rabbit serums between the two MYXV strains was not due to limitations in the assay's analytical sensitivity. The high reactivity of the hyperimmune serum with both strains indicated the presence of conserved epitopes highly immunogenic in both strains, or the presence of a broad-specific and redundant humoral response. This justified the use of either strain as the coating antigen, ensuring a versatile tool for detecting antibodies against MYXV.

Using complete MYXV particles as antigen in the iELISA presents certain manufacturing complexities associated with the scale-up process of production. For the generation of infectious viruses, specific facilities, culture media and specifically trained laboratory personnel are required, which increases the cost of production. Constant viral replication may also introduce certain variability of the different virus batches; therefore, it is relevant to maintain control of

verification of the homogeneity of the stock. Culturing and handling infectious virus also inevitably pose biosafety risks to the personnel and the workplace. To mitigate this risk, we tested the effect of thermal inactivating the virus at 60°C. The use of the heat inactivated MYXV-Lu as antigen for the iELISA test resulted in a dramatic decrease in the $OD_{450\ nm}$ values. Although the protocol could have been re-optimized and adjusted to the inactivated MYXV, the fact that more than half of the reactivity was lost, revealed the high relevance of conformational epitopes in the elicitation of specific anti-MYXV antibodies.

The use of recombinant viral proteins as coating agents in indirect ELISA tests is an alternative for eliminating the biosafety risks and facilitating the manufacturing process. It has been explored for the antibody detection in various poxvirus diseases, although not for MYXV. The IMV is the most stable and predominant form of poxviruses, considered to play a crucial role in transmission between hosts. Surface proteins of the IMV are directly exposed to the host immune system and are targets of neutralizing antibodies. Hence, they are commonly used as antigens in the development of immunoassays. However, core proteins (Hermanson et al., 2012) or EEV proteins (Berguido et al., 2022; Fogg et al., 2004; García et al., 2007) have also been screened for using them as coating antigens in iELISAs. The use of proteins orthologous to M071 (VACV H3L) and M115 (VACV A27) proteins, two of the candidates that were proposed for serology in MYXV, has been extensively studied among all viral proteins. For instance, the homologous gene of the M071 protein has been completely of partially expressed for being used in the serologic diagnosis of capripoxvirus, and displayed a good sensitivity in iELISA, although its full-length expression in prokaryotic cells was difficult and showed low stability (Carn et al., 1994; Heine et al., 1999). In this regard, strategies that improved its manufacture like using antigenic synthetic peptides or truncated recombinant M071 homologous of capripoxvirus, also showed high Se and Sp for the detection of anti-GTPV and SPPV (Tian et al., 2010; Venkatesan et al., 2018). Building on the evidence presented and the current use of a monoclonal antibody against MYXV M071 in the reference cELISA test, M071 stands out as a promising candidate for future serological diagnosis of myxomatosis. Its potential for improving diagnostic accuracy makes it highly suitable for inclusion in future screening tests.

The homologous genes of VACV A27 (MYXV M115) capripoxvirus and buffalopoxvirus have been used as coating antigens in the developing of their corresponding iELISAs. The iELISA developed using the A27 homologous, ORF117 in goatpox virus (GTPV), showed a 98.5% Se and 88.7% Sp compared to the gold-standard technique, for samples from both sheep and goat specimens (Dashprakash et al., 2015, 2019). The homologous A27L protein of buffalopox virus also displayed high specificity but the iELISA was not further validated (A. Kumar et al., 2015).

Additionally, the A27 of capripoxvirus was used in an antigen capture, or "sandwich" ELISA developed for the genus-specific detection of up to 11 different orthopoxvirus (OPXV) isolates, pathogenic to humans (Stern et al., 2016). The second candidate for developing the sandwich ELISA was the homologous of VACV D8 (MYXV M083), which sharply contrasts with the lack of immunogenic ability of the M083 protein in MYXV suggested by the results presented in this thesis. However, screening of antigenic candidates in VACV revealed that D8L offered the best sensitivity and specificity for monitoring the antibody responses in vaccination against smallpox (Hermanson et al., 2012).

For MYXV, indirect ELISAs that were developed to address the persistence of antibodies to MYXV in wild rabbit populations, as well as the seroconversion on vaccinated animals, use whole MYXV particles as coating antigens (Gelfi et al., 1999; P. J. Kerr, 1997). To explore a new approach, an indirect ELISA was developed using the antigen(s) selected from the initial proposed candidates: M022, M029, M071, M083, M115, and M141. The recombinant proteins that could not be successfully expressed or purified in their native form (M029, M071, M141), were discarded. Whereas those that were purified under native conditions, M022, M083 and M115, were further tested to analyze their antigenic properties. The exploration for linear and conformational antigenic epitopes revealed that only the recombinant proteins M022 and M115 displayed specific reactivities with the control sera. Notably, M022 is associated with the EEV, and M115 with the IMV particle. This involuntarily fact could indeed provide a wider understanding of the humoral response against MYXV infections.

Despite the existence of commonly recognized viral antigens, the immune response to poxviruses stands out for its inherent complexity and variability at an individual level (Duke-Cohan et al., 2009). Some poxviral antigens are more frequently recognized by the immune system of the hosts, which may be attributed to the intrinsic properties of the protein and the way it is exposed to the immune system. A differential pattern of reactivity was even found in some VACV antigens for distinguishing primary and secondary responses to vaccination with Dryvax (Hermanson et al., 2012). Even if the same antigens are recognized by the immune system, the strength or effectiveness of the humoral response can differ from one subject to another, due to diverse factors like main individual differences in their genetic background and immune system, amongst others. This variability was evident when the results obtained for the same serum, analyzed by the three iELISA systems, where the anti-M022, anti-M115 and anti-MYXV antibody responses, were compared amongst them.

Control serum samples would preferably be obtained from individual animals (Jacobson, 1998), but looking into the individual variability in antibody responses to MYXV, and specifically in this situation where one single viral protein would be the antigen, 9 high-titered samples from seropositive animals was pooled and used as the positive control (PC) serum to assure a representative level of anti-rM022 and anti-M115 antibodies. The negative control (NC) was a rabbit serum purchased from Invitrogen.

Using the MYXV M022 protein as an antigen for the development of serological tests is unprecedented. Despite several EEV-specific proteins having been screened for their use in iELISA, no proteins homologous to M022 (VACV F13L) have previously been used in diagnostic tests, or even be targets of antibody recognition (Duke-Cohan et al., 2009; García et al., 2007). In fact, F13L is only recognized after vaccination on 32.6% and 35.3% of the VACV naïve individuals (Hermanson et al., 2012). This introduced an additional contribution to the field and offered an opportunity for novel approach in the detection of specific immune responses to poxviruses, and MYXV in particular.

The optimization of the iELISA-rM022 and iELISA-rM115 was straightforward, and relatively low amounts of protein were needed for an efficient differential reactivity with the PC and NC sera: 1 µg/ml for M022, and 250 ng/ml for M115. The reactivity of saturating concentration of GST alone was studied to identify potential non-specific interactions of this fusion tag with any of the antibodies present in the rabbit sera. The results showed that the reactivity observed in the iELISA-rM022 belonged to anti-M022 interactions with the viral antigen, discarding any potential interference due to the GST tag. The amount of M115 used for the plate coating was four times less than M022, indicating a higher antigenicity power, in agreement with the results that were obtained in the Western blot, and the dot-blot analysis.

Regarding the reproducibility of the assays, the variability within-run in iELISA-rM022 analysis for the control sera showed an accurate precision within PC replicates and good precision for the NC measurements, as well as the inter-plate variability (CV% of 2.18% for the PC and 9.10% for the NC). The iELISA-rM115 also displayed a good intra-plate precision for both PC and NC measurements and thus, and an acceptable inter-plate variability (CV% of 14.87% for the PC, and 9.02% for the NC). The low variability on the P/N ratio values across different runs indicated a robust diagnostic behavior for both tests: the CV% for the iELISA-rM022 was 7.22%, and for the iELISA-rM115 was 5.64%.

The consistent results given by the M022-coated plates after one month of storage showed slightly better stability of the antigen, over the M115 protein. The analysis of PC serum with the

iELISA-rM115 showed lower OD_{450} readings already one week after coating the plate and subsequent storing, however the although the variability of PC measurements was high, the discriminatory power of the test, given by the P/N rate had an acceptable CV% value of 14.98%. The loss of M115 reactivity with the PC might be a consequence of loss of some conformational epitopes, but it seemed to maintain its integrity over time. In contrast, the analysis of PC on the iELISA-rM022 assay showed higher consistency of this measurements across the time points, with a good precision of 8.59% CV%. In fact, the P/N ratio even increased over time, suggesting an improvement of the test sensitivity.

Upon the independent optimization of the iELISA protocols, each serological test was validated was defined by different sensibility and specificity values, that were used for the analysis of a total of 259 sera samples obtained from 3 different panels. Each panel contained sera samples collected from animals subjected to specific and controlled experimental conditions. Panels 1 and 2 were obtained from a vaccination and challenge experiment, in which rabbits were vaccinated against myxomatosis using a homologous MYXV vaccine, either subcutaneously (SC) or intradermally (ID). Both panels also contained sera obtained from NV animals, that were not vaccinated but were challenged, but while rabbits in panel 1 were animals individually selected from a farm, that were relocated to laboratory conditions to take part on a challenge experiment, sera from panel 2 were obtained from experimental rabbits that were kept in a confined and controlled conditions from the beginning. On the other hand, the totality of samples from panel 3 were collected from naïve or non-vaccinated rabbits. Within this heterogenicity, the fact that samples were obtained from experimental rabbits allowed the control and reduction of variability related to environmental factors, and to have a tighter control over their health status. However, it is worth noting that these conditions fail to replicate the natural vaccination events or the exposure to pathogens, potentially skewing the results when applied in real-world scenarios.

The sera samples were analyzed using the commercial INgezim ELISA test and categorized into positives or negatives for the presence of anti-MYXV antibodies. This serological test was chosen as the gold-standard due to its accessibility and practicality for performing routinary serological diagnostics. In addition, its good diagnostic sensitivity (98%) and specificity (>99%) values provided certain reliability to its power of discrimination true positives from negative cases. While 188 sera (128 from panel 1 and 60 from panel 2) were used in the validation of the optimized *in house* iELISA-Lu, all 259 sera were analyzed as one large panel during the validation of the optimized iELISA based on the recombinant proteins (iELISA-M022 and iELISA-M115).

Selecting an optimal cut-off point for the diagnostic tests was a critical stage, as it directly impacts the diagnostic sensitivity (DSe), specificity (DSp), and overall clinical relevance. The Receiver Operating Characeteristic (ROC) analysis is a powerful tool to assess and optimize the performance of a binary classification model or test. It indicates the ability of the test to discriminate between two groups by evaluating the compensation between correct identification of true positives) and DSp (correct identification of true negatives) at every possible decision threshold. The area under the curve (AUC) of a classifier indicates the discriminatory power of the model and comprises values between 0 and 1. An AUC value of 0.5 indicates that the model has no discriminatory power, and the true positive rate (DSe) is equal to the false positive rate (1-Sp) at all thresholds. An AUC < 0.5 suggests that the test performs worse than random chance, while an AUC > 0.5 indicates that the test has some discriminatory power, with its performance improving as the value approaches 1.

The %ROD cut-off for the in-house iELISA-Lu test obtained by analyzing the data resulting from testing the 188 rabbit sera samples with this test, was 25.28%. The ROC analysis of the in house iELISA-Lu test demonstrated excellent discriminatory power, as evidenced by the AUC value of 0.9816. Using a threshold or cut-off value of 25.28% ROD, the test achieved a DSe of 92.25% and a DSp of 93.22%. While these values indicated a good performance and underscored the iELISA-Lu test reliability, they were far from the DSe 98% and DSp >99% achieved by the gold-standard commercial iELISA. However, the detection of the heterogeneous spectra of anti-MYXV antibodies in rabbit sera revealed several discrepancies between the outcomes of both tests. Notably, the majority of the misclassified sera were obtained from SC vaccinated rabbits: 10 samples had an %ROD below the threshold (FN), while other 3 sera showed higher anti-MYXV reactivity (FP) than when analyzed with the reference commercial iELISA test.

The ROC analysis showed an overall outstanding performance for the iELISA's based on the viral recombinant proteins (iELISA-rM022 and iELISA-rM115), with AUC values > 0.9. High AUC indicated a great ability of both tests to distinguish between positive and negative cases across the possible threshold values. The threshold value was set maximizing Youden's Index, which provides the best balance that the test can give between DSe and DSp. The cut-off for the iELISA-rM022 test was set at -0.895% ROD, giving a DSe of 90.97% and a DSp of 83.65%; and the cut-off value for the iELISA-rM115 was set at -0.559% ROD, giving a DSe of 96.77% and DSp of 75%.

The negative sign of both values determined as the %ROD cut-off indicated that samples would be classified as negative when their OD_{450nm} was below that of the negative control. Unlike in this situation, it is not usual that the NC gives higher OD values than the main negative serum

samples. The fact that a commercial rabbit serum was chosen to be used as the NC for the optimization of the recombinant iELISAs aimed to guarantee a standardized and batch-tested and validated sample, which could give assurance of specificity. Its higher background or baseline value would probably be due to the presence of an overall higher level of endogenous antibodies or different composition (presence of additives, stabilizers, etc? is heat inactivated?). Since the commercial NC did not contain antibodies against MYXV, it still represented a true negative response.

The re-classification of samples from the panel of 259 sera was based on the outcomes obtained through the analysis with iELISA-rM022 or iELISA-rM115. This allowed for the comparison of the discrimination performance of both iELISA tests against the "true" classification of samples determined by the "gold-standard" test used in this analysis (the commercial iELISA test). iELISA-rM022 showed a PPV of 89.24% and a NPV of 86.14%, and the iELISA-rM115 showed a PPV of 85.23% and a NPV of 93.98%, altogether indicating a good reliability on the diagnostic outcomes.

The iELISA-rM115 only had 5 false negative counts, but up to 26 false positives, indicating that although it has an excellent sensibility and efficiently recognizes the true positives, the high rate of false positives would not be suitable to fully replace a commercial ELISA. Although the PPV (85.23%) could give confidence that most positive results would be actually true positives, due to the moderate DSp (75%), animals without specific humoral response to MYXV, or without the infection could have positive anti-M115 outcomes. The routinary use of iELISA-rM115 would need follow-up testing to confirm positive results and to ensure accurate diagnosis. This test displayed a substantial degree of agreement with the test outcomes obtained by the reference iELISA (kappa value = 0.742 ± 0.043), indicating that both tests have similar classification power.

However, in the context of a DIVA serologic test, the iELISA-rM115 test could ensure the effective identification of infected animals and that negative outcomes would be reliable, regarding its excellent DSe (96.77%) and high NPV (93.98%), respectively. A test with high sensitivity would be crucial for preventing spread, ensuring that infected animals are not missed. In addition, a high NPV indicated that the iELISA-rM115 test would confidently assume that rabbits testing negative would be indeed free of infection. However, the moderate DSp of the test indicated a high rate of false positives (around 25% of vaccinated animals could be incorrectly identified as infected). While not ideal, the trade-off of having moderate specificity and some false positives and efficiently identifying the infected animals was considered acceptable, as the overall reliability of negative results ensures that the test is suitable for controlling the infection in a population. Regarding the test diagnostic performance, the iELISA-

rM115 test had certain usefulness in confirming the disease (LR+ of 3.87) but could provide high confidence in the negative results (LR- of 0.081). The agreement κ value

The total positive and negative counts with the iELISA-rM022 were close to the "true counts", but at the individual level, a total of 31 samples had discordant outcomes to those of the gold standard: 14 false negatives and 17 false positives. The moderate DSp (83.65%) of the test could be a limitation for its implementation as a substitution of a typical commercial ELISA test, since it displayed a higher rate of false positives. Nevertheless, the test shows high DSe of 90.97%, which indicated that most vaccinated/infected animals would be correctly identified, minimizing false negatives. The PPV of 89.24% and NPV of 86.14%, although were not the highest, showed acceptable predictive values, indicating that both positive and negative results would be generally reliable. On top of that, the likelihood ratios from the iELISA-rM022 test demonstrated a moderate positive diagnostic performance (LR+ of 5.565) that indicated that while a positive test result increases the probability of disease, it does not absolutely confirm it. Conversely, the test exhibited good negative diagnostic performance (LR- of 0.1092), where a negative outcome would significantly reduce the likelihood of the disease. The iELISA-rM022 test displayed a substantial degree of agreement with the reference iELISA test (kappa value = 0.75 ± 0.042), indicating that both tests have similar classification power. Although this test did not perfectly match the performance of the commercial ELISA test, given its high sensitivity and PPV, the test ensured that rabbits with M022-specific immune response are correctly identified as positives, while positive test results would indeed be reliable indicators of exposure. The iELISA-rM022 test could be valuable for assessing vaccination success in farm rabbits, or seroprevalence in wild rabbits, as long as its trade off in potentially overestimating the positivity. Results will need to be interpreted carefully and the use of complementary methods might be necessary to validate the findings.

Although the antibody titre is an indicative parameter of the humoral immune response to myxomatosis, seroconversion of rabbits does not always guarantee an efficient immune protection to myxomatosis (Marlier et al., 2000). The presence of antibodies against MYXV could indicate an activation of the immune system upon vaccination, but ultimately, cellular immunity and neutralizing antibodies would be primary responsible for the effective clearance of the virus and protection towards future infections (Panchanathan et al., 2008; P. J. Kerr, 2012). The only reliable method to assess the efficacy of a vaccine is to challenge the immunized rabbit with a virulent MYXV strain.

Sera samples from panel 1 were collected from rabbits that participated in a challenge experiment. Initially, 77 animals from a rabbit farm were serologically screened, including those that had been vaccinated either ID or SC, as well as some that were not vaccinated. Out of the total, 34 rabbits were selected to participate in the experiment where they were infected with a virulent MYXV strain under controlled laboratory conditions. Among these, only 2 rabbits were vaccinated ID, 23 rabbits were vaccinated SC, and the remaining 8 were NV. The fact that the majority were SC was intentional, based on prior evidence which found less robust seroconversion associated with this administration route (Dalton et al., 2015). The selection of a wide representation of these subjects was meant to clarify and obtain a more accurate description of those findings.

Previous studies reported no correlation between pre-challenge antibody titers and the intensity of clinical signs or mortality following a viral challenge (Marlier et al., 2000). In order to further explore this, available survival data at the end of the experiment were used to analyze a possible correlation between the reactivity of specific antibodies, such as anti-M022 and anti-M115, in the 34 sera samples obtained before a challenge with MYXV, and the survival outcomes.

While only two rabbits were ID vaccinated, both of them developed a high anti-M022 response prior to challenge and the 100% survived the infection with the virulent MYXV. These consistent and positive outcomes of the ID vaccination align with previous findings that suggest that ID administration may lead to better antigen presentation and more effective immune response. In contrast, the anti-M115 response was more heterogeneous, since one of the rabbits showed a high intensity response while the other barely surpassed the %ROD threshold level. SC vaccination displayed a less consistent survival rate of only 43.47%, and heterogeneous anti-M022 and anti-M115 responses. Overall, the control group constituted by NV rabbits exhibited low anti-M022 and anti-M115 immune response (% ROD values in the iELISA-rM022) prior to the virus challenge and did not survive. Two NV samples tested positive, though they were very close to the threshold, indicating marginal M115 reactivity.

The ROC analysis using the iELISA-rM115 test results and the survival outcome of the rabbits (if they were protected or non-protected against the challenge with MYXV) performed with 83.33% DSe and 72.73% DSp at a cut-off of 0.082 % ROD. The test minimizes the risk of false negatives, which in the context of vaccination controls could help to reduce the economic and logistical resources destined for revaccination animals that are already protected. However, the rate of false positives obtained from this analysis is considerable, and the fact that non-protected

animals could be classified as protected (due to the presence of sufficient anti-M115 reactivity) could lead to them being mistakenly considered safe when it will not be the case.

By comparison, the iELISA-rM022 analysis showed a perfect discriminating ability between the two outcomes (AUC of 1), achieving 100% DSe and 100% DSp values when the threshold was set at 2.074 % ROD. This indicated that the anti-M022 reactivity of rabbit sera, measured prior to an imminent MYXV challenge, could completely distinguish between animals that would survive such challenge (showing test results above 2.074 % ROD), and those that will not (showing results below 2.074 % ROD). Monitoring anti-M022 antibody levels with the iELISA-rM022 test analysis could help to assess the protection level acquired after vaccination, and to evaluate the risk of mortality in case those rabbits would be exposed to the virus.

The reliability of this result can be debated due to the small number of samples used in the ROC analysis, which were the only available ones at the time. But in essence, these preliminary findings demonstrated that the intensity of the anti-M022 immune response on rabbit sera are an accurate predictor of survival following viral challenge. However, the homologous of M022 protein in VACV, F13L, has not been shown to elicit neutralizing antibodies, which has been attributed to its inner location within the virus particle (Ahsendorf et al., 2022; Demkowicz et al., 1992). Considering the results presented above, regarding that anti-M022 reactivity can predict the outcome upon infection with MYXV, it would be reasonable to evaluate the neutralizing capacity of the anti-M022 in the future. Moreover, the strong correlation between the F13L-specific antibody response intensity and enhanced antibody-dependent cellular cytotoxicity (ADCC) responses suggested that F13L could play a critical role in the stimulation of the cellular immune response (Frey et al., 2021). Notably, this correlation was only observed in subjects vaccinated intradermally, which emphasizes the individual variability in immune responses depending on the administration route, consistent with previous results.

This preliminary results regarding the measurement of anti-M022 response could lead the way for conducting broader immunological profiling of MYXV with the aim to identify other potential correlates of protection. Besides that, considering that the cellular immune response to MYXV has not been characterized, it could be relevant to conduct the corresponding assays for assessing T cell responses (CTL) and their correlation with survival outcomes.

Analyzing hare sera with a diagnostic test originally designed for rabbits, was done to assess particularly cross-reactivity with ha-MYXV, since it is a pathogen antigenically related to MYXV affecting both rabbits and hares. This approach aimed to determine whether antibodies in hare sera could recognize and react to MYXV antigens, similar to those targeted in rabbits. Conducting

such analyses could shed light on shared immune responses against the same pathogen across closely related species.

The immune condition of the animals from which the 20 hare sera were obtained was not documented, so they first were categorized using the commercial iELISA (gold-standard) into positive and negative groups depending on the detection of antibodies against the MYXV. The restricted number and volume of hare sera samples imposed significant constraints on the ability to conduct extensive characterization and optimization of the iELISA tests specific to these samples. The 20 hare sera samples were therefore analyzed using the iELISA-rM022 and iELISA-rM115 tests using the same protocol optimized for rabbit sera samples. The correlation analysis showed a statistically significant positive monotonic relationship between the results obtained from both tests. On average, the M022-specific reactivity was slightly higher than the M115-specific reactivity, but at the individual level there was no evident bias towards any of the two tests. The 11 hare sera categorized as negative by the commercial iELISA, showed high agreement between the two recombinant iELISA tests. Two of the negative samples had % ROD values minimally above the threshold reactivity determined for the iELISA-rM022 test, which would make them to be considered positive for the anti-M022 response if the same criteria would be applied for hare samples. On the other hand, the results of the screening showed a consistent and robust categorization of the 9 positive hare samples by both tests. Although the intensity of the antigen-specific responses was heterogeneous in these positive samples, no systematic bias was identified between the two tests. Again, this underscored the relevance of individual immune response variability against poxviruses.

The results obtained from these preliminary screenings established an exploratory baseline for future studies with more extensive samples and known animal conditions. Besides offering critical insights into the cross-species prevalence of the disease and potentially guiding towards the enhancement of diagnostic methods. Indeed, results obtained from these analyses could represent a significant step in understanding interspecies immunity and diagnostic test applicability.

A safe and effective viral vaccine against myxomatosis should induce both adaptive immune responses effectively, inducing neutralizing antibodies to prevent the spread of infectious particles, and additionally, the activation of cytotoxic T-cells that can perform an antigen-specific CTL response and kill virus-infected cells at early infection times, preventing its amplification and spread.

Immunization with inactivated virus might result in a rise of antibody levels due to the high immunogenicity of IMV proteins, but even when some anti-IMV neutralizing antibodies are present, immune protection to an infectious challenge is not guaranteed (Appleyard et al., 1971; Boulter, 1969). Neutralizing anti-EEV titers developed during a life VACV immunization are lower than anti-IMV titers; however, they presumably have a more critical role upon virus challenge, in preventing the spread of infection. B5R is the EEV protein that makes the largest contribution to EEV-neutralization (Law & Smith, 2001; Payne, 1980). Removal of this protein altered the sensitivity of the VACV to anti-EEV neutralizing activity, but gene knockouts targeting immune components responsible for EEV neutralization did not interfere with the protective effectiveness of a VACV vaccine strain in a mouse challenge model (Meseda et al., 2013).

Some of the homologous vaccines are MYXV strains that were attenuated on the lab by the loss of several immunomodulatory and virulence genes during serial passage in cell culture (Cavadini et al., 2010). The development of homologous live attenuated MYXV vaccines with targeted site-directed deletions of virulence genes has been contemplated for providing "safer" immunogenic conditions and reducing the side effects on immunocompromised or juvenile subjects. Deletions of MYXV host range genes have been successfully deleted in the reference Lu-MYXV strain, such as M-T5, M128L, M141R, Serp-3, M150R, M153R, M13L (reviewed in (Stanford et al., 2007). The resulting mutants did not suffer any reduction in the *in vitro* replication levels in rabbit fibroblasts, although some showed a restricted replication in lymphocytes. Overall, these mutants showed an attenuated replication profile *in vivo.*

In addition to these strains, deletions of other virulence genes have been performed on an attenuated MYXV strain. For instance, a triple M007L, M010L and M011L gene knock-out was carried out in the attenuated Ur strain. Immunization with this mutant resulted in minimal clinical signs of disease, mainly at the inoculation site, while inducing a consistent immune response that protected adult and young rabbits from lethal challenge (Adams, Van Leeuwen, & Kerr, 2008).

M141R is a virulence factor that mimics the CD200 cellular protein and ligates to CD200 receptor (CD200R), which is expressed in the myeloid-lineage cells such as monocytes, macrophages, and dendritic cells (Cameron et al., 1999). Although M141R is not essential for MYXV replication, it is an element obviously involved in the pathogenesis of virulent MYXV strains. M141 is localized in the MYXV virions, and it is expressed in the surface of host cells early during infection, at 1 hpi. M141R interaction with the CD200R molecule in the surface of myeloid-lineage cells, such as macrophages, initiates a signaling cascade that inhibits the polarization into their pro-

inflammatory M1 phenotype, by blocking the NF-κB pathway (Zhang et al., 2009). This inhibition strategy prevents the transcription of inflammatory factors such as inducible nitric oxide synthase (iNOS), which downregulates the localized production of nitric oxide (NO), a relevant proinflammatory and virotoxic agent (Yu et al., 2022). MYXV mutant lacking this gene displayed the same replication kinetic but had an attenuated disease profile *in vivo*. Rabbits infected with this virus exhibited higher activation of the immune system in the local lymph node, involving a greater antigen presentation, and an increased activation of macrophages and T lymphocytes, and production of IFN-γ (Cameron et al., 2005).

Finally, two approaches have been developed regarding the "conscious" design of live attenuated MYXV vaccines, regarding their transmissibility. On one hand, a host-range defective vaccine unable to replicate in rabbit cells, due to a deletion of the M063L gene, was designed to avoid unwanted or accidental transmissions (Adams et al., 2008b). The M029L gene encodes a E3-like dsRNA binding protein (homologous to E3 VACV) that antagonizes innate immune signaling pathways triggered in response to viral dsRNA, such as the activation of the IFN-induced dsRNA dependent protein kinase (PKR), or the type I IFN antiviral response (Rahman & McFadden, 2017). A MYXV mutant lacking M029L is unable to efficiently replicate and spread *in vitro* and *in vivo* (Rahman et al., 2013). The deletion of this host range gene results in a highly attenuated strain which could make it a suitable candidate for a safer vaccine. However, challenge experiments with wildtype MYXV on rabbits vaccinated with these mutants suggested a trade-off between safety of the vaccine, and long-term protection. The attenuated profile of these mutants facilitates rapid clearance of the infection at the primary inoculation site, potentially too soon to fully engage the acquired immune responses. The second approach is focused on the development of transmissible vaccines, to promote immunization of uninoculated animals by contact or a vector-mediated process (Bárcena, Morales, et al., 2000).

As poxviruses can be used as vaccine vectors, an attenuated MYXV strain was used as parental genomic background for the generation of a recombinant virus expressing the VP60 gene of RHDV1 in the MGF/M11L locus by homologous recombination (Spibey et al., 2012). Deletion of these two genes arranged in tandem, which in fact, are MYXV virulence factors, results in a safer profile for the recombinant MYXV (Graham et al., 1992; Opgenorth et al., 1992). The high attenuation of the VP60-vectored MYXV vaccine restricts its spread within the host and its dissemination, but it proved to induce a protective immune response against both diseases, myxomatosis and RHD. Following the emergence of a new genotype of RHDV (RHDV2) that showed limited cross-protection by RHDV, a novel trivalent vaccine against both genotypes was

designed to address the gaps in immunity presented by the new genotype (Dalton et al., 2012; Reemers et al., 2020).

Homologous recombination has been widely used for basic research about the biology of VACV and other poxviruses, in determining the essentiality and role of several viral genes. Indeed, it is still the usual way for recombinant poxvirus generation (Wyatt et al., 2017). Multiple transfer vectors available use different strategies for the selection of the recombinant virus, from thymidine kinase (TK) selection, chloramphenicol acetyltransferase (CAT) selection, β-galactosidase screening, GUS screening, XGPRT selection, luciferase or fluorescence screening, to plaque size selection (Blasco & Moss, 1995; Falknert & Moss, 1990; Jackson & Bults, 1992a; J. F. Rodriguez & Esteban, 1989; Scheiflinger et al., 1998). New innovative strategies for generating recombinant viruses have been developed recently, based on modern technologies such as CRISPR (Laudermilch & Chandran, 2021).

Since the genomic background in which the deletions are performed has great influence on further characterization *in vitro* studies and virulence studies *in vivo*, two parental strains were used to create the recombinant viruses: the virulent wild-type reference MYXV strain, Lausanne (Lu-MYXV), and an attenuated homologous vaccine strain (Vac-MYXV). The genetically modified viral strain candidate to constitute a DIVA vaccine had to retain its immunogenicity and protective efficacy. To ensure that this was achieved, the attenuated Vac-MYXV strain was selected as the genetic background for the subsequent gene deletions. This choice was crucial because this attenuated strain has already been demonstrated to provoke a strong immune response while being safe for use in animals. By using it as the parental backbone, the vaccine development could focus on deleting specific antigenic genes without compromising the safety profile of the Vac-MYXV strain.

The isolation of a MYXV mutant in which the *m071l* gene was replaced by the *dTmt* fluorescent marker gene was unsuccessful. Single homologous cross-over events were eventually identified by the development of virus foci with red fluorescence that were resistant to MPA. However, after eliminating the selective pressure and performing several isolation and amplification passages, the phenotypes of the foci that developed in the infected cultures indicated that the insertion was reversed back to the parental genomic background (non-fluorescent) or were still the intermediates a single cross-over recombination (fluorescent).

The homologous gene of *m071l* in VACV, H3L, was not found to be essential for the life cycle of the virus since the deletion mutant was successfully isolated by two independent research groups (da Fonseca et al., 2000b; Lin et al., 2000). The VACV H3L protein is involved in the

adsorption of IMV to cells through HS binding, but it is also involved in virion morphogenesis. It accumulates in viral factory areas, and it associates with the membranes of maturing viral particles during the assembly process (da Fonseca et al., 2000a). Although the ΔH3L mutant was still infectious, it displayed lower infectivity *in vitro* and showed an attenuated profile *in vivo*. Its characterization revealed a significant reduction in the amount of infectious intracellular virus that was attributed to an impaired IMV morphogenesis, as infected cells showed an accumulation of IVs and viral crescents (Lin et al., 2000). In consequence, it also exhibited a small plaque phenotype and reduced EEV production, yet the formation of actin tails was not affected (da Fonseca et al., 2000b).

Usually, the inability for isolating plaques or foci with a double-crossover recombinant poxvirus with a deletion mutation implies that the target gene, at least, is essential for plaque or focus formation (Blasco & Moss, 1991). An interesting finding was that at 48 hpi of the amplification infections, several isolated fluorescent cells were commonly observed, which later in infection appeared to suffer cell lysis. Suspecting that Vac-ΔM071*dTmt* mutant could be a "non-plaquing" phenotype and that these cells were actually infected with the double-crossover recombinant virus, they were isolated for further characterization and lysed to extract the intracellular mutant. However, neither the amplification of the mutant virus inside these cells, nor the PCR analysis were successful (data not shown). In this particular situation, given that the amplification of the Vac-ΔM071*dTmt* mutant failed and it was not even possible to isolate its genome, it was suggested that the recombinant virus resulting from the deletion of M071 was so attenuated that it was not able to efficiently replicate under normal culture conditions, or it even resulted in a non-viable mutant.

In order to provide evidence that confirmed or refuted the previous findings, complementary RK13 cell lines expressing the M071 protein of MYXV were intended to be generated using lentiviral vectors (Rahman et al., 2013; Rico et al., 2019). Under these conditions, a successful generation and isolation of the Vac-ΔM071*dTmt* mutant would confirm the significance on the presence of the M071 protein in the MYXV's life cycle. Data on this issue is not available because the construction of lentiviral vectors containing the *m071l* coding sequence was unfinished at the time this thesis was written. An alternative approach for studying the viability of Vac-ΔM071*dTmt* mutant in the future could involve the generation of an inducible recombinant virus in which M071 expression would be dependent on the presence of IPTG, as used in the study by Fonseca (da Fonseca et al. (2000)).

The isolation of MYXV mutants in which the *m022l* gene was replaced by the *gfp* fluorescent marker gene were successful after multiple attempts, in both the vaccine (Vac) and the virulent (Lu) genomic backgrounds, successfully generating the Vac-ΔM022*gfp* and Lu-ΔM022*gfp* mutants. First, single homologous cross-over events were identified by the development of foci resistant to MPA that showed green fluorescent. These viral clones were individually purified and amplified without selective pressure for several isolation and amplification rounds, until a homogeneous fluorescent phenotype was obtained during the RK13 infections. In turn, the deletion of the *m115l* gene was also successful in the vaccine genomic background. Since the isolation of the ΔM115 infection phenotype involved challenging technical considerations, the Lu mutant could not be isolated due to the insufficient time.

The purity of the knockouts was confirmed by two PCR analyses. One reaction was designed to amplify the target locus using a pair of primers designed to hybridize within the 5' and 3' flanking regions of the target genes, used for the construction of the transfer vectors. This strategy allowed to confirm the difference between the size of the genomic background belonging to the parental MYXV strain. There was no sign of wildtype *m022l* or *m115l* genes in the knockout viruses. The second reaction was focused on the differential amplification of the knockout genomes, since at least one primer was designed to hybridize inside the *gfp* fluorescent marker coding sequence. This amplification verified the site-directed insertion of the GFP cassette deleting and replacing the *m022l* or *m115l* coding region, respectively. After the knockout viruses were identified, one clone of each mutant (Lu-ΔM022*gfp,* Vac-ΔM022*gfp,* Vac-ΔM115*gfp*) was selected and sequenced by Sanger to confirm the genotype. Further passages of the selected clones were done to generate larger recombinant virus stocks.

Analyzing virus spread under two different culture conditions (liquid medium, and a semi-solid agarose overlay), provided crucial insights into the effects that could cause the deletion of the *m022l* or *m115l* genes in the virus biologic cycle. The use of a semi-solid overlay retained the IMV particles released by cell lysis and the EEVs, therefore, increasing the concentration of progeny virions around the initial focus, and enhancing localized infections around a limited area (Flores et al., 2020). The plaque/focus size under a semi-solid overlay provides information exclusively about the cell-to-cell spread ability of the virus, since under this culture condition the infection can only spread through the cell culture to adjacent cells. Cell-to-cell spread is an efficient way for virus transmission and constitutes a mechanism to evade the anti-viral systems and immune barriers of the host by limiting the exposure of virions to neutralizing antibodies in the extracellular environment (Law et al., 2002). This has already been reported for several

viruses; the higher infection rates occur under conditions of cell-to-cell compared to lower infection by cell-free virus infection (Kolodkin-Gal et al., 2013).

VACV uses (at least) two mechanisms to spread enveloped VACV particles between cells in an antibody resistant way: using an actin-dependent and actin-independent manner (Law et al., 2002). In the first pathway, CEV virions that are still attached to the membrane are projected towards neighboring cells for direct cell-to-cell spread through actin tails that are polymerized underneath them. In VV the phosphorylation of A36R initiates the recruitment of several cellular factors that stimulate the actin tail initiation and elongation (Frischknecht et al., 1999). The actin-independent pathway, not so well studied, is dependent on the A33R protein (Krupovič et al., 2010; Law et al., 2002).

The actin-dependent mechanism is also conserved in MYXV, but no homolog of the A36R gene has been identified in MYXV. Instead, there is a functional ortholog (M125R) that seemed to play a similar role (Dodding & Way, 2009). Since MYXV seemed to conserve most of the genes involved in the formation of EEV and actin tails, differences between the large VACV plaques and small MYXV foci were partly studied by Irwin & Evans (2012).

Despite having homologs of the genes required for promoting the formation of actin projectiles, MYXV has a significantly limited spread via actin filaments because it is not able to disrupt cortical actin. MYXV lacks the homolog of the VACV F11L gene, which is involved in modifying the cellular cytoskeleton and promoting virus egress and spread, and cell motility (Cordeiro et al., 2009). Compared to the phenotype of VACV infection in cell culture, which rapid develops cytolytic plaques characterized by a ring of infected cells surrounding a central lytic zone, the tumorigenic MYXV produces smaller clusters of infected cells with significantly slower growth, called foci (Barrett et al., 2001). Given that MYXV produces low amount of EEV, but normal amounts of CEV, cell-to-cell contact would become the preferential route for MYXV spread (Flores et al., 2020).

The size of viral foci or clusters of infected cells generated *in vitro* under a semi-solid overlay is influenced by the characteristics of the virus itself and its interactions with host cells. Under these culture conditions, the transmission of the virus is restricted to cell-to-cell spread and IMV infection after cell lysis. Therefore, foci size analysis provides valuable information about relevant aspects of viral infection.

VACV mutants with EEV-protein deletions show a compromised cell-to-cell spread due to an inability to produce actin tails (Law et al., 2002). The lack or restricted formation of IEV and ultimately CEV, prevents the cell-to-cell transmission in infected cell cultures, but the

intracellular particles produced by the deletion mutants are still fully infectious (Smith & Law, 2004). VACV-ΔF13 mutant also produced small size plaques in cell culture (Blasco & Moss, 1991).

These IMV particles can successfully complete the viral replication cycle intracellularly, producing abundant progeny. Inhibition of F13 (M022) or A27 protein (M115) expression in VACV virions do not affect the generation or infectivity of IMVs (Hsiao et al., 1999a; J. F. Rodriguez & Smith, 1990). According to these results, the deleted (ΔM022 and ΔM115) MYXV mutants were propagated by harvesting the cell cultures infected at high MOIs and the newly formed virions released by cell lysis, indicating the viable production of IMVs.

Following a long incubation time, ΔM022 and ΔM115 mutants were able to develop virus foci of limited size in the infected cell cultures. In particular, after 6 days of incubation, the mutant viruses (Lu-ΔM022*gfp,* Vac-ΔM022*gfp,* and Vac-ΔM115*gfp*) were able to propagate and develop foci with a characteristic morphology. IMVs are insufficient for cell-to-cell transmission, but over time, the virus foci developed from the mutant strains could be the result of the lysis of infected cells, the release of the recombinant progeny to the media, and the subsequent reinfection of the surrounding cells by the IMV.

Although the production of EEV particles is not correlated with plaque size (McIntosh & Smith, 1996; Wolffe et al., 1997), the amount of EEV released does correlate very closely with the ability of VACV to cause comet-shaped plaques in cell cultures at low MOI (Payne, 1980). The ability of VV to form a comet-shaped plaque under liquid overlay has been noted for years, where the unidirectionally spread of the virus from the primary infection focus, produces secondary infection sites that appear as a comet tail. These plaques are formed by distant unidirectional spread of EEVs by convection currents, not because of gravity (Law et al., 2002). Comet-shaped plaques can be blocked by antibodies against EEV proteins; thus, the anti-comet assay is usually a way of measuring the activity of EEV-specific antibodies (Appleyard et al., 1971; Law et al., 2002; Law & Smith, 2001).

The comet-shaped phenotype has not been well described for MYXV infection in the literature. Infection with the virulent Lu-MYXV*gfp* strain, for instance, did not display any comet-shaped foci in the liquid culture conditions, nor did the corresponding ΔM022 mutant (Figures…). However, comet-shaped foci were described for the ΔM022 mutant in the vaccine genetic background (Vac-ΔM115*gfp*), but not in Vac-ΔM115*gfp* infection.

The M022 homologous in VACV, F13L, together with B5R, are two of the viral proteins that are incorporated into or associated with the wrapping membranes (Blasco & Moss, 1991; Engelstad

& L.Smith, 1993). These two EEV proteins and the IMV-associated protein A27L, are required for the IEV formation through a process which is still not well described.

Considering the number of difficulties that we faced during the generation of these MYXV mutants, the fact that three of the recombinant viruses were successfully isolated and amplified to a working stock represented a significant achievement. However, due to time constraints at this point on the development of the project, only one of them was further used in the *in vittro* characterization and functional assays: Vac-ΔM022*gfp.*

Transmission electron microscopy (TEM) images of the parental Vac-MYXV and the mutant Vac-ΔM022*gfp* obtained using negative staining with uranyl acetate. Information about structural and morphological features of both MYXV types were obtained from the examination of these images. In the first place, two MYXV different forms were distinguished in the images, in agreement with the observations for VACV, which depend on the integrity of the particle (Moussatche & Condit, 2015). While the most abundant form is characterized by the presence of randomly arranged surface tubule elements (*mulberry*-like form), the negative-stained VACV preparations also contain virions lacking these elements and instead have a clearly delineated boundary surrounding the particle (*capsule*-like form) (Westwood et al., 1964). The first form is more abundant in freshly prepared samples, and corresponds with particles that maintained their integrity, while any damage experienced in the viral membrane (e.g. excessive drying during sample preparation) allows the stain to penetrate, resulting in the altered capsule-like appearance of the particle (Harris & Westwood, 1964). These two forms of VACV can also be differentiated by their size; the capsular virion has larger dimensions than the mulberry form (Condit et al., 2006; Moussatche & Condit, 2015). In agreement with these observations in VACV, the TEM images obtained in both preparations of MYXV, revealed that the majority of virions displayed the first *mulberry*-like form. One single virus particle within the Vac-MYXV sample appeared as a larger and more electron-dense body that was identified by *capsule*-like virion. In the TEM image where this particular particle was identified, it appeared besides what was identified as a *mulberry*-like form, which facilitated a direct comparison of their morphological features.

In these TEM images, the parental strain Vac-MYXV seemed larger than the ΔM022 mutant. Therefore, a comparative analysis of the length and width of the virions was performed, making the measurements from the particles identified in the TEM images. The analysis confirmed the hypothesis and revealed a robust statistical significance regarding the overall difference in size of the MYXV particles, without the symmetry of the particle being affected (L/W rate).

While the progression of the disease may extend over a longer period during *in vivo* or within an animal MYXV infection, the *in vitro* infectious cycle of Myxoma virus typically spans around 12 to 24 hours. Although this duration might be subjected to variation based on specific conditions or viral strains, it represents the average time required for the virus to enter a host cell, replicate its genome, and produce a whole new generation of virus particles. For a viral infection to successfully result in virus production, host cells must be susceptible, allowing them to be infected, and permissive, enabling them to support viral replication once the virus is inside. To examine the role of M022 in primary virus replication efficiency within the RK13 susceptible cell line, the production of infective virus was monitored using a single-step growth curve.

Lack of F13L in VACV results in a virus that produces normal amounts of IMV, but fails to generate CEV and EEV, which is reflected in a defective plaque formation (Blasco & Moss, 1991).

While M022 was not required for IMV synthesis, its absence significantly impaired foci formation, indicating its crucial role in viral dissemination. This was further addressed through a kinetic analysis of the Vac-ΔM022*gfp* mutant during multiple infection cycles, compared to the parental Vac-MYXV strain. Three independent infections with both viruses were performed at an MOI of 0.1 and monitored over a period of 96 hours. Both cells and medium of the infected samples were indistinctly harvested at multiple time points. The rate of infection spread across the RK13 monolayer indicated a better viral fitness for the parental strain. Indeed, the Vac-MYXV showed a stronger and more extensive cytopathic effect, such as higher cell rounding, detachment and lysis, than the ΔM022 mutant, especially at later times of infection. The efficient dissemination of Vac-MYXV within the host cells even led to the partial disruption of the cell monolayer at 96 hpi (Figure…). Under these infection conditions (low MOI), the kinetics of virus spread is associated with the amount of virus released from the initially infected cells. Therefore, the lower recovery of the mutant ΔM022 progeny during secondary stages of multi-step growth curves, compared to the parental Vac-MYXV, supported a role for M022 in an efficient *in vitro* virus spread.

Although EEV represents a minor fraction of the total viral progeny, they are crucial for mediating long-range virus spread both in cell culture and *in vivo.* EEV released in early stages of the infection are crucial for systemic spread and immune evasion. Indeed, VACV strains releasing higher EEV progeny correlate with more pathogenesis *in vivo* (Payne, 1980). Mutations on viral proteins that are critical for the production of EEV usually result in attenuated virus phenotypes. Deletion or mutation of viral proteins that are involved in extracellular virus particle formation result in reduction of plaque size in Vaccinia virus: A36 (B. M. Ward & Moss, 2004;

Wolffe et al., 1998), A33 (Roper et al., 1998), A34 (Wolffe et al., 1997), B5R (Engelstad & L.Smith, 1993). Not all mutations in these genes result in attenuated virus strains (e.g. A56R is still virulent). A34R glycoprotein found in the EEV is involved in the retention of CEV on the surface of the cell membrane (Blasco et al., 1993).

The lack of the M115 viral protein displayed a higher restriction on EEV generation than the ΔM022 mutant in Vac-MYXV. The same ΔM022 mutation caused a different degree of EEV formation restriction depending on the genomic background of the parental MYXV strain. In particular, the amount of EEV produced by the ΔM022 deletion mutants was 3 times lower when compared to the attenuated parental strain Vac-MYXV, and 10 times lower in case of the virulent Lu-MYXV strain. When interpreting these results, it may be noted that it was assumed that all viral particles found in the culture medium corresponded to EEV, although some of them could belong to IMV released by cell lysis, since the sample was taken at 96 hpi. Additionally, the fragility of the EEV outer envelope would also contribute to the presence of contaminating IMV in the culture medium samples (Boulter & Appleyard, 1973). The lack of anti-IMV sera or commercially available monoclonal/polyclonal antibodies specific to MYXV IMV proteins excluded the possibility of pretreating the culture medium samples to remove contaminant IMV particles (Appleyard et al., 1971). Therefore, it would be prudent to consider these results as preliminary and to conduct additional experiments that provide more conclusive data, such as analyzing EEV formation within the infected cells by electron microscopy.

EEV might also be involved in the modulation of the host's innate immune system (Pickup, 2015). A single-gene knockout of cowpox virus study found that several genes involved in the efficient production and transport of EEVs, including the homologs of the VACV A33R, A34R, A36R and B5R genes, were required for the suppression of the innate immune responses. The cowpox deletion mutant lacking the homolog of the VACV F13L (M022 in MYXV) was not able to develop pocks in infected chorioallantoic membranes of chick embryos (Z. Xu et al., 2014). These findings were demonstrated in a study involving cowpox virus proteins, and although these genes are well conserved in Orthopoxviruses, they need to be carefully interpreted when extrapolating them to MYXV. In any case, the development of poxvirus vaccine vectors in which the efficient production or spread of EEVs is compromised, may avoid the EV-mediated suppression of the innate immune responses, in turn, enhancing the immunization effect of the vaccine. Targeting viral proteins involved in EEV formation or release are expected to have a protective role against a systemic poxviral dissemination and disease progression (H. Yang et al., 2005).

In summary, from the six candidates that were initially selected based on bioinformatic analysis and relevant findings in homologous proteins of other poxviruses reported in the scientific literature (M022, M029, M071, M083, M115 and M141), only three were able to be produced in a soluble, and thus, putatively native form: M022, M83 and M115. The production of soluble M083 in the prokaryotic expression system was straightforward and yielded a high ratio compared to the same insoluble protein. Soluble M022 and M115 proteins were also produced in this system, albeit in lower ratios when compared to their insoluble form. Due to the higher soluble M022 and M115 yields and post-translational benefits using the recombinant baculoviruses, it was decided that the BEVS system would be used for large-scale production and purification of these proteins. As opposed to findings reported in other studies, the M083 protein did not appear to elicit a specific immune response in rabbit sera. While M022 and M115 proteins displayed specific reactivity to seropositive rabbit sera, confirming that they are recognized by the immune system of the host. Therefore, the two viral proteins, M022 and M115 were selected to continue analysis with regard to their potential as diagnostic antigens.

The creation of these serologic diagnostic tests would offer valuable resources for a range of different applications in clinical and public health settings. These tests could be instrumental in conducting seroprevalence studies to ascertain the prevalence of MYXV in specific wild rabbit populations, as well as monitoring changes in their immunity levels over time. Such data are essential for understanding the transmission dynamics of myxomatosis and could play a pivotal role in guiding public health decisions aimed at preventing outbreaks in rabbitries located in areas with a high incidence of the disease. Furthermore, these tests would be useful for the retrospective diagnosis of myxomatosis and assessing the vaccination-induced immune response in rabbits. They could be used to assess the efficacy of vaccination protocols (administration route, vaccine type, dosage, number of shots, etc) by determining whether they induced protective immunity. This is particularly important given the current lack of a direct link between serum anti-MYXV antibody titers and the actual protection level against this disease in animals. The results obtained in the present dissertation also suggest that the administration

route is indeed relevant for an effective (and protective) activation of the humoral immune response. The consistent and robust protection observed with the ID vaccination indicates that this route should be considered in future vaccination programs to achieve higher seroconversion and more uniform immune responses. While SC vaccination might be easier and more straightforward to administer, it involves less reliable and more heterogeneous results.

CHAPTER 9: CONCLUSIONS

1) Heterologous expression studies and characterization of MYXV proteins M022, M029, M071, M083, M115, and M141, selected for their putative antigenic properties, reveal that recombinant proteins M022, M083, and M115 are successfully expressed and purified in a soluble form. In contrast, proteins M029, M071, and M141 were not able to be expressed in a soluble and/or stable form under the experimental conditions evaluated in this thesis.

2) The recombinant M071 protein displays specific antigenic properties, indicating significant potential for the development of serological diagnostic assays for MYXV in the future.

3) The recombinant M022 protein shows specific reactivity in serum samples from myxomatosis-seropositive rabbits, primarily due to its conformational epitopes.

4) The recombinant M115 protein shows specific reactivity in serum samples from rabbits seropositive for myxomatosis. In addition to having conformational epitopes, it also displays highly immunogenic linear epitopes.

5) The viral proteins M022 and M115 are successfully used as antigens for the development of serological assays for the specific detection of anti-M022 and anti-M115 antibodies in rabbit sera.

6) The iELISA-rM115 test ensures effective identification of infected animals, although at the expense of yielding false positives.

7) The iELISA-rM022 test shows good diagnostic potential. Although it does not reach the discriminatory capacity of the reference (commercial) ELISA test, it remains useful for monitoring the presence of antibodies against MYXV.

8) The level of anti-M022 reactivity perfectly correlates with the survival of vaccinated rabbits imminently exposed to MYXV.

9) Serological analysis using the iELISA-rM022 test predicts protection against myxomatosis in vaccinated rabbits.

10) The iELISA-rM022 and iELISA-rM115 serological tests cross-detect antibodies against ha-MYXV and can be employed for diagnosing myxomatosis in hares

11) While neither M022 nor M115 proteins are essential for MYXV viability, the absence of M115 significantly reduces the virus's fitness.

12) Deletion of the M022 or M115 protein in the Vac-ΔM022gfp and Vac-ΔM115gfp viruses moderately and severely affects, respectively, the cell-to-cell transmission of these viruses.

13) The M022 protein might play a significant, though not exclusive, role in the formation of EEV and viral spread.

14) The mutant Vac-ΔM022gfp virus exhibits significantly reduced length and width compared to the parental Vac-MYXV, although the morphology of its virion is not altered by the ΔM022 mutation. The M022 protein may play a significant role in some stage of IMV morphogenesis.

15) The genetic background of MYXV is relevant when characterizing recombinant viruses and assessing the effect of certain mutations through functional assays.

CHAPTER 10: CONCLUSIONES

1) A través de estudios de expresión heteróloga y caracterización llevados a cabo para las proteínas M022, M029, M071, M083, M115, M141 del MYXV, seleccionadas por su putativo carácter antigénico, se determina las proteínas recombinantes M022, M083 y M115 se expresan y purifican en forma soluble. Por el contrario, las proteínas M029, M071 y M141 no logran expresarse de forma soluble y/o estable bajo las condiciones experimentales evaluadas en esta tesis.

2) La proteína recombinante M071 muestra propiedades antigénicas específicas, lo cual indica un potencial significativo para el desarrollo de ensayos serológicos de diagnóstico de MYXV en el futuro.

3) La proteína recombinante M022 tiene reactividad específica en muestras de sueros de conejo con seropositividad para mixomatosis y su inmunogenicidad se basa esencialmente en la presencia de epítopos conformacionales.

4) La proteína recombinante M115 tiene reactividad específica en muestras de sueros de conejo con seropositividad para mixomatosis. Además de poseer epítopos conformacionales, también exhibe epítopos lineales altamente inmunogénicos.

5) Las proteínas virales M022 y M115 se usan de forma satisfactoria como antígenos para el desarrollo de ensayos serológicos para la detección específica de anticuerpos anti-M022 y anti-M115 en sueros de conejo.

6) La prueba iELISA-rM115 asegura una identificación efectiva de los animales infectados, aunque a expensas de dar lugar a falsos positivos.

7) La prueba iELISA-rM022 muestra buen potencial diagnóstico. Aunque no alcanza la capacidad de discriminación de la prueba ELISA de referencia (comercial), sigue siendo útil para monitorear la presencia de anticuerpos frente a MYXV.

8) El nivel de reactividad anti-M022 se correlaciona perfectamente con la supervivencia en conejos vacunados y expuestos inminentemente al MYXV.

9) El análisis serológico mediante la prueba iELISA-rM022 pronostica la protección contra la mixomatosis en conejos vacunados.

10) Las dos pruebas serológicas iELISA-rM022 e iELISA-rM115 detectan de forma cruzada la presencia de anticuerpos contra ha-MYXV y pueden usarse para el diagnóstico serológico de la mixomatosis en liebres.

11) Las proteínas virales M022 y M115 no son esenciales para la viabilidad del MYXV, pero la ausencia de M115 perjudica en mayor grado el fitness viral de MYXV.

12) La deleción de la proteína M022 o M115 en los virus Vac-ΔM022gfp y Vac-ΔM115gfp afecta de forma moderada y grave, respectivamente, la transmisión célula a célula de estos virus.

13) La proteína M022 podría desempeñar una función relevante, aunque no exclusiva, en la formación de EEV y la propagación viral.

14) El virus mutante Vac-ΔM022gfp exhibe una longitud y un ancho significativamente reducidos en comparación con el virus parental Vac-MYXV, aunque la morfología de su virión no se ve alterada por la mutación ΔM022. La proteína M022 podría desempeñar alguna función relevante en alguna etapa de la morfogénesis del IMV.

15) El fondo genético del MYXV es relevante a la hora de caracterizar virus recombinantes y valorar el efecto de ciertas mutaciones mediante ensayos funcionales.

REFERENCES

Abade dos Santos, F. A., Carvalho, C. L., Monteiro, M., Carvalho, P., Mendonça, P., Peleteiro, M. da C., & Duarte, M. D. (2021). Recombinant myxoma virus infection associated with high mortality in rabbit farming (Oryctolagus cuniculus). *Transboundary and Emerging Diseases*, *68*(4), 2616–2621. https://doi.org/10.1111/tbed.13899

Abade dos Santos, F. A., Carvalho, C. L., Parra, F., Dalton, K. P., Peleteiro, M. C., & Duarte, M. D. (2021). A quadruplex qPCR for detection and differentiation of classic and natural recombinant myxoma virus strains of leporids. *International Journal of Molecular Sciences*, *22*(21). https://doi.org/10.3390/ijms222112052

Abade dos Santos, F. A., Carvalho, C. L., Pinto, A., Rai, R., Monteiro, M., Carvalho, P., Mendonça, P., Peleteiro, M. C., Parra, F., & Duarte, M. D. (2020). Detection of recombinant hare myxoma virus in wild rabbits (Oryctolagus cuniculus algirus). *Viruses*, *12*(10). https://doi.org/10.3390/v12101127

Abade dos Santos, F. A., Carvalho, C. L., Valente, P. C. L. G., Armés, H., Reemers, S. S., Peleteiro, M. C., Calonge-Sanz, I., Dalton, K. P., Parra, F., & Duarte, M. D. (2022). Evaluation of Commercial Myxomatosis Vaccines against Recombinant Myxoma Virus (ha-MYXV) in Iberian Hare and Wild Rabbit. *Vaccines*, *10*(3). https://doi.org/10.3390/vaccines10030356

Adams, M. M., Van Leeuwen, B. H., & Kerr, P. J. (2004). Limitations of plasmid vaccines to complex viruses: Selected myxoma virus antigens as DNA vaccines were not protective. *Vaccine*, *23*(2), 198–204. https://doi.org/10.1016/j.vaccine.2004.05.023

Adams, M. M., Van Leeuwen, B. H., & Kerr, P. J. (2008). Construction and evaluation of live attenuated myxoma virus vaccines with targeted virulence gene deletions. *Vaccine*, *26*(46), 5843–5854. https://doi.org/10.1016/j.vaccine.2008.08.036

Adams, M. M., Van Leeuwen, B. H., McFadden, G., & Kerr, P. J. (2008). Construction and testing of a novel host-range defective myxoma virus vaccine with the M063 gene inactivated that is non-permissive for replication in rabbit cells. *Veterinary Research*, *39*(6), 60–60. https://doi.org/10.1051/vetres:2008037

Ahsendorf, H. P., Diesterbeck, U. S., Hotop, S. K., Winkler, M., Brönstrup, M., & Czerny, C. P. (2022). Characterisation of an Anti-Vaccinia Virus F13 Single Chain Fragment Variable from a Human Anti-Vaccinia Virus-Specific Recombinant Immunoglobulin Library. *Viruses*, *14*(2). https://doi.org/10.3390/v14020197

Albini, S., Sigrist, B., Güttinger, R., Schelling, C., Hoop, R. K., & Vögtlin, A. (2012). Development and validation of a Myxoma virus real-time polymerase chain reaction assay. *Journal of Veterinary Diagnostic Investigation*, *24*(1), 135–137. https://doi.org/10.1177/1040638711425946

Alfonso, M., & Pagés-Mantè, A. (2003). Serological response to myxomatosis vaccination by different inoculation systems on farm rabbits. *World Rabbit Science*, *11*, 145–156.

Altmann, F., Staudacher, E., Wilson, I., & März, L. (1999). Insect cells as hosts for the expression of recombinant glycoproteins. *Glycoconjugate Journal*, *16*(2), 109–123. https://doi.org/10.1023/A:1026488408951

Angulo, E., & Bárcena, J. (2007). Towards a unique and transmissible vaccine against myxomatosis and rabbit haemorrhagic disease for rabbit populations. In *Wildlife Research* (Vol. 34, Issue 7, pp. 567–577). CSIRO. https://doi.org/10.1071/WR06160

Appleyard, G., Hapel, A. J., & Boulter, E. A. (1971). An Antigenic Difference between Intracellular and Extracellular Rabbitpox Virus. *Journal of General Virology*, *13*, 9–17.

Aragão, H. B. (1927). Myxoma of rabbits. *Memórias Do Instituto Oswaldo Cruz*, *20*, 237–247.

Arenas, A. J., Napp, S., Arenas-Montes, A., Borge, C., Carbonero, A., Perea, A., Cadenas, R., & García-Bocanegra, I. (2012). Serological response against myxoma virus and rabbit hemorrhagic disease virus in European wild rabbits using commercial vaccines. *Journal of Wildlife Management*, *76*(1), 102–107. https://doi.org/10.1002/jwmg.207

Baek, S.-H., Kwak, J.-Y., Haeng Lee, S., Lee, T., Ryu, S. H., Uhlinger, D. J., & Lambeth, J. D. (1997). Lipase Activities of p37, the Major Envelope Protein of Vaccinia Virus. *The Journal of Biological Chemistry*, *272*(December 19), 32042–32049.

Ball, L. A. (1987). High-Frequency Homologous Recombination in Vaccinia Virus DNA. *JOURNAL OF VIROLOGY*, *61*(6), 1788–1795.

Baraitareanu, S., sona Doina, D., Dan, M., Bărăităreanu, S., & Daneş, D. (2014). Serosurveillance of Myxomatosis by Competitive ELISA. *Bulletin UASVM Veterinary Medicine*, *71*(1), 266–267. http://www.oie.int/fileadmin/

Bárcena, J., Morales, M., Vázquez, B., Boga, J. A., Parra, F., Lucientes, J., Pagès-Manté, A., Sánchez-Vizcaíno, J. M., Blasco, R., & Torres, J. M. (2000). Horizontal Transmissible Protection against Myxomatosis and Rabbit Hemorrhagic Disease by Using a Recombinant Myxoma Virus. *JOURNAL OF VIROLOGY*, *74*(3), 1114–1123.

Bárcena, J., Pagès-Manté, A., March, R., Morales, M., Ramírez, M. A., Sánchez-Vizcaíno, J. M., & Torres, J. M. (2000). Isolation of an attenuated myxoma virus field strain that can confer protection against myxomatosis on contacts of vaccinates. *Archives of Virology*, *145*(4), 759–771. https://doi.org/10.1007/s007050050669

Barlow, A., Lawrence, K., Everest, D., Dastjerdi, A., Finnegan, C., & Steinbach, F. (2014). Confirmation of myxomatosis in a European brown hare in Great Britain. In *Veterinary Record* (Vol. 175, Issue 3, pp. 75–76). British Veterinary Association. https://doi.org/10.1136/vr.g4621

Barrett, J. W., Cao, J. X., Hota-Mitchell, S., & McFadden, G. (2001). Immunomodulatory proteins of myxoma virus. *Seminars in Immunology*, *13*(1), 73–84. https://doi.org/10.1006/smim.2000.0298

Barrett, J. W., Shun Chang, C., Wang, G., Werden, S. J., Shao, Z., Barrett, C., Gao, X., Belsito, T. A., Villenevue, D., & McFadden, G. (2007). Myxoma virus M063R is a host range gene essential for virus replication in rabbit cells. *Virology*, *361*(1), 123–132. https://doi.org/10.1016/j.virol.2006.11.015

Barros, S. C., Cruz, B., Luís, T. M., Ramos, F., Fagulha, T., Duarte, M., Henriques, M., & Fevereiro, M. (2009). A DIVA system based on the detection of antibodies to non-structural protein 3 (NS3) of bluetongue virus. *Veterinary Microbiology*, *137*(3–4), 252–259. https://doi.org/10.1016/j.vetmic.2009.01.033

Beaud, G. (1995). Vaccinia virus DNA replication: A short review. *Biochimie*, *77*, 774–779.

Belsham, G. J., Polacek, C., Breum, S., Larsen, L. E., & Bøtner, A. (2010). Detection of myxoma viruses encoding a defective M135R gene from clinical cases of myxomatosis; Possible implications for the role of the M135R protein as a virulence factor. *Virology Journal*, *7*. https://doi.org/10.1186/1743-422X-7-7

Benhnia, M. R.-E.-I., McCausland, M. M., Su, H.-P., Singh, K., Hoffmann, J., Davies, D. H., Felgner, P. L., Head, S., Sette, A., Garboczi, D. N., & Crotty, S. (2008). Redundancy and Plasticity of Neutralizing Antibody Responses Are Cornerstone Attributes of the Human Immune Response to the Smallpox Vaccine. *Journal of Virology*, *82*(7), 3751–3768. https://doi.org/10.1128/jvi.02244-07

Berguido, F. J., Chibssa, T. R., Loitsch, A., Liu, Y., Krstevski, K., Djadjovski, I., Tuppurainen, E., Petrović, T., Vidanović, D., Caufour, P., Settypalli, T. B. K., Grünwald-Gruber, C., Grabherr, R., Diallo, A., Cattoli, G., & Lamien, C. E. (2023). Harnessing Attenuation-Related Mutations of Viral Genomes: Development of a Serological Assay to Differentiate between Capripoxvirus-Infected and -Vaccinated Animals. *Viruses*, *15*(12). https://doi.org/10.3390/v15122318

Berguido, F. J., Gelaye, E., Liu, Y., Davaasuren, B., Krstevski, K., Djadjovski, I., Ivanova, E., Goujgoulova, G., Loitsch, A., Tuppurainen, E., Chibssa, T. R., Caufour, P., Samojlović, M., Lazić, S., Petrović, T., Vidanović, D., Bertagnoli, S., Grabherr, R., Diallo, A., … Lamien, C. E. (2022). Development and Optimization of Indirect ELISAs for the Detection of Anti-Capripoxvirus Antibodies in Cattle, Sheep, and Goat Sera. *Microorganisms*, *10*(10). https://doi.org/10.3390/microorganisms10101956

Berhanu, A., Wilson, R. L., Kirkwood-Watts, D. L., King, D. S., Warren, T. K., Lund, S. A., Brown, L. L., Krupkin, A. K., VanderMay, E., Weimers, W., Honeychurch, K. M., Grosenbach, D. W., Jones, K. F., & Hruby, D. E. (2008). Vaccination of BALB/c Mice with Escherichia coli - Expressed Vaccinia Virus Proteins A27L, B5R, and D8L Protects Mice from Lethal Vaccinia Virus Challenge . *Journal of Virology*, *82*(7), 3517–3529. https://doi.org/10.1128/jvi.01854-07

Bertagnoli, S., Gelfi, J., Le Gall, G., Boilletot, E., Vautherot, J.-F., Rasschaert, D., Laurent, S., Petit, F., Boucraut-Baralon, C., & Milon, A. (1996). Protection against Myxomatosis and

Rabbit Viral Hemorrhagic Disease with Recombinant Myxoma Viruses Expressing Rabbit Hemorrhagic Disease Virus Capsid Protein. In *JOURNAL OF VIROLOGY* (Vol. 70, Issue 8).

Bertolotti, L., Muratore, E., Nogarol, C., Caruso, C., Lucchese, L., Profiti, M., Anfossi, L., Masoero, L., Nardelli, S., & Rosati, S. (2015). Development and validation of an indirect ELISA as a confirmatory test for surveillance of infectious bovine rhinotracheitis in vaccinated herds. *BMC Veterinary Research*, *11*(1). https://doi.org/10.1186/s12917-015-0612-5

Best, S. M., Collins, S. V., & Kerr, P. J. (2000). Coevolution of host and virus: Cellular localization of virus in myxoma virus infection of resistant and susceptible European rabbits. *Virology*, *277*(1), 76–91. https://doi.org/10.1006/viro.2000.0505

Best, S. M., & Kerr, P. J. (2000). Coevolution of host and virus: The pathogenesis of virulent and attenuated strains of myxoma virus in resistant and susceptible european rabbits. *Virology*, *267*(1), 36–48. https://doi.org/10.1006/viro.1999.0104

Blasco, R., & Moss, B. (1991). Extracellular Vaccinia Virus Formation and Cell-to-Cell Virus Transmission Are Prevented by Deletion of the Gene Encoding the 37,000-Dalton Outer Envelope Protein. *Journal of Virology*, *65*(11), 5910–5920. https://journals.asm.org/journal/jvi

Blasco, R., & Moss, B. (1995). Selection of recombinant vaccinia viruses on the basis of plaque formation. *Gene*, *158*, 157–162.

Blasco, R., Sisler, J. R., & Moss, B. (1993). Dissociation of Progeny Vaccinia Virus from the Cell Membrane Is Regulated by a Viral Envelope Glycoprotein: Effect of a Point Mutation in the Lectin Homology Domain of the A34R Gene. *JOURNAL OF VIROLOGY*, *67*(6), 3319–3325.

Boag, B., Hernandez, A. D., & Cattadori, I. M. (2013). Observations on the epidemiology and interactions between myxomatosis, coccidiosis and helminth parasites in a wild rabbit population in Scotland. *European Journal of Wildlife Research*, *59*(4), 557–562. https://doi.org/10.1007/s10344-013-0704-0

Boulter, E. A. (1969). Protection against Poxviruses. *Proc. Roy. Soc. Med.*, *62*, 295–297.

Boulter, E. A., & Appleyard, G. (1973). Differences between extracellular and intracellular forms of poxvirus and their implications. *Progress in Medical Virology. Fortschritte Der Medizinischen Virusforschung. Progres En Virologie Medicale*, *16*, 86–108.

Boulter, E. A., Zwartouw, H. T., J Titmuss, D. H., Maber, H. B., & Zwartouw, T. (1971). The nature of the immune state produced by inactivated Vaccinia virus in Rabbits. *American Journal of Epidemiology*, *94*(6), 612–620. https://academic.oup.com/aje/article-abstract/94/6/612/249958

Braun, C., Thürmer, A., Daniel, R., Schultz, A.-K., Bulla, I., Schirrmeier, H., Mayer, D., Neubert, A., & Czerny, C.-P. (2017). Genetic Variability of Myxoma Virus Genomes. *Journal of Virology*, *91*(4). https://doi.org/10.1128/jvi.01570-16

Broder, C. C., & Earl, P. L. (1999). Recombinant Vaccinia Viruses. Design, Generation, and Isolation. *Molecular Biotechnology*, *13*, 223–245.

Broyles, S. S. (2003). Vaccinia virus transcription. In *Journal of General Virology* (Vol. 84, Issue 9, pp. 2293–2303). https://doi.org/10.1099/vir.0.18942-0

Cabezas, S., Blas, J., Marchant, T. A., & Moreno, S. (2007). Physiological stress levels predict survival probabilities in wild rabbits. *Hormones and Behavior*, *51*(3), 313–320. https://doi.org/10.1016/j.yhbeh.2006.11.004

Cabezas, S., Calvete, C., & Moreno, S. (2006). Vaccination Success and Body Condition in the European Wild Rabbit: Applications for Conservation Strategies. *Journal of Wildlife Management*, *70*(4), 1125–1131. https://sci-hub.im/10.2193/0022-541X(2006)70[1125:VSABCI]2.0.CO;2

Cairns, J. (1960). The Initiation of Vaccinia Infection. *Virology*, *11*, 603–623.

Calvete, C., Angulo, E., Estrada, R., Moreno, S., & Villafuerte, R. (2005). Quarantine length and survival of translocated European wild rabbits. *Journal of Wildlife Management*, *69*, 1063–1072.

Calvete, C., Estrada, R., Lucientes, J., Osacar, J. J., & Villafuerte, R. (2004). Short-term negative effects of vaccination campaigns against Myxomatosis and Viral Haemorrhagic Disease (VHD) on the survival of European wild rabbits. *Journal of Wildlife Management*, *68*(1), 198–205. https://www.researchgate.net/publication/232686758_Short-term_negative_effects_of_vaccination_campaigns_against_Myxomatosis_and_Viral_Haemorrhagic_Disease_VHD_on_the_survival_of_European_wild_rabbits

Calvete, C., Estrada, R., Villafuerte, R., Osácar, J. J., & Lucientes, J. (2002). Epidemiology of viral haemorrhagic disease and myxomatosis in a free-living population of wild rabbits. *Veterinary Record* , *150*, 776–782. http://veterinaryrecord.bmj.com/

Calvete, C., Villafuerte, R., Lucientes, J., & Osacar, J. J. (1997). Effectiveness of traditional wild rabbit restocking in Spain. *Journal of Zoology* , *241*, 271–277. https://doi.org/10.1111/j.1469-7998.2007.tb01957.x

Camacho-Sillero, L., Cardoso, B., Beato-Benítez, A., Gómez-Guillamón, F., Díaz-Cao, J. M., Jiménez-Martín, D., Caballero-Gómez, J., Castro-Scholten, S., Cano-Terriza, D., & García-Bocanegra, I. (2022). Spatiotemporal monitoring of myxomatosis in European wild rabbit (*Oryctolagus cuniculus*) in Spanish Mediterranean ecosystems. *Transboundary and Emerging Diseases*, *69*(6), 3494–3505. https://doi.org/10.1111/tbed.14709

Camacho-Sillero, L., Cardoso, B., Beato-Benítez, A., Gómez-Guillamón, F., Manuel Díaz-Cao, J., Jiménez Martín, D., Caballero-Gómez, J., Castro-, S., Cano-Terriza, D., & García-Bocanegra, I. (2022). Spatiotemporal monitoring of myxomatosis in European wild rabbit (Oryctolagus 1 cuniculus) in Spanish Mediterranean ecosystems. *Transboundary and Emerging Diseases*, *69*(6), 3499–3505.

Cameron, C., Hota-Mitchell, S., Chen, L., Barrett, J., Cao, J.-X., Macaulay, C., Willer, D., Evans, D., & Mcfadden, G. (1999). The Complete DNA Sequence of Myxoma Virus. *Virology*, *264*, 298–318. http://www.idealibrary.com

Cameron, C. M., Barrett, J. W., Liu, L., Lucas, A. R., & McFadden, G. (2005). Myxoma Virus M141R Expresses a Viral CD200 (vOX-2) That Is Responsible for Down-Regulation of Macrophage and T-Cell Activation In Vivo. *Journal of Virology*, *79*(10), 6052–6067. https://doi.org/10.1128/jvi.79.10.6052-6067.2005

Carn, V. M., Kitching, R. P., Hammond, J. M., & Chand, P. (1994). Use of a recombinant antigen in an indirect ELISA for detecting bovine antibody to capripoxvirus. *Journal of Virological Methods*, *49*, 285–294.

Carter, G. C., Law, M., Hollinshead, M., & Smith, G. L. (2005). Entry of the vaccinia virus intracellular mature virion and its interactions with glycosaminoglycans. *Journal of General Virology*, *86*(5), 1279–1290. https://doi.org/10.1099/vir.0.80831-0

Carvalho, C. L., Abade Dos Santos, F. A., Monteiro, M., Carvalho, P., Mendonça, P., & Duarte, M. D. (2020). First cases of myxomatosis in Iberian hares (Lepus granatensis) in Portugal. *Veterinary Record Case Reports*, *8*(2). https://doi.org/10.1136/vetreccr-2019-001044

Cavadini, P., Botti, G., Barbieri, I., Lavazza, A., & Capucci, L. (2010). Molecular characterization of SG33 and Borghi vaccines used against myxomatosis. *Vaccine*, *28*(33), 5414–5420. https://doi.org/10.1016/j.vaccine.2010.06.017

Cesari, V., Zucali, M., Bava, L., Gislon, G., Tamburini, A., & Toschi, I. (2018). Environmental impact of rabbit meat: The effect of production efficiency. *Meat Science*, *145*, 447–454. https://doi.org/10.1016/j.meatsci.2018.07.011

Chakrabarti, S., Sisler, J. R., & Moss, B. (1997). Compact, Synthetic, Vaccinia Virus Early/Late Promoter for Protein Expression. *Biotechniques*, *23*(6), 1094–1097.

Chang, S.-J., Shih, A.-C., Tang, Y.-L., & Chang, W. (2012). Vaccinia Mature Virus Fusion Regulator A26 Protein Binds to A16 and G9 Proteins of the Viral Entry Fusion Complex and Dissociates from Mature Virions at Low pH. *Journal of Virology*, *86*(7), 3809–3818. https://doi.org/10.1128/jvi.06081-11

Chang, T. H., Chang, S. J., Hsieh, F. L., Ko, T. P., Lin, C. T., Ho, M. R., Wang, I., Hsu, S. T. D., Guo, R. T., Chang, W., & Wang, A. H. J. (2013). Crystal Structure of Vaccinia Viral A27 Protein Reveals a Novel Structure Critical for Its Function and Complex Formation with A26 Protein. *PLoS Pathogens*, *9*(8). https://doi.org/10.1371/journal.ppat.1003563

Chapple, P. J., & Muirhead-Thomson, R. C. (1964). Effect of Varying the Site of Intradermal Inoculation of Myxoma Virus on the Course of Tthe Disease. *Journal of Comparative Pathology and Therapeutics*, *74*, 366–372. https://doi.org/10.1016/S0368-1742(64)80042-4

Coelho, J., Pacheco, H., Rafael, M., Jiménez-Ruiz, S., Alves, P. C., & Santos, N. (2023). Dynamics of Humoral Immunity to Myxoma and Rabbit Hemorrhagic Disease Viruses in Wild European Rabbits Assessed by Longitudinal Semiquantitative Serology. *Microbiology Spectrum*, *11*(4). https://doi.org/10.1128/spectrum.00050-23

Condit, R. C., Moussatche, N., & Traktman, P. (2006). In A Nutshell: Structure and Assembly of the Vaccinia Virion. *Advances in Virus Research*, *65*, 31–124. https://doi.org/10.1016/S0065-3527(06)66002-8

Cordeiro, J. V., Guerra, S., Arakawa, Y., Dodding, M. P., Esteban, M., & Way, M. (2009). F11-mediated inhibition of RhoA signalling enhances the spread of vaccinia virus in vitro and in vivo in an intranasal mouse model of infection. *PLoS ONE*, *4*(12). https://doi.org/10.1371/journal.pone.0008506

Crowther, John. R. (2009). Titration of Reagents. In J. M. Walkers (Ed.), *The ELISA Guidebook* (Second Edition, Vol. 516, pp. 79–109). Humana Press. www.springer.com/series/7651

da Fonseca, F. G., Wolffe, E. J., Weisberg, A., & Moss, B. (2000a). Characterization of the Vaccinia Virus H3L Envelope Protein: Topology and Posttranslational Membrane Insertion via the C-Terminal Hydrophobic Tail. *Journal of Virology*, *74*(16), 7508–7517. https://doi.org/10.1128/JVI.74.16.7508-7517.2000

da Fonseca, F. G., Wolffe, E. J., Weisberg, A., & Moss, B. (2000b). Effects of Deletion or Stringent Repression of the H3L Envelope Gene on Vaccinia Virus Replication. *Journal of Virology*, *74*(16), 7518–7528. https://doi.org/10.1128/jvi.74.16.7518-7528.2000

Dalton, K. P., Martín, J. M., Nicieza, I., Podadera, A., de Llano, D., Casais, R., Gimenez, S., Badiola, I., Agüero, M., Duran, M., Buitrago, D., Romero, L. J., García, E., & Parra, F. (2019). Myxoma virus jumps species to the Iberian hare. *Transboundary and Emerging Diseases*, *66*(6), 2218–2226. https://doi.org/10.1111/tbed.13296

Dalton, K. P., Nicieza, I., Balseiro, A., Muguerza, M. A., Rosell, J. M., Casais, R., Álvarez, Á. L., & Parra, F. (2012). Variant rabbit hemorrhagic disease virus in young rabbits, Spain. *Emerging Infectious Diseases*, *18*(12), 2009–2012. https://doi.org/10.3201/eid1812.120341

Dalton, K. P., Nicieza, I., de Llano, D., Gullón, J., Inza, M., Petralanda, M., Arroita, Z., & Parra, F. (2015). Vaccine breaks: Outbreaks of myxomatosis on Spanish commercial rabbit farms. *Veterinary Microbiology*, *178*(3–4), 208–216. https://doi.org/10.1016/j.vetmic.2015.05.008

Dalton, K. P., Ringleb, F., Martín Alonso, J. M., & Parra, F. (2009). Rapid identification of myxoma virus variants by long-range PCR and restriction fragment length polymorphism analysis. *Journal of Virological Methods*, *161*(2), 284–288. https://doi.org/10.1016/j.jviromet.2009.06.026

Dashprakash, M., Venkatesan, G., Kumar, A., Sankar, M., Arya, S., Ramakrishnan, M. A., Pandey, A. B., & Mondal, B. (2019). Prokaryotic expression, purification and evaluation of goatpox virus ORF117 protein as a diagnostic antigen in indirect ELISA to detect goatpox. *Archives of Virology*, *164*(4), 1049–1058. https://doi.org/10.1007/s00705-019-04170-8

Dashprakash, M., Venkatesan, G., Ramakrishnan, M. A., Muthuchelvan, D., Sankar, M., Pandey, A. B., & Mondal, B. (2015). Genetic diversity of fusion gene (ORF 117), an analogue of vaccinia virus A27L gene of capripox virus isolates. *Virus Genes*, *50*(2), 325–328. https://doi.org/10.1007/s11262-015-1172-2

Davies, D. H., McCausland, M. M., Valdez, C., Huynh, D., Hernandez, J. E., Mu, Y., Hirst, S., Villarreal, L., Felgner, P. L., & Crotty, S. (2005). Vaccinia Virus H3L Envelope Protein Is a Major Target of Neutralizing Antibodies in Humans and Elicits Protection against Lethal Challenge in Mice. *Journal of Virology*, *79*(18), 11724–11733. https://doi.org/10.1128/jvi.79.18.11724-11733.2005

Davies, D. H., Molina, D. M., Wrammert, J., Miller, J., Hirst, S., Mu, Y., Pablo, J., Unal, B., Nakajima-Sasaki, R., Liang, X., Crotty, S., Karem, K. L., Damon, I. K., Ahmed, R., Villarreal, L., & Felgner, P. L. (2007). Proteome-wide analysis of the serological response to vaccinia and smallpox. *PROTEOMICS*, *7*(10), 1678–1686. https://doi.org/10.1002/pmic.200600926

Delibes-Mateos, M., Ramírez, E., Ferreras, P., & Villafuerte, R. (2008). Translocations as a risk for the conservation of European wild rabbit Oryctolagus cuniculus lineages. *ORYX*, *42*(2), 259–264. https://doi.org/10.1017/S0030605308006984

Delibes-Mateos, M., Redpath, S. M., Angulo, E., Ferreras, P., & Villafuerte, R. (2007). Rabbits as a keystone species in southern Europe. *Biological Conservation*, *137*(1), 149–156. https://doi.org/10.1016/j.biocon.2007.01.024

Demkowicz, W. E., Maa, J. S., & Esteban, M. (1992). Identification and Characterization of Vaccinia Virus Genes Encoding Proteins That Are Highly Antigenic in Animals and Are Immunodominant in Vaccinated Humans. *Journal of Virology*, *66*(1), 386–398. https://journals.asm.org/journal/jvi

DiGiacomo, R. F., & Maré, C. J. (1994). Viral Diseases. In P. J. Manning, D. H. Ringler, & C. E. Newcomer (Eds.), *The Biology of the Laboratory Rabbit* (Second Edition, pp. 171–204). American College of Laboratory Animal Medicine. https://doi.org/https://doi.org/10.1016/C2009-0-02399-X

Dodding, M. P., & Way, M. (2009). Nck- and N-WASP-Dependent Actin-Based Motility Is Conserved in Divergent Vertebrate Poxviruses. *Cell Host and Microbe*, *6*(6), 536–550. https://doi.org/10.1016/j.chom.2009.10.011

Domi, A., & Beaud, G. (2000). The punctate sites of accumulation of vaccinia virus early proteins are precursors of sites of viral DNA synthesis. *Journal of General Virology*, *81*, 1231–1235.

Duarte, M. D., Barros, S. C., Henriques, A. M., Fagulha, M. T., Ramos, F., Luís, T., & Fevereiro, M. (2013). Development and validation of a real time PCR for the detection of myxoma virus based on the diploid gene M000.5L/R. *Journal of Virological Methods*, *196*, 219–224. https://doi.org/10.1016/j.jviromet.2013.11.014

Duke-Cohan, J. S., Wollenick, K., Witten, E. A., Seaman, M. S., Baden, L. R., Dolin, R., & Reinherz, E. L. (2009). The heterogeneity of human antibody responses to Vaccinia Virus revealed through use of focused protein arrays. *Vaccine*, *27*(8), 1154–1165. https://doi.org/10.1016/j.vaccine.2008.12.035

Duteyrat, J. L., Gelfi, J., & Bertagnoli, S. (2006). Ultrastructural study of myxoma virus morphogenesis. *Archives of Virology*, *151*(11), 2161–2180. https://doi.org/10.1007/s00705-006-0791-2

Engelstad, M., & L.Smith, G. (1993). The Vaccinia Virus 42-kDa Envelope Protein is required for the envelopment and egress of Extacellular Virus and for Virus virulence. *Virology*, *194*, 627–637.

Espinosa, J., Ferreras, M. C., Benavides, J., Cuesta, N., Pérez, C., Iglesias, M. J. G., Marín, J. F. G., & Pérez, V. (2020). Causes of mortality and disease in rabbits and hares: A retrospective study. *Animals*, *10*(1). https://doi.org/10.3390/ani10010158

Falknert, F. G., & Moss, B. (1988). Escherichia coli gpt Gene Provides Dominant Selection for Vaccinia Virus Open Reading Frame Expression Vectors. In *JOURNAL OF VIROLOGY* (Vol. 62, Issue 6).

Falknert, F. G., & Moss, B. (1990). Transient Dominant Selection of Recombinant Vaccinia Viruses. *JOURNAL OF VIROLOGY*, *64*(6), 3108–3111.

Fenner, F. (2010). Deliberate introduction of the European rabbit, Oryctolagus cuniculus, into Australia. *Rev. Sci. Tech. Off. Int. Epiz*, *1*, 103–111.

Fenner, F., Dayt, M. F., & Woodroofet, G. M. (1956). Epidemiological consequences of the mechanical transmission of myxomatosis by mosquitoes*. *The Journal of Hygiene*, *54*(2), 284–303. https://doi.org/10.1017/s0022172400044521

Fenner, F., & Marshall, I. D. (1954). Passive immunity in myxomatosis of the European rabbit (Oryctolagus cu- niculus): the protection conferred on kittens by immune does. *J Hyg (Cambridge)*, *52*, 321–336.

Fenner, F., & Marshall, I. D. (1957). A comparison of the virulence for European rabbits (Oryctolagus cuniculus) of strains of myxoma virus recovered in the field in Australia, Europe and America. *Journal of Hygiene*, *55*(2), 149–191. https://doi.org/10.1017/S0022172400037098

Fenner, F., Marshall, I. D., & Woodroofe, G. M. (1953). Studies in the epidemiology of infectious myxomatosis of rabbits. I. Recovery of Australian wild rabbits (Oryctolagus cuniculus) from myxomatosis under field conditions. *Journal of Hygiene (Cambridge University Press)*, *25*, 225–244.

Fenner, F., Poole, W. E., Marshall, I. D., & Dyce, A. L. (1957). Studies in the epidemiology of infectious myxomatosis of rabbits: VI. The Experimental Introduction of the European Strain of Myxoma Virus into Australian Wild Rabbit Populations. *Journal of Hygiene*, *55*(2), 192–206. https://doi.org/10.1017/S0022172400037104

Fenner, F., & Ratcliffe, F. N. (1965, April). Myxomatosis. *Cambridge University Press*, *8*(4), 254–254. https://doi.org/10.1017/s0030605300004907

Fenner, F., & Woodroofe, G. M. (1953). The pathogenesis of infectious myxomatosis: The mechanism of infection and the immunological response in the European Rabbit (Oryctolagus cuniculus). *British Journal of Experimental Pathology*, *34*, 400–410.

Fenner, P., & Woodroofe, G. M. (1954). Protection of laboratory rabbits against myxomatosis by vaccination with Fibroma virus. *Australian Journal of Experimental Biology*, *32*, 653–668.

Ferreira, C., Ramírez, E., Castro, F., Ferreras, P., Alves, P. C., Redpath, S., & Villafuerte, R. (2009). Field experimental vaccination campaigns against myxomatosis and their effectiveness in the wild. *Vaccine*, *27*(50), 6998–7002. https://doi.org/10.1016/j.vaccine.2009.09.075

Ferrer, M., & Negro, J. J. (2003). The Near Extinction of Two Large European Predators: Super Specialists Pay a Price. *Conservation Biology*, *18*(2), 334–349.

Firth, C., Kitchen, A., Shapiro, B., Suchard, M. A., Holmes, E. C., & Rambaut, A. (2010). Using time-structured data to estimate evolutionary rates of double-stranded DNA viruses. *Molecular Biology and Evolution*, *27*(9), 2038–2051. https://doi.org/10.1093/molbev/msq088

Flores, E. B., Bartee, M. Y., & Bartee, E. (2020). Reduced cellular binding affinity has profoundly different impacts on the spread of distinct poxviruses. *PLOS ONE*, *15*(4), e0231977. https://doi.org/10.1371/journal.pone.0231977

Fogg, C., Lustig, S., Whitbeck, J. C., Eisenberg, R. J., Cohen, G. H., & Moss, B. (2004). Protective Immunity to Vaccinia Virus Induced by Vaccination with Multiple Recombinant Outer Membrane Proteins of Intracellular and Extracellular Virions. *Journal of Virology*, *78*(19), 10230–10237. https://doi.org/10.1128/jvi.78.19.10230-10237.2004

Fouchet, D., Guitton, J. S., Marchandeau, S., & Pontier, D. (2008). Impact of myxomatosis in relation to local persistence in wild rabbit populations: The role of waning immunity and the reproductive period. *Journal of Theoretical Biology*, *250*(4), 593–605. https://doi.org/10.1016/j.jtbi.2007.10.037

Fouchet, D., Marchandeau, S., Langlais, M., & Pontier, D. (2006). Waning of maternal immunity and the impact of diseases: The example of myxomatosis in natural rabbit populations. *Journal of Theoretical Biology*, *242*(1), 81–89. https://doi.org/10.1016/j.jtbi.2006.02.003

Fountain, S., Holland, M. K., Hinds, L. A., Janssens, P. A., & Kerr, P. J. (1997). Interstitial orchitis with impaired steroidogenesis and spermatogenesis in the testes of rabbits infected with an attenuated strain of myxoma virus. *Journal of Reproduction and Fertility*, *110*, 161–169.

Freuling, C. M., Müller, T. F., & Mettenleiter, T. C. (2017). Vaccines against pseudorabies virus (PrV). *Veterinary Microbiology*, *206*, 3–9. https://doi.org/10.1016/j.vetmic.2016.11.019

Frey, S. E., Stapleton, J. T., Ballas, Z. K., Rasmussen, W. L., Kaufman, T. M., Blevins, T. P., Jensen, T. L., Huw Davies, D., Tary-Lehmann, M., Chaplin, P., Hill, H., Goll, J. B., Belshe, R. B., Wald, A., Johnston, C., Jackson, L. A., Winokur, P., Keitel, W., El Sahly, H., … Buddy Creech, C. (2021). Human Antibody Responses following Vaccinia Immunization Using Protein Microarrays and Correlation with Cell-Mediated Immunity and Antibody-Dependent Cellular Cytotoxicity Responses. *Journal of Infectious Diseases*, *224*(8), 1372–1382. https://doi.org/10.1093/infdis/jiab111

Frischknecht, F., Moreau, V., Röttger, S., Gonfloni, S., Reckmann, I., Superti-Furga, G., & Way, M. (1999). Actin-based motility of vaccinia virus mimics receptor tyrosine kinase signalling. *Nature*, *401*, 926–929. www.nature.com

García, A. D., Meseda, C. A., Mayer, A. E., Kumar, A., Merchlinsky, M., & Weir, J. P. (2007). Characterization and use of mammalian-expressed vaccinia virus extracellular membrane proteins for quantification of the humoral immune response to smallpox vaccines. *Clinical and Vaccine Immunology*, *14*(8), 1032–1044. https://doi.org/10.1128/CVI.00050-07

García-Bocanegra, I., Astorga, R. J., Napp, S., Casal, J., Huerta, B., Borge, C., & Arenas, A. (2010). Myxomatosis in wild rabbit: Design of control programs in Mediterranean ecosystems. *Preventive Veterinary Medicine*, *93*(1), 42–50. https://doi.org/10.1016/j.prevetmed.2009.09.013

García-Bocanegra, I., Camacho-Sillero, L., Caballero-Gómez, J., Agüero, M., Gómez-Guillamón, F., Manuel Ruiz-Casas, J., Manuel Díaz-Cao, J., García, E., José Ruano, M., & de la Haza, R. (2021). Monitoring of emerging myxoma virus epidemics in Iberian hares (Lepus granatensis) in Spain, 2018–2020. *Transboundary and Emerging Diseases*, *68*(3), 1275–1282. https://doi.org/10.1111/tbed.13781

García-Bocanegra, I., Camacho-Sillero, L., Risalde, M. A., Dalton, K. P., Caballero-Gómez, J., Agüero, M., Zorrilla, I., & Gómez-Guillamón, F. (2019). First outbreak of myxomatosis in Iberian hares (Lepus granatensis). *Transboundary and Emerging Diseases*, *66*(6), 2204–2208. https://doi.org/10.1111/tbed.13289

García-Fruitós, E. (2015). *Insoluble Proteins* (J. M. Walker, Ed.; Vol. 1258). Methods and Protocols Methods in Molecular Biology . http://www.springer.com/series/7651

García-Pereira, S., González-Barrio, D., Fernández-García, J. L., Gómez-Martín, A., Habela, M. Á., García-Bocanegra, I., & Calero-Bernal, R. (2021). Detection of myxoma virus DNA in ticks from lagomorph species in spain suggests their possible role as competent vector in viral transmission. *Journal of Wildlife Diseases*, *57*(2), 423–428. https://doi.org/10.7589/JWD-D-20-00116

Gelfi, J., Chantal, J., Phong, T. T., Py, R., & Boucraut-Baralon, C. (1999). Development of an ELISA for detection of myxoma virus-specific rabbit antibodies: Test evaluation for diagnostic applications on vaccinated and wild rabbit sera. *Journal of Veterinary Diagnostic Investigation*, *11*(3), 240–245. https://doi.org/10.1177/104063879901100306

Geshelin, P., & Berns, K. I. (1974). Characterization and Localization of the Naturally Occurring Cross-links in Vaccinia Virus DNA. *J. Mol. Biol*, *88*, 785–796.

Gilbert, Y., Picavet, D.-P., & Chantal, J. (1989). Diagnostic de la myxomatose : mise au point d'une technique d'immunofluorescence indirecte. Utilisation de prélèvements sanguins sur papier buvard pour la recherche d'anticorps *. *Rev. Sci. Tech. Off. Int. Epiz*, *8*(1), 209–220.

Graham, K. A., Opgenorth, A., Upton, C., & Mcfadden', G. (1992). Myxoma Virus Ml 1 L ORF Encodes a Protein for Which Cell Surface Localization Is Critical in Manifestation of Viral Virulence. In *VIROLOGY* (Vol. 191, pp. 112–136).

Granados, R. R., Guoxun, L. X., Derksen, A. C. G., & Mckenna, K. A. (1994). A New Insect Cell Line from Trichoplusia ni (BTI-Tn-5B1-4) Susceptible to Trichoplusia ni Single Enveloped Nuclear Polyhedrosis Virus. *JOURNAL OF INVERTEBRATE PATHOLOGY*, *64*, 260–266. https://doi.org/10.1016/S0022-2011(94)90400-6

Guitton, J. S., Devillard, S., Guénézan, M., Fouchet, D., Pontier, D., & Marchandeau, S. (2008). Vaccination of free-living juvenile wild rabbits (Oryctolagus cuniculus) against myxomatosis improved their survival. *Preventive Veterinary Medicine*, *84*(1–2), 1–10. https://doi.org/10.1016/j.prevetmed.2007.10.001

Harris, W. J., & Westwood, J. C. N. (1964). Phosphotungstate Staining of Vaccinia Virus. In *J. gen. Microbiol* (Vol. 34).

Hatherley, D., & Barclay, A. N. (2004). The CD200 and CD200 receptor cell surface proteins interact through their N-terminal immunoglobulin-like domains. *European Journal of Immunology*, *34*(6), 1688–1694. https://doi.org/10.1002/eji.200425080

Heine, H. G., Stevens, M. P., Foord, A. J., & Boyle, D. B. (1999). A capripoxvirus detection PCR and antibody ELISA based on the major antigen P32, the homolog of the vaccinia virus H3L gene. *Journal of Immunological Methods*, *227*, 187–196. www.elsevier.nlrlocaterjim

Hermanson, G., Chun, S., Felgner, J., Tan, X., Pablo, J., Nakajima-Sasaki, R., Molina, D. M., Felgner, P. L., Liang, X., & Davies, D. H. (2012). Measurement of antibody responses to Modified Vaccinia virus Ankara (MVA) and Dryvax ® using proteome microarrays and development of recombinant protein ELISAs. *Vaccine*, *30*(3), 614–625. https://doi.org/10.1016/j.vaccine.2011.11.021

Hiller, G., & Weber, K. (1985). Golgi-Derived Membranes That Contain an Acylated Viral Polypeptide Are Used for Vaccinia Virus Envelopment. *Journal of Virology*, *55*(3), 651–659. https://journals.asm.org/journal/jvi

Hirt, P., Hiller, G., & Wittek, R. (1986). Localization and Fine Structure of a Vaccinia Virus Gene Encoding an Envelope Antigen. *Journal of Virology*, *58*(3), 757–764.

Hollinshead, M., Rodger, G., Van Eijl, H., Law, M., Hollinshead, R., Vaux, D. J. T., & Smith, G. L. (2001). Vaccinia virus utilizes microtubules for movement to the cell surface. *Journal of Cell Biology*, *154*(2), 389–402. https://doi.org/10.1083/jcb.200104124

Howard, A. R., Senkevich, T. G., & Moss, B. (2008). Vaccinia Virus A26 and A27 Proteins Form a Stable Complex Tethered to Mature Virions by Association with the A17 Transmembrane Protein. *Journal of Virology*, *82*(24), 12384–12391. https://doi.org/10.1128/jvi.01524-08

Hoy, S. M. (2018). Tecovirimat: First Global Approval. *Drugs*, *78*(13), 1377–1382. https://doi.org/10.1007/s40265-018-0967-6

Hsiao, J.-C., Chung, C.-S., & Chang, W. (1998). Cell Surface Proteoglycans Are Necessary for A27L Protein-Mediated Cell Fusion: Identification of the N-Terminal Region of A27L Protein as the Glycosaminoglycan-Binding Domain. *Journal of Virology*, *72*(10), 8374–8379. https://doi.org/10.1128/JVI.72.10.8374-8379.1998

Hsiao, J.-C., Chung, C.-S., & Chang, W. (1999a). Vaccinia Virus Envelope D8L Protein Binds to Cell Surface Chondroitin Sulfate and Mediates the Adsorption of Intracellular Mature Virions to Cells. *JOURNAL OF VIROLOGY*, *73*(10), 8750–8761. https://journals.asm.org/journal/jvi

Hsiao, J.-C., Chung, C.-S., & Chang, W. (1999b). Vaccinia Virus Envelope D8L Protein Binds to Cell Surface Chondroitin Sulfate and Mediates the Adsorption of Intracellular Mature Virions to Cells. In *JOURNAL OF VIROLOGY* (Vol. 73, Issue 10). https://journals.asm.org/journal/jvi

Husain, M., & Moss, B. (2003). Intracellular Trafficking of a Palmitoylated Membrane-Associated Protein Component of Enveloped Vaccinia Virus. *Journal of Virology*, *77*(16), 9008–9019. https://doi.org/10.1128/jvi.77.16.9008-9019.2003

Ichihashi, Y. (1996). Extracellular Enveloped Vaccinia Virus Escapes Neutralization. *VIROLOGY*, *217*, 478–485.

Irwin, C. R., & Evans, D. H. (2012). Modulation of the Myxoma Virus Plaque Phenotype by Vaccinia Virus Protein F11. *Journal of Virology*, *86*(13), 7167–7179. https://doi.org/10.1128/jvi.06936-11

Jackson, R. J., & Bults, H. G. (1992a). A myxoma virus intergenic transient dominant selection vector. *Journal of General Virology*, *73*(12), 3241–3245. https://doi.org/10.1099/0022-1317-73-12-3241

Jackson, R. J., & Bults, H. G. (1992b). The myxoma virus thymidine kinase gene: sequence and transcriptional mapping. *Journal of General Virology*, *73*, 323–328.

Jackson, R. J., Hall, D. F., & Kerr, P. J. (1999). Myxoma Virus Encodes an α2,3-Sialyltransferase That Enhances Virulence. *Journal of Virology*, *73*(3), 2376–2384. https://doi.org/10.1128/JVI.73.3.2376-2384.1999

Jan, E., Mohr, I., & Walsh, D. (2016). A Cap-to-Tail Guide to mRNA Translation Strategies in Virus-Infected Cells. In *Annual Review of Virology* (Vol. 3, pp. 283–307). Annual Reviews Inc. https://doi.org/10.1146/annurev-virology-100114-055014

Jeklova, E., Leva, L., Matiasovic, J., Kovarcik, K., Kudlackova, H., Nevorankova, Z., Psikal, I., & Faldyna, M. (2008a). Characterisation of immunosuppression in rabbits after infection with myxoma virus. *Veterinary Microbiology*, *129*(2), 117. https://doi.org/10.1016/j.vetmic.2007.11.039ï

Jeklova, E., Leva, L., Matiasovic, J., Kovarcik, K., Kudlackova, H., Nevorankova, Z., Psikal, I., & Faldyna, M. (2008b). Characterisation of immunosuppression in rabbits after infection with myxoma virus. *Veterinary Microbiology*, *129*(1–2), 117–130. https://doi.org/10.1016/j.vetmic.2007.11.039

Jerabek, J. (1980). Applicability of Shope Fibroma Virus Replicated in Cell Cultures for Immunoprophylaxis of Rabbit Myxomatosis. *ACTA VET. BRNO*, *49*, 259–267. https://doi.org/10.2754/avb198049030259

Johnson, G. P., Goebel, S. J., & Paoletti, E. (1993). An update on the Vaccinia Virus genome. *Virology*, *196*, 381–401.

Jones, D. T. (1999). Protein secondary structure prediction based on position-specific scoring matrices 1 1Edited by G. Von Heijne. *Journal of Molecular Biology*, *292*(2), 195–202. https://doi.org/10.1006/jmbi.1999.3091

Joubert, L., Duclos, P., & Toaillen, P. (1982). La myxomatose des garennes dans le sud-est. La myxomatose amyxomateuse. *Reviste Médique Véterinaire*, *133*, 739–753.

Karstad, L., Thorsen, L. J., Davies, G., & Kaminjoloo, J. S. (1977). Poxvirus fibromas on African hares. *Journal of Wildlife Diseases*, *13*. http://meridian.allenpress.com/jwd/article-pdf/13/3/245/2335075/0090-3558-13_3_245.pdf

Kato, N., Eggers, H. J., & Rolly, H. (1969). INHIBITION OF RELEASE OF VACCINIA VIRUS BY N1-ISONICOTINOYL-N2-3-METHYL-4-CHLOROBENZOYLHYDRAZINE. *Journal of Experimental Medicine*, *129*(4), 795–808.

Kerr, P. J. (1997). An ELISA for epidemiological studies of myxomatosis: Persistence of antibodies to myxoma virus in European rabbits (Oryctolagus cuniculus). *Wildlife Research*, *24*(1), 53–65. https://doi.org/10.1071/WR96058

Kerr, P. J. (2012). Myxomatosis in Australia and Europe: A model for emerging infectious diseases. *Antiviral Research*, *93*(3), 387–415. https://doi.org/10.1016/j.antiviral.2012.01.009

Kerr, P. J. (2020). Rabbit Myxoma Virus and the Fibroma Viruses (Poxviridae). In *Encyclopedia of Virology: Volume 1-5, Fourth Edition* (Vols. 1–5, pp. 730–737). Elsevier. https://doi.org/10.1016/B978-0-12-809633-8.20935-7

Kerr, P. J., & Best, S. M. (1998). Myxoma virus in rabbits. In *Rev. sci. tech. Off. int. Epiz* (Vol. 17, Issue 1).

Kerr, P. J., Cattadori, I. M., Rogers, M. B., Fitch, A., Geber, A., Liu, J., Sim, D. G., Boag, B., Eden, J. S., Ghedin, E., Read, A. F., & Holmes, E. C. (2017). Genomic and phenotypic characterization of myxoma virus from Great Britain reveals multiple evolutionary pathways distinct from those in Australia. *PLoS Pathogens*, *13*(3). https://doi.org/10.1371/journal.ppat.1006252

Kerr, P. J., Ghedin, E., DePasse, J. V., Fitch, A., Cattadori, I. M., Hudson, P. J., Tscharke, D. C., Read, A. F., & Holmes, E. C. (2012). Evolutionary History and Attenuation of Myxoma Virus on Two Continents. *PLoS Pathogens*, *8*(10). https://doi.org/10.1371/journal.ppat.1002950

Kerr, P. J., Hone, J., Perrin, L., French, N., & Williams, C. K. (2010). Molecular and serological analysis of the epidemiology of myxoma virus in rabbits. *Veterinary Microbiology*, *143*(2–4), 167–178. https://doi.org/10.1016/j.vetmic.2009.11.025

Kerr, P. J., Liu, J., Cattadori, I., Ghedin, E., Read, A. F., & Holmes, E. C. (2015). Myxoma virus and the leporipoxviruses: An evolutionary paradigm. In *Viruses* (Vol. 7, Issue 3, pp. 1020–1061). MDPI AG. https://doi.org/10.3390/v7031020

Kerr, P. J., Merchant, J. C., Silvers, L., Hood, G. M., & Robinson, A. J. (2003). Monitoring the spread of myxoma virus in rabbit Oryctolagus cuniculus populations on the southern tablelands of New South Wales, Australia. II. Selection of a strain of virus for release. *Epidemiology and Infection*, *130*(1), S0950268802007860. https://doi.org/10.1017/S0950268802007860

Kerr, P., & McFadden, G. (2002). Immune Responses to Myxoma Virus. *Viral Immunology*, *15*(2).

Khlusevich, Y., Matveev, A., Emelyanova, L., Goncharova, E., Golosova, N., Pereverzev, I., & Tikunova, N. (2022). New p35 (H3L) Epitope Involved in Vaccinia Virus Neutralization and Its Deimmunization. *Viruses*, *14*(6), 1224. https://doi.org/10.3390/v14061224

Kilham, L., Herman, C. M., & Fisher, E. R. (1953). Naturally Occurring Fibromas of Grey Squirrels Related to Shope's Rabbit Fibroma. *Experimental Biology and Medicine*, *82*(2), 298–301. https://doi.org/10.3181/00379727-82-20099

King, J. M., Woolf, A., & Shively, J. N. (1972). Naturally occurring Squirrel fibroma with involvement of internal organs. *Journal of Wildlife Diseases*, *8*, 321–324. http://meridian.allenpress.com/jwd/article-pdf/8/4/321/2237678/0090-3558-8_4_321.pdf

Kollewe, C., & Vilcinskas, A. (2013). Production of recombinant proteins in insect cells. *American Journal of Biochemistry and Biotechnology*, *9*(3), 255–271. https://doi.org/10.3844/ajbbsp.2013.255.271

Kolodkin-Gal, D., Hulot, S. L., Korioth-Schmitz, B., Gombos, R. B., Zheng, Y., Owuor, J., Lifton, M. A., Ayeni, C., Najarian, R. M., Yeh, W. W., Asmal, M., Zamir, G., & Letvin, N. L. (2013). Efficiency of Cell-Free and Cell-Associated Virus in Mucosal Transmission of Human Immunodeficiency Virus Type 1 and Simian Immunodeficiency Virus. *Journal of Virology*, *87*(24), 13589–13597. https://doi.org/10.1128/jvi.03108-12

Kool, M., Voncken, J. W., Lier, F. L. V., Tramper, J., & Vlak, J. M. (1991). Detection and analysis of Autographa californica nuclear polyhedrosis virus mutants with defective interfering properties. *Virology*, *183*, 739–746. https://doi.org/10.1016/0042- 6822(91)91003-Y

Koonin, E. V. (1996). A duplicated catalytic motif in a new superfamily of phosphohydrolases and phospholipid synthases that includes poxvirus envelope proteins. *Trends Biochemistry Science*, *21*, 242–243.

Krauss, O., Hollinshead, R., Hollinshead, M., & Smith, G. L. (2002). An investigation of incorporation of cellular antigens into vaccinia virus particles. *Journal of General Virology*, *83*, 2347–2359.

Kritas, S. K., Dovas, C., Fortomaris, P., Petridou, E., Farsang, A., & Koptopoulos, G. (2008). A pathogenic myxoma virus in vaccinated and non-vaccinated commercial rabbits. *Research in Veterinary Science*, *85*(3), 622–624. https://doi.org/10.1016/j.rvsc.2008.03.008

Krupovič, M., Cvirkaite-Krupovič, V., & Bamford, D. H. (2010). Protein A33 responsible for antibody-resistant spread of Vaccinia virus is homologous to C-type lectin-like proteins. *Virus Research*, *151*(1), 97–101. https://doi.org/10.1016/j.virusres.2010.03.004

Kubelka, V., Altmann, F., Kornfeld, G., & März, L. (1994). Structures of the N-linked oligosaccharides of the membrane glycoproteins from three lepidopteran cell lines (Sf-21, IZD-Mb-0503, Bm-N). *Archives of Biochemistry and Biophysics*, *308*(1), 148–157.

Kumar, A., Tiwari, S., Thavaselvam, D., Sathyaseelan, K., Prakash, A., Barua, A., Arora, S., & Kameswara Rao, M. (2012). Optimization and efficient purification of recombinant Omp28 protein of Brucella melitensis using Triton X-100 and β-mercaptoethanol. *Protein Expression and Purification*, *83*(2), 226–232. https://doi.org/10.1016/j.pep.2012.04.002

Kumar, A., Yogisharadhya, R., Bhanuprakash, V., Venkatesan, G., & Shivachandra, S. B. (2015). Structural analysis and immunogenicity of recombinant major envelope protein (rA27L) of buffalopox virus, a zoonotic Indian vaccinia-like virus. *Vaccine*, *33*(41), 5396–5405. https://doi.org/10.1016/j.vaccine.2015.08.058

Kumar, B., Gono Bishwabidyalay, S., Jahan, N., Sil, B. K., Haq, M. A., Oishee, M. J., Ali, T., Saif Khandker, S., Kobatake, E., Mie, M., Khondoker, M. U., Raeed Jamiruddin, M., & Adnanid, N. (2021). Development and performance evaluation of a rapid in-house ELISA for retrospective serosurveillance of SARS-CoV-2. *Plos ONE*. https://doi.org/10.1101/2020.12.10.20244350

Kwit, E., Osiński, Z., Lavazza, A., & Rzeżutka, A. (2020). Detection of myxoma virus in the classical form of myxomatosis using an AGID assay: Statistical assessment of the assay's diagnostic performance. *Journal of Veterinary Research (Poland)*, *64*(3), 369–372. https://doi.org/10.2478/jvetres-2020-0049

Kwit, E., Osiński, Z., & Rzeżutka, A. (2019). Detection of viral DNA of myxoma virus using a validated PCR method with an internal amplification control. *Journal of Virological Methods*, *272*. https://doi.org/10.1016/j.jviromet.2019.113709

Labudovic, A., Perkins, H., Van Leeuwen, B., & Kerr, P. (2004). Sequence mapping of the Californian MSW strain of Myxoma virus. *Archives of Virology*, *149*(3), 553–570. https://doi.org/10.1007/s00705-003-0222-6

Lai, C., Gong, S., & Esteban, M. (1990). Structural and Functional Properties of the 14-kDa Envelope Protein of Vaccinia Virus Synthesized in Escherichia coli. *The Journal of Biological Chemistry*, *265*(36), 22174–22180.

Lai, C., Gong, S., & Esteban, M. (1991). The Purified 14-Kilodalton Envelope Protein of Vaccinia Virus Produced in Escherichia coli Induces Virus Immunity in Animals. *Journal of Virology*, *65*(10), 5631–5635.

Landis, J. R., & Koch, G. G. (1977). The Measurement of Observer Agreement for Categorical Data. *Biometrics*, *33*(1), 159–174.

Laudermilch, E., & Chandran, K. (2021). MAVERICC: Marker-free Vaccinia Virus Engineering of Recombinants through in vitro CRISPR/Cas9 Cleavage. *Journal of Molecular Biology*, *433*(9). https://doi.org/10.1016/j.jmb.2021.166896

Lavazza, A. (2023). *Myxomatosis-WOAH Reference Laboratory Reports Activities 2022*.

Law, M., Carter, G. C., Roberts, K. L., Hollinshead, M., & Smith, G. L. (2006). Ligand-induced and nonfusogenic dissolution of a viral membrane. *PNAS*, *103*, 5989–5994. www.pnas.orgcgidoi10.1073pnas.0601025103

Law, M., Hollinshead, R., & Smith, G. L. (2002). Antibody-sensitive and antibody-resistant cell-to-cell spread by vaccinia virus : role of the A33R protein in antibody-resistant spread. *Journal of General Virology*, *83*, 209–222.

Law, M., & Smith, G. L. (2001). Antibody neutralization of the extracellular enveloped form of vaccinia virus. *Virology*, *280*(1), 132–142. https://doi.org/10.1006/viro.2000.0750

Lees, A. C., & Bell, D. J. (2008). A conservation paradox for the 21st century: The European wild rabbit Oryctolagus cuniculus, an invasive alien and an endangered native species. *Mammal Review*, *38*(4), 304–320. https://doi.org/10.1111/j.1365-2907.2008.00116.x

Levin, C., Perrin, H., & Combadiere, B. (2015). Tailored immunity by skin antigen-presenting cells. *Human Vaccines and Immunotherapeutics*, *11*(1), 27–36. https://doi.org/10.4161/hv.34299

Lin, C.-L., Chung, C.-S., Heine, H. G., & Chang, W. (2000). Vaccinia Virus Envelope H3L Protein Binds to Cell Surface Heparan Sulfate and Is Important for Intracellular Mature Virion Morphogenesis and Virus Infection In Vitro and In Vivo. In *JOURNAL OF VIROLOGY* (Vol. 74, Issue 7). https://journals.asm.org/journal/jvi

Liu, S. J., Xue, H. P., Pu, B. Q., & Qian, N. H. (1984). A new viral disease in rabbits. *Animal Husbandry and Veterinary Medicine (Xumu Yu Shouyi)*, *16*(6), 253–255.

López-Lorenzo, G., López-Novo, C., Prieto, A., Díaz, J. M., Gullón, J., Arnal, J. L., Benito, A., Díaz, P., Panadero, R., Díez-Baños, P., Dalton, K. P., Parra, F., & Fernández, G. (2021). Molecular detection of myxoma virus in the environment of vaccinated rabbitries. *Transboundary and Emerging Diseases*, *68*(3), 1424–1431. https://doi.org/10.1111/tbed.13809

Ludwiczak, J., Winski, A., Szczepaniak, K., Alva, V., & Dunin-Horkawicz, S. (2019). DeepCoil - A fast and accurate prediction of coiled-coil domains in protein sequences. *Bioinformatics*, *35*(16), 2790–2795. https://doi.org/10.1093/bioinformatics/bty1062

Manev, I., Genova, K., Lavazza, A., & Capucci, L. (2018). Humoral immune response to different routes of myxomatosis vaccine application. *World Rabbit Science*, *26*(2), 149–154. https://doi.org/10.4995/wrs.2018.7021

Marchandeau, S., Pontier, D., Guitton, J. S., Letty, J., Fouchet, D., Aubineau, J., Berger, F., Léonard, Y., Roobrouck, A., Gelfi, J., Peralta, B., & Bertagnoli, S. (2014). Early infections by myxoma virus of young rabbits (Oryctolagus cuniculus) protected by maternal antibodies activate their immune system and enhance herd immunity in wild populations. *Veterinary Research*, *45*(1). https://doi.org/10.1186/1297-9716-45-26

Marlier, D., Cassart, D., Boucraut-Baralon, C., Coignoul, F., & Vindevogel, H. (1999). Experimental Infection of Specific Pathogen-free New Zealand White Rabbits with Five Strains of Amyxomatous Myxoma Virus. In *J. Comp. Path* (Vol. 121).

Marlier, D., Herbots, J., Detilleux, J., Lemaire, M. Á., Thiry, E., & Vindevogel, H. (2001). Cross-sectional study of the association between pathological conditions and myxoma-virus seroprevalence in intensive rabbit farms in Europe. *Preventive Veterinary Medicine*, *40*, 55–64.

Marlier, D., Mainil, J., Boucraut-Baralon, C., Linden, A., & Vindevogel, H. (2000). The efficacy of two vaccination schemes against experimental infection with a virulent amyxomatous or a virulent nodular myxoma virus strain. *Journal of Comparative Pathology*, *122*(2–3), 115–122. https://doi.org/10.1053/jcpa.1999.0346

Matho, M. H., de Val, N., Miller, G. M., Brown, J., Schlossman, A., Meng, X., Crotty, S., Peters, B., Xiang, Y., Hsieh-Wilson, L. C., Ward, A. B., & Zajonc, D. M. (2014). Murine Anti-vaccinia Virus D8 Antibodies Target Different Epitopes and Differ in Their Ability to Block D8 Binding to CS-E. *PLoS Pathogens*, *10*(12), e1004495. https://doi.org/10.1371/journal.ppat.1004495

Matho, M. H., Maybeno, M., Benhnia, M. R.-E.-I., Becker, D., Meng, X., Xiang, Y., Crotty, S., Peters, B., & Zajonc, D. M. (2012). Structural and Biochemical Characterization of the Vaccinia Virus Envelope Protein D8 and Its Recognition by the Antibody LA5. *Journal of Virology*, *86*(15), 8050–8058. https://doi.org/10.1128/JVI.00836-12

McConkey, S. J., Reece, W. H. H., Moorthy, V. S., Webster, D., Dunachie, S., Butcher, G., Vuola, J. M., Blanchard, T. J., Gothard, P., Watkins, K., Hannan, C. M., Everaere, S., Brown, K., Kester, K. E., Cummings, J., Williams, J., Gray Heppner, D., Pathan, A., Flanagan, K., … Hill, A. V. S. (2003). *Enhanced T-cell immunogenicity of plasmid DNA vaccines boosted by recombinant modified vaccinia virus Ankara in humans*. *503*(6). http://www.nature.com/naturemedicine

McIntosh, A. A. G., & Smith, G. L. (1996). Vaccinia Virus glycoprotein A34R is required for infectivity of Extracellular Enveloped Virus. *Journal of Virology*, *70*(1), 44–1865. https://journals.asm.org/journal/jvi

McKercher, D. G. (1952). Infectious myxomatosis. I. Vaccination. II. Antibiotic therapy. *American Journal of Veterinary Research*, *13*(48), 425–429.

McKercher, D. G., & Saito, J. K. (1964). An Attenuated Live Virus Vaccine for Myxomatosis. *Nature*, *202*(4935), 933–934.

Mercer, A. A., Schmidt, A., Weber, O., Barrett, J. W., & McFadden, G. (2007). Genus Leporipoxvirus. *Poxviruses*, *183*.

Meseda, C. A., Campbell, J., Kumar, A., Garcia, A. D., Merchlinsky, M., & Weir, J. P. (2013). Effect of the Deletion of Genes Encoding Proteins of the Extracellular Virion Form of

Vaccinia Virus on Vaccine Immunogenicity and Protective Effectiveness in the Mouse Model. *PLoS ONE*, *8*(6). https://doi.org/10.1371/journal.pone.0067984

Mims, C. A. (1964). Aspects of the pathogenesis of virus diseases. *Bacteriological Reviews*, *28*(1), 30–71. https://doi.org/10.1128/br.28.1.30-71.1964

Monterroso, P., Garrote, G., Serronha, A., Santos, E., Delibes-Mateos, M., Abrantes, J., De Ayala, R. P., Silvestre, F., Carvalho, J., Vasco, I., Lopes, A. M., Maio, E., Magalhães, M. J., Mills, L. S., Esteves, P. J., Simón, M. N., & Alves, P. C. (2016). Disease-mediated bottom-up regulation: An emergent virus affects a keystone prey, and alters the dynamics of trophic webs. *Scientific Reports*, *6*. https://doi.org/10.1038/srep36072

Morales, M., Ramírez, M. A., Cano, M. J., Párraga, M., Castilla, J., Pérez-Ordoyo, L. I., Torres, J. M., & Bárcena, J. (2009). Genome Comparison of a Nonpathogenic Myxoma Virus Field Strain with Its Ancestor, the Virulent Lausanne Strain. *Journal of Virology*, *83*(5), 2397–2403. https://doi.org/10.1128/jvi.02189-08

Moreno, S., & Villafuerte, R. (1995). Traditional management of scrubland for the conservation of rabbits Oryctolagus cuniculus and their predators in Doñana National park, Spain. *Biological Conservation*, *73*, 81–85.

Moreno, S., Villafuerte, R., Cabezas, S., & Lombardi, L. (2004). Wild rabbit restocking for predator conservation in Spain. *Biological Conservation*, *118*(2), 183–193. https://doi.org/10.1016/j.biocon.2003.07.020

Moss, B. (2012). Poxvirus cell entry: How many proteins does it take? In *Viruses* (Vol. 4, Issue 5, pp. 688–707). https://doi.org/10.3390/v4050688

Moss, B. (2013). Poxvirus DNA replication. *Cold Spring Harbor Perspectives in Biology*, *5*(9). https://doi.org/10.1101/cshperspect.a010199

Moss, B. (2016). Membrane fusion during poxvirus entry. In *Seminars in Cell and Developmental Biology* (Vol. 60, pp. 89–96). Academic Press. https://doi.org/10.1016/j.semcdb.2016.07.015

Moss, B., & Rosenblum, E. N. (1973). Protein Cleavage and Poxvirus Morphogenesis: Tryptic Peptide Analysis of Core Precursors Accumulated by Blocking Assembly with Rifampicin. *Journal of Molecular Biology*, *81*, 267–269.

Moss, B., & Salzman, N. P. (1968). Sequential Protein Synthesis Following Vaccinia Virus Infection. In *JOURNAL OF VIROLOGY* (Vol. 2, Issue 10).

Moussatche, N., & Condit, R. C. (2015). Fine structure of the vaccinia virion determined by controlled degradation and immunolocalization. *Virology*, *475*, 204–218. https://doi.org/10.1016/j.virol.2014.11.020

Mutze, G., Bird, P., Kovaliski, J., Peacock, D., Jennings, S., & Cooke, B. (2002). Emerging epidemiological patterns in rabbit haemorrhagic disease, its interaction with

myxomatosis, and their effects on rabbit populations in South Australia. *Wildlife Research*, *29*(6), 577–590. https://doi.org/10.1071/WR00100

Nallamsetty, S., & Waugh, D. S. (2006). Solubility-enhancing proteins MBP and NusA play a passive role in the folding of their fusion partners. *Protein Expression and Purification*, *45*(1), 175–182. https://doi.org/10.1016/j.pep.2005.06.012

Nash, P., Barrett, J., Cao, J.-X., Everett, H., Xu, X.-M., Robichaud, J., Hnatiuk, S., Ainslie, C., Seet, B. T., & McFadden, G. (1999). Immunomodulation by viruses: the myxoma virus story. *Immunological Reviews*, *168*(1), 103–120.

Nash, P., Barrett, J., Jing-Xin, C., Hota-Mitchell, S., Lalani, A. S., Everett, H., Xiao-Ming, X., Robichaud, J., Hnatiuk, S., Ainslie, C., Seet, B. T., & McFadden, G. (1999). Immunomodulation by viruses: The myxoma virus story. *Immunological Reviews*, *168*(1), 103–120. https://doi.org/10.1111/j.1600-065X.1999.tb01286.x

Newsome, T. P., Scaplehorn, N., & Way, M. (2004). Src Mediates a Switch from Microtubule-to Actin-Based Motility of Vaccinia Virus. *Science*, *306*(9), 124–129. www.sciencemag.org/cgi/content/full/306/5693/120/

Niles, E. G., & Seto, J. (1988). Vaccinia virus gene D8 encodes a virion transmembrane protein. *Journal of Virology*, *62*(10), 3772–3778. https://doi.org/10.1128/jvi.62.10.3772-3778.1988

Nuismer, S. L., Althouse, B. M., May, R., Bull, J. J., Stromberg, S. P., & Antia, R. (2016). Eradicating infectious disease using weakly transmissible vaccines. *Proceedings of the Royal Society B: Biological Sciences*, *283*(1841). https://doi.org/10.1098/rspb.2016.1903

Nuismer, S. L., & Bull, J. J. (2020). Self-disseminating vaccines to suppress zoonoses. In *Nature Ecology and Evolution* (Vol. 4, Issue 9, pp. 1168–1173). Nature Research. https://doi.org/10.1038/s41559-020-1254-y

OIE. (2018). Mixomatosis. In *Manual Terrestre*.

Opgenorth, A., Graham, K., Nation, N., Strayer, D., & McFadden, G. (1992). Deletion analysis of two tandemly arranged virulence genes in myxoma virus, M11L and myxoma growth factor. *Journal of Virology*, *66*(8), 4720–4731. https://doi.org/10.1128/jvi.66.8.4720-4731.1992

Ostrout, N. D., McHugh, M. M., Tisch, D. J., Moormann, A. M., Brusic, V., & Kazura, J. W. (2007). Long-term T cell memory to human leucocyte antigen-A2 supertype epitopes in humans vaccinated against smallpox. *Clinical and Experimental Immunology*, *149*(2), 265–273. https://doi.org/10.1111/j.1365-2249.2007.03401.x

Parrish, S., & Moss, B. (2007). Characterization of a Second Vaccinia Virus mRNA-Decapping Enzyme Conserved in Poxviruses. *Journal of Virology*, *81*(23), 12973–12978. https://doi.org/10.1128/jvi.01668-07

Payne, L. G. (1980). Significance of Extracellular Enveloped Virus in the in vitro and in vivo Dissemination of Vaccinia. *J. Gen. Virol*, *50*, 89–100.

Payne, L. G. (1986). Archives of Virology The Existence of an Envelope on Extracellular Cowpox Virus and Its Antigenic Relationship to the Vaccinia Envelope. In *Archives of Virology* (Vol. 90).

Pennington, T. H. (1974). Vaccinia Virus Polypeptide Synthesis: sequential Appearance and Stability of Pre- and Post-replicative Polypeptides. *J. Gen. Virol. (I974)*, *25*, 433–444.

Pickup, D. J. (2015). Extracellular Virions: The Advance Guard of Poxvirus Infections. *PLoS Pathogens*, *11*(7). https://doi.org/10.1371/journal.ppat.1004904

Pütz, M. M., Midgley, C. M., Law, M., & Smith, G. L. (2006). Quantification of antibody responses against multiple antigens of the two infectious forms of Vaccinia virus provides a benchmark for smallpox vaccination. *Nature Medicine*, *12*(11), 1310–1315. https://doi.org/10.1038/nm1457

Rahman, M. M., Liu, J., Chan, W. M., Rothenburg, S., & McFadden, G. (2013). Myxoma Virus Protein M029 Is a Dual Function Immunomodulator that Inhibits PKR and Also Conscripts RHA/DHX9 to Promote Expanded Host Tropism and Viral Replication. *PLoS Pathogens*, *9*(7). https://doi.org/10.1371/journal.ppat.1003465

Rahman, M. M., & McFadden, G. (2017). Myxoma virus dsRNA binding protein M029 inhibits the type I IFN-induced antiviral state in a highly species-specific fashion. *Viruses*, *9*(2). https://doi.org/10.3390/v9020027

Reemers, S., Peeters, L., van Schijndel, J., Bruton, B., Sutton, D., van der Waart, L., & van de Zande, S. (2020). Novel trivalent vectored vaccine for control of myxomatosis and disease caused by classical and a new genotype of rabbit haemorrhagic disease virus. *Vaccines*, *8*(3), 1–15. https://doi.org/10.3390/vaccines8030441

Rico, A. B., Olson, A. T., & Wiebe, M. S. (2019). Generation of Vaccinia Virus Gene Deletion Mutants Using Complementing Cell Lines. In *Methods in Molecular Biology* (Vol. 2023, pp. 93–108). Humana Press Inc. https://doi.org/10.1007/978-1-4939-9593-6_5

Rivers, T. M. (1930). Infectious myxomatosis of rabbits: Observations on the pathological changes induced by virus myxomatosum (Sanarelli). *The Journal of Experimental Medicine*, *51*(6), 965–976.

Roberts, K. L., & Smith, G. L. (2008). Vaccinia virus morphogenesis and dissemination. In *Trends in Microbiology* (Vol. 16, Issue 10, pp. 472–479). https://doi.org/10.1016/j.tim.2008.07.009

Rodriguez, D., Rodriguez, J. R., & Esteban, M. (1993a). The vaccinia virus 14-kilodalton fusion protein forms a stable complex with the processed protein encoded by the vaccinia virus

A17L gene. *Journal of Virology*, *67*(6), 3435–3440. https://doi.org/10.1128/jvi.67.6.3435-3440.1993

Rodriguez, D., Rodriguez, J.-R., & Esteban, M. (1993b). The Vaccinia Virus 14-Kilodalton Fusion Protein Forms a Stable Complex with the Processed Protein Encoded by the Vaccinia Virus A17L Gene. *Journal of Virology*, *67*(6), 3435–3440.

Rodriguez, J. F., & Esteban, M. (1989). Plaque Size Phenotype as a Selectable Marker To Generate Vaccinia Virus Recombinants. In *JOURNAL OF VIROLOGY* (Vol. 63, Issue 2).

Rodriguez, J. F., Janeczko, R., & Esteban, M. (1985). Isolation and characterization of neutralizing monoclonal antibodies to vaccinia virus. *Journal of Virology*, *56*(2), 482–488. https://doi.org/10.1128/jvi.56.2.482-488.1985

Rodriguez, J. F., & Smith, G. L. (1990). IPTG-dependent vaccinia virus: identification of a virus protein enabling virion envelopment by Golgi membrane and egress. *Nucleic Acids Research*, *18*(18), 5347–5351.

Rodríguez, J.-R., Rodríguez, D., & Esteban, M. (1992). Insertional Inactivation of the Vaccinia Virus 32-Kilodalton Gene Is Associated with Attenuation in Mice and Reduction of Viral Gene Expression in Polarized Epithelial Cells. *JOURNAL OF VIROLOGY*, *66*(1), 183–189. https://journals.asm.org/journal/jvi

Romano, P. R., Zhang, F., Tan, S.-L., Garcia-Barrio, M. T., Katze, M. G., Dever, T. E., & Hinnebusch, A. G. (1998). Inhibition of Double-Stranded RNA-Dependent Protein Kinase PKR by Vaccinia Virus E3: Role of Complex Formation and the E3 N-Terminal Domain. *Molecular and Cellular Biology*, *18*(12), 7304–7316. https://doi.org/10.1128/MCB.18.12.7304

Roper, R. L., Wolffe, E. J., Weisberg, A., & Moss, B. (1998). The Envelope Protein Encoded by the A33R Gene Is Required for Formation of Actin-Containing Microvilli and Efficient Cell-to-Cell Spread of Vaccinia Virus. In *JOURNAL OF VIROLOGY* (Vol. 72, Issue 5). https://journals.asm.org/journal/jvi

Rosell, J. M., de la Fuente, L. F., Parra, F., Dalton, K. P., Badiola Sáiz, J. I., Pérez de Rozas, A., Badiola Díez, J. J., Fernández de Luco, D., Casal, J., Majó, N., Casas, J., Garriga, R., & Fernández Magariños, X. M. (2019). Myxomatosis and Rabbit Haemorrhagic Disease: A 30-Year Study of the Occurrence on Commercial Farms in Spain. *Animals*, *9*(10), 780. https://doi.org/10.3390/ani9100780

Rouco, C., Moreno, S., & Santoro, S. (2016). A case of low success of blind vaccination campaigns against myxomatosis and rabbit haemorrhagic disease on survival of adult European wild rabbits. *Preventive Veterinary Medicine*, *133*, 108–113. https://doi.org/10.1016/j.prevetmed.2016.09.013

Saint, K. M., French, N., & Kerr, P. (2001). Genetic variation in Australian isolates of myxoma virus: an evolutionary and epidemiological study. *Arch Virol*, *146*, 1105–1123.

Saito, J. K., Mckercher, D. G., & Castrucci, G. (1964a). Attenuation of the myxoma virus and use of the living attenuated virus as an immunizing agent for myxomatosis. *Journal of Infectious Diseases*, *114*, 417–422. http://jid.oxfordjournals.org/

Saito, J. K., Mckercher, D. G., & Castrucci, G. (1964b). Attenuation of the myxoma virus and use of the living attenuated virus as an immunizing agent for myxomatosis. *Journal of Infectious Diseases*, *114*, 417–428. https://doi.org/10.1093/infdis/114.5.417

Sakhatskyy, P., Wang, S., Chou, T. hui W., & Lu, S. (2006). Immunogenicity and protection efficacy of monovalent and polyvalent poxvirus vaccines that include the D8 antigen. *Virology*, *355*(2), 164–174. https://doi.org/10.1016/j.virol.2006.07.017

Salaün, H. A., Bougeard, S., Balaine, L., Eono, F., Le Bouquin, S., & Chauvin, C. (2015). Husbandry factors and health conditions influencing the productivity of French rabbit farms. *World Rabbit Science*, *23*(1), 27–37. https://doi.org/10.4995/wrs.2015.3076

Sanderson, C. M., Hollinshead, M., & Smith, G. L. (2000). The vaccinia virus A27L protein is needed for the microtubule-dependent transport of intracellular mature virus particles. *Journal of General Virology*, *81*, 47–58.

Santoro, S., Pacios, I., Moreno, S., Bertó-Moran, A., & Rouco, C. (2014). Multi-event capture-recapture modeling of host-pathogen dynamics among European rabbit populations exposed to myxoma and Rabbit Hemorrhagic Disease Viruses: Common and heterogeneous patterns. *Veterinary Research*, *45*(1). https://doi.org/10.1186/1297-9716-45-39

Scheiflinger, F., Dorner, F., & Falkner, F. G. (1998). Transient marker stabilisation: a general procedure to construct marker-free recombinant vaccinia virus. In *Arch Virol* (Vol. 143).

Schmelz, B., Sodeik, M., Ericsson, M., Wolffe, E. J., Shida, H., Hiller, G., & Griffithsi, G. (1994). Assembly of Vaccinia Virus: the Second Wrapping Cisterna Is Derived from the Trans Golgi Network. *Journal of Virology*, *68*(1), 130–147.

Schmidt, F. I., Bleck, C. K. E., & Mercer, J. (2012). Poxvirus host cell entry. In *Current Opinion in Virology* (Vol. 2, Issue 1, pp. 20–27). https://doi.org/10.1016/j.coviro.2011.11.007

Schmutz, C., Rindisbacher, L., Galmiche, M. C., & Wittek Riccardo. (1995). Biochemical analysis of the major Vaccinia Virus envelope antigen. *Virology*, *213*, 19–27.

Schramm, B., & Locker, J. K. (2005). Cytoplasmic organization of POXvirus DNA replication. *Traffic*, *6*(10), 839–846. https://doi.org/10.1111/j.1600-0854.2005.00324.x

Sell, S., & Scott, C. B. (1981). An immunohistologic study of Shope fibroma virus in rabbits: tumor rejection by cellular reaction in adults and progressive systemic reticuloendothelial infection in neonates. *Journal of the National Cancer Institute*, *66*(2), 363–373.

Senkevich, T. G., Ojeda, S., Townsley, A., Nelson, G. E., & Moss, B. (2005). Poxvirus multiprotein entry-fusion complex. *PNAS*, *102*(51), 18572–18577. www.pnas.orgcgidoi10.1073pnas.0509239102

Shih, P.-C., Yang, M.-S., Lin, S.-C., Ho, Y., Hsiao, J.-C., Wang, D.-R., Yu, S. S.-F., Chang, W., & Tzou, D.-L. M. (2009). A Turn-like Structure "KKPE" Segment Mediates the Specific Binding of Viral Protein A27 to Heparin and Heparan Sulfate on Cell Surfaces. *Journal of Biological Chemistry*, *284*(52), 36535–36546. https://doi.org/10.1074/jbc.M109.037267

Shope, R. E. (1932a). A filtrable virus causing a tumor-like condition in rabbits and its relationship to virus mixomatosum. *Journal of Experimental Medicine*, *56*(6), 803–822. https://doi.org/10.1084/jem.56.6.803

Shope, R. E. (1932b). A transmissible tumor-like condition in rabbits. *Journal of Experimental Medicine*, *56*(6), 793–802. https://doi.org/10.1084/jem.56.6.793

Singh, A., Upadhyay, V., Upadhyay, A. K., Singh, S. M., & Panda, A. K. (2015). Protein recovery from inclusion bodies of Escherichia coli using mild solubilization process. In *Microbial Cell Factories* (Vol. 14, Issue 1). BioMed Central Ltd. https://doi.org/10.1186/s12934-015-0222-8

Smallwood, S. E., Rahman, M. M., Smith, D. W., & McFadden, G. (2010). Myxoma virus: Propagation, purification, quantification, and storage. In *Current Protocols in Microbiology* (Issue SUPPL. 17). https://doi.org/10.1002/9780471729259.mc14a01s17

Smith, G. L., Benfield, C. T. O., Maluquer de Motes, C., Mazzon, M., Ember, S. W. J., Ferguson, B. J., & Sumner, R. P. (2013). Vaccinia virus immune evasion: Mechanisms, virulence and immunogenicity. In *Journal of General Virology* (Vol. 94, Issue PART 11, pp. 2367–2392). https://doi.org/10.1099/vir.0.055921-0

Smith, G. L., & Law, M. (2004). The exit of Vaccinia virus from infected cells. *Virus Research*, *106*(2 SPEC.ISS.), 189–197. https://doi.org/10.1016/j.virusres.2004.08.015

Smith, G. L., Vanderplasschen, A., & Law, M. (2002). The formation and function of extracellular enveloped vaccinia virus. *Journal of General Virology*, *83*, 2915–2931. www.sanger.ac.uk

Sobey, W. R., Conolly, D., & Adams, K. M. (1966). Myxomatosis: A simple method of sampling blood and testing for circulating soluble antigens or antibodies to them. *Australian Journal Science* , *28*(9), 354–355.

Spibey, N., McCabe, V. J., Greenwood, N. M., Jack, S. C., Sutton, D., & Van Der Waart, L. (2012). Novel bivalent vectored vaccine for control of myxomatosis and rabbit haemorrhagic disease. *Veterinary Record*, *170*(12), 309. https://doi.org/10.1136/vr.100366

Spiesschaert, B., McFadden, G., Hermans, K., Nauwynck, H., & Van De Walle, G. R. (2011). The current status and future directions of myxoma virus, a master in immune evasion. In

Veterinary Research (Vol. 42, Issue 1, pp. 1–18). BioMed Central. https://doi.org/10.1186/1297-9716-42-76

Stanford, M. M., Werden, S. J., & McFadden, G. (2007). Myxoma virus in the European rabbit: Interactions between the virus and its susceptible host. *Veterinary Research*, *38*(2), 299–318. https://doi.org/10.1051/vetres:2006054

Stern, D., Pauly, D., Zydek, M., Miller, L., Piesker, J., Laue, M., Lisdat, F., Dorner, M. B., Dorner, B. G., & Nitsche, A. (2016). Development of a Genus-Specific AntigenCapture ELISA for Orthopoxviruses–Target Selection and Optimized Screening. *PloS ONE*, *11*(3).

Subdirección General de Producciones Ganaderas y Cinegéticas, & Dirección general de producciones y mercados agrarios. (2024). *Informe trimestral Indicadores del sector cunícola (abril 2024)*. http://publicacionesoficiales.boe.es/

Sung, T.-C., Roper, R. L., Zhang, Y., Rudge, S. A., Temel, R., Hammond, S. M., & Morris, A. J. (1997). Mutagenesis of phospholipase D defines a superfamily including a trans-Golgi viral protein required for poxvirus pathogenicity. *The EMBO Journal*, *16*(15), 4519–4530.

Sypula, J., Wang, F., Ma, Y., Bell, J., & McFadden, G. (2004). Myxoma virus tropism in human tumour cells. *Gene Ther. Mol. Biol*, *8*, 103–114.

Tian, H., Chen, Y., Wu, J., Shang, Y., & Liu, X. (2010). Serodiagnosis of sheeppox and goatpox using an indirect ELISA based on synthetic peptide targeting for the major antigen P32. *Virology Journal*, *7:245*. http://www.virologyj.com/content/7/1/245

Tolonen, N., Doglio, L., Schleich, S., & Locker, J. K. (2001). Vaccinia Virus DNA Replication Occurs in Endoplasmic Reticulum-enclosed Cytoplasmic Mini-Nuclei. In *Molecular Biology of the Cell* (Vol. 12).

Torres, J. M., Ramírez, M. A., Morales, M., Bárcena, J., Vázquez, B., Espuña, E., Pagès-Manté, A., & Sánchez-Vizcaíno, J. M. (2001). Safety evaluation of a recombinant myxoma-RHDV virus inducing horizontal transmissible protection against myxomatosis and rabbit haemorrhagic disease. *Vaccine*, *19*, 174–182. www.elsevier.com/locate/vaccine

Torres, J. M., Sánchez, C., Ramírez, M. A., Morales, M., Bárcena, J., Ferrer, J., Espuña, E., Pagès-Manté, A., & Sánchez-Vizcaíno, J. M. (2001). First field trial of a transmissible recombinant vaccine against myxomatosis and rabbit hemorrhagic disease. *Vaccine*, *19*(31), 4536–4543. https://doi.org/10.1016/S0264-410X(01)00184-0

Townsley, A. C., Weisberg, A. S., Wagenaar, T. R., & Moss, B. (2006). Vaccinia Virus Entry into Cells via a Low-pH-Dependent Endosomal Pathway. *Journal of Virology*, *80*(18), 8899–8908. https://doi.org/10.1128/jvi.01053-06

Trottier, Y.-L., Wright, P. F., & Lariviere1, S. (1992). Optimization and Standardization of an Enzyme-Linked Immunosorbent Assay Protocol for Serodiagnosis of Actinobacillus

pleuropneumoniae Serotype 5. In *JOURNAL OF CLINICAL MICROBIOLOGY* (Vol. 30, Issue 1).

Van Eijl, H., Hollinshead, M., Rodger, G., Zhang, W.-H., & Smith, G. L. (2002). The vaccinia virus F12L protein is associated with intracellular enveloped virus particles and is required for their egress to the cell surface. *Journal of General Virology*, *83*, 195–207.

Van Oirschot, J. T. (1999). Diva vaccines that reduce virus transmission. In *Journal of Biotechnology* (Vol. 73). www.elsevier.com/locate/jbiotec

Van Oirschot, J. T., Rziha, H. J., Moonen, P. J. L. M., Pol, J. M. A., & Van Zaane, D. (1986). Differentiation of Serum Antibodies from Pigs Vaccinated or Infected with Aujeszky's Disease Virus by a Competitive Enzyme Immunoassay. In *J. gen. Virol* (Vol. 67).

Vanderplasschen, A., Hollinshead, M., & Smith, G. L. (1997). Antibodies against vaccinia virus do not neutralize extracellular enveloped virus but prevent virus release from infected cells and comet formation. *Journal of General Virology*, *78*, 2041–2048.

Vanderplasschen, A., Mathew, E., Hollinshead, M., Sim, R. B., Smith, G. L., William, S., & Joklik, W. K. (1998). Extracellular enveloped vaccinia virus is resistant to complement because of incorporation of host complement control proteins into its envelope. *Immunology*, *95*, 7544–7549. www.pnas.org.

Vanderplasschen, A., & Smith, G. L. (1997). A Novel Virus Binding Assay Using Confocal Microscopy: Demonstration that the Intracellular and Extracellular Vaccinia Virions Bind to Different Cellular Receptors. *Journal of Virology*, *71*(5), 44–1865.

Vaughn, J. L., Goodwin, R. H., Tompkins, G. J., & McCawley, P. (1977). The establishment of two cell lines from the insect spodoptera frugiperda (lepidoptera; noctuidae). *In Vitro*, *13*, 213–217.

Vázquez, M.-I., & Esteban, M. (1999). Identification of Functional Domains in the 14-Kilodalton Envelope Protein (A27L) of Vaccinia Virus. *JOURNAL OF VIROLOGY*, *73*(11), 9098–9109.

Vázquez, M.-I., Rivas, G., Cregut, D., Serrano, L., & Esteban, M. (1998). The Vaccinia Virus 14-Kilodalton (A27L) Fusion Protein Forms a Triple Coiled-Coil Structure and Interacts with the 21-Kilodalton (A17L) Virus Membrane Protein through a C-Terminal α-Helix. *Journal of Virology*, *72*(12), 10126–10137. https://doi.org/10.1128/JVI.72.12.10126-10137.1998

Venkatesan, G., Kumar Teli, M., Sankar, M., Kumar, A., Dashprakash, M., Arya, S., Madhavan, A., Ramakrisnan, M. A., & Pandey, A. B. (2018). Expression and evaluation of recombinant P32 protein based ELISA for sero-diagnostic potential of capripox in sheep and goats. *Molecular and Cellular Probes*, *37*, 48–54. https://doi.org/10.1016/j.mcp.2017.11.005

Villa, N. Y., Bartee, E., Mohamed, M. R., Rahman, M. M., Barrett, J. W., & McFadden, G. (2010a). Myxoma and vaccinia viruses exploit different mechanisms to enter and infect

human cancer cells. *Virology*, *401*(2), 266–279. https://doi.org/10.1016/j.virol.2010.02.027

Villa, N. Y., Bartee, E., Mohamed, M. R., Rahman, M. M., Barrett, J. W., & McFadden, G. (2010b). Myxoma and vaccinia viruses exploit different mechanisms to enter and infect human cancer cells. *Virology*, *401*(2), 266–279. https://doi.org/10.1016/j.virol.2010.02.027

Villafuerte, R., Castro, F., Ramírez, E., Cotilla, I., Parra, F., Delibes-Mateos, M., Recuerda, P., & Rouco, C. (2017). Large-scale assessment of myxomatosis prevalence in European wild rabbits (Oryctolagus cuniculus) 60 years after first outbreak in Spain. *Research in Veterinary Science*, *114*, 281–286. https://doi.org/10.1016/j.rvsc.2017.05.014

Wagenaar, T. R., & Moss, B. (2007). Association of Vaccinia Virus Fusion Regulatory Proteins with the Multicomponent Entry/Fusion Complex. *Journal of Virology*, *81*(12), 6286–6293. https://doi.org/10.1128/jvi.00274-07

Walker, J. M. (2009). *The ELISA Guidebook Second Edition Series Editor* (John M.Walker, Ed.; Second Edition). www.springer.com/series/7651

Wang, D. R., Hsiao, J. C., Wong, C. H., Li, G. C., Lin, S. C., Yu, S. S. F., Chen, W., Chang, W., & Tzou, D. L. M. (2014). Vaccinia viral protein A27 is anchored to the viral membrane via a cooperative interaction with viral membrane protein A17. *Journal of Biological Chemistry*, *289*(10), 6639–6655. https://doi.org/10.1074/jbc.M114.547372

Ward, B. M. (2005). Visualization and Characterization of the Intracellular Movement of Vaccinia Virus Intracellular Mature Virions. *Journal of Virology*, *79*(8), 4755–4763. https://doi.org/10.1128/jvi.79.8.4755-4763.2005

Ward, B. M., & Moss, B. (2004). Vaccinia Virus A36R Membrane Protein Provides a Direct Link between Intracellular Enveloped Virions and the Microtubule Motor Kinesin. *Journal of Virology*, *78*(5), 2486–2493. https://doi.org/10.1128/jvi.78.5.2486-2493.2004

Ward, D. (2005). *Reversing Rabbit Decline: One of the biggest challenges for nature conservation in Spain and Portugal*. https://doi.org/10.13140/RG.2.2.26144.00009

Welsch, S., Doglio, L., Schleich, S., & Krijnse Locker, J. (2003). The Vaccinia Virus I3L Gene Product Is Localized to a Complex Endoplasmic Reticulum-Associated Structure That Contains the Viral Parental DNA. *Journal of Virology*, *77*(10), 6014–6028. https://doi.org/10.1128/jvi.77.10.6014-6028.2003

Westwood, J. C. N., Harris, W. J., Zwartouw, H. T., Titmuss, D. H. J., & Appleyard, G. (1964). Studies on the Structure of Vaccinia Virus. *J. Gen. Microbial*, *34*, 67–78.

Whitbeck, J. C., Foo, C. H., Ponce de Leon, M., Eisenberg, R. J., & Cohen, G. H. (2009). Vaccinia virus exhibits cell-type-dependent entry characteristics. *Virology*, *385*(2), 383–391. https://doi.org/10.1016/j.virol.2008.12.029

Willer, D. O., McFadden, G., Evans, D. H., Barrett, J., Cao, J., Macaulay, C., Willer, D., Evans, D., & McFadden, G. (1999). *The Complete Genome Sequence of Shope (Rabbit) Fibroma Virus*. http://www.idealibrary.com

Wolfe, A. M., Dunlap, K. M., Smith, A. C., Bartee, M. Y., & Bartee, E. (2018). Myxoma Virus M083 Is a Virulence Factor Which Mediates Systemic Dissemination. *Journal of Virology*, *92*(7). https://doi.org/10.1128/jvi.02186-17

Wolffe, E. J., Katz, E., Weisberg, A., & Moss, B. (1997). The A34R Glycoprotein Gene Is Required for Induction of Specialized Actin-Containing Microvilli and Efficient Cell-to-Cell Transmission of Vaccinia Virus. In *JOURNAL OF VIROLOGY* (Vol. 71, Issue 5). https://journals.asm.org/journal/jvi

Wolffe, E. J., Weisberg, A. S., Moss, B., Wolffe, E. J., Katz, A., Weisberg, B., Roper, E. J., & Wolffe, A. (1998). Role for the Vaccinia Virus A36R Outer Envelope Protein in the Formation of Virus-Tipped Actin-Containing Microvilli and Cell-to-Cell Virus Spread. In *J. Virol* (Vol. 71).

Wyatt, L. S., Earl, P. L., & Moss, B. (2017). Generation of Recombinant Vaccinia Viruses. *Current Protocols in Protein Science*, *89*, 5.13.1-5.13.18. https://doi.org/10.1002/cpps.33

Xu, Z. J., & Chen, W. X. (1989). Viral haemorrhagic disease in rabbits: A review. *Veterinary Research Communications*, *13*(3), 205–212. https://doi.org/10.1007/BF00142046

Xu, Z., Zikos, D., Tamošiūnaitė, A., Klopfleisch, R., Osterrieder, N., & Tischer, B. K. (2014). Identification of 10 Cowpox Virus Proteins That Are Necessary for Induction of Hemorrhagic Lesions (Red Pocks) on Chorioallantoic Membranes. *Journal of Virology*, *88*(15), 8615–8628. https://doi.org/10.1128/jvi.00901-14

Yang, G., Pevear, D. C., Davies, M. H., Collett, M. S., Bailey, T., Rippen, S., Barone, L., Burns, C., Rhodes, G., Tohan, S., Huggins, J. W., Baker, R. O., Buller, R. L. M., Touchette, E., Waller, K., Schriewer, J., Neyts, J., DeClercq, E., Jones, K., … Jordan, R. (2005). An Orally Bioavailable Antipoxvirus Compound (ST-246) Inhibits Extracellular Virus Formation and Protects Mice from Lethal Orthopoxvirus Challenge. *Journal of Virology*, *79*(20), 13139–13149. https://doi.org/10.1128/jvi.79.20.13139-13149.2005

Yang, H., Kim, S.-K., Kim, M., Reche, P. A., Morehead, T. J., Damon, I. K., Welsh, R. M., & Reinherz, E. L. (2005). Antiviral chemotherapy facilitates control of poxvirus infections through inhibition of cellular signal transduction. *Journal of Clinical Investigation*, *115*(2), 379–387. https://doi.org/10.1172/jci23220

Yang, Z., Reynolds, S. E., Martens, C. A., Bruno, D. P., Porcella, S. F., & Moss, B. (2011). Expression Profiling of the Intermediate and Late Stages of Poxvirus Replication. *Journal of Virology*, *85*(19), 9899–9908. https://doi.org/10.1128/jvi.05446-11

Yu, S., Ge, H., Li, S., & Qiu, H. J. (2022). Modulation of Macrophage Polarization by Viruses: Turning Off/On Host Antiviral Responses. In *Frontiers in Microbiology* (Vol. 13). Frontiers Media S.A. https://doi.org/10.3389/fmicb.2022.839585

Zachertowska, A., Brewer, D., & Evans, D. H. (2006). Characterization of the major capsid proteins of myxoma virus particles using MALDI-TOF mass spectrometry. *Journal of Virological Methods*, *132*(1–2), 1–12. https://doi.org/10.1016/j.jviromet.2005.08.015

Zhang, L., Stanford, M., Liu, J., Barrett, C., Jiang, L., Barclay, A. N., & McFadden, G. (2009). Inhibition of Macrophage Activation by the Myxoma Virus M141 Protein (vCD200). *Journal of Virology*, *83*(18), 9602–9607. https://doi.org/10.1128/JVI.01078-09

Zhao, Y., Chapman, D. A. G., & Jones, I. M. (2003). Improving baculovirus recombination. *Nucleic Acids Research*, *31*(2). https://doi.org/10.1093/nar/gng006

Zinkernagel, R. M. (2001). Maternal antibodies, childhood infections, and autoimmune diseases. *N Engl J Med*, *345*(18), 1331–1335. www.nejm.org

Zinovieva, V. V, Tchikaev, N. A., Chertovb, O. Y., & Malygina, E. G. (1994). Identification of the gene encoding vaccinia virus immunodominant protein ~35. *Gene*, *147*(2), 209–214.